UNIVERSITÀ
DEGLI STUDI
FIRENZE

DOTTORATO DI RICERCA IN
INGEGNERIA INDUSTRIALE

CICLO XXVII

Modeling and simplification methods for machine tool dynamics prediction in high speed milling

Settore Scientifico Disciplinare ING/IND-16

Candidato
Ing. Niccolò Grossi

Tutori
Dott. Ing. Antonio Scippa

Dott. Ing. Gianni Campatelli

Controrelatore
Prof. Dr. Yusuf Altintas

Coordinatore del Dottorato
Prof. Ing. Maurizio De Lucia

Anni 2012/2014

ISBN XXX–XX–XXXX–XXX–X
D/XXXX/XXXX/XX

To my brothers,
Lapo and Giacomo

Abstract

Unstable vibration phenomenon known as chatter is the most limiting factor to the performances of modern milling machine. Stability Lobe Diagram (SLD) is the main tool adopted to avoid chatter, and improve machine tool productivity, since it allows selecting optimal cutting parameters (spindle speed and engagement condition) to ensure a stable operation at the highest material removal rate. This chart can be obtained with simulation, thanks to predictive approaches, or directly by means of experimental tests.

The aim of this thesis was to increase the reliability of Stability Lobe Diagram, and to propose and develop new identification techniques in order to support its industrial applications. Different methods have been analyzed both for chatter prediction, and experimental detection.

In particular for prediction, research has been principally focused on the main inputs required: tool-tip Frequency Response Functions (FRFs) and cutting force coefficients. Machine tool dynamics has been investigated with the aim at developing methods to quickly and accurately identify tool-tip FRFs, key factor for a reliable chatter prediction. Both full Finite Element models of machine tool, and hybrid experimental-numerical methods have been analyzed and implemented, studying their application limits. On the other hand cutting speed dependence of cutting force coefficients has been investigated in order to improve their reliability in High Speed Milling (HSM).

Moreover this work presents an experimental detection technique called Spindle Speed Ramp-up test. Thanks to this technique with few cutting tests Stability Lobe Diagram can be accurately identified without any approximation introduced by predictive approaches. All the proposed methods have been validated and critically discussed.

The main goal of this Ph.D. thesis is to improve industrial application of vibrations prediction and detection approaches in milling, proposing simplified methods and easy-to-use systems. In order to do so an extensive critical analysis on advantages and drawbacks of different techniques is here presented.

Preface

Parts of this thesis have been published in peer reviewed journals and conference proceedings. The publications reported work carried out during my Ph.D. research under the supervision of Dr. Antonio Scippa and Dr. Gianni Campatelli.

A version of Chapter 5 has been published as Law M., Grossi N., Scippa A., Phani A.S., Altintas Y., 2014, Modeling the Orientation-Dependent Dynamics of Machine Tools with Gimbal Heads, 3rd International Chemnitz Manufacturing Colloquium ICMC 2014, Chemnitz [1]. Developed technique was a result of collaboration with Dr. M. Law supervised by Prof. Dr. Altintas. I was mainly responsible of spindle FE modeling.

Parts of Chapter 8 (section 8.5) have been published in two conference proceedings: Campatelli G., Scippa A., Grossi N., Velenosi A., 2012, Hybrid FE-experimental modeling of machine tool dynamics, MTTRF Annual Meeting 2012, Iga, Japan [2] and Grossi N., Scippa A., Campatelli G., Tool point dynamics prediction using a hybrid FE-experimental modeling of milling machine, 2013, XI AITeM Conference, San Benedetto del Tronto [3]. I developed the theory, performed experiments and wrote most of the manuscript.

A version of Chapter 9 has been published as Grossi N., Sallese L., Scippa A., Campatelli G., 2014. Chatter Stability Prediction in Milling Using Speed-varying Cutting Force Coefficients, Procedia CIRP [4]. I formulated presented techniques, conducted experiments and wrote most of the manuscript with contributions from other authors.

Contents of Chapter 10 has been published as N. Grossi, A. Scippa, L. Sallese, R. Sato, G. Campatelli, Spindle speed ramp-up test: A novel experimental approach for chatter stability detection, International Journal of Machine Tools and Manufacture [5]. I worked on test formulation, experimental activities and elaboration of the results. I wrote most of the manuscript.

Developed methods and results presented in this work are under consideration to be published in peer reviewed journals.

Activities presented in this thesis have been carried out both in Machine Tool Research Laboratory in Firenze and Manufacturing Automation Laboratory in Vancouver, Canada, under Prof. Dr. Yusuf Altintas supervision.

Table of contents

List of figures

List of tables

Acronyms List

CNC	Computer Numerical Control
DOF	Degree Of Freedom
EMA	Experimental Modal Analysis
FE	Finite Element
FEM	Finite Element Method
FRF	Frequency Response Function
HSM	High Speed Machining
OA	Order Analysis
RCSA	Receptance Coupling Substructure Assembly
MAL	Manufacturing Automation Laboratory
MRR	Material Removal Rate
MTRL	Machine Tool Research Laboratory
MTTRF	Machine Tool Technologies Research Foundation
MPC	Multi-Point Constraint
SLD	Stability Lobe Diagram
SLE	Surface Location Error
SPC	Single Point Constraint
SSR	Spindle Speed Ramp-up
UBC	University of British Columbia

Introduction

Machining is the most widespread manufacturing technology to produce final shape metal components. Precision and productivity of such technology is increased in the last decades thanks to improvements in materials, computers, and sensors [6]. Nowadays computer numerically controlled (CNC) machine tools cut extra material to obtain desired part by different types of operation (e.g., turning, drilling, milling, boring).

Among these, milling has assumed a central role in manufacturing industries due to its versatility and wide range of metal cutting potentials. Multi-flutes cutting tool removes material rotating and advancing in the workpiece, this process is hence inherently periodic characterized by time-dependent forces that cause vibration phenomena potentially affecting machine surface quality, tool wear and productivity.

The actual trend in milling is to increase cutting parameters (e.g., feed and spindle speed) to enhance process productivity without compromising surface finish. This leads to the development of modern High Speed Machining (HSM) milling technology, which results in higher Material Removal Rate (MRR) and better surface quality. HSM is a powerful cutting technology increasingly exploited by manufacturing industries, especially in aerospace field where components are being machined as monolithic structures [7]. Monolithic components are commonly used in that field due to their homogeneity and excellent strength-to-weight-ratio. In order to ensure enough stiffness to the whole component, monolithic parts are often made of thin walls, and webs, obtained usually starting from a blank of material and removing up to 95% of the weight of the initial blank. Therefore, increasing the removal rate as much as possible is the main condition to reach high productivity. The drawback is that, at high removal rate conditions (high feed, large depth of cut), vibrations induced by the milling process can be an issue that limits HSM operation performances.

On the other hand the application of advanced materials is continuously increasing in many fields of industry, primarily in the medical, energy and aerospace industry. Machining of high performance materials such as hardened steel, titanium alloys or metallic super-alloys, is a challenge for modern manufacturing. The high strength and hardness of these materials causes high cutting forces, and under high cutting forces, detrimental vibrations are more likely to occur [8]. It is thus necessary to select right cutting conditions to control cutting vibrations and possible chatter instabilities, but parameters range is limited by cutting temperature and tool wear.

The most detrimental vibrations affecting milling operation is chatter [9]. Chatter is an unstable vibration particularly dangerous because it grows as result of dynamic modulation of chip thickness, leading to unstable variation of cutting force and consequently tool motion, resulting in poor surface finish, increase of tool wear and possible tool breakage.

For this reasons chatter prediction and avoidance are topics of great interest for academic and industry research. Chatter drastically reduces performance of milling process, increasing scraps and additional operation required, resulting in increase of cost for precision manufacturing enterprises. As example automotive sector gives this issue high consideration. Ford Motors Company is promoting chatter avoidance strategies [10] that return an increase of productivity of the manufacturing division. Renault S.A. estimated chatter cost in production, the results of the research are quite impressive: cost due to the unstable phenomenon on cylinder block is estimated 0.35€ per piece, that is significant considering that Renault produced around 3 millions engines a year [11].

Chatter has been thus widely studied and different techniques to predict and detect chatter onset have been developed [12, 13]. Actually most of the machine tool users adopts trial and error experimental tests in order to evaluate a feasible dataset of chatter-free parameters, but this approach has two main disadvantages: the cost of experimental tests is usually high and time consuming, the obtained dataset is able to meet the product specification but is not granted that it would be the optimal one. So simulation of machining process is an economical alternative. The goal of combining high productivity and high workpiece quality can be achieved simulating process behavior in order to identify optimal cutting parameters. A reliable dynamics milling simulation requires accurate machine dynamic behavior and cutting force simulation.

The main output of chatter investigation techniques is a graphic chart showing the stable conditions known as Stability Lobe Diagram (SLD). By means of this graph, optimal cutting parameters can be selected to avoid chatter occurrence and increase MRR of the milling operation. An accurate SLD allows improving drastically milling performances and it is crucial for the competiveness of a modern precision manufacturing industry. However reliability of this chart is still an open issue.

In this work Stability Lobe Diagram identification techniques are analyzed, developed and critically discussed. Both chatter simulation and experimental detection methods are considered. This work aims at improving these methods thanks to a deep analysis of machine tool dynamics, development of dynamics identification techniques, accurate chatter prediction approaches and experimental chatter detection methods. The main goal is to develop simplified and easy-to-use techniques able to provide optimal cutting parameters for chatter-free operations thanks to accurate SLD identification.

1. Thesis structure and goals

This thesis aims at returning useful guidelines and techniques for industrial application of chatter avoidance strategies. Chatter-free cutting parameters can be obtained thanks to Stability Lobe Diagram, but its identification and implementation could be difficult in industrial context. This work tries to improve effectiveness of SLD identification approaches, reducing time-consuming procedures and repetitive experimental tests generally required.

The goal of this thesis is therefore developing simplified and easy-to-use techniques to chatter identification, granting adequate accuracy. Both predictive and experimental approaches are investigated. Predictive approaches compute SLD thanks to process simulation without the need of direct experimental cutting tests in unstable condition. Unfortunately these methods are highly sensitive on input data: machine tool dynamics and cutting force coefficients.

In this work reliability of predictive approaches input data is investigated and improved. Machine tool dynamics is deeply studied since it is the most important parameter for chatter process simulation: is the main responsible of SLD lobes positioning in the spindle speed range, and thus accurate dynamics identification is essential to identify best spindle speed to be exploited in order to maximize MRR.

SLDs are highly influenced by machine tool dynamics, i.e., tool-tip Frequency Response Functions (FRFs). An example is presented in Figure 1.1 to highlight this aspect.

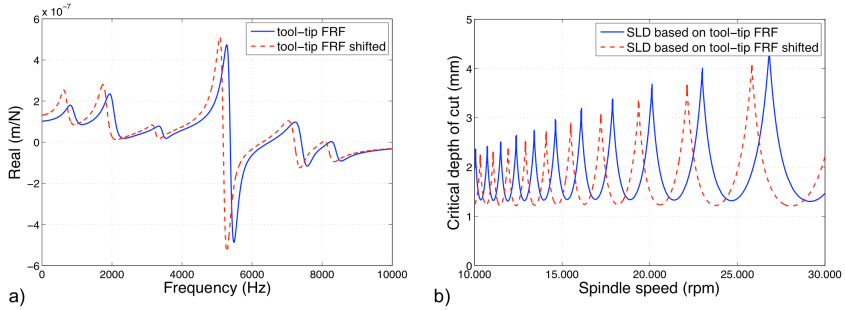

Figure 1.1 Tool-tip FRF influence on Stability Lobe Diagram

Starting from experimental FRF (in solid blue), considered equal in the two directions (x and y), SLD can be calculated (slotting on Aluminum is simulated as example). If an error of 4% on natural frequency is hypothesized on the FRF (dotted red), resulted SLD appears significantly changed. A small error on FRFs identification leads to confuse stable and

unstable zones, reducing the effectiveness of resulted SLD. It is thus essential and goal of this thesis to developed high accurate and reliable FRFs identification techniques. The most reliable technique is Experimental Modal Analysis (EMA): it consists on performing an experimental test on the machine, generally by means of accelerometer and impact hammer. However this technique is not easily implementable in the industrial context, because experimental test has to be repeated for every new tool mounted on the machine: this leads to an increase of production downtime, not affordable by precision manufacturing companies. Different approaches to overcome this issue have been presented in literature. In this work both full numerical and hybrid experimental-numerical approaches are analyzed and new methods proposed in order to improve efficiency and accuracy (Chapter 4-8). Beside machine tool dynamics, a deep analysis of specific cutting force coefficients, studying their reliability at high spindle speed has been carried out: a technique to implement speed-varying coefficients to chatter stability prediction is then proposed (Chapter 9). This part of the work aims at improving predictive approaches reliability and diffusion, identifying the limits of their application.

When prediction is not possible, predictive approaches can be replaced by experimental cutting tests. These are generally time-consuming and hardly applicable to the shop floor. This work aims at improving experimental chatter detection of SLD by a simplified and easy-to-use test, called Spindle Speed Ramp-up test. This developed test, presented in Chapter 10, allows to easily experimentally reconstruct SLD.

This thesis is structured around SLD, its identification and industrial implementation. Contents of thesis is schematized in Figure 1.2.

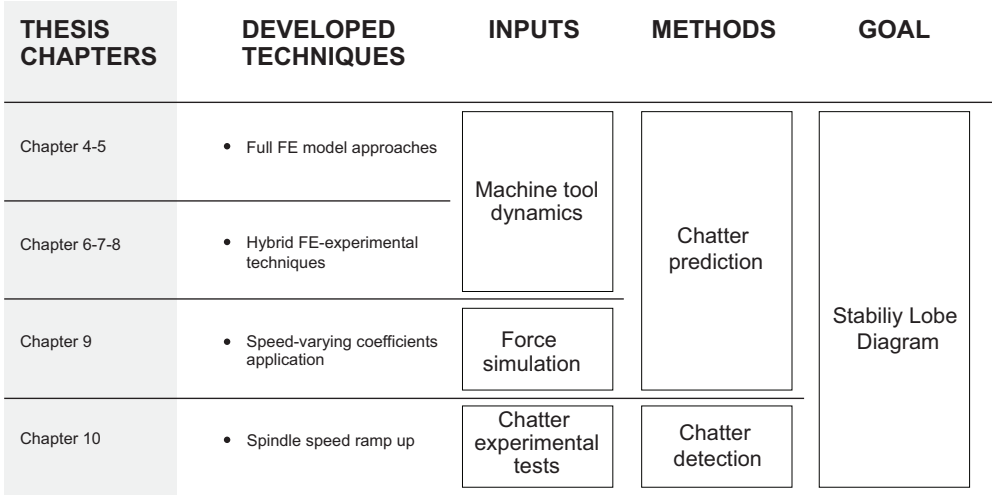

Figure 1.2 Structure of the thesis scheme based on involved topics

According to the scheme the thesis is organized as follow.

In Chapter 2 vibratory phenomena in milling process are summarized and briefly explained to introduce the topic of interest (i.e., chatter and SLD).

Chapter 3 is focused on machine tool dynamics: some experimental results are shown in order to critically present dynamics identification techniques.

In Chapter 4 and Chapter 5 two new machine tool dynamics identification methods by means of full FE model are presented, while Chapter 6, 7, and 8 are focused on hybrid FE-

experimental techniques: toolkit modeling is investigated (Chapter 6), holder-tool connection modeling techniques are proposed (Chapter 7), analytical coupling formulations are discussed and applied to build a simplified machine tool FE model (Chapter 8). In Chapter 9 Stability Lobe Diagram prediction theory is adapted using speed-varying cutting force coefficients.

Finally Chapter 10 is about chatter experimental detection: the new Spindle Speed Ramp-up test is presented.

2. Vibrations in milling

Machine tool vibrations affect milling operation, playing an important role in precision manufacturing. Detrimental vibrations accelerate tool wear, cause poor surface finish and may damage tool and spindle bearings. Cutting parameters (speed, feed and depth of cut) have to be controlled in order to achieve a reduction in the vibrations level [14].

Three are the main types of vibrations in milling [12]:

- Random or free-vibrations, e.g., machine tool oscillating at its natural frequency after a strike. This vibration effect is often neglected;
- Forced vibrations, caused by excitation forces (e.g., cutting forces);
- Self-excited vibrations (known as chatter vibration), regenerative unstable vibration caused by phase difference of subsequent tooth passing on chip thickness.

2.1. Forced vibration

Forced vibrations are produced by periodic excitation forces: spindle imbalance, tool run-out, periodic cutting forces generated by tooth entry in the workpiece. The machine system will vibrate according to the excitation force frequency content. These excitation forces can be amplified through the structure of the machine when a resonance frequency of the structure is excited. This kind of vibration can be reduced changing exciting frequency so that is not close to the natural frequency of the system [15] or by means of active or passive damping system [14].

In milling forced vibrations are mainly caused by cutting forces that are inherently periodic, characterized by tooth pass frequency and its harmonics that can be calculated by equation (**2.1**):

$$f_{tp} = \frac{n \cdot Z}{60} \tag{2.1}$$

where f_{tp} is tooth pass frequency, n spindle speed, Z number of flutes. In Figure 2.1 cutting forces frequency spectra are presented as example (n=2500 rpm, Z=2) [16].

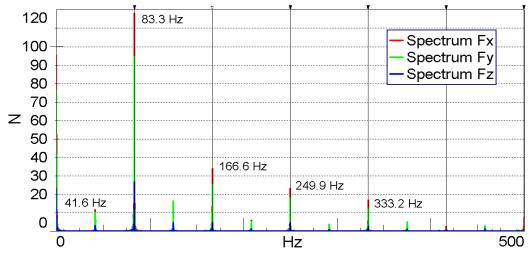

Figure 2.1 Cutting forces frequency spectra [16]

Direct measurement of tool forced vibrations is not an easy task due to the cutting process interaction. This type of vibrations is generally studied investigating frequency content of cutting forces and machine tool dynamics, i.e., tool-tip FRF. Tool vibrations are the result of cutting forces amplified by dynamics: consequently tool motion under cutting force effect can be obtained indirectly by multiplying measured cutting forces with measured flexibility of the tool. Once tool motion is identified, surface finish can be predicted thanks to a surfaced generation model based on tool path, as the one presented in [17]. Particularly prediction of errors in respect of nominal surface, known as Surface Location Error (SLE), and surface roughness is generally investigated [18]. An example of measured and predicted SLE is presented in Figure 2.2 [17].

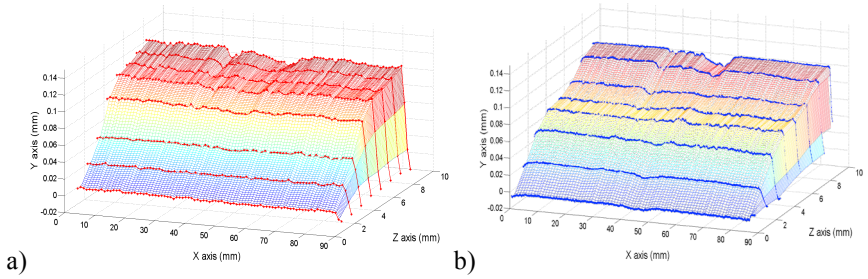

Figure 2.2 SLE predicted (a) and measured (b) [17]

2.2. Self-excited vibration

Chatter is one of the main limiting factors to machining performance, deeply studied in academic and industrial field since 1961 when Tobias [19] defined it. However after few decades of studies chatter is still an open issue because of difficulties in modeling, prediction and detection of this instability. It is not surprising that Taylor in 1907 [20] stated that chatter is the “most obscure and delicate of all problems facing the machinist”.

Despite many different classification [12, 19], generally the term chatter is used to identify the regenerative unstable phenomenon affecting machining process that occurs due to overlapping cuts. The cutter vibrations leave a wavy surface, when milling the next tooth in cut attacks this wavy surface and generates a new wavy surface. The chip thickness and, hence, the force on the cutting tool vary due to the phase difference between the wave left by the previous teeth and the wave left by the current ones (Figure 2.3).

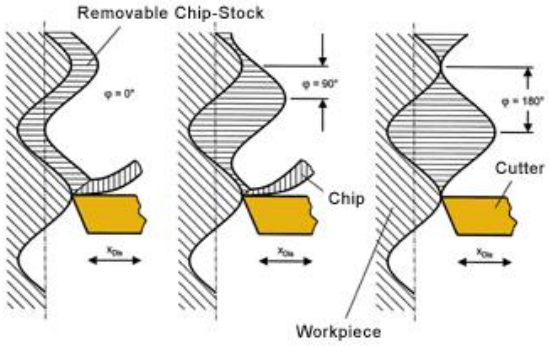

Figure 2.3 Effect of phase of subsequent tooth pass on chip thickness [21]

This phenomenon can greatly amplify vibrations, become dominant and build up chatter [12]. This happens at some critical depth of cut in which the static cutting forces become so large, that even a small transient force can provoke this self-excitation mechanics. Forces then grow over a period of time generating a variation in the chip thickness, which results in further varying cutting forces. If the phase between previous cut and current cut is 180°, the varying cutting forces can grow and oscillate at the chatter frequency (close to the resonant frequency of excited mode of the structure).

2.2.1. Chatter prediction in milling

Graphic chart showing the stable conditions known as Stability Lobe Diagram (SLD) is the most common result of chatter analysis. This diagram is used to select optimal operating conditions (i.e., cutting parameters) in order to avoid chatter. SLD represents the borderline between a stable cut (i.e., no chatter) and an unstable cut (i.e., with chatter) visualized in terms of the axial depth-of cut as a function of the spindle speed (Figure 2.4). SLD is then divided in two zones: stable region and unstable region. If the couple spindle speed-depth of cut is located in the unstable zone, chatter will occur: thanks to this diagram, during cutting parameters definition, it is possible to select a couple spindle speed-depth of cut to maximize MRR.

Analyzing the diagram three key features can be identified: depth of cut limit, lobes and process damping. Depth of cut limit represents the minimum depth of cut below which cutting operation is stable at every spindle speed. Lobes are the characteristic shape of the diagram: lobbing effect of SLD can be exploited to achieve high productivity once the right spindle speed is selected. However at low speed lobes are narrow and exploitation of diagram is limited only to depth of cut limit. Lastly, process damping is a stabilizing effect that occurs at low spindle speeds and provides stability. This effect is due to the short undulations left on the part's surface by high-frequency vibrations. These surface waves interfere with the cutting tool flank face and dampen the cutting tool vibration.

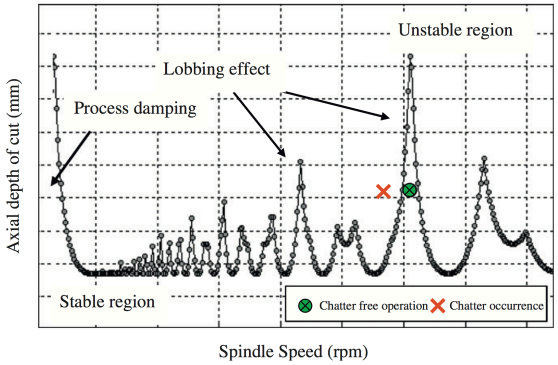

Figure 2.4 Stability Lobe Diagram [12]

In the last decades chatter has been widely investigated and different predictive methods have been developed, summarized in [12, 13]. Basic theory of dynamics model was introduced by Tlusty and Polacek [22], and Tobias and Fiswick [23] studying one-dimensional chatter for orthogonal operation. By means of simplified chip thickness formulation and a linear cutting model, it is possible to obtain the dynamic cutting equation (delayed differential equation) solved by the transfer function:

$$\frac{h(s)}{h_0(s)} = \frac{1}{1 + (1 - e^{-sT})K_r a \Phi(s)} \tag{2.2}$$

where h is the chip thickness, T is the spindle period, K_r cutting force coefficient, a depth of cut and Φ tool-tip FRF. Characteristic equation of (**2.2**) returns chatter stability condition that the following absolute chatter stability laws for orthogonal cutting:

$$a_{lim} = \frac{-1}{2K_r G(\omega)} \tag{2.3}$$

$$\psi = tan^{-1}\frac{H(\omega)}{G(\omega)}, \varepsilon = 3\pi + 2\psi \tag{2.4}$$

$$T = \frac{2k\pi + \varepsilon}{2\pi f_c} \rightarrow n = \frac{60}{NT} \tag{2.5}$$

where G and H are the real and imaginary part of the FRF. Scanning possible chatter frequencies on the FRF, these formulations allow to identify SLD as schematized in Figure 2.5.

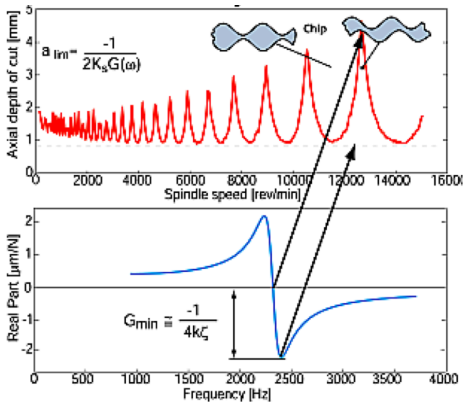

Figure 2.5 Stability Lobe Diagram in orthogonal cutting [13]

This theory provides fundamental understanding of dynamic cutting and chatter stability lobes, however milling operation cannot be accurately modeled as an orthogonal cutting. Multiple teeth rotating tool, periodical cutting forces, different chip-load direction, and multi-degree-of freedom structural dynamics characterize milling cutting process compared to orthogonal cutting mechanism. Advance models are hence required, and different techniques have been developed [13, 24-26]. Even if literature counts several complex and accurate predictive models generally based on time domain simulations [24], the most widely used method still refers to zero-order analytical approach proposed by Altintas [25] because its simplicity and efficient SLD evaluation. Milling tool can be modeled as a two degree of freedom, as shown in Figure 2.6.

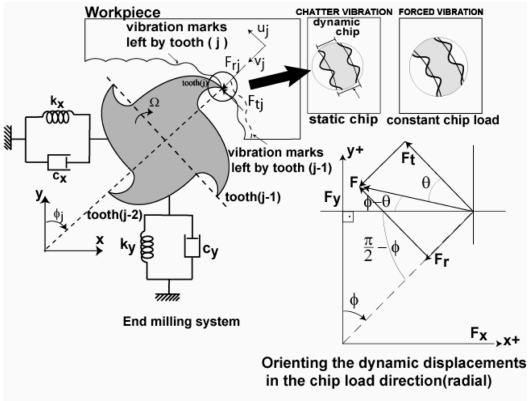

Figure 2.6 Milling process dynamics scheme [13]

According to this theory, chatter stability conditions can be calculated by solving the equation (2.6):

$$\det\left[[I]-\frac{1}{2}K_{tc}a(1-e^{-i\omega_c T})[A_0(K_r)][\Phi(i\omega_c)]\right]=0 \tag{2.6}$$

where $\Lambda = \Lambda_R + i\Lambda_I = -\frac{1}{4\pi} N_t K_{tc} a (1 - e^{-i\omega_c T})$ (2.7)

is the eigenvalue of the characteristic equation, Λ_R and Λ_I are its real and imaginary parts; N_t is the number of teeth on the cutter; K_t is the cutting force coefficient of the material being cut; a is the axial depth of cut; ω_c is the chatter frequency; T is the tooth passing period; Φ is the directional FRFs matrix and A_0 is the directional cutting coefficient matrix. A_0 is dependent on K_r, relative coefficient, defined as:

$$K_r = \frac{K_{rc}}{K_{tc}} \tag{2.8}$$

The limiting depth of cut, described by the parameters in Eq. (2.6), may be analytically determined as [25]:

$$a_{\lim} = -\frac{2\pi\Lambda_R}{N_t K_{tc}} \left[1 + \left(\frac{\Lambda_I}{\Lambda_R} \right)^2 \right] \tag{2.9}$$

The details of evaluating stability charts can be found in reference [25].
Accordingly, despite the differences, every process model requires two main inputs (as Tlusty and Altintas theories suggest):

- Machine tool dynamics, i.e., tool-tip FRF (Φ in the equations (**2**.**2**) and (2.6));
- Coefficients for cutting forces prediction (basically K_{rc} and K_{tc}).

As presented in the theory, tool-tip dynamics governs lobes position and depth of cut limit. Stability is influenced basically by dominant modes: natural frequency shift returns a shift in the lobes and modal damping returns an increase of depth of cut limit (Figure 2.5). On the other hand cutting force coefficients are mainly accountable of depth of cut limit: higher values of the coefficients (i.e., in case of hard-to-machine material) results in a lower stable limit depth of cut.

Thus, once the frequency response functions (FRFs) of the machine tool system are identified, and coefficients for specific cutter and workpiece material obtained, the SLD can be calculated for a specific cutting operation, allowing the workshop operator to select the right combinations of axial depth-of-cut and spindle speed that ensure chatter-free operations.

A significant part of this work is focused on reliability of these data entries that strongly affected SLD prediction. Considering that this work does not aim at developing new chatter stability methods, in order to present results, the widespread zero-order analytical approach [25], briefly presented here, will be adopted.

3. Machine tool dynamics

Machine tool dynamics knowledge is essential to perform accurate milling process simulation with the goal of identifying vibrations phenomena. With respect to other structures or components, machine tool dynamics investigation can be restricted: main forces (i.e., cutting forces) are applied on a single zone (end of the tool) and motion of that point is generally sufficient to perform accurate simulation of the process. Therefore analysis is focused on tool-tip dynamic behavior, i.e., its driving point Frequency Response Functions (FRFs).

Such system response is obtained mainly by experimental test directly on the machine tool. This technique, known as Experimental Modal Analysis (EMA), is generally performed by means of impact testing: tool-tip is equipped with an accelerometer, and instrumental hammer is used to apply impulsive force, exciting a wide frequency range (Figure 3.1). A more comprehensive explanation is given in section 6.4.2.

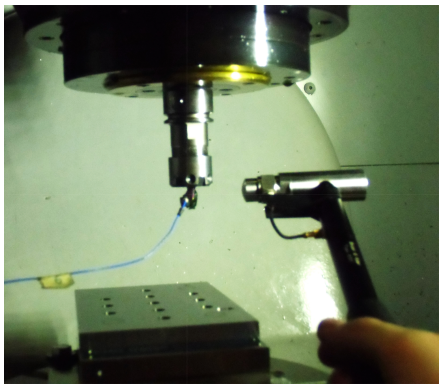

Figure 3.1 Experimental Modal Analysis set-up

Although measurement set up is easy to implement, this method is time consuming since machine tool dynamics is strongly dependent on milling tool and could be influenced by axis position and rotation. This aspect will be clarified and highlighted in the next sections thanks to some preliminary tests, fundamental to define scope and area of applicability of developed modeling techniques.

3.1. Toolkit dependent dynamics

Machine dynamics may change significantly with a new tool clamped to the spindle, because tool is generally the most flexible part of the assembly and more apt to vibration. Experimental measurements have been performed on a five-axis machine tool (FAGIMA JAZZ 5Ax), equipped with HSK63 spindle.

Different toolkits (holder and tool) characterized by different connection systems and overhangs, summarized in Table 3.1 and presented in Figure 3.2, have been tested.

Table 3.1 Toolkit dimensions and characteristics

N°	Spindle Taper	Holder Joint	Holder length (mm)	Shank overhang (mm)	Tool Diameter (mm)	N° flutes
1	HSK63	Hydraulic	90	24.5	12	4
2	HSK63	Hydraulic	170	42	16	4
3	HSK63	Hydraulic	170	82	16	4
4	HSK63	Shrink Fit	160	24.5	12	4
5	HSK63	Shrink Fit	160	84	12	4
6	HSK63	Shrink Fit	90	24.5	12	4
7	HSK63	Hydraulic	170	84	12	4
8	HSK63	Hydraulic	170	24.5	12	4
9	HSK63	Hydraulic	200	120	12	4
10	HSK63	Hydraulic	90	84	12	4

Figure 3.2 Tested toolkits

Experimental Modal Analysis has been performed by impact testing with Brüel & Kjær type-8202 impact hammer equipped with a hard tip. In order to minimize noise and leakage errors, suitable trigger level and windowing were set up: a force window for input and an exponential window for output have been chosen. Data were collected by LMS SCADAS III acquisition system, considering a measurements bandwidth of 8192 Hz with 1 Hz resolution. Mono-axial PCB 352C22 accelerometers, with a nominal mass of 0.4 grams, have been mounted on the machine tool.

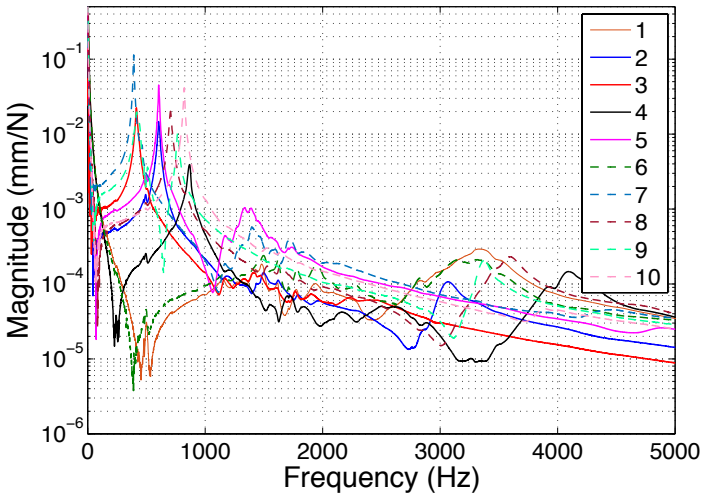

Figure 3.3 Tool-tip FRFs of different toolkits clamped on machine

Figure 3.3 clarifies that machine tool dynamics is drastically influenced by toolkit, e.g., the same tool composes toolkit 4 and 6 that are only different for the holder, however machine tool dynamics significantly changes. This influence is evident and already highlighted in literature [6, 27] considering that toolkit is generally the most flexible part of the machine. When a new tool is mounted a new experimental test should be performed. Any modeling technique must consider toolkit change in order to accurately model dynamic behavior.

3.2. Position and orientation dependent dynamics

Machine tool dynamics is strictly related to the configuration of the machine itself. Machine tool market offers a wide variety of milling machine structures for various applications: e.g., small-medium machine for HSM with Box-in-Box construction, large bridge type machine, gantry type machine equipped with gimbal head. In this section some experimental investigations carried out on different types of machine are described: three different machines have been selected in order to present different dynamic behavior changing with position and orientation. Investigated machine tools are:

- 5-axis Mori Seiki NMV1500 DCG, loaned by Machine Tools Research Foundation (MTTRF) to Machine Tool Research Lab. (MTRL) of University of Firenze;
- Three axis FADAL2216, located at the Machine Automation Laboratory (MAL) of University of British Columbia [28];
- Mill-Turn MORI SEIKI NT-3150 DCG, located at the Machine Automation Laboratory (MAL) of University of British Columbia.

3.2.1. Mori Seiki NMV 1500 DCG

Mori Seiki NMV1500 DCG is a 5-axis milling machine equipped with high-speed spindle. Its Box-in-Box structure is suitable for HSM. Machine and structure is presented in Figure 3.4.

Figure 3.4 Mori Seiki NMV 1500

Tool-tip FRFs responses have been measured at different positions on the workspace with only a tool-holder (HSK32) clamped on the machine. Impact testing has been performed by means of Brüel & Kjær type-8202 impact hammer and mono-axial PCB 352C22 accelerometer. Test setup is reported in Figure 3.5.

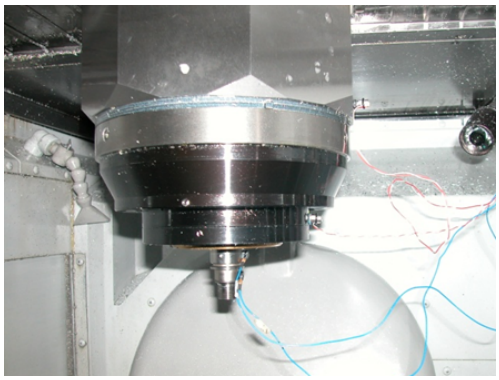

Figure 3.5 Experimental set-up

Analyzed positions in the workspace in the machine tool coordinate system are reported in Table 3.2 and FRFs resulted are presented in Figure 3.6.

Table 3.2 Axis position for FRFs evaluation on Mori Seiki NMV 1500 DCG machine

Axis position – Machine Tool coordinate system								
X axis	240	240	240	240	0	0	420	-240
Y axis	-100	-100	-210	-210	0	210	-210	-210
Z axis	-315	0	0	-175	-175	-400	-400	-340

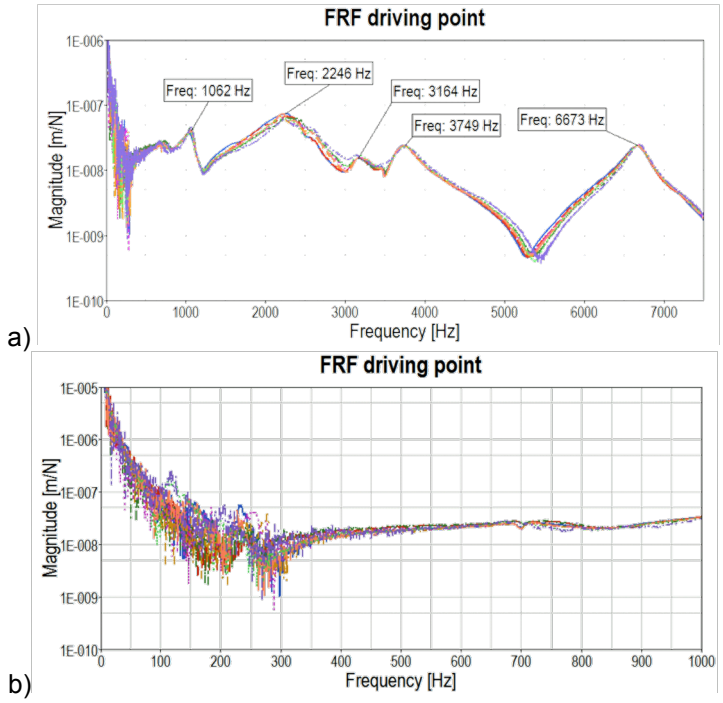

Figure 3.6 Driving point FRFs of Mori Seiki NMV 1500 DCG (a), low frequency zoom (b)

Experimental tests have proven that in this type of machine the FRFs at the tool-tip are only slightly dependent by the axis position within the machine workspace. This means that the FRFs of the machine at the tool tip are nearly independent by the structural machine dynamics but depend only on the dynamic characteristic of the spindle and tool-tool holder assembly. In particular, frequency range can be split in two regions:

- High frequency dynamics (> 400 Hz) is independent on position and it is characterized by all the dominant modes (related to spindle-holder-tool assembly);
- Low frequency dynamics is position dependent (Figure 3.6b) and not dominant

3.2.2. **FADAL 2216**

FADAL 2216 is a vertical three-axis machine tool. Figure 3.7 shows the machine and FRFs results in different position presented in [28].

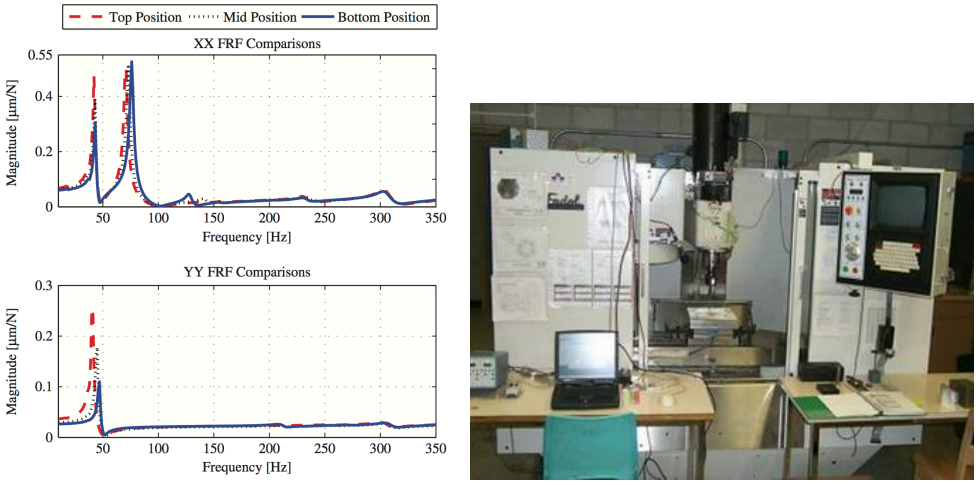

Figure 3.7 FRFs and picture of FADAL 2216 machine

Authors in [28] state that, for this machine, dominant modes are related to the structure and they change in amplitude and frequency with position. It is thus required to consider the structure and its change with axis position to achieve an accurate dynamic simulation.

3.2.3. **Mori Seiki NT 3150 DCG**

Even with rotation position dominant modes could change, this is highlighted analyzing results for Mill-Turn Mori Seiki NT3150 DCG. The machine is equipped with two spindles, one for turning operation and one for milling on the rotating turret. Dynamic behavior investigation has been carried out focusing on turret rotation. Machine picture and structure scheme are presented in Figure 3.8.

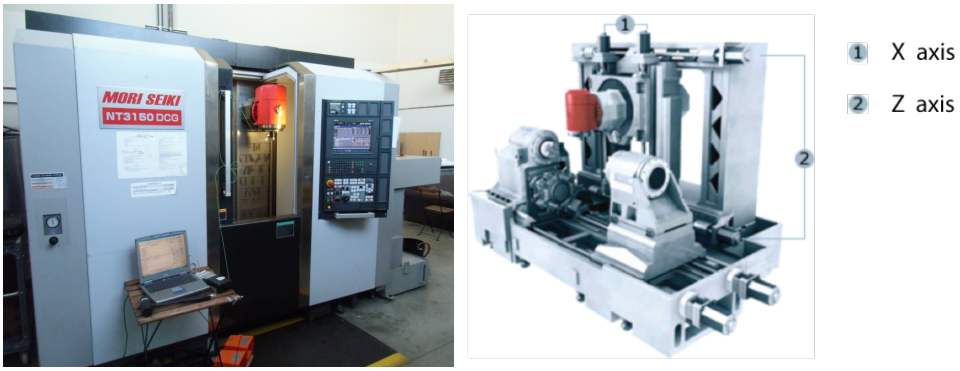

Figure 3.8 Mori Seiki NT3150 DCG

A Sandvik CoroGrip chunk C5-391.HMD-25 078 tool-holder has been connected to the spindle, without tool. In the experimental modal testing, a PCB 086C41 impulse hammer, a PCB 353B31 mono-axial accelerometer and CutPro 10 software for signal acquisition and processing have been used. Different rotation positions have been tested in the machine coordinate system zero position. Measurements have been performed in order to identify the FRFs need for chatter stability prediction, i.e., both normal directions to the spindle as shown in Figure 3.9 (one is Y direction on the machine coordinate system and the other is changing respect to the machine system, remaining normal to the spindle, called T in the figures).

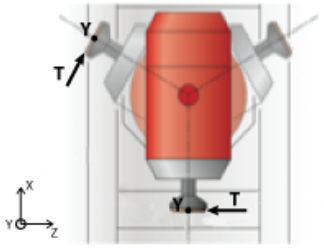

Figure 3.9 FRFs directions scheme

FRFs results are shown in Figure 3.10.

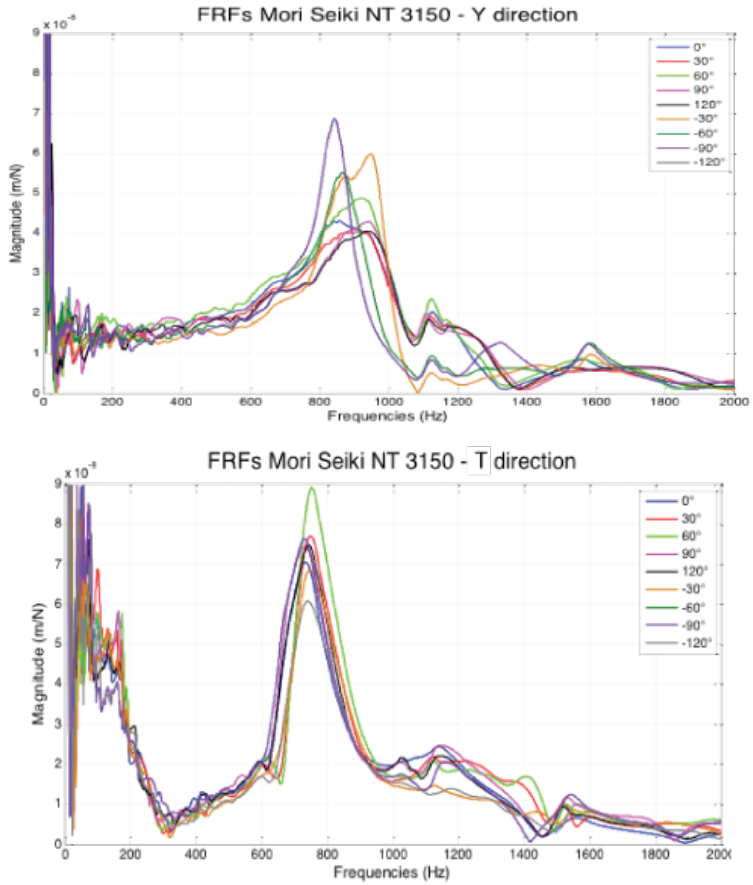

Figure 3.10 FRFs normal to spindle direction on Mori Seiki NT3150 DCG

Results show a dependency of FRF on rotation, particularly:

- On Y direction FRFs are different in the entire frequency range
- FRFs on T direction are different in the low frequency range but are quite similar at high frequency.

Rotation dependency can be highlighted isolating two orientation positions: 0° and -90° (Figure 3.11).

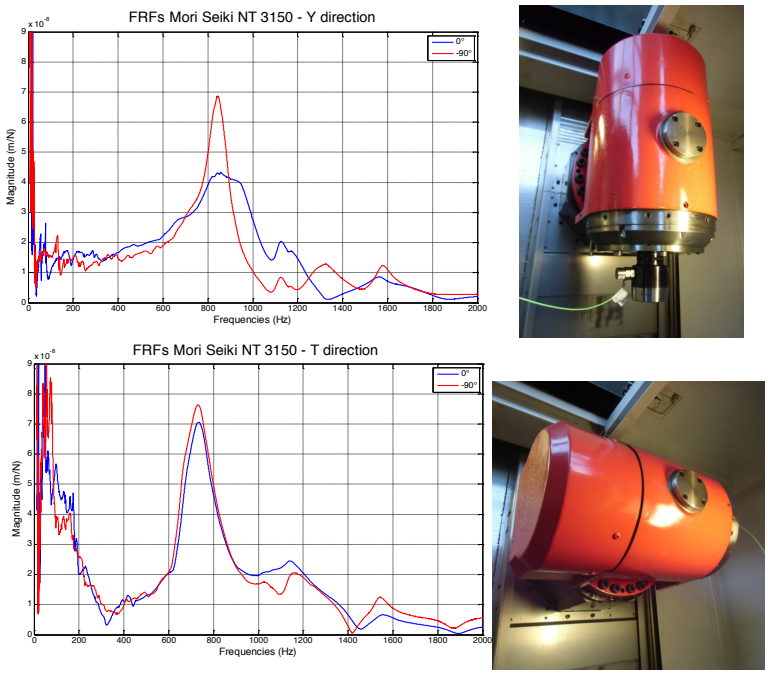

Figure 3.11 FRFs for two orientation positions: 0° and -90°

Depending on the structure, machine tool dynamics could change with position and orientation.

3.3. Machine tool dynamics identification methods

Presented results and research literature show how machine tool dynamics could change varying working configurations: i.e., different toolkits, position and orientation in the workspace. While toolkit always significantly influences machine tool dynamics, position and orientation dynamics influence depend on machine tool structure and work area. For some machine tools (e.g., Mori Seiki NMV 1500 DCG) this dependency is not dominant and affects only lower frequency range: in this case machine tool dynamics is influenced mainly by spindle-holder-tool assembly.

Experimental approach, i.e., EMA, to identify machine tool dynamics should be repeated every time these conditions (i.e., toolkits and eventually position) are modified, resulting in a costly and time-consuming procedure. To make simulation process feasible in an industrial context it is crucial to develop fast tool-tip dynamics identification procedures, to reduce production downtimes.

Therefore Finite Element (FE) simulations have been introduced to avoid repeated experimental characterizations. FE model of the entire machine tool, including all the components and substructures, allows simulating machine tool dynamics in every configuration (position and rotation) and toolkit set-up. Otherwise, despite modern commercial FE software solutions provide several instruments to model complex system, a FE analysis of complete machine tool structure can be troublesome and involve high pre-process and analysis time, because of the complexity of the modeled structures.

Moreover building an accurate FE model of the machine tool is still a time-consuming operation: experimental validation and tuning is unavoidable to reach high-accurate FE model due mainly to joints modeling procedure. Therefore depending on application and required accuracy this kind of modeling approach can be effectively replaced by hybrid experimental-numerical techniques, that reduce pre-processing modeling phase exploiting experimental tests. The basic idea of hybrid techniques is coupling FE model and experimental ones. Finite Element Method (FEM) can be used for tool and workpiece modeling, since as earlier mentioned these are the variable components in machine tool structure, while the milling structure can be experimentally identified. The models can then be connected with proper techniques to identify assembled structure dynamics. It is hence possible to consider toolkit change quickly without the need of a new experimental test or a full FE model of the machine. Combining a FE analysis of a small part of machine tool structure with an experimental model of the most complex substructure allows overcoming the disadvantages of both fully experimental and FE approaches. It is clear how these techniques could be efficiently adopted in case that dynamics is not influenced significantly by position: only one measurement set up for the single machine tool is required. On the other hand when position affects dynamics these techniques are less efficient, considering that more measurements should be repeated in order to predict machine behavior changing with position.

In conclusion, taking into account these consideration, in this work machine tool dynamics prediction methods will be divided in:

- Full FE model techniques
- Hybrid experimental-numeric approaches.

Full FE model is required if position dependent dynamics must be considered. In this case methods to reduce computational time and remove pre-processing phase have been developed and presented in Chapter 3 and 4.

On the other hand hybrid techniques are interesting approaches in order to evaluate machine tool dynamics when position dependency is not significant. Particularly in case of machine tool behavior such as the one presented for the Mori Seiki NMV 1500 DCG, tool-tip FRFs obtained by this kind of approach can be effectively used for:

- Chatter stability prediction, since dominant modes are due to spindle-holder-tool assembly and chatter stability is basically driven by dominant dynamics (Chapter 1.2);
- HSM forced vibrations simulation, since at high speed frequency content of forces is characterized by high frequency harmonics that are not influenced by axis positions (Chapter 1.1).

This work, focused on High Speed Milling, will examine extensively this kind of approaches. Two are the common requirements that affect accuracy of hybrid approaches (presented in Chapter 8):

- Toolkit modeling: identification of dynamics of each substructure and joints connecting them is critical;
- Experimental response of the machine: the main issue is the identification of moments and rotational deformations that are hard to directly measure.

Toolkit modeling techniques will be deeply analyzed in Chapter 6 and 7. Improved analytical formulations to overcome rotational identification issue will be explained in Chapter 8, developing a coupling approach to build a simplified FE model of milling machine.

4. Position dependent dynamics

FE models of entire machine can be very effective to evaluate structural modification in design stage [29] or to identify dynamics of process-machine interaction. However analyses of such models is computational costly, considering the high number of degrees of freedom (DOFs) required. These cumbersome models have to be used when simplification strategies cannot be applied: this is the case of machine tool dynamics significantly influenced by tool position and orientation in the workspace. The FE model of the entire machine tool can predict position-dependent dynamics, but tool-tip FRFs should be simulated separately for each position, resulting in:

- increase of computational time: response analysis of full machine models is computational costly (machine tool model is generally characterized by 1,000,000 DOFs or more [28]);
- increase of pre-processing time: connection between different substructures should be re-designed.

Substructures of a machine are generally modeled separately resulting in dissimilar mesh when coupling. Ensuring mesh compatibility during synthesis for such models, which are simultaneously in contact over multiple nodes, requires qualified operator to introduce connection strategies, and this has to be modified for position to be analyzed, increasing pre-processing time. Despite advanced modeling technique are nowadays used in many fields of engineering, machine tool modeling strategies have not been extensively investigated. Co-simulation in which FE solver is coupled to multi-body simulation code has been adopted, but these models have been mainly developed for rigid body motion analysis [30], only few attempts with flexible bodies have proposed [2, 31, 32].

In the last years few methods and investigations on machine tool model issues have been carried out, the main goal of these techniques is to create efficient and effective tool to simulate position-dependent dynamics. One of the most comprehensive works has been presented by Law in his Ph.D. thesis [33]. The basic idea (firstly proposed by Fonseca [34]) is to build FE models of the different substructures of machine tools, perform a modal reduction on them and then, for each position, perform coupling between substructures. Therefore Law's approach is basically composed by two stages:

- Reduction: machine tool substructures are modal reduced (to do once for a single machine);
- Synthesis: coupling stage between the reduced substructures in the selected position in workspace (to repeat for each position of interest).

FE models of the main substructures of the considered machine tool are reduced during the first phase by means of an improved modal reduction that result to be more accurate compared to the traditional Craig-Bampton modal reduction [35]. The second stage, synthesis, consists in coupling substructures by Multi-Point Constraint (MPC) equations, in order to simplify the connection between the coupled substructures and make easy coupling reduced models when substructures position changes, also for component with dissimilar mesh (e.g. different mesh resolution). Surface interaction is approximate by a virtual condensation node for each of the interface surfaces, as shown in Figure 4.1, and then enforcing displacement compatibility between these virtual nodes as:

$$u_C^{(1)} - u_C^{(2)} = 0 \tag{4.1}$$

where $u_c^{(1)}$ and $u_c^{(2)}$ are the displacements of the two condensation nodes.

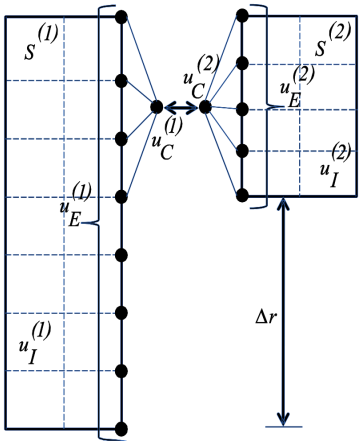

Figure 4.1 Substructures synthesis in Law's method [33]

Each condensed node is then connected with the surfaces by means of MPC equations. Different connection types have been evaluated in order to obtain the same dynamic behavior of the full FE model: interpolated MPC underestimates model connection while a rigid MPC overestimates [28]. The best approach seems to be an interpolated MPC, even because this choice makes the linear system to be resolved more efficient (less number of constrain equations).

The main advantage of this comprehensive technique is to simulate quickly multi-position dynamics and create a workspace map of dynamics and stability of machine. This approach has been applied effectively to two different machine tools: three-axis machine (FADAL 2216) [28] and serial-parallel kinematic machine [36]. In Figure 4.2 results for the cases are presented.

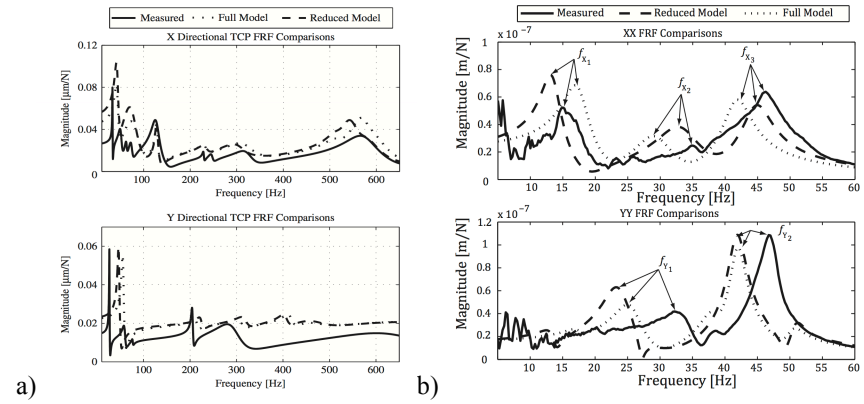

Figure 4.2 Measured tool-tip FRF compared to Full FE model and Reduced Model for FADAL machine [28] (a) serial-parallel [36] (b)

Figure 4.2 shows discrepancies between full FE model and experimental results due to issues in the validation procedure, however this cannot be attributed to the proposed technique. On the contrary it is interesting to point out that there are significant errors even between full FE model results and the ones obtained by Law's approach (Reduced model in Figure 4.2). These errors are ascribable to the method and it is quite odd to obtain such results in a numeric-numeric comparison, even after reduction phases. The reason is in the synthesis phase: MPC formulation proposed by Law is very easy to implement, but too simple to accurately model mesh surface connection. Condensing interface connection in a single node simplifies algorithm and procedure but approximates the dynamic behavior: introduced errors increase when interface surfaces become larger. These errors are acceptable in early design stage: in this phase there are a lot of uncertainties, first of all experimental and model agreement. On the contrary they can be unsatisfactory in other stages when a full-validated model is used. Moreover advanced commercial FE software solutions are able to carry out reduction phase and synthesize phase thanks to internal features. It is then possible to develop similar approach entirely in FE environment in order to reach higher reliability and accuracy.

In this section a fully FE approach developed by means of MSC Nastran® has been proposed, in order to improve existing methods and hence achieve efficiently and accurately tool-tip FRF simulation changing with position. Results obtained by proposed approach have been compared with full FE model and Law's method [28] on different test cases in order to prove new method capabilities.

4.1. Proposed method

Proposed method aims at developing a quick and easy-to-use procedure to identify tool-tip FRFs in different position on the workspace based on the FE model of entire machine tool. Basically the same idea presented by Law [33] has been developed in full FE environment by means of MSC Nastran® features, in order to overcome the main limitation of the method, improving accuracy of predicted dynamics.

Two main Nastran features have been used: reduction is performed creating reduced component called "superelement" in Nastran, and coupling is carried out by means of double

sided linear contact called “glued contact”. In reduction Nastran applies Craig-Bampton theory [35]: a component (FE model) is reduced to a small number of nodes of interest creating a superelement, that is characterized practically by the same dynamic behavior of the full FE model but a lower number of DOFs (i.e., lower computational time). Superelements are assembled using glued contact, double sided linear contact algorithm that permits to join components having dissimilar meshes [37].

Proposed method inputs are:

- FE models of all the substructures. The machine tool should be divided in the moving substructures required;
- Nodes to which reduce the substructures. In order to improve computational efficiency each substructure is reduced to only the required nodes: interface nodes and nodes of interest (e.g., tool-tip);
- Models of the surface in contact. Interface is required to perform connection routine (glued contact).

A demonstrator of the method has been developed in Matlab® used to manage process and write Nastran files to be launched. Based on these information the algorithm is able to compute efficiently tool-tip FRF in different configurations. Scheme of proposed approach is presented in Figure 4.3.

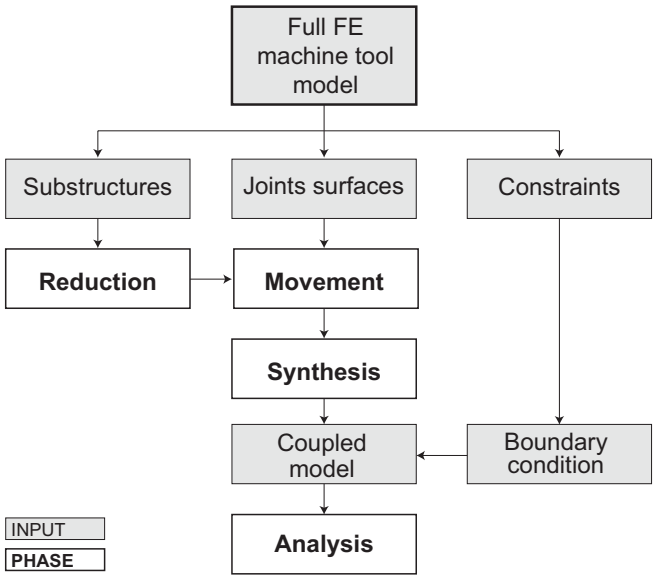

Figure 4.3 Proposed approach scheme

Algorithm procedure is composed by four stages: reduction, movement, synthesis and analysis. These stages are summarized below thanks to a description and a figure based on a simple slide example.

1. Reduction. A first reduction phase is performed in Nastran for each substructure: components are reduced to the selected nodes. Reduced model matrices and nodes called "superelement" are stored in external files. This stage is carried out only one time for each machine tool and each substructure. In Figure 4.4 a scheme is shown.

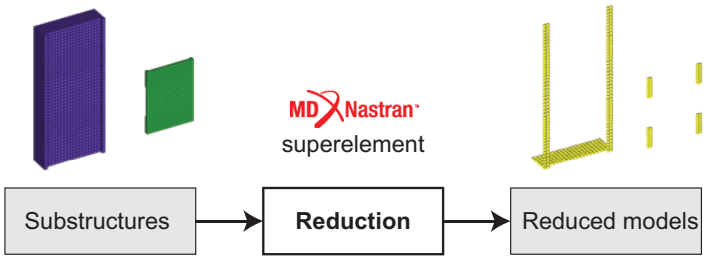

Figure 4.4 Reduction stage scheme

This phase does not present relevant differences compared to Law's method [28], except for working in FE environment that allows easily handling full and reduced substructures matrices.

2. Movement. Superelements can be moved and rotated in any different position, according to the new position of the tool tip investigated. In Figure 4.5 a scheme of movement phase is shown.

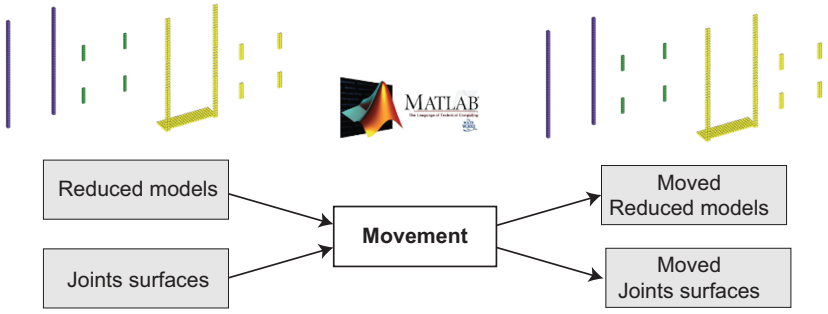

Figure 4.5 Movement stage scheme

3. Synthesis is performed by Nastran "glued contact". With glued contact it is possible to connect different FE components without the need of mesh compatibility. This Nastran feature creates coefficients for mathematical formulation (Multi-Point Constraints - MPC) to connect surfaces nodes. In the method presented, MPC are written in an external file to be used later in the analysis. In Figure 4.6 synthesis stage is summarized.

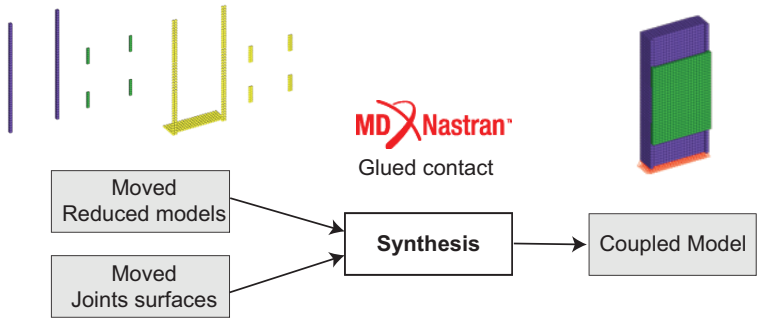

Figure 4.6 Synthesis stage scheme

Glued contact feature is more complex than synthesis strategy adopted in [28]. Interface surfaces nodes are rigidly connected directly, without the adoption of condensed node, according to equation (4.2), valid for each node.

$$u_s = u_m + \alpha_m \wedge r_{s-m} \tag{4.2}$$

where u_s is the displacement of node on one surface (called SLAVE in Nastran), u_m and α_m are the displacement and rotation of node on the other surface (called MASTER in Nastran), and r_{s-m} is the vector from slave to master nodes. These specific formulations are calculated for all the nodes and combined in MPC general equation (4.3).

$$\sum A_j u_j = 0 \tag{4.3}$$

where A_j and u_j are the weight factor and the displacement for the j node. Weight factors (value from 0 to 1) are calculated based on the distance between connected nodes: if connecting nodes are close, value is high, decreasing with the distance and becoming zero when the distance is too high. Thanks to this connection strategy only close nodes between interface surfaces are connected. In Figure 4.7 a scheme is reported as example.

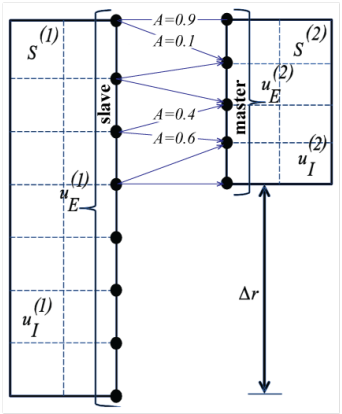

Figure 4.7 Substructures synthesis with glued contact

In case of compatible mesh, glued method returns the same connection configuration obtainable merging surface nodes; on the other hand in case of dissimilar mesh, it reproduces merging surface thanks to a selective, dedicated nodes connection strategy. This procedure is more complex than Law's approach, but generally returns more accurate results.

4. Analysis. Once all the elements are placed in the right position and MPC are created, all these data are used in the launch to perform the required analysis (e.g., modal or FRF) by means of Nastran.

When a new position has to be investigated, new movement and synthesis stages are repeated and analysis is performed, achieving a reduction of time for pre-processing and analysis. Method allows considering any kind of FE model (1D, 2D, 3D), any motion of the parts (translation and rotation) and any size of the FE model (any type of machine tool or other moving structures). Validation test performed on case study proves method efficiency and accuracy: comparison of proposed method results with Law's approach and time-consuming full FE model is provided in the next section.

4.1.1. Results for a machine tool architecture

Proposed approach has been tested on simple machine tool architecture. The case study assembly is composed by column and spindle housing of FADAL 2216 machine tool used in [28] (Figure 4.8a).

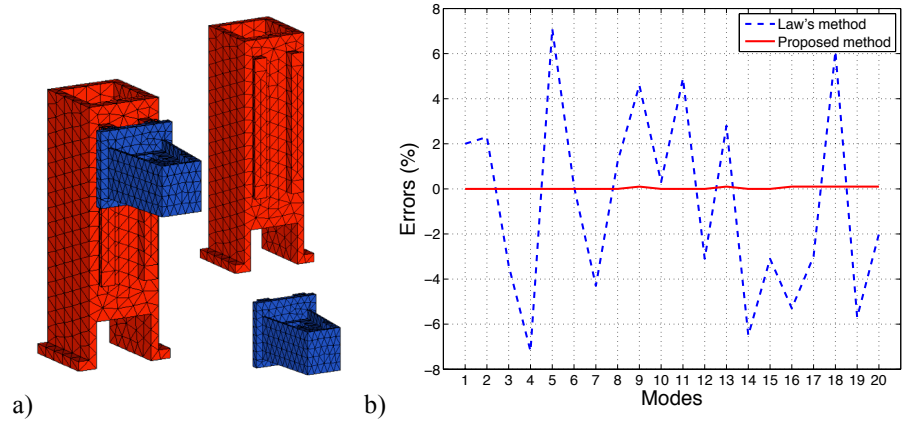

a) b)

Figure 4.8 Column and spindle housing of FADAL 2216 machine (a) Comparison on Natural Frequency errors (b)

20 natural frequencies of full model are compared to the ones obtained with the proposed model and with Law's approach. Results are summarized in Table 4.1 and Figure 4.8b.

Table 4.1 Natural frequencies comparisons for FADAL model

Natural frequencies FADAL					
Modes	**Full Model (Hz)**	**Proposed method (Hz)**	**Law's method (Hz)**	**Proposed method Error**	**Law's method Error**
1	73.8	73.8	75.3	0.0%	2.0%
2	75.9	75.9	77.7	0.0%	2.3%
3	131.8	131.8	127.3	0.0%	-3.4%
4	251.1	251.1	233.1	0.0%	-7.2%
5	263.5	263.5	282.2	0.0%	7.1%
6	306.4	306.4	306.6	0.0%	0.1%
7	481.6	460.7	481.7	0.0%	-4.3%
8	492.1	492.1	497.8	0.0%	1.2%
9	534.8	535.1	559.6	0.1%	4.6%
10	563.1	563.3	564.6	0.0%	0.3%
11	608.3	608.4	638.2	0.0%	4.9%
12	677.4	677.5	656.1	0.0%	-3.1%
13	682.6	683.0	701.5	0.1%	2.8%
14	840.7	841.0	785.8	0.0%	-6.5%
15	866.5	866.7	839.2	0.0%	-3.1%
16	887.6	888.3	840.4	0.1%	-5.3%
17	889.9	890.6	862.8	0.1%	-3.0%
18	1018.1	1018.6	955.5	0.1%	6.1%
19	1043.5	1044.4	973.6	0.1%	-5.7%
20	1081.6	1082.6	1060.1	0.1%	-2.0%

Results show a very good agreement for proposed method between reduced and full model (less than 0.2% in the first 20 modes), Law's method presents higher errors (around 5%). This difference is due mainly to the synthesis stage: MPC built in Nastran are a more robust and accurate approach compared to simple interpolation used in Law's method [33].

4.2. Conclusions

Machine tool FE model is a suitable approach to evaluate position-dependent dynamics. The main drawback, that limits the use of FEM for the simulation of machine tool dynamics, is the effort required to validate the model, due to the difficulties related to the joint modeling [33]. Even in case of fully validated models, the evaluation of the position-dependent tooltip dynamics is however limited by the high pre-processing and computational time. Actually for every toolkit, according to the required accuracy, many FRFs have to be calculated, considering different positions and orientations of the toolkit. These configurations with standard commercial software solutions have to be manually pre-processed by qualified operator. In this chapter a fully FE approach has been presented in order to overcome these issues and create a procedure to accurately model position-dependent dynamics efficiently and accurately. Based on similar approach presented by Law [33] a technique developed entirely in FE environment has been defined by means of MSC Nastran: superelement reduction and glued contact features have been used to achieve this result. Case study application shows the accuracy of the developed method comparing numerically full and reduced order model. Proposed method application to industrial context is still limited by validation of full FE model. Proposed method could be an interesting approach to identify machine tool dynamics and consequently chatter stability quickly and accurately, but the machine tool FE model used should be accurate enough to represent experimental behavior.

5. Orientation dependent dynamics

As for position, orientation could influence machine tool dynamics: this issue is significant for machine tool structures in which spindle unit can swivel and pivot (i.e., gimbal head). As already explained in the previous chapter, FE models of the machine are able to predict this behavior but their application is still limited by the high pre-processing and computational time. In this chapter a specific method to overcome this issue, achieving efficiently dynamics and chatter prediction is presented. Proposed method is tailored on gimbal head machine tools and takes advantage of detailed and efficient spindle FE model and Receptance Coupling techniques [1].

5.1. Overview

Machining of complex free-form surface requires large multi-axis machine tools able to continuously modify tool lead and tilt angles. This capability is normally provided by a gimbal head type kinematic configuration with a continuously rotating and/or swiveling spindle head. By swiveling the spindle head, these machines offer additional functionality and versatility by making it possible to approach the part from underneath.

Changing in orientation by head rotating and pivoting could influence tool-tip dynamics reducing stiffness and leading to detrimental vibrations occurrence, such as chatter that can compromise performance and productivity [13, 25]. This orientation-dependency, though important has been less investigated in literature. Recent investigations by Hung et. al. in [38] also confirmed the importance and influence of the spindle orientation on tool point dynamics and machining stability. Thus it is crucial to investigate machine dynamics varying with orientation and propose efficient technique to predict it.

In this chapter a generalized comprehensive approach to model and evaluate the orientation-dependent dynamics in machine tools is presented and summarized in Figure 5.2. As a separate substructure rotary head is modeled using Timoshenko beam elements. A dynamic substructuring approach based on receptance coupling is used to synthesize spindle head with the machine tool model. Consolidated techniques (i.e., receptance coupling and FE beam modeling of spindle unit), already adopted for other purposes in this field [39] [40], are used by proposed method to model machine tool orientation-dependent dynamics, slightly investigated in literature.

Proposed methodology is applied to an archetype of a 5-axis gantry mill machine tool with a gimbal head, based on [36] and shown in Figure 5.1. The 5 axes of the machine are decomposed into 3 linear axes (X, Y, and Z) on the gantry and 2 rotary/swivel (A and C) axes on the gimbal head (Figure 5.1).

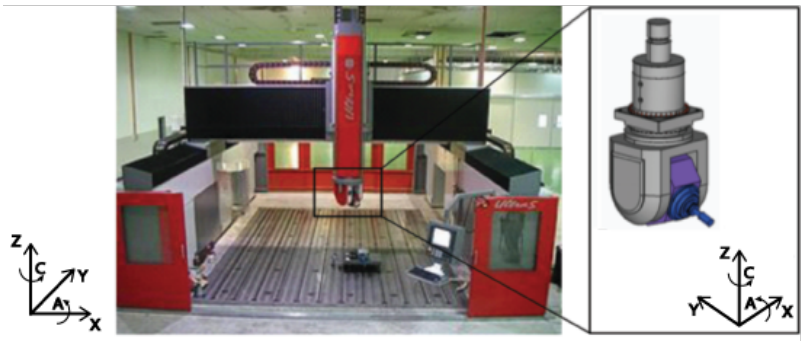

Figure 5.1 Representative example of a gantry mill with a gimbal head [41] , Gimbal head [31]

Simulation driven investigations of the influence of spindle orientation on the tool point dynamics and chatter stability for representative machining operations are discussed.

5.2. Proposed modeling approach

Proposed technique can be summarized in Figure 5.2. The two substructures (machine tool and spindle head) are simulated separately and then coupled together after rotation. Compared to the technique proposed in previous chapter, coupling is performed between Frequency Response Functions, thanks to Receptance Coupling Substructure Analysis (RCSA) in order to calculate tool-tip FRFs efficiently. Substructure FRFs are coupled in the spindle unit reference system in order to obtain tool-tip FRFs ready to be used for chatter prediction application.

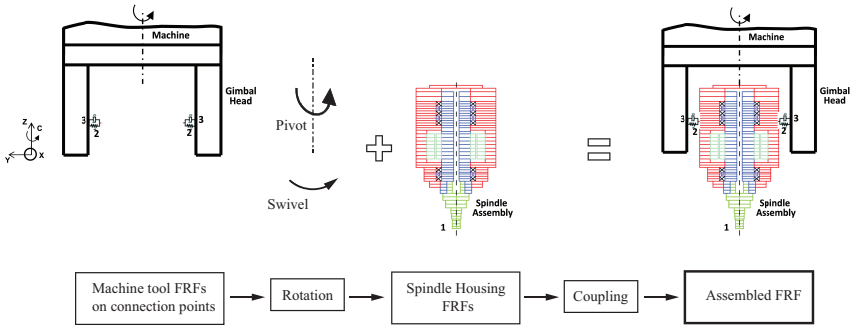

Figure 5.2 Scheme of the proposed technique

Three inputs are consequently required for the approach:

- Machine tool FRFs without the spindle housing calculated on connection points.
- Spindle housing FE model.
- Orientation of the tool.

5.2.1. **Machine tool response**

Detailed FE model of the gantry type machine tool [36] is constructed within the finite element environment from its available CAD model. The dynamic response at the connection end of the gimbal head is then simulated and presented in Figure 5.3.

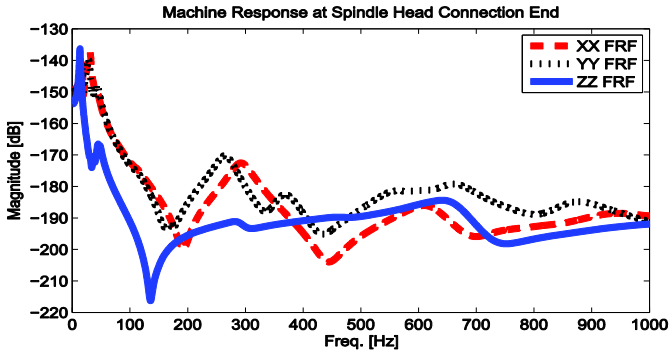

Figure 5.3 FRF at the gimbal head connection point on the machine [1]

A uniform damping of the level of $\zeta = 0.06$ for all structural modes is assumed [42]. The response in the machine Z direction, i.e., along the length of the Z-slide is stiffer than in the machine X and Y directions in a wide range of frequency. The low-frequency modes in the X and Y directions correspond to the bending modes of the Z-slide of the machine.

5.2.2. **Spindle Head FE model**

The spindle assembly, shown in Figure 5.4, includes the tool-tool-holder, spindle shaft, spindle cartridge, bearings, spacers, rotor, stator, housing and other accessories such as nuts and caps. An end-mill cutter of 30 mm diameter with an overhang of 145 mm from the spindle nose with a HSK100 type tool-holder is modeled. All components of the spindle assembly are modeled with Timoshenko beam elements based on design guidelines in [40]. Bearings are modeled as radial-axial springs, stiffness whose is obtained from the manufacturer's catalogue.

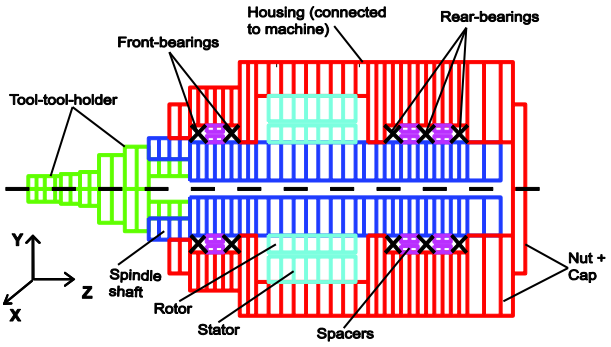

Figure 5.4 Detailed finite element model of the spindle assembly including holder and tool [1]

The free-free response at the tool-tip for the spindle head assembly, shown in Figure 5.4, is given in Figure 5.5. A uniform damping of the level of $\zeta = 0.02$ is assumed in constructing the FRFs. The spindle assembly response is symmetric in the X-Y plane. The response along the spindle Z direction, i.e., along the axis of the spindle shaft, is also stiffer than in the spindle X and Y directions.

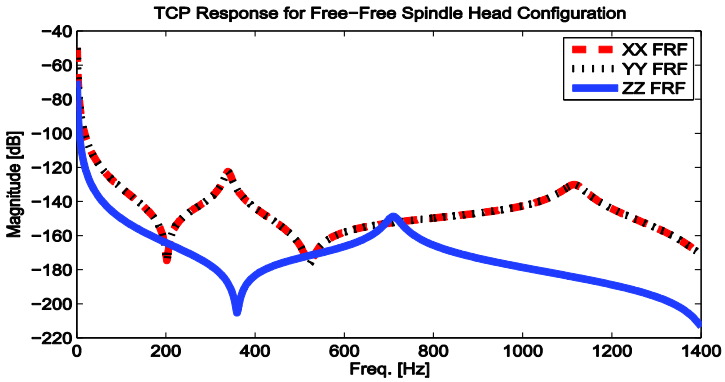

Figure 5.5 FRFs at the tool-tip for free-free spindle assembly configuration [1]

5.2.3. Modeling the orientation-dependence

Either spindle housing, using beam transformation matrices at the elemental level (as in [36]), or machine response may be rotated to the given orientation before synthesis. In this work machine response is rotated in order to obtain directly response in the spindle unit reference system (required for chatter prediction). Swivel motion (A axis), as well as gimbal head rotation (C axis) is accounted for by introducing rotational operators, such that the oriented machine tool transfer function matrix $\Phi_{\mathrm{OR_{MC}}}$ becomes:

$$\Phi_{\mathrm{OR_{MC}}} = \mathrm{R_{x/z}}^{\mathrm{T}} \Phi_{\mathrm{MC}} \mathrm{R_{x/z}} \tag{5.1}$$

where Φ_{MC} is the machine tool FRF matrix at the connection point and includes machine FRFs in machine principal directions (OXYZ):

$$\Phi_{\mathrm{MC}} = \begin{bmatrix} \Phi_{\mathrm{xx}} & \Phi_{\mathrm{xy}} & \Phi_{\mathrm{xz}} \\ \Phi_{\mathrm{yx}} & \Phi_{\mathrm{yy}} & \Phi_{\mathrm{yz}} \\ \Phi_{\mathrm{zx}} & \Phi_{\mathrm{zy}} & \Phi_{\mathrm{zz}} \end{bmatrix} \tag{5.2}$$

$\mathrm{R_{x/z}}$ within Eq. (**5.1**) is the transformation matrix necessary for rotations about the X or Z axis; and may be expressed as:

$$\mathrm{R_x} = \begin{bmatrix} 1 & 0 & 0 \\ 0 & \cos\alpha_{\mathrm{x}} & -\sin\alpha_{\mathrm{x}} \\ 0 & \sin\alpha_{\mathrm{x}} & \cos\alpha_{\mathrm{x}} \end{bmatrix}, \text{ and } \mathrm{R_z} = \begin{bmatrix} \cos\gamma_{\mathrm{z}} & -\sin\gamma_{\mathrm{z}} & 0 \\ \sin\gamma_{\mathrm{z}} & \cos\gamma_{\mathrm{z}} & 0 \\ 0 & 0 & 1 \end{bmatrix} \tag{5.3}$$

wherein α_x and γ_z are the rotations angles to be carried out about the A and C axis respectively.

As demonstration of the effect of rotation on the response of the machine at the connection points, transformed machine tool FRFs in X and Y directions are compared in Figure 5.6 for rotation only about the A axis. As evident in Figure 5.6, there remains no change in the dynamics (FRFs) about the axis of rotation; and only the Y and Z axis (not shown) response will change due to transformations.

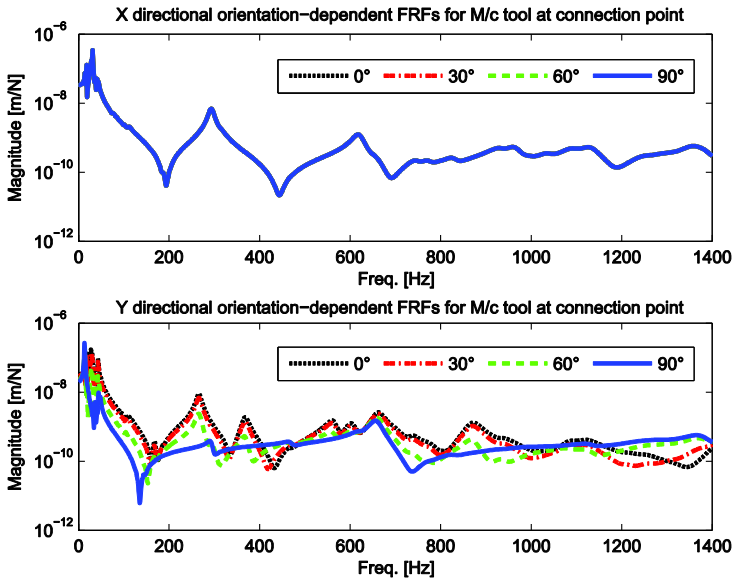

Figure 5.6 X and Y direction orientation-dependent FRFs for the machine tool at the connection point [1]

5.2.4. **Dynamic coupling**

The rotated (oriented) response of the machine tool at the connection point is combined with the free-free response of the spindle head assembly in the same point, to obtain the synthesized orientation-dependent tool-tip dynamic behavior. The component receptances for each of the substructures, i.e., the machine tool and the spindle assembly, are coupled thanks to RCSA technique as presented in [39] and explained in 8.1.

The assembled receptances, G_{11}, at the tool-tip in the generalized form are given as [39]:

$$G_{11} = R_{11} - R_{12}(R_{22} + R_{33})^{-1}R_{21} \tag{5.4}$$

where G_{11} and R_{ij}, are the receptance matrix that describes translational component behavior, and i and j are the respective measurement and excitation locations.

Each time the tool-tip response is desired at a different orientation, the machine tool receptances are first transformed to the desired configuration using Eq. (**5.1**), and subsequently substituted into Eq. (5.4) wherein they are combined with the spindle head response.

5.3. Results

Considering the two motions of spindle unit presented, orientation dependence has been investigated for two cases as shown in Figure 5.7: for swivel motion of the tool; and for rotation about the Z axis (C axis motion) for when the tool is inclined at 30˚ about the X axis.

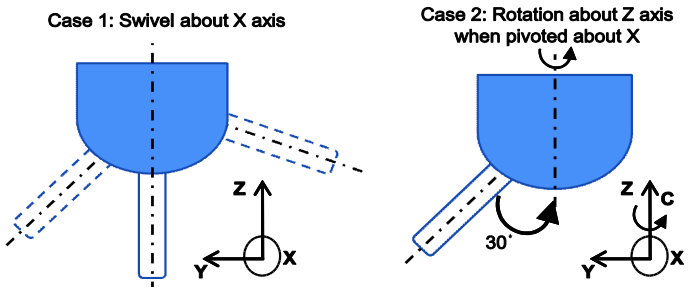

Figure 5.7 Investigation of orientation-dependent dynamics for two cases: (1) for swivel motion about X axis; and, (2) for pivot about X axis + rotation about Z axis

Tool-tip FRF changing with orientation is studied and applied to chatter stability in order to investigate the impact on machining process.

5.3.1. Orientation-dependent dynamics

Case 1. Swivel motion

Orientation-dependent response for swivel motion of the tool is shown in Figure 5.8. In the case study the tool-tip response is symmetric about the neutral position of the tool, there only motion positive direction will be shown in Figure 5.8. Moreover as shown in Figure 5.6 X directional response does not change for the case study: only the changing Y directional response is compared in Figure 5.8. Furthermore, since the Z directional response is stiffer than the machine X and Y directions, as observed earlier in Figure 5.5, Z direction response is also neglected for comparisons.

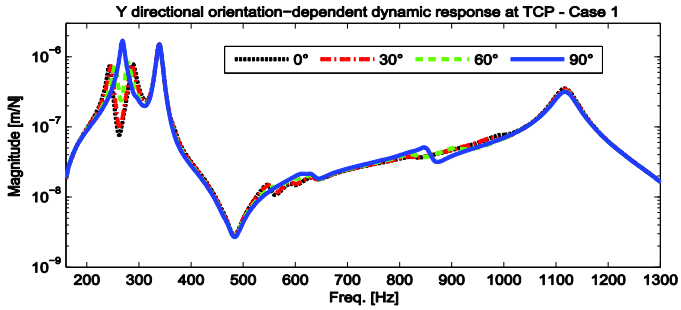

Figure 5.8 Orientation-dependent dynamics for the case of swivel motion about the X axis

As evident in Figure 5.8, the response changes more significantly for higher swivel motions and is found to be more flexible at 90˚ orientation than between 0-60˚. The dynamic stiffness for the mode at ~260 Hz at 90˚ orientation is ~100% less than at the at 0˚ orientation. A slight change in frequency of this mode is also observed due to the effect of

orientation. The mode at ~260 Hz corresponds to the global bending mode of the Z-slide of the machine tool along with the spindle head assembly; whereas the dominant mode at ~340 Hz corresponds to the first local bending mode of the spindle head assembly.

Case 2. Pivoting motion

Orientation-dependent response for rotation about the Z axis (i.e., C axis motion) for tool pivoted at 30˚ about the X axis is shown in Figure 5.9. When the spindle head rotates 90˚ about the Z axis, the local X and Y tool-tip directions get switched. This behavior, which repeats for every 90˚ rotation about the Z axis, is captured by the model – as is evident from comparisons in Figure 5.9.

The dynamic behavior for rotation about the Z axis is also observed to change, causing both a shift in the frequencies of the dominant modes as well as a change in the dynamic stiffness. Dynamic stiffness for the mode at ~260 Hz is observed to change by as much as 60% for rotation from 0-90˚. The higher frequency response corresponds to the local tool-tool-holder bending modes and is not observed to be a strong function of orientation for either of the cases.

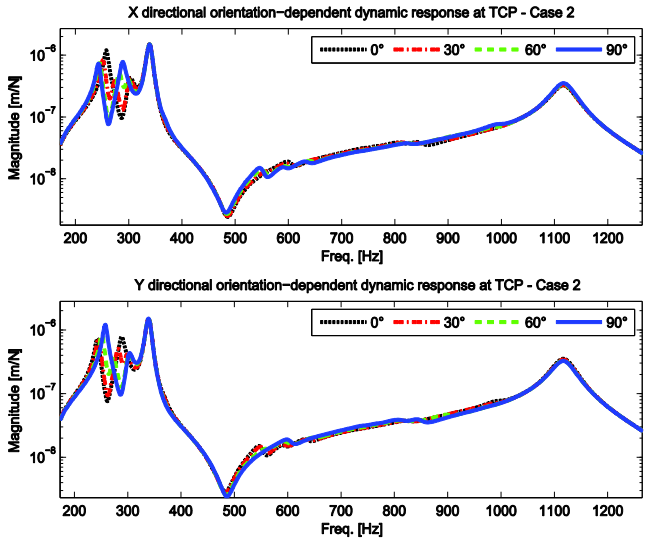

Figure 5.9 Orientation-dependent dynamics for the case of rotational motion about the Z axis when pivoted at 30˚ about the X axis

5.3.2. Orientation-dependent chatter stability

When the structural dynamics of the machine vary within the machine's workspace due to the tool's constantly changing orientation during continuous cutting, the chatter stability and the resulting limits on the material removal rates vary as well. The changing stability of the milling system is determined using a modal model of the machine and the characteristic equations (2.6)-(2.9) according to Altintas and Budak theory [25], as presented in Chapter 1. Stability was simulated for continuous cutting for swivel and pivoting motion cases in Figure 5.7 for full immersion milling (slotting) of AISI 1045 steel with $N_t = 4$; $K_t =$ 2,362 MPa; and the radial coefficient, $K_r = 0.5$. End-milling of steel is treated as the representative machining operation to be carried out on this machine. Orientation-dependent

machining stability, i.e., stability lobes along with the corresponding chatter frequencies are shown in Figure 5.10 and Figure 5.11 for Cases 1 and 2 respectively.

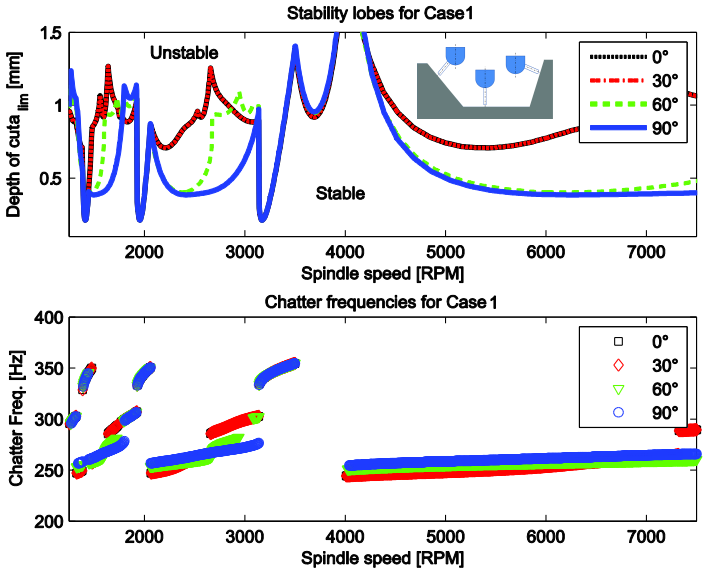

Figure 5.10 Orientation-dependent machining stability for Case 1, i.e., for swivel motion about X axis. Stability lobes (top), with the corresponding chatter frequencies (bottom)

The stability lobes for Case 1 are significantly influenced by orientation; with the stability boundary being lower for higher swivel motions; due to the dynamic stiffness being lower at the 90˚ orientation than between 0-60˚. The absolute minimum stability limit is found to be independent of the orientation and occurs around the dominant spindle bending mode of ~340 Hz; however, the stability limits at some speeds, for example at 2500 RPM and 5000 RPM, is found to vary by as must as ~80-100% - depending on the orientation angle. This is explained by the change in the chatter frequencies observed at these two speeds. Chatter at these two speeds occurs at ~260 Hz which corresponds to the global bending mode of the Z-slide and the spindle head, which is also observed to become dominant at certain orientations – as evident from earlier comparisons in Figure 5.8.

Orientation-dependent machining stability comparisons for Case 2 is shown in Figure 5.11. The machining operation would be akin to a circular milling operation. As evident in Figure 5.11, the stability lobes for the 0˚ and the 90˚ are the same – since the dynamics between 0˚ and 90˚ for the X and Y directions get switched – as observed in earlier comparisons in Figure 5.9.

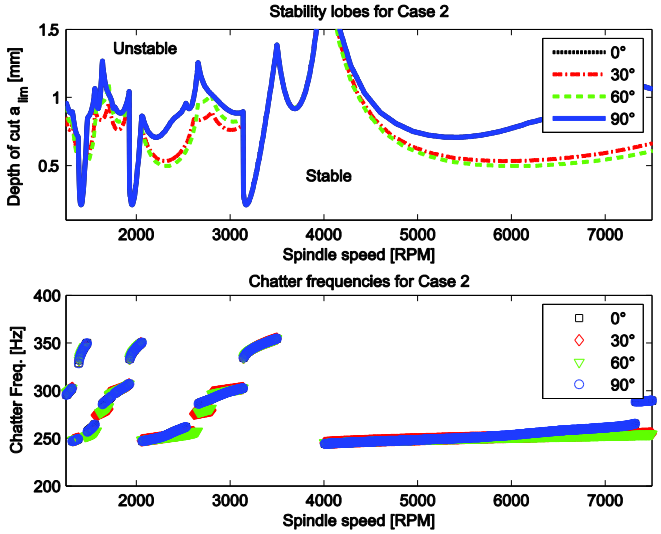

Figure 5.11 Orientation-dependent machining stability for Case 2, i.e., for rotary motion about Z axis when the tool is pivoted at 30˚ about the X axis. Stability lobes (top), with the corresponding chatter frequencies (bottom)

As was observed in Figure 5.10 for Case 1, the absolute minimum stability limit for Case 2 is also independent of orientation. However, as before, the stability limits are different at certain speeds, and chatter is observed to occur at different frequencies for these speeds. For example, the absolute minimum stable depth of cut is limited by chatter occurring at the ~340 Hz bending mode, whereas at a spindle speed of 6000 RPM, chatter occurs between ~240-260 Hz – depending on orientation.

The changing machining stability observed may need the planning of dynamically changing machining trajectories such as to ensure stable cutting – which poses its own set of challenges; or, alternatively and more conservatively, it may result in selection of cutting parameters below the lowest of all possible stability thresholds, thereby resulting in a slower material removal process – which is undesirable.

5.4. Conclusions

For machine tools with gimbal heads, which have spindle heads that may rotate and/or swivel during continuous cutting operations, the changing dynamics due to change in orientation was taking into account in this study, and its influence on machining stability of the system was demonstrated. The spindle head assembly modeled as a separate substructure was coupled to a virtual machine tool model using a receptance coupling approach, as part of a dynamic sub-structuring strategy.

Changing dynamics and stability were investigated for two different cases for swivel and rotational motion of the machine tool gimbal head. Simulation driven investigations show a strong dependence of the tool-tip dynamics and stability on orientation – for the case considered varying by as much as 100% in dynamic stiffness and depth of cuts limit for change in orientation within the 0-90˚ rotation and swivel motion. Experimental investigations are required to validate proposed method and form part of the future work.

6. Toolkit modeling

Hybrid experimental-numeric methods are efficient techniques able to identify machine tool dynamics, i.e., tool-tip FRF. As mentioned in the Chapter 2, these methods combine experimental results of machine without toolkit clamped, and dynamic behavior of toolkit obtained via numeric computation (FEM) or analytical formulation. Compared to fully experimental approach, in which for each toolkit one measurement is required, these methods allow to drastically reduce experimental phase time: only one experimental set-up is required for each machine in case of machine tool dynamics does not change significantly with position. One of the main drawbacks of these techniques is the need of high-accurate model of milling tool in order to return reliable and accurate results.

In this Chapter toolkit modeling is investigated. The goal of the tool modeling activity is the implementation of the simplest algorithm that could predict accurately milling tool dynamics (including tool-holder), in order to perform hybrid experimental-numerical approach and predict tool-tip dynamic response efficiently. RCSA effectiveness is predicting tool-tip FRFs performing a single test for machine tool, independently from the toolkit (holder-tool assembly) clamped on it. To achieve such result, entire toolkit should be assumed as the changeable part, hence it should be FE modeled. In this Chapter simplified FE modeling technique, based on beam elements, has been tested and limits of its application have been highlighted comparing it with 3D solid approach.

6.1. Overview

Toolkit model is essential to perform hybrid experimental-numerical methods. Considering the preferential dimension of general toolkits, 1D beam is definitely the most adopted element type to achieve this goal because of three main advantages:

- Computational efficiency;
- Easily automation of pre-processing operations;
- No commercial software required.

The computational efficiency is mainly due to i) the reduced number of degree of freedoms required to perform the geometry discretization, and ii) the analytical formulation of beam elements [43], which means that no numerical integration is required for elements matrices calculation. The possibility of easily automate the mesh process occurs for the same reasons explained above. Furthermore, since an analytical formulation of the elements is

present, commercial finite element software is not required, since pre-processing and analysis operations can be carried out by an own written code.

In Schmitz and Donalson work [39] (first receptance coupling implementation) the tool was modeled using an analytical formulation according to Euler-Bernoulli beam model, i.e., no geometry discretization was performed and an analytical tool FRFs formulation given. An analytical Timoshenko beam formulation was instead used by Ertürk et al. to model the spindle - tool holder – tool assembly response [44]. Namazi et al. [45] presented a model of the tool holder-spindle contact stiffness: in their work a FE modeling of the holder-tool assembly was realized using Timoshenko beam elements.

The main lack of analytical approach is that just prismatic components, with no cross section variations along their axis, can be modeled. This problem can be overcame analytically in several ways, for example using a receptacle coupling approach between components prismatic segments [44]. Despite strategies to overcome analytical formulations limitations exist in literature, numerical approach (FE) simplifies modeling operations if tapered segments are present [45]. Moreover a relevant distinction has to be made between Timoshenko and Euler-Bernoulli beam models. The latter represents the simplest approximation, but it is well known that it cannot provide a reliable prediction of milling tool dynamics [46]. This lack of accuracy occurs because the Euler-Bernoulli model considers just bending contribution to the beam deflection and shear deformation is neglected.

Euler approximation is acceptable for slender structures, because the shearing deformation contribution is very small with respect to the overall deformation. In structures with low length to thickness ratio, instead, deflection due to shearing deformation has the same magnitude order of bending deflection; hence it cannot be neglected. To overcome these limitations, Stephen Timoshenko [47] developed a beam model including shearing contributions. Figure 6.1 shows a comparison between Timoshenko and Euler model in beam displacement calculation. The accuracy gap between the two models is larger in dynamic modeling applications, such as normal modes or FRFs computing.

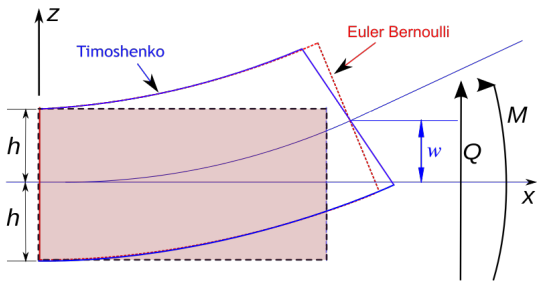

Figure 6.1 Comparison between Euler-Bernoulli and Timoshenko beams

One-dimensional (1D) models represent the most used strategy for tool modeling, even if this implementation could lead to inaccuracies, mainly related to:

- Flutes modeling;
- Holder-tool connection identification;
- No-axisymmetric geometry modeling

To improve flutes modeling in beam models Kivanc and Budak [48] presented simplified equations for end mills and Bediz et al. [49] developed a new three-dimension dynamics modeling technique in which, thanks to spectral-Tchebychev (ST), actual fluted geometry is taken into account. Holder-tool connection identification is still an open issue: different techniques have been proposed and will be discussed in Chapter 6. In order to avoid modeling issues, in some works [50, 51] 3D-solid FE models are preferred in RCSA approach in order to reach high accurate dynamics simulation. A summary of modeling techniques used in literature is reported in Table 6.1.

Table 6.1 Tool modeling literature summary

First Author Ref.	Year	Paper's Scope	Cutting process	Modeling techniques	Toolkit connection
Schmitz [39]	2000	Chatter SLD	Milling	Analytic Euler Beam	Collet
Schmitz [52]	2001	Chatter SLD	Milling	Analytic Euler Beam	Collet Φ 6.35 mm
Park [27]	2003	Tool-tip FRF	Milling	FE Timoshenko Beam	Collet Φ 19.05 mm
Kivanc [48]	2004	Flutes modeling Tool deflection Tool-tip FRF	Milling	Analytic Euler Beam	Φ 6-20 mm
Schmitz [53]	2005	Chatter SLD	Milling	Analytic Euler Beam	Shrink Fit Φ 19.1 mm
Erturk [44]	2006	Tool-tip FRF	Milling	Analytic Timoshenko Beam	
Cao [40]	2006	Spindle model	Milling	FE Timoshenko Beam	
Namazi [45]	2007	Tool-tip FRF	Milling	FE Timoshenko Beam	
Ahmadi [54]	2007	Chatter SLD	Milling	Analytic Euler Beam	
Mascardelli [51]	2008	Chatter SLD	Micro-Milling	FE 3D solid	Collet
Madoliat [55]	2011	Chatter suppression	Milling	FE 3D solid	Slender endmill
Ostsevicius [56]	2012	Modal response	Drilling	FE 3D solid	Φ 10 mm
Albertelli [50]	2013	Chatter SLD	Milling	FE 3D solid	Collet Φ 8-14 mm
Mancisidor [57]	2014	Chatter SLD	Milling	FE Timoshenko Beam	

As clear from Table 6.1, the most used technique is 1D beam model; recently few works are reporting the use of 3D solid FE model. In this thesis both 1D beam and 3D solid FE models have been investigated.

6.2. 1D Beam Model

In this section Timoshenko beam modeling has been investigated, since it allows dramatically reducing modeling pre-process time. A numerical approach has been

implemented since analytical strategy has not been considered feasible in complex tool modeling. Therefore the tool geometry is discretized with Timoshenko beam elements and dynamic analyses (modal or FRF) are performed with numerical methods.

6.2.1. **Timoshenko beam theory**

Stephen Timoshenko developed the beam theory that takes its name early in the 20th century. As briefly stated in the introduction, the main difference between Euler-Bernoulli theory is that it considers shear deformation, but from a dynamic point of view, the main advantage is that Timoshenko theory takes into account rotational inertial effects, making it suitable for dynamic analysis of beam structures. Figure 6.2 shows a comparison between Timoshenko and Euler models in static deflection prediction, pointing out the difference between the two mathematical formulations.

Euler – Bernoulli Theory:

$$\begin{cases} EJ\dfrac{d^4w(x)}{dx^4} = q(x) \\ \varphi(x) = \dfrac{dw}{dx} \end{cases}$$

Timoshenko Theory:

$$\begin{cases} \dfrac{d^2}{dx^2}\left(EJ\dfrac{d\varphi(x)}{dx}\right) = q(x) \\ \dfrac{dw(x)}{dx} = \varphi - \dfrac{1}{k_S AG}\dfrac{d}{dx}\left(EJ\dfrac{d\varphi(x)}{dx}\right) \end{cases}$$

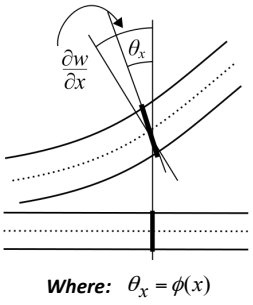

Where: $\theta_x = \phi(x)$

Figure 6.2 Comparison between Euler-Bernoulli and Timoshenko theories

In Euler theory, the approximation of pure bending deformation leads to a direct correlation between cross section rotation angle and displacement. If shearing contribution is considered, rotation and displacement are not so closely bonded as in Euler model and this leads to better displacement approximation, especially for structures with a low length to thickness ratio. The displacement related to shearing deformations is computed making the approximation that a shearing force produces a constant stress along beam cross section:

$$\gamma = \frac{\tau}{G} \tag{6.1}$$

$$\tau = \frac{T}{Ak_S} \tag{6.2}$$

$$\gamma = \frac{T}{GAk_S} \tag{6.3}$$

where γ is shear strain, τ is shear stress, T is the applied load, A is the beam section, G is shearing elasticity modulus and k_S is the shear factor, that acts as a scale factor for beam cross section area compensating the non uniformity of stress field. In literature several formulation for shear factor calculation have been presented. Generally it depends on Poisson ratio and cross section shape and dimension. Hence there is not a widely accepted

theory for this parameter calculation. In this work Hutchinson [58] and Shames [59] formulations have been tested, since they have been already used in machine-tool research application [60, 61]. The analysis of tool resonance frequencies has shown just little differences between the two formulations. Despite this, Shames' approach seems to provide a better agreement with the experimental data, especially in high frequency modes computing. Equation (**6**.**4**) and (**6**.**5**) reports Shames formulation for solid and hollow circular sections:

$$k_s = \frac{6(1+\nu)}{7+6\nu} \tag{6.4}$$

$$k_S = \frac{6(1+\nu)(1+p^2)^2}{(7+6\nu)(1+p^2)^2 + (20+12\nu)p^2} \tag{6.5}$$

where p is the ratio between outer radius and inner radius. For a beam of constant cross section that respects every hypothesis mentioned for static displacement equations, the flexural dynamic behavior is described by equation (6.6):

$$EJ\frac{\partial^4 w}{\partial x^4} + m\frac{\partial^2 w}{\partial t^2} - \left(I + \frac{EJm}{k_s AG}\right)\frac{\partial^4 w}{\partial x^2 \partial t^2} + \frac{mI}{k_s AG}\frac{\partial^4 w}{\partial t^4} = \\ ...q(x,t) + \frac{I}{k_s AG}\frac{\partial^2 q}{\partial t^2} - \frac{EJ}{k_s AG}\frac{\partial^2 q}{\partial x^2} \tag{6.6}$$

where:

- m is the mass per unit length.
- J is the second moment area.
- I=Jρ
- q(x,t) is the distributed load per unit length

The analytical formulation shown in equation (6.6) can be applied to solve free or forced vibration problem. Analytical equations are the basis for Timoshenko beam finite element (FE) formulation. This element has two nodes, each one with six degree of freedom (Figure 6.3), it means that also torsional and axial vibrations can be modeled. This leads to twelve by twelve stiffness and mass matrices. Since each element represents a constant section beam segment, its dynamic behavior is described by the Timoshenko beam theory, i.e., element matrices can be yielded directly from analytical formulation, without involving any numerical integration process.

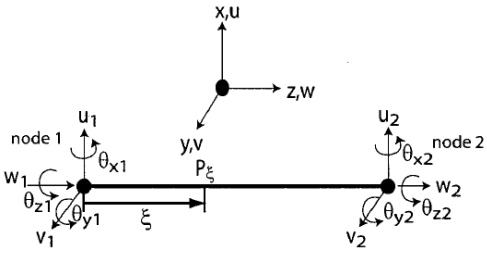

Figure 6.3 Timoshenko beam element

Systems matrices are computed from element matrices with the assembling process, allowing to solve forced or free vibration problems for variable cross section beams.

6.2.2. **Timoshenko beam implementation**

A Matlab® code has been implemented to build Timoshenko beam FE models of milling tools and perform modal and FRF analysis. Each beam element is identified by nodes positions, cross section properties and material properties. Since milling tools have a linear geometry, nodes position can be determined just by one coordinate. Furthermore, these components have a prevailing axial symmetric structure with little asymmetries that can be usually considered negligible. This simplifies cross section property evaluation, since the tool has an isotropic flexural behavior and just two geometric parameters are required to characterize beam section. In Figure 6.4 a flow chart summarizing algorithm steps is presented.

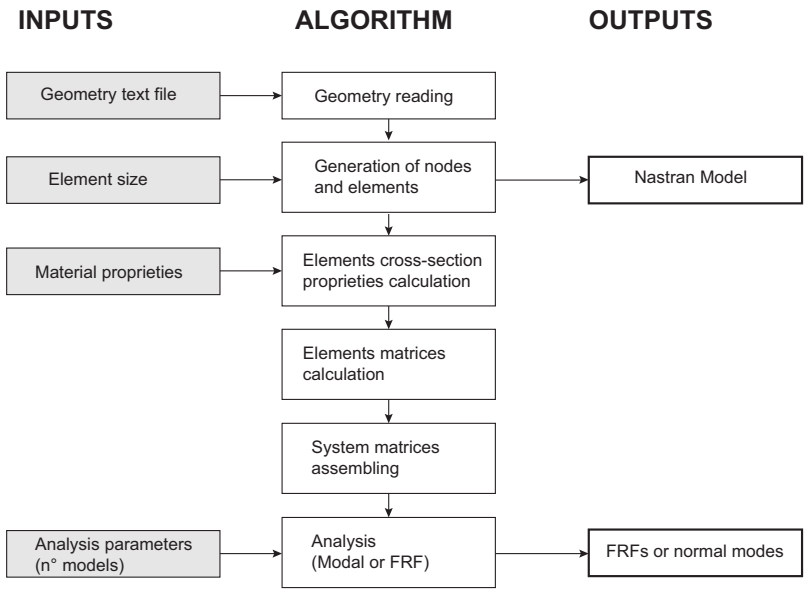

Figure 6.4 Timoshenko beam algorithm flow chart

Linear structure and axial symmetry allowed automating the mesh process, so that no model pre-process operation is required. Algorithm inputs are:

- Tool geometry text file.
- Element size.
- Number of modes to compute.
- Material properties.

Tool geometry is written in a text file in a specific format: starting from tooltip the segments with continuous radius variation along tool axis are identified. Since, as earlier mentioned, tool geometry is approximated as axial symmetric, each segment is characterized by outer and inner radius at both its ends and by its length, hence every line of the text file represents one segment. In Figure 6.5 an example of segments definition is given.

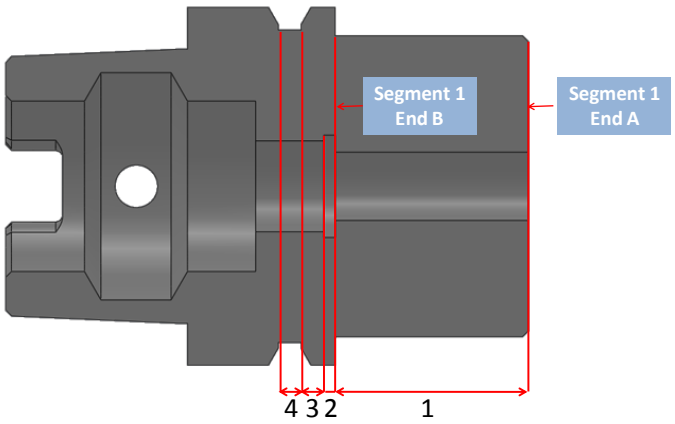

Outer Radius End A	Inner Radius End A	Outer radius End B	Inner Radius End B	Length
26.5	6	26.5	6	15
31.5	9	31.5	9	2
31.5	8	31.5	8	2.25
31.5	8	27.5	8	1.75

Figure 6.5 Segment definition example.

Since the goal is to model the holder-tool assembly, a joint between these two components will be present. In the implemented code, joints are treated as rigid connections, it means that assembly is modeled as a continuous component. Joint zones geometry are specified considering the overall dimensions as shown in Figure 6.6.

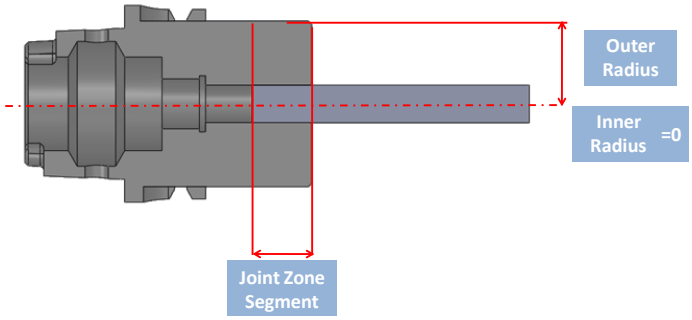

Figure 6.6 Joint zone segment definition example.

Material is assumed to be homogeneous, linear elastic, isotropic according to Timoshenko beam theory hypothesis. Tool damping is considered according to a structural proportional model, i.e., complex stiffness matrix is defined computing a complex Young modulus as in equation (**6.7**):

$$E_c = E(1 + j\eta) \tag{6.7}$$

According to the exposed hypothesis, the code requires the following material parameters:

- Young modulus.
- Poisson coefficient.
- Mass density.
- Structural damping coefficient (η).

As outlined in Figure 6.4 the first operation performed by the code is geometry text file reading. After that meshing process begins. Nodes coordinates identify elements location and length. Nodes coordinates are specified in a coordinate system with z-axis along tool axis, while x and y axis orientation is not relevant because of tool axial symmetry. Nodes positions are established considering segments position and mesh size. Node placing algorithm ensures that a node is always present at each segment's ends: if segment is longer than the chosen mesh size then a proper number of nodes (elements) is created, otherwise segment is modeled with just one element.

After the meshing process, the following elements cross-section properties are computed:

- Flexural second moment area (J_{xx}, J_{yy}).
- Polar moment area (J_{zz}).
- Area.
- Shear Factor (computed according to Shames formulation).

For tapered segments, code interpolates inner and outer radius with a linear function yielding radius values at nodes positions. Elements section properties are then computed considering an average radius value between the two ends of each element as shown in Figure 6.7.

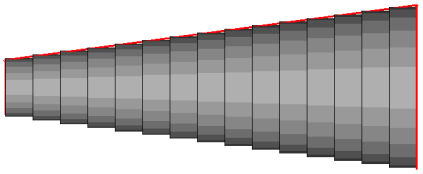

Figure 6.7 Tapered segment modeling example. Red line is the tapered surface, while cylinders are beam elements.

Once that properties have been computed, the algorithm proceed to element mass and stiffness matrices calculation, according to the formulation presented in [62]. Last step is matrices assembling [43]: in this phase elements matrices are combined together to create the assembly matrices. To explain how matrices assembling phase works, the model composed by two elements (Figure 6.8) is considered as example.

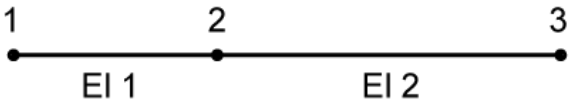

Figure 6.8 Simple model for assembling process example.

Let K^k, M^k be respectively stiffness and mass matrices for element k:

$$K^1 = \begin{vmatrix} K^1_{11} & K^1_{12} \\ K^1_{21} & K^1_{22} \end{vmatrix} \qquad M^1 = \begin{vmatrix} M^1_{11} & M^1_{12} \\ M^1_{21} & M^1_{22} \end{vmatrix} \tag{6.8}$$

$$K^2 = \begin{vmatrix} K^2_{11} & K^2_{12} \\ K^2_{21} & K^2_{22} \end{vmatrix} \qquad M^2 = \begin{vmatrix} M^2_{11} & M^2_{12} \\ M^2_{21} & M^2_{22} \end{vmatrix} \tag{6.9}$$

where K^k_{ij} and M^k_{ij} are sub-matrices corresponding to nodes i and j. Matrices are assembled as shown in equation (**6.10**).

$$K = \begin{vmatrix} K^1{}_{11} & K^1{}_{12} & 0 \\ K^1{}_{21} & K^1{}_{22} + K^2{}_{22} & K^2{}_{23} \\ 0 & K^2{}_{32} & K^2{}_{33} \end{vmatrix} \quad M = \begin{vmatrix} M^1{}_{11} & M^1{}_{12} & 0 \\ M^1{}_{21} & M^1{}_{22} + M^2{}_{22} & M^2{}_{23} \\ 0 & K^2{}_{32} & M^2{}_{33} \end{vmatrix} \tag{6.10}$$

This method is yielded from kinetic and potential energy balance, considering that energy is additive. Once matrices have been assembled, FRFs and modal analyses can be performed.

Modal analysis is the extraction of eigenvalues and eigenvectors of the matrix:

$$A = K - \omega^2 M \tag{6.11}$$

This extraction is performed using *eigs* Matlab function that computes the lowest n eigenvalues (and eigenvectors), where n is specified in software input. Eigenvectors represent normal modes and eigenvalues are related to natural frequencies according to equation (**6.12**).

$$f_{ni} = \frac{\sqrt{\omega^2 i}}{2\pi} \tag{6.12}$$

The analysis are carried out in free-free conditions, it means that no constrain are used. This because experimental modal analysis (EMA) has performed in free-free conditions as will be later presented. In Figure 6.9 an example of modal analysis results is given on an HSK-63A tool holder with a hypothetic milling tool.

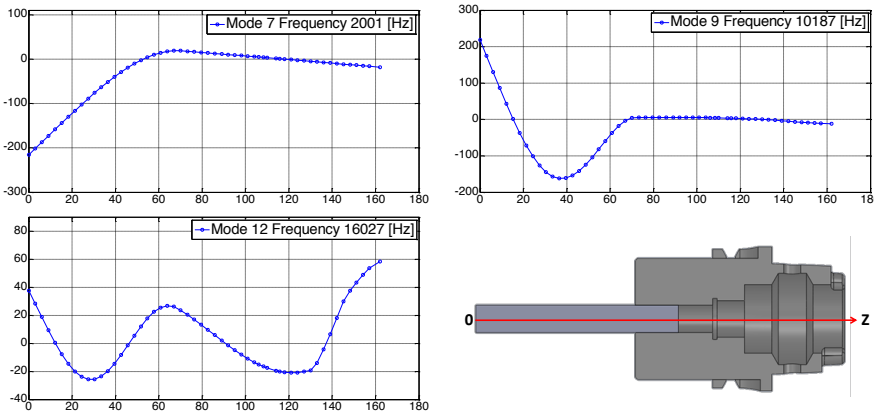

Figure 6.9 Modal analysis results example: first three bending modes

FRF analysis on a FE model can be carried out with two methods [43]:

- Direct method.
- Modal superposition method.

Direct method consist in dynamic stiffness matrix inversion for a selected frequency set as shown in equation (**6.13**):

$$(K - \omega^2 M)X_0 = F_0 \tag{6.13}$$

F_0 is external force vector, while X_0 is nodes displacement vector, therefore if a unit load is applied on a single degree of freedom (DOF), the computed displacements represent displacements due to a unit load, hence the receptance functions. Unlike in direct method, in modal superposition no matrix inversion is performed: as first a modal analysis step is carried out, then FRFs are computed with linear system dynamics relations:

$$G_{jk}(\omega) = \sum_{r=1}^{N} \frac{\phi_i{}^r \phi_k{}^r}{\omega^2{}_r - \omega + j\eta_r\omega_r} \tag{6.14}$$

where:

- $G_{jk}(\boldsymbol{\omega})$ is j-th DOF displacement for a unit load on k-th DOF.
- $\boldsymbol{\omega}_r$ is r-th natural pulsation.
- $\boldsymbol{\eta}_r$ is r-th modal damping factor.
- $\boldsymbol{\phi}_j^{\,r}$ is r-th component of j-th mode.

Usually not all systems modes are used in the analysis, but a sub-set is chosen, therefore direct method produces more accurate results. However direct analysis involves higher process time, especially for models with a large number of DOFs or if many frequency steps are involved. The implemented code produces all information needed to process FRFs analysis with both direct and modal method.
In order to have a graphic representation of the FE model realized, the code can write down an ASCII file in Nastran input file format. This allows the model to be viewed with FE pre-processing software able to read Nastran format, as shown in Figure 6.10.

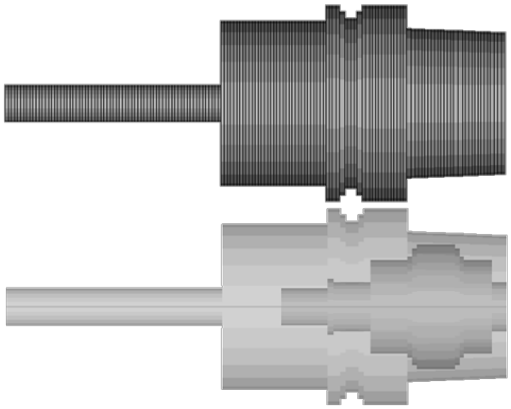

Figure 6.10 Three dimensional view of a tool model.

Thanks to the presented algorithm, a computational efficient, easy to use method to calculate toolkit dynamics has been developed. This approach is suitable for industrial applications, since simple inputs are required (geometry file and material) without the need of commercial software.

6.3. 3D solid model

1D beam model are generally preferred to simulate toolkit dynamics because of their simplicity. In this work toolkit components are also modeled using three-dimensional (3D) elements in order to deep investigate beam model limitations. Models are simulated using MSC Nastran commercial FE solver. Toolkit components are assembled using glued contact,

a MSC Nastran double sided linear contact algorithm [37], that permits to join components having dissimilar meshes. This choice allows using different mesh patterns and element types for every component, optimizing elements quality. Component mesh size has been chosen smaller than required from convergence analysis to allow better components description. Toolkit modeling has been performed using first order prismatic elements (CHEXA and CPENTA in Nastran) for all the components except for tools with twisted cutting edge, because of complexity of their geometry. Tools have been hence modeled using second order tetrahedral elements (CTETRA in Nastran), exploiting glued contact potential to join meshes with dissimilar elements formulations.

6.4. Model validation method

Once models are created, modeling accuracy is studied by means of an experimental validation. In this work proposed modeling techniques have been evaluate according to Modal Testing theory [63]. Component in free-free condition has been tested and simulated to evaluate accuracy of the modeling techniques proposed. In this section this procedure is explained using, as tested component, the toolkit shown in Figure 6.11.

Figure 6.11 Dummy tool for model validation procedure: physical component (a), beam FE model (b)

The toolkit is composed by a tool-holder HSK32ER20 and a shank connected by means of collet chuck connection with 220 mm overhang. All the components are made of steel. The toolkit is easy to model and suitable for simplified 1D beam modeling due to its high slenderness and simple geometry (e.g., no flutes). The same toolkit presented here will be used in other sections for validation purpose as “dummy toolkit”.

Model validation procedure can be synthetized in the following steps:

- Pre Test
- Experimental Modal Analysis (EMA)
- Correlation
- Model Updating (optional)

6.4.1. Pre-Test

Pre-test phase is carried out in order to ensure experimental test returning proper and accurate results. This phase gives useful guidelines on measurement points locations, thanks to modal analysis on the tested component model. In this work both natural frequency and modes shape are investigated: an appropriate placement of measurement points (accelerometers) is required to correctly observe all the mode shapes of interest. Different

measurement locations can be simulated on component model, in order to avoid time-consuming trial and error approach during EMA phase.

As example in Figure 6.12 the first four flexural mode shapes of the dummy toolkit beam model are shown. It is not relevant to specify modes bending plane, since FE model is axial symmetry: this means that bending modes on yz and xz planes will have the same natural frequencies and deformed shapes. Modes from 1st to 6th are rigid body motions since the analysis has been carried out in free-free condition. The modes between the plotted ones have been excluded because they are torsional, or axial modes, or because they are the dual of the plotted modes lying on another bending plane. Accelerometers layout is proposed as shown in Figure 6.13, where measurement points positions are marked by blue dots.

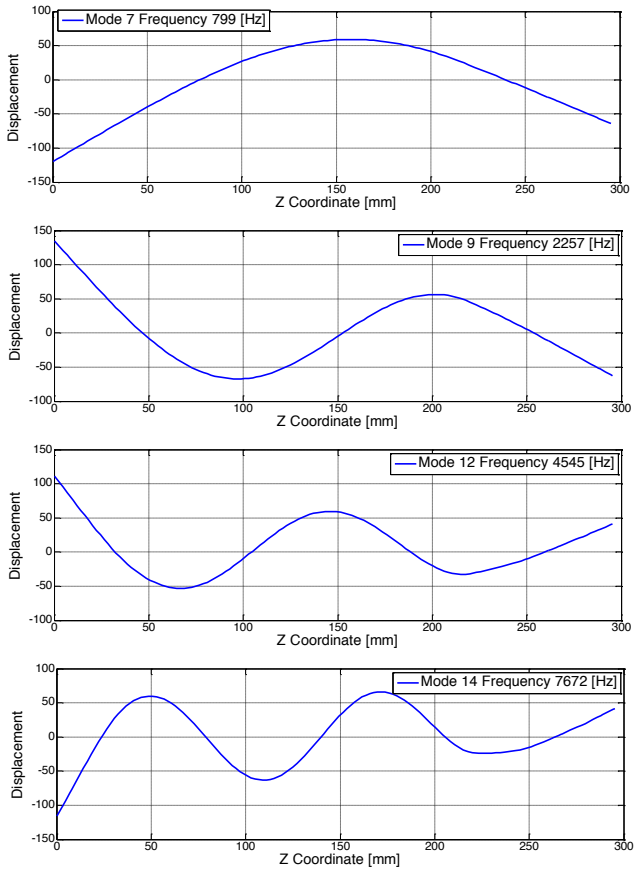

Figure 6.12 Configuration one: flexural mode shapes.

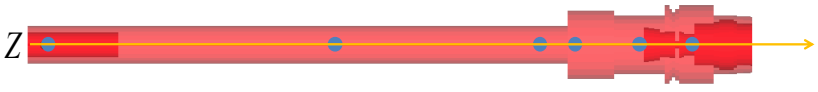

Figure 6.13 Configuration one: accelerometers layout.

To verify if accelerometers layout is correct, the AutoMAC parameter has been evaluated. The MAC acronym stands for modal-assurance-criterion and it is a correlation method between two sets of mode shapes [64], generally the predicted and the measured one. Basically when a modal analysis is performed, the goal is to have the corresponding mode shapes of the two sets proportional to each other. At the same time no corresponding modes should be orthogonal vectors, in order to be able to discern them. So the mathematical formulation of the MAC is substantially a dot product, as shows equation (**6.15**):

$$MAC = \frac{\left|\left\{\Psi^{i}{}_{ex}\right\}^{T}\left\{\Psi^{j}{}_{FE}\right\}\right|^{2}}{\left\{\Psi^{i}{}_{ex}\right\}^{T}\left\{\Psi^{i}{}_{ex}\right\}\left\{\Psi^{j}{}_{FE}\right\}^{T}\left\{\Psi^{j}{}_{FE}\right\}} \tag{6.15}$$

- Ψ^{i}_{ex} is the ith experimental mode shape
- Ψ^{j}_{FE} is the jth FE model mode shape

If i=j the MAC should theoretically be one (perfect correlation), while if i≠j should be zero. All these products compose the MAC Matrix. So the AutoMAC is a MAC between model modes and themselves (equation (**6.16**)):

$$AUTOMAC = \frac{\left|\left\{\Psi^{i}{}_{FE}\right\}^{T}\left\{\Psi^{j}{}_{FE}\right\}\right|^{2}}{\left\{\Psi^{i}{}_{FE}\right\}^{T}\left\{\Psi^{i}{}_{FE}\right\}\left\{\Psi^{j}{}_{FE}\right\}^{T}\left\{\Psi^{j}{}_{FE}\right\}} \tag{6.16}$$

AutoMAC verifies if the accelerometers layout allows to correctly observing the desired mode shapes: performing the AutoMAC using all model's Degrees-of-Freedom (DOFs) a perfect correlation would be obtained. Otherwise considering just a subset of the measured DOFs, the diagonal AutoMAC terms (corresponding modes) will still be unitary, but the off diagonal terms will not be zero. This helps to verify if the chosen accelerometers layout will allow discerning the measured modes. Figure 6.14 shows AutoMAC matrix computed on accelerometers layout presented in Figure 6.13: x and y coordinates are modes indexes and bars high represent AutoMAC value.

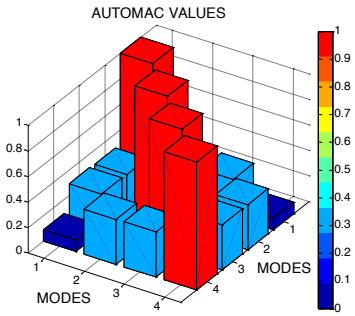

Figure 6.14 AutoMAC example

It is important to point out that both MAC and AutoMAC are global indices, i.e., they give a general metric of correlation but they are not able to give information about which part of the structure is responsible of eventual inaccuracy in mode shapes prediction. Furthermore, the AutoMAC is computed assuming that the predicted modes will give a good approximation of the real modes. For this reason after the EMA another AutoMAC test is performed on the experimental data. AutoMAC values are considered acceptable if maximum off diagonal value is lower than a specific value (0.4 in this work). If this condition is not satisfied accelerometers layout must be rearranged.

6.4.2. **EMA**

Once pre-test operations have been carried out, Experimental Modal Analysis (EMA) is performed. Basically it consists in exciting the tested structure in correspondence of the points chosen in pre-test phase, and measure accelerometer responses. The outputs of the measurements are the ratios between accelerometers response and excitation force, i.e., the FRFs. Natural frequencies and mode shapes are yielded from the FRFs using a specific algorithm for modal parameter estimation. The excitation method chosen to perform the analysis has been impact testing [63]. It consists in exciting the structure with an impulsive force produced by an impact hammer equipped with a force sensor. The alternative method is to excite the structure with vibration shakers. In this work EMA is performed by impact hammer testing.

The most important advantage of the excitation instrument is reduced analysis and setup time. In fact the basis of this excitation technique is that an impulsive load excites a large frequency bandwidth, so one hit excites the whole frequency measurement range. Shakers instead require more time to set-up and excite all the frequency range. Figure 6.15 shows impact testing execution on dummy tool.

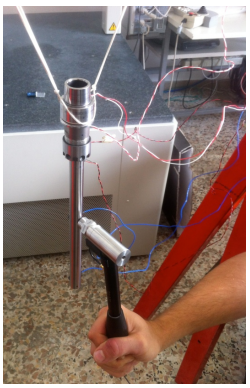

Figure 6.15 Impact testing on dummy tool.

It is not mandatory for EMA to acquire the complete matrix since for the reciprocity condition [63] a subset of FRFs allows to correctly identify modal parameters. Tests have been carried out using roving hammer procedure: it means that accelerometers positions have been kept fixed during tests execution and FRFs matrix has been acquired exciting all chosen points. Table 6.2 lists the accelerometers used in experimental modal analysis and reports their main technical features.

Table 6.2: Accelerometer used for EMA.

Accelerometer Manufacture	Acceleromter Model	Nominal Sensitivity (mV/g)	Mass (kg*10^-3)
PCB	35c22	10	0.5
PCB	u35c22	10	0.5
PCB	3252c67	100	2
ENDEVECO	2250am10	10	0.5

Accelerometers have been calibrated before each test, using a Bruel and Kjiaer handheld shaker type 4294 operating at fixed frequency (159.15 Hz) and known velocity (10 mm/s RMS).

EMA is usually carried out testing components in free-free conditions, since if the FE model is validated in absence of constraints then it can be used in other analysis where it is coupled with other models. Otherwise if a constrained condition had been validated, it would have been hard to remove constraint from the model in order to use it in other analyses. During tests, the free-free condition is realized suspending the toolkit from a support framework with soft springs, that should be as compliant as possible in order to approximate the absence of constraints [63]. Although suspension could add a resonance frequency (the suspended system can be approximated as a single DOF system), this would be very low and not affect measures accuracy. Figure 6.16a exemplified accelerometers layout and free-free condition realization.

a) 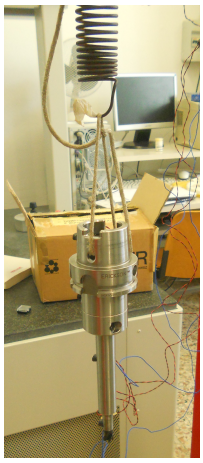 b) 

Figure 6.16 EMA of tool 1: (a) free-free condition realization, (b) LMS Scadas III data acquisition system.

Data acquisition and signal conditioning has been carried out using a LMS Scadas III frontend system and LMS Test.Lab software, as shown in Figure 6.16b. Scadas system handles all signal conditioning operations like anti-aliasing filtering, signal amplification, force signal windowing, accelerometers signals windowing and FRFs computing. Scadas hardware can be directly controlled via LMS Test.Lab software, allowing reducing pre process time during tests execution.

Correct load application is important during impact testing, since it should be as similar as possible to an ideal impulsive force applied in the desired direction. An incorrect hitting could produce noisy FRFs measurements, and a wrong load application direction could lead to a wrong FRFs estimation. For this reason, FRFs measurements are repeated during tests, and an average measurement is taken in order to compensate the aforementioned errors. In this work, every measure has been evaluated as the average of ten hits. Despite these cautions a quality check of measured FRFs is required, a widely used parameter for these evaluations is coherence function. Coherence estimates the power transfer between input and output of a linear system. Coherence between two signals x(t) and y(t) is a real-valued function that is defined as:

$$C_{xy}(f) = \frac{\left|G_{xy}(f)\right|^2}{G_{xx}(f)G_{yy}(f)} \tag{6.17}$$

where $G_{xy}(f)$ is the cross-spectral density between x and y, and $G_{xx}(f)$ and $G_{yy}(f)$ the auto-spectral density of x and y respectively. For an ideal linear system with single input x(t) and single output y(t), coherence will be equal to one. In FRF estimation, coherence function is calculated between excitation and response signals and allows to perform a rapid estimation of signal to noise ratio on the measured frequency range.

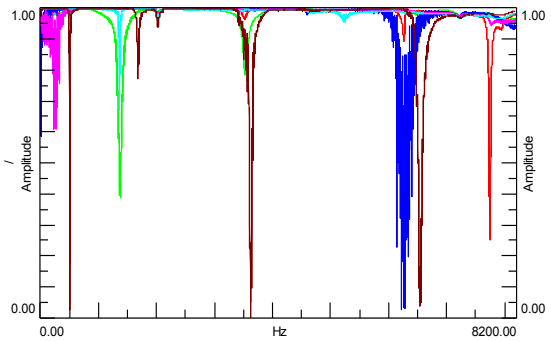

Figure 6.17 Coherence functions of configuration 1 point 1 FRFs.

Coherence functions extracted from one of the performed tests is shown in Figure 6.17 as example. This function should ideally be unitary on all the measurement bandwidth, although lower values of coherence are acceptable in correspondence of anti-resonance points because of the low accelerometer signal level. A lack of coherence usually is present in low frequency range, since piezoelectric accelerometers have a lower bound in their measurement frequency range. This inaccuracy could be present in high frequency too, since impact hammer excitation is not perfectly impulsive, therefore the applied load will have an upper bound excitation frequency, i.e., if measurement bandwidth is too large experimental FRFs could show a lack of coherence in high frequency range. A good practice is to exclude from data analysis, FRFs bandwidths having low coherence values, except for anti-resonances: in this work an acceptability threshold of 0.95 has been assumed.

After tests, modal parameter estimation has been carried out using Polymax algorithm embedded in LMS Test.Lab software. This is a frequency domain modal parameter

estimation algorithm [65], it performs a fitting of the measured FRFs with a proper complex function and evaluates natural frequencies, mode shapes and modal damping ratios.

6.4.3. Correlation

Correlation is the next step in model validation: a comparison between FE model and experimental model to evaluate the accuracy of model natural frequencies and mode shapes prediction has been carried out. Therefore FE models of selected components have been analyzed, using standard material properties values, and correlation parameters have been evaluated. In this work natural frequencies prediction accuracy is estimated using the percentage errors between computed and measured modes, while mode shapes correlation is evaluated with the MAC matrix. Standard material properties have been used for materials, which values are reported in Table 6.3, according to the units system used in FE analyses (seconds, millimeters, tons). Structural damping coefficient is not introduced in these analyses since its values does not modify natural frequencies or mode shapes [63].

Table 6.3: Materials property values used in correlation analyses.

	Young Modulus (MPa)	Poisson Ratio	Density (tons/mm^3)
Steel	2.06E+05	0.3	7.8E-09

After these preliminary considerations, correlation analysis results are presented for all the modeled tools. To evaluate models correlation quality, the following metric has been used:

- Percentage errors on natural frequencies.
- MAC matrix diagonal and extra-diagonal values.

Table 6.4 reports the correlation between dummy tool experimental and FE model in terms of natural frequencies percentage error, while in Figure 6.18 a bar plot of the MAC matrix is shown.

Table 6.4: Predicted and measured natural frequencies of Dummy Tool.

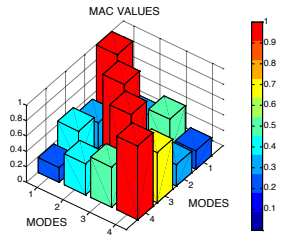

	Experimental (Hz)	Computed (Hz)	Percentage Error
Mode 1	777	799	3%
Mode 2	2110	2257	6%
Mode 3	4296	4545	7%
Mode 4	7193	7672	6%

Figure 6.18: Dummy Tool MAC matrix plot.

Despite random values of material properties have been used, percentage errors on natural frequencies are lower than 8%, and MAC matrix diagonal terms are all greater than

0.9. For this configuration the Timoshenko beam model can provide a reliable prediction of tool dynamics using standard values of material properties and rigid connection modeling.

6.4.4. **Model updating**

Starting from experimental results is possible to improve FEM-experimental correlation results performing a model updating operations. This step consists in carrying out an optimization to find the uncertain models parameters, for example material properties that provide the best correlation with experimental data. This phase can be useful if tool modeled is going to be used in further analyses where it is coupled with other components. This improvement could be very interesting for hybrid approach application, considering the need of very high accurate model to reach accurate tool-tip FRF prediction, key factor for a correct SLD prediction. The main drawback is this procedure requires experimental test. A model updating has been carried out on dummy tool as example. Uncertain model parameters have been identified:

- Young modulus.
- Density.
- Poisson ratio.
- Shear factor.
- Accelerometers positions.
- Accelerometers masses.

Material properties values are not known, since Young modulus, density and Poisson ratio can be different from the standard values assigned in correlation analyses. Shear factors are another uncertain parameters, since their formulation is based on approximations [59] of cross section shearing stiffness yielded for continuous structures. Since the modeled configurations are constituted by different components linked together, Shames formulation might not be accurate enough to estimate shearing stiffness. For this reason a shear factor correction coefficient has been introduced, as stated in equation (6.18):

$$\left[k^{c}{}_{s1} \cdots k^{c}{}_{sn}\right] = \lambda\left[k_{s1} \cdots k_{sn}\right] \tag{6.18}$$

k_{sj} is the shear factor of the j^{th} beam element, λ is the shear factor correction coefficient and k^{c}_{sj} is the corrected shear factor for the j^{th} beam element. Correction coefficients acts as a scale parameter for beams shear factors, modifying them proportionally to their values. If λ is unitary, Shames formulation is applied, while if it is zero valued shear stiffness is not considered and Timoshenko model becomes equal to Euler beam model. A parameter that has not been considered in correlation analyses is accelerometers mass loading effect, i.e., accelerometers can modify dynamics of the tested structure since additional mass is introduced. Despite these measurement instruments have very low masses, their effect could be relevant because of high values of component natural frequencies that make them more sensitive to small variations of mass and geometry. Mass loading effect can be considered positioning grid points in correspondence of accelerometers locations and introducing concentrated mass elements in these nodes. These elements have no stiffness matrix, and their mass matrix is defined in equation (**6**.**19**):

$$M_{acc} = \begin{vmatrix} m_{acc} & 0 & 0 \\ 0 & m_{acc} & 0 \\ 0 & 0 & m_{acc} \end{vmatrix} \tag{6.19}$$

where m_{acc} is accelerometer mass. These elements can be included in the assembling process assigning them zero values to the terms corresponding to rotational DOFs. Hence, to perform a correct modeling of mass loading effect it is necessary to accurately identify accelerometers positions and masses. This operation could be difficult, since errors could be present in accelerometers positions measurement and accelerometers masses could not be the effective additional masses since their wires could contribute to mass loading effect. Hence, accelerometers masses and positions have been included in model updating operation.

Model updating optimization has been performed using the genetic algorithm implemented in Matlab Global Optimization Toolbox ® *ga* function. This routine performs constrained and unconstrained optimizations with genetic algorithm method allowing to solve global minimum problems. Design variables have been defined as the previously identified uncertain parameters. The genetic algorithm fitness function has been defined as stated in equation (**6**.**20**).

$$F(\vec{D_v}) = 0.4\frac{\left|f^{FE}{}_{n1}(\vec{D_v}) - f^{\exp}{}_{n1}\right|}{f^{\exp}{}_{n1}} + 0.25\frac{\left|f^{FE}{}_{n2}(\vec{D_v}) - f^{\exp}{}_{n2}\right|}{f^{\exp}{}_{n2}} + \\ + 0.2\frac{\left|f^{FE}{}_{n3}(\vec{D_v}) - f^{\exp}{}_{n3}\right|}{f^{\exp}{}_{n3}} + 0.15\frac{\left|f^{FE}{}_{n4}(\vec{D_v}) - f^{\exp}{}_{n4}\right|}{f^{\exp}{}_{n4}} \tag{6.20}$$

- $f^{FE}{}_{nj}$ is the j^{th} natural frequency of the FE model.
- $f^{exp}{}_{nj}$is the j^{th} natural frequency of the experimental model.
- D_v is the design variables vector.

Fitness function defined in this work is simply a weighted sum of relative errors on natural frequencies. Weights have been introduced in order to have a better approximation on the lowest frequencies modes, therefore their values have been assigned as stated in equation (**6**.**20**) (their sum must be one). Fitness function evaluation consists in running a modal analysis and reading the natural frequencies corresponding to the required modes, i.e., the first four flexural shapes. The method used to locate the required frequencies is to locate the first four modes, which have the successive one with the same natural frequency. A Matlab code has been implemented to perform the presented operations. Fitness function does not consider MAC values for two main issues: a) it is reasonable to assume that design variables modifications would not significantly affects mode shapes correlation, b) introducing them in the fitness function could complicate its formulation affecting optimization results. For these reasons MAC values have been checked after the optimization, in order to verify that model updating would not have affected modes correlation. In order to force the genetic algorithm not to introduce non-physical combinations of design variables, lower and upper boundaries constraints have been introduced, as reported in Table 6.5.

Table 6.5: Design variables boundaries.

Optimization Lower bound					
	Young Modulus (MPa)	**Poisson ratio**	**Density (tons/mm^3)**	**Correction Coefficient**	
	1.9E+5	0.21	7.7E-9	0.1	
Accelerometers Positions – Z coordinate (mm)					
4.5	124.5	209.5	222.5	248.5	270.5
Accelerometers Masses (tons)					
4.0E-7	4.0E-7	4.0E-7	4.0E-7	2.5E-6	3.0E-6

Optimization Upper bound					
	Young Modulus (MPa)	**Poisson ratio**	**Density (tons/mm^3)**	**Correction Coefficient**	
	2.06E+5	0.33	7.99E-9	1.0	
Accelerometers Positions – Z coordinate (mm)					
7.5	127.5	212.5	224.5	251.5	273.5
Accelerometers Masses (tons)					
6.0E-7	6.0E-7	6.0E-7	6.0E-7	3.0E-6	4.0E-6

Table 6.6 reports model updating results in terms of percentage errors on natural frequencies. Negative values of these parameters mean that computed natural frequencies are lower than the experimental ones. Table 6.7 reports the optimized model parameters.

Table 6.6: Model Updating results.

	Mode 1	Mode 2	Mode 3	Mode 4
Experimental	777	2110	4296	7193
Starting FEM	799	2257	4545	7672
Updated FEM	777	2155	4202	6847
Starting FEM (Percentage Error)	3%	7%	6%	7%
Updated FEM (Percentage Error)	0%	2%	-2%	-5%

Table 6.7: Optimized model parameters.

	Young Modulus (MPa)	**Poisson ratio**	**Density (tons/mm^3)**	**Correction Coefficient**	
	2.01+5	0.2309	7.87E-9	0.3316	
Accelerometers Positions – Z coordinate (mm)					
5.74	127.29	211.21	224.06	249.42	270.68
Accelerometers Masses (tons)					
5.89E-7	5.53E-7	5.99E-7	5.60E-7	2.79E-6	3.00E-6

Figure 6.19 shows a comparison between MAC matrices of the starting and the updated model.

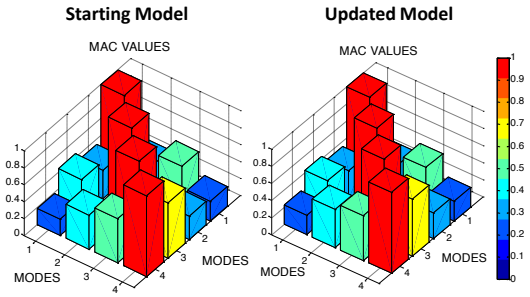

Figure 6.19: Comparison of starting model and updated model MAC matrices.

It is clear that the proposed model updating procedure caused just a reduction of natural frequencies percentage errors and did not compromised mode shapes correlation. A lower value of shear factor has been identified.

Model updating operation can be performed also on structural damping coefficient. As earlier mentioned, this parameter does not affect natural frequencies that are independent from its values, furthermore according to structural proportional damping model, resonance frequencies are equal to natural frequencies [63]. Hence, if this model is applied, damping value affects only resonance peaks magnitude without modifying their positions. Therefore since beam model natural frequencies have already been optimized, a further optimization can be carried out to minimize the difference between experimental model FRFs resonance peaks magnitude and the ones of the FE model. This operation can be performed using one or more FRFs. Optimizing peaks values on a single FRF could lead to an inaccurate damping estimation. Otherwise experimental FRFs could have different coherence function values, hence some FRFs could have a lack of accuracy that could compromise correct damping estimation. In this work one driving point FRF corresponding to the first accelerometer (the closest to tool tip) has been optimized as example.

This analysis has been carried out using the Matlab® *fminbnd* function that performs constrained optimizations with a gradient based method. The objective function has been defined as reported in equation (**6**.**21**):

$$F(\eta) = \sum_{i=1}^{n} w_i \left| \frac{G_{kj}^{FE}(f_i^{FE}, \eta) - G_{kj}^{Exp}(f_i^{Exp})}{G_{kj}^{Exp}(f_i^{Exp})} \right| \tag{6.21}$$

1. Subscript I rows from 1 to n that is the number of optimization modes (peaks).
2. G_{kj}^{FE} is the selected FRF computed with the FE model.
3. G_{kj}^{Exp} is the selected FRF of the experimental model.
4. f_i^{FE} is the i^{th} natural frequency of the FE model.
5. f_i^{Exp} is the i^{th} natural frequency of the experimental model.
6. w_i are modes weights.

The objective function is similar to the one adopted for natural frequencies optimization, i.e., a weighted sum of relative errors on peaks magnitude values that are computed as FRF values in correspondence of models natural frequencies. In this optimization weights values equal to the ones of equation (**6**.**20**) have been used. Objective

function evaluation involves FE model FRF analysis, that has been performed using direct computing method. The proposed optimization technique lead to the identification of an optimal value of damping coefficient η=0.1398. Figure 6.20 shows a comparison between the FRF computed with the optimized damping value and the one computed with η=0.

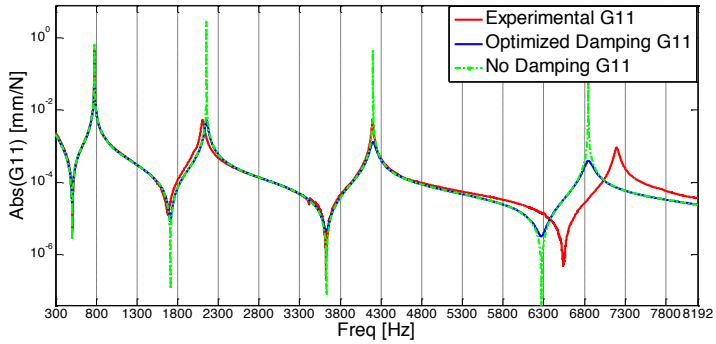

Figure 6.20: Comparison between optimized damping and no damping FRF (Magnitude, log scale).

The proposed damping estimation procedure provides a good estimation of structural damping coefficient, allowing to correctly compute tool FRFs values. Method performances should be deeper investigated, including more than one FRF in the objective function in order to find the most reliable procedure.

In conclusion model updating technique allows to reduce percentage errors on natural frequencies and to correctly estimate structural damping coefficient for the tested tool, without compromising mode shapes prediction accuracy. However it requires that tool is experimentally characterized, therefore they are not directly implementable in industrial application. Otherwise this operation allowed to understand how influent shear stiffness can be in tool modal behavior modeling. Model updating technique could be useful to identify an experimentally based correlation between tool slenderness, tool clamping system and shear factor correction coefficient λ. This could be an interesting way to make the beam models suitable even for thick tools dynamics modeling.

6.5. Results

Model validation strategies presented in the previous section has been applied to toolkit test cases in order to investigate modeling strategies: both 1D modeling and 3D modeling have been compared to experimental results. Tools manufacturers propose a wide range selection of milling tools and holder. In this work six different toolkits have been tested, two main parameters have been taken into account to select the different configurations:

- Tool holder - end mill clamping system.
- Component slenderness.

Clamping system is an important parameter as reported in literature (an overview is presented in Chapter 7): in the modeling approaches presented in this Chapter, components connections are treated as rigid, therefore it is important to understand in which cases this

approximation is correct. Moreover tool slenderness is crucial because 1D beam elements can be theoretically used to model components with high length to thickness ratio, therefore it is important to understand which is the limit of this approach. Considering the mentioned issues, tests configurations have been chosen as outlined in Table 6.8. Tested toolkit are presented in Figure 6.21.

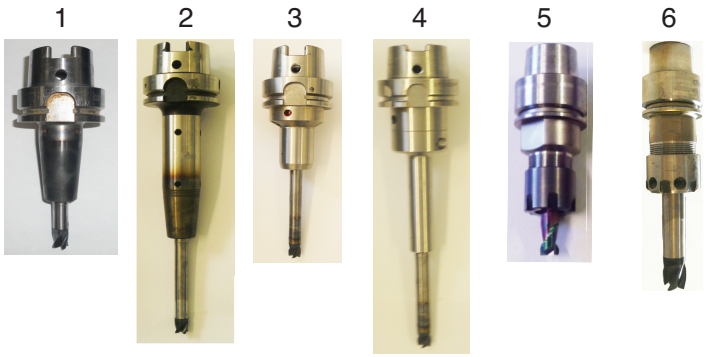

Figure 6.21 Tested toolkits

Table 6.8 Tested toolkits (tool and tool-holder)

N°	Spindle Connection	Holder	Holder connection	Shank length (mm)	Overhang (mm)	Tool Diameter (mm)	Number of flutes
1	HSK63	12x90	Shrink Fit	70	41	12	4
2	HSK63	12x160	Shrink Fit	130	100.5	12	4
3	HSK63	12x90	Hydraulic	130	98	12	4
4	HSK63	12x170	Hydraulic	130	100.5	12	4
5	HSK32	ER16	Collet	-	19.5	8	2
6	HSK32	ER20	Collet	70	48.9	12	4

Three different clamping systems have been tested:

- Shrink fit: tool-holder is heated up to cause thermal expansion of tool housing, allowing the end mill to fit in;
- Hydraulic chuck: a piston compresses a fluid inside a pressure chamber surrounding tool bore, the deformation of pressure chamber allows tool clamping.
- Collet chuck: tool is housed inside a deformable component (collet) that is tightened around tool shank by means of shaped bolt (nut), providing the required connection force;

Different holder and overhangs have been used in order to test different toolkit slenderness: in particular for each connection one short and one long toolkit are selected. To perform correlation steps, all the tested assemblies have been modeled using 1D beam and 3D solid modeling approach as explained in sections 6.2 and 6.3. Holder components are

made of steel, shanks (used in 5 of 6 toolkit) are constituted by two welded component made of steel and carbide, end-mills are made of carbide.

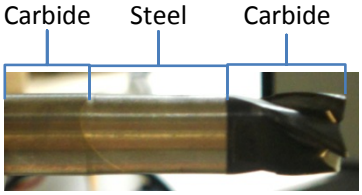

Figure 6.22 End mill used in configuration 1, 2, 3, 4 and 5.

Figure 6.22 shows the assembly shank and end mill used in the first 5 configurations. These material discontinuities cannot be neglected for low slenderness, since carbide density and Young modulus are significantly different with respect to the steel: they are hence introduced in 3D solid model and 1D beam model. Standard material properties have been used for carbide and steel, values are reported in Table 6.3.

Table 6.9: Materials property values used in correlation analyses.

	Young Modulus (MPa)	Poisson Ratio	Density (tons/mm^3)
Steel	2.06E+05	0.3	7.8E-09
Carbide	6.60E+05	0.23	1.39E-08

In 1D beam modeling end-mill cutting edges are modeled as a tapered segment. This has been done since modeling cutting segment as a solid cylindrical segment will bring to an overestimation of its mass. Therefore tool tip radius has been chosen to ensure that cutting segment beams have the same mass of the real one. In 3D solid model, edges geometry has been modeled accurately thanks to second order tetrahedral elements (CTETRA in Nastran). In this Chapter connections have been modeled as rigid both in 3D and 1D modeling techniques. With respect to hydraulic and shrink fit toolkit, collet chuck toolkits are characterized by higher number of components (nut, collet, holder and tool) and no-axisymmetric collet geometry. This leads to a higher modeling complexity. However in this Chapter their geometry has been simplified as axisymmetric, both for 1D beam modeling (not able to reproduce such complex geometry) and for 3D modeling in order to reduce modeling effort. Axisymmetric 3D modeling is presented in Figure 6.23 to show this modeling strategy.

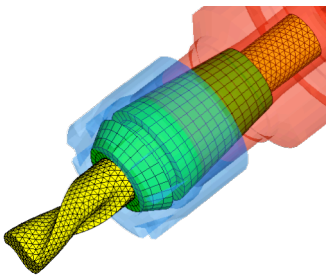

Figure 6.23 Axisymmetric collet for simplified solid 3D modeling

Models and natural frequencies comparison results for the six configurations are shown in Table 6.10-Table 6.15. For the sake of brevity MAC matrices are not presented since they all report good agreement on mode shapes reproduction without significant differences between 1D and 3D modeling.

Table 6.10 Correlation report on toolkit 1 (Shrink Fit – Short)

Figures			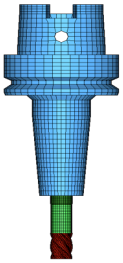	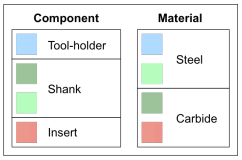	
Modes	**Experimental (Hz)**	**1D beam model (Hz)**	**3D solid model (Hz)**	**1D beam Error**	**3D solid Error**
1	4296	4631	4249	7.8%	-1.1%
2	8635	9665	8628	9.4%	-0.1%

Table 6.11 Correlation report on toolkit 2 (Shrink Fit – Long)

Figures		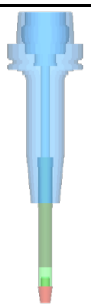	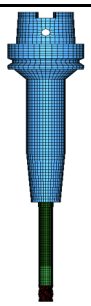	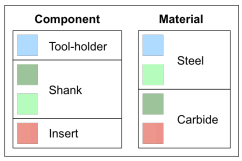	
Modes	**Experimental (Hz)**	**1D beam model (Hz)**	**3D solid model (Hz)**	**1D beam Error**	**3D solid Error**
1	1195	1254	1204	5.0%	0.7%
2	3423	3469	3420	1.3%	-0.1%
3	5698	5505	5776	6.5%	1.4%
4	9121	9508	9290	4.2%	1.9%

Table 6.12 Correlation report on toolkit 3 (Hydraulic – Short)

Figures			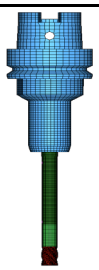	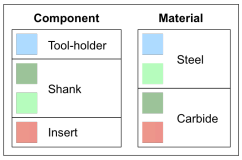	
Modes	**Experimental (Hz)**	**1D beam model (Hz)**	**3D solid model (Hz)**	**1D beam Error**	**3D solid Error**
1	1304	1531	1452	17.4%	11.4%
2	4785	5696	5336	19.0%	11.5%
3	8862	10177	9684	14.8%	9.3%

Table 6.13 Correlation report on toolkit 4 (Hydraulic – Long)

Figures		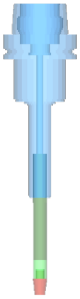	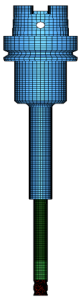	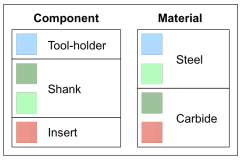	
Modes	**Experimental (Hz)**	**1D beam model (Hz)**	**3D solid model (Hz)**	**1D beam Error**	**3D solid Error**
1	837	912	886	8.9%	5.7%
2	2186	2355	2260	7.8%	3.4%
3	4776	5045	5085	10.8%	6.5%
4	7978	8927	8517	11.9%	6.8%

Table 6.14 Correlation report on toolkit 5 (Collet – Short)

Figures			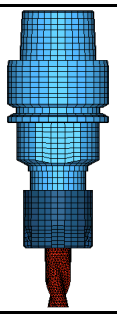	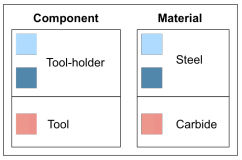	
Modes	**Experimental (Hz)**	**1D beam model (Hz)**	**3D solid model (Hz)**	**1D beam Error**	**3D solid Error**
1	10401	11670	10612	12.2%	2.0%
2	16895	19193	17543	13.6%	3.8%

Table 6.15 Correlation report on toolkit 6 (Collet – Long)

Figures		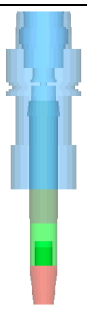	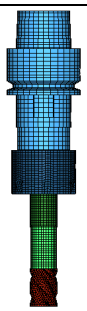	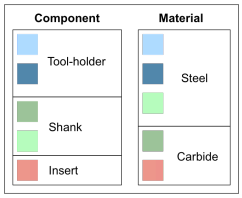	
Modes	**Experimental (Hz)**	**1D beam model (Hz)**	**3D solid model (Hz)**	**1D beam Error**	**3D solid Error**
1	4610	5284	4686	14.6%	1.7%
2	12744	14182	12869	11.3%	1.0%

Results shown in the tables suggest that beam models are not always suitable for toolkit dynamics simulation in free-free boundary condition. Particularly, beam model fails in presence of low slenderness (toolkit 1, 3, 5), as expected. For what concern holder-tool connection, only shrink fit is able to return high-accurate results (about 5% error on toolkit 2), on the contrary beam model looses accuracy on hydraulic and collet chucks. Low slenderness issue can be fixed with 3D solid modeling strategy that results in better accuracy on all the toolkits. Even though on shrink fit solid models return very high accuracy (about 1% error) on both long and short toolkit, for different connections this modeling approach is less accurate: particularly for hydraulic chuck 3D solid modeling approach seems to fail in reproducing accurately toolkit dynamic behavior (error > 5% for hydraulic toolkits). These results can be summarized in Figure 6.24 in which average error of the first two modes for each toolkit is shown in a bar plot.

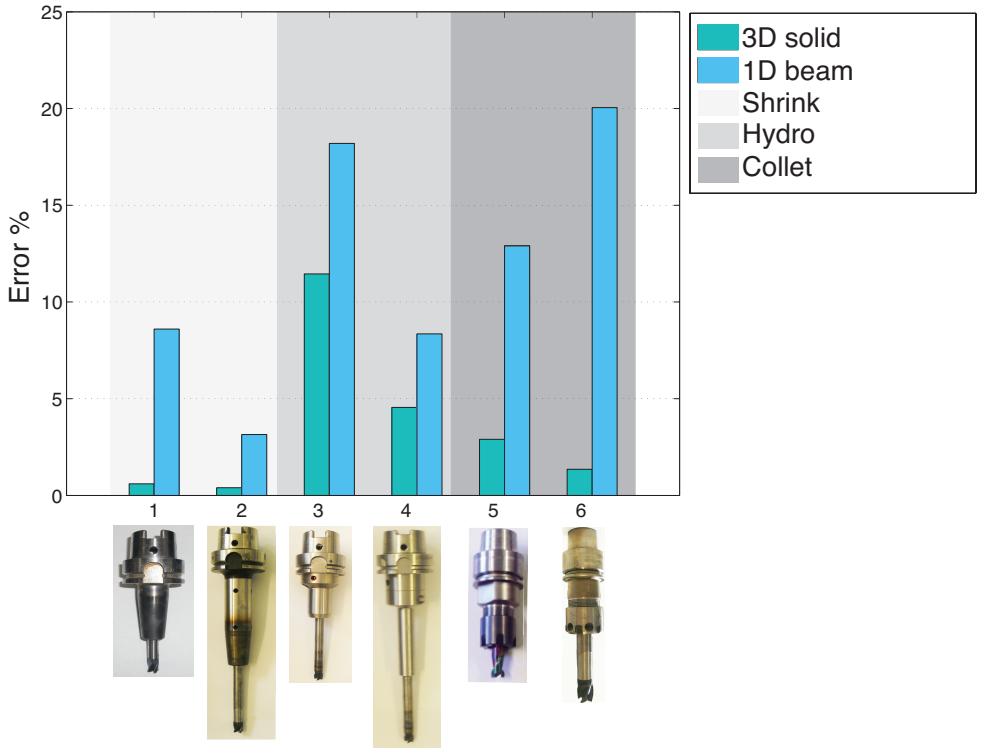

Figure 6.24 1D and 3D modeling errors on selected toolkits

Figure 6.24 shows how shrink fit connection is the easiest to model, both 1D and 3D modeling return good results, on the other hand the most complex one seems hydraulic connection, not accurately modeled both via 1D and 3D models.

6.6. Conclusion

In conclusion in this chapter 1D and 3D modeling technique have been presented, developed beam algorithm, able to quickly and easily implement beam approach, has been proposed. Model validation method has been explained and a model updating procedure has been proposed to improve correlation parameters between model and experimental results.

Dynamic correlation has been applied to six different toolkits. Modeling strategies performances have been tested selecting different configurations. Two main parameters are investigated: slenderness and holder-tool clamping system.

Results show that 1D modeling is influenced by slenderness, as beam theory suggests. Moreover holder-tool connection seems to be a crucial factor for dynamics prediction both for 1D and 3D modeling strategies.

In the next chapter this aspect will be examined and a novel modeling technique will be suggested to overcome modeling issues here presented.

7. Holder-tool connection modeling

7.1. Overview

As observed in the previous chapter, one of the key factors to achieve an accurate dynamic toolkit model is a proper joint modeling. This aspect has been already highlighted in literature. Spindle-holder joint has been studied: Hanna et al. [66] presented an analysis on HSK interface investigating stresses generated by spindle drawbar forces and rotational speed; Namazi et al. [45] presented a modeling and iterative identification technique for tool holder–spindle interface using translational and rotational springs uniformly distributed at the contact zone. Recently Xiao et al. [67] proposed a new technique based on a "tapered zero-thickness finite element" to model connection stiffness between spindle and BT holder: to characterize this element an experimental iterative procedure is used.

Nevertheless for RCSA application the most interesting joint is between holder and tool. Modeling holder-tool connection is not an easy task because of the different types (e.g., collet chuck, shrink fit and hydraulic clamping) and the influence of this connection on accuracy of toolkit model. For this reason, most of the RCSA approaches have been applied to simple connection type (easier to be modeled), such as thermal shrink fit [52, 68]. In some works [50, 51] authors preferred to model just the tool (i.e., endmill) without the holder: connection modeling is hence avoided but experimental modal test is required for every new holder clamped on the machine, making RCSA approach less effective and efficient.

On the other hand, several papers investigate this connection by means of lumped stiffness applied between holder and tool model: Movahhedy et al. [69] proposed a joint modeling method with two parallel linear springs, Ahamadi [54] used a distributed elastic layer including damping, Ostasevicius et al. used elastic elements placed at fixed nodes connected to the holder both for turning [70] and drilling [56] tools. However all these methods introduce an iterative procedure based on experimental tests to identify connection stiffness: elastic elements parameters are identified minimizing difference between measured and calculated FRFs of the tool-holder assembly. Therefore each connection requires a new modal test on the toolkit increasing the number of tests required.

Table 7.1 Connection modeling literature summary

First Author Ref.	Year	Paper's Scope	Cutting process	Connection technique	Identification method	Toolkit connection
Schmitz [39]	2000	Chatter SLD	Milling	Lumped stiffness	Experiments	Collet

First Author Ref.	Year	Paper's Scope	Cutting process	Connection technique	Identification method	Toolkit connection
Schmitz [52]	2001	Chatter SLD	Milling	Lumped stiffness	Experiments	Collet
Schmitz [68]	2007	Tool-tip FRF	Milling	Modeling Shrink Fit	FE	Shrink-fit
Hanna [66]	2003	Stress investigation	Milling	Modeling HSK spindle connection	FE	Collet Φ 19.05 mm
Park [27]	2003	Tool-tip FRF	Milling	No connection	Only tool modeled	Collet Φ 19.05 mm
Erturk [44]	2006	Tool-tip FRF	Milling	No experimental validation	Values from other works	Collet
Namazi [45]	2006	Tool-tip FRF	Milling	Lumped stiffness	Experiments	
Ahmadi [54]	2007	Chatter SLD	Milling	Distributed parameter interface	Experiments	
Ostsevicius [56]	2012	Modal response	Drilling	Lumped stiffness	Experiments	Φ 10 mm
Albertelli [50]	2013	Chatter SLD	Milling	Lumped stiffness	Experiments	Collet Φ 8-14 mm

As clear form Table 7.1, despite all the presented methods, a likely connection modeling technique taking into account real contact behavior has not been developed: as consequence experimental measurements are needed to overcome connection modeling issue. The goal of RCSA methods is to reduce the number of tests required in order to apply vibrations predictive methods on shop floor, therefore the requirement of new experimental tests makes this method less attractive, limiting its industrial diffusion.

In this Chapter modeling strategies of holder-tool connection are presented, focusing on milling application. Proposed procedures are fully implemented in FE environment without the use of any tuning experimental test. Solid finite elements are used to model the most common connection types: collet chuck, shrink fit and hydraulic clamping. The main advantage of these novel modeling approaches is to model connection and contact properly without requiring lumped stiffness and iterative identification procedures.

The goal of proposed techniques is to return modeling guidelines for toolkits in dynamics applications and extend the industrial diffusion of vibrations predictive methods thanks to a significant reduction of experimental tests required.

Modeling strategies are presented in section 2 divided in subsections for each type of connection, in section 3 experimental validation performing EMA on different test cases is provided.

7.2. Proposed approach

As earlier mentioned, traditional connection modeling techniques are based on regressive approaches, in which spring elements are introduced between tool and holder and their stiffness is tuned to fit modal behavior of a test case toolkit, yielded by EMA. The main drawback of these approaches is the need of carrying out experimental tests for each tool holder required to be modeled. This because different tool holder geometries and clamping systems will have different connection stiffness, therefore every tool holder requires its own tuning phase.

In this work is proven that regressive approach can be replaced by an accurate modeling of contact conditions between toolkit components. The goal is to develop a fully predictive modeling technique to avoid the experimental testing phase. The basic idea of the proposed approach is that connection spring elements are not required to implement an accurate contact stiffness model. One of the main reasons because those elements are introduced, is that toolkit (holder-tool assembly) components are modeled by using simplified one dimensional (1D) techniques, such as Timoshenko beams, that may not be accurate in reproducing contact conditions. Therefore, springs do not represent the likely contact stiffness but compensate modeling inaccuracies instead. In this work the regressive approach is overcome by investigating toolkit connection to identify the key factors for a correct contact stiffness evaluation in a FE model, such as contact region extension or accurate component modeling. Toolkit components are modeled using three dimensional (3D) elements; this strategy allows to correctly simulate the contact between tool and holder. Same procedure presented in section 6.3 is applied to proposed modeling approach. Toolkit components (holder-tool) are assembled by means of MSC Nastran glued contact feature [13]: a linear double sided contact algorithm that allows joining components with non conformal interfaces, i.e., different meshes. The reason of using such a solution is twofold: it allows to achieve a better component description since mesh pattern and size can be different with respect to the component, and it reduces pre-processing time since conformal mesh interfaces are not required.

As highlighted in Figure 7.1, where proposed modeling workflow is shown, different connections follow specific pre-processing operations requiring different modeling efforts. Details of modeling procedures are given in following sub-sections.

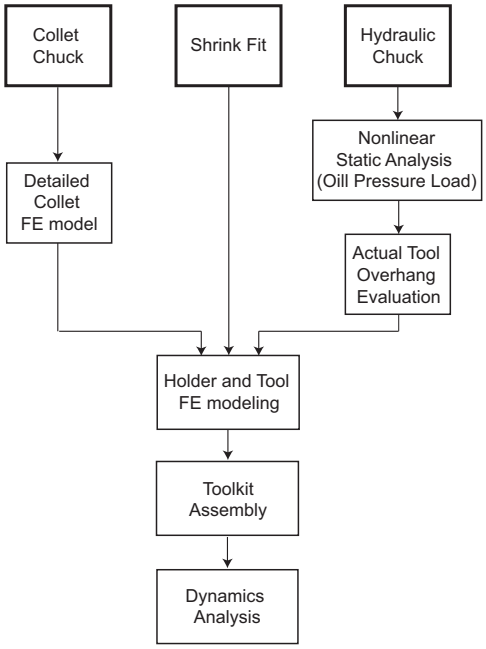

Figure 7.1 Workflow of the proposed modeling techniques

7.2.1. Collet Chuck

In Figure 7.2a an example of conical collet chuck tool holding is presented.

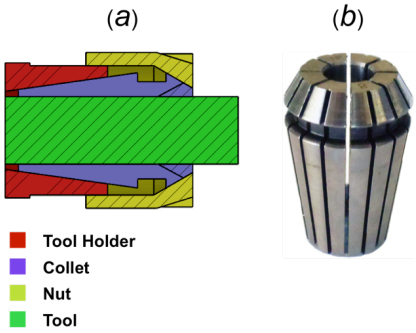

Figure 7.2 Collet chuck connection example (a) and tapered collet detail (b).

Nut fastening pushes the collet inside its conical housing, tightening tool shank. Collet shrinkage clamps the tool inside the holder, allowing spindle torque to be transmitted during milling operations. In accordance with previous considerations, in this connection type, tool and holder are not directly in contact because of the collet, making such component crucial for correct contact stiffness evaluation.

Proposed modeling technique is based on including collet in toolkit model, avoiding excessive approximation of its geometry to achieve an accurate dynamics prediction. In Figure 7.2b an example of collet (tapered class) is given. Basically it is a metallic sleeve with a sequence of longitudinal slots to increase its compliance, directly related to the available clamping force. Therefore, compared to the 3D solid modeling proposed in the previous Chapter, slots are included in the FE analysis, since a filled modeling could lead to a connection stiffness overestimation. On the other hand 1D beam modeling is not suitable for such component, since it cannot model tangential expansion that could affect dynamic compliance of assembled toolkit.

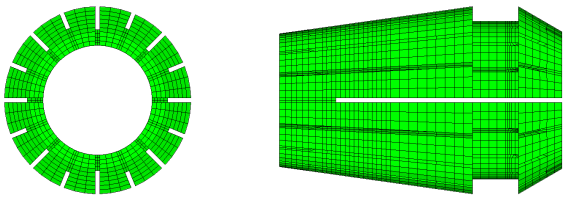

Figure 7.3 Collet model according to the proposed technique.

In Figure 7.3 an example of detailed collet modeling is given.

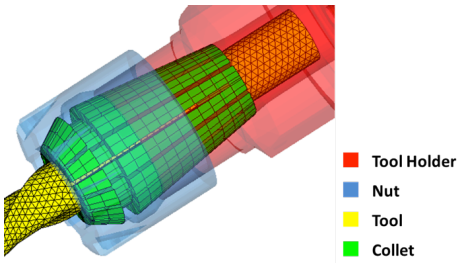

Figure 7.4 Assembled collet chuck toolkit FE model.

Figure 7.4 shows a collet chuck toolkit in assembled configuration, with the collet modeled according to the proposed technique.

7.2.2. **Shrink-fit**

In Shrink fit toolkits, holding force is provided by thermal radial contraction of the tool-holder. Figure 7.5 gives an example of this toolkit type.

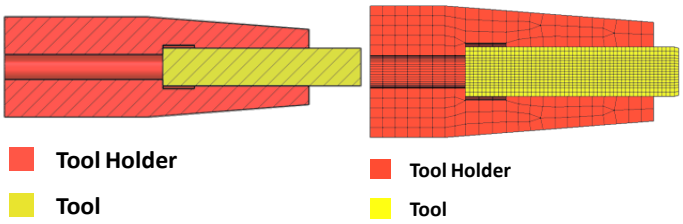

Figure 7.5 Shrink-fit connection example.

Although Schmitz et al. [68] present a complex modeling technique for shrink-fit connection, in this work, as previously presented in section 6.5, shrink-fit toolkits show good accuracy modeled with glued contact. Actually these tool-holders can provide a high flexural stiffness, since there is no component between tool and holder as in the collet chuck connection. Furthermore, since shrink fit is a tight fit connection, it is reasonable to hypothesize toolkits components to be in contact in the entire interface region. Therefore this connections type can be modeled just merging components interface nodes (or via glued contact as in this work) without using specific techniques.

7.2.3. **Hydraulic chuck**

In Figure 7.6 hydraulic chuck working principle scheme and real component cross-section are shown.

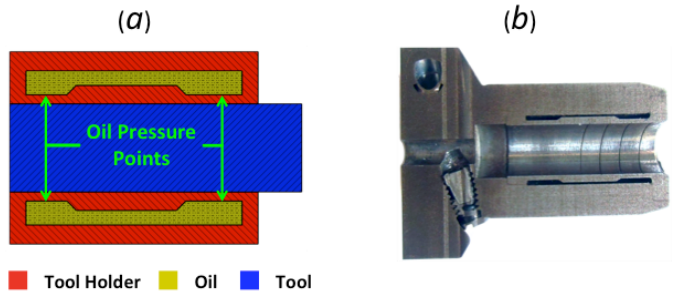

Figure 7.6 Hydraulic chuck holder scheme (a), real cross-section (b).

The oil inside the pressure chamber is compressed by means of a screw. Oil compresses tool holder, mainly in correspondence of pressure points (pointed out in Figure 7.6a), allowing tool shank to be clamped.

As in shrink-fit toolkits there is no flexible components between tool and holder, but unlike the previous connection such components could not be in contact along the entire tool housing length [71]. When oil is compressed, pressure chamber undergoes a radial deformation, tightening tool housing in correspondence of pressure points. Since pressure acts on both oil chamber inner and outer faces, the final part of tool-holder (on tool tip side) could be pushed far from tool shank.

Therefore tool could not be clamped in the front part of the housing, leading to an increased overhang [71]: this parameter must be accurately identified, since it has a great influence on toolkit modal behavior [27].

In this work, a method for actual tool overhang evaluation is proposed: holder deformation is evaluated performing a nonlinear static analysis in which oil pressure effect is simulated. A FE 3D model of the toolkit portion, corresponding to the shank clamping region, is implemented.

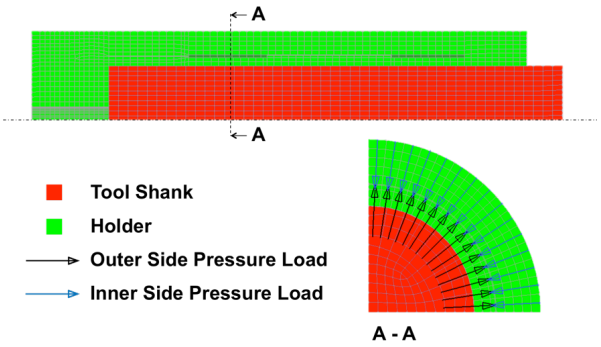

Figure 7.7 Proposed nonlinear static analysis to identify actual tool overhang

Figure 7.7 shows the proposed modeling technique. Toolkit axial symmetry is exploited, modeling just a quarter of it and applying symmetry constraints. Oil pressure is introduced in the model as pressure loads (PLOAD entry in Nastran [37]) applied on oil chamber inner and outer faces. External loads magnitude has been set to 300 MPa, considering oil pressure values range between 200 and 300 MPa [71]. It is important to remark that a likely pressure value is sufficient since the goal is not focused on accurate

toolkit deformation estimation, but on contact regions evaluation. Components contact is modeled using MSC Nastran one sided contact algorithm [37].

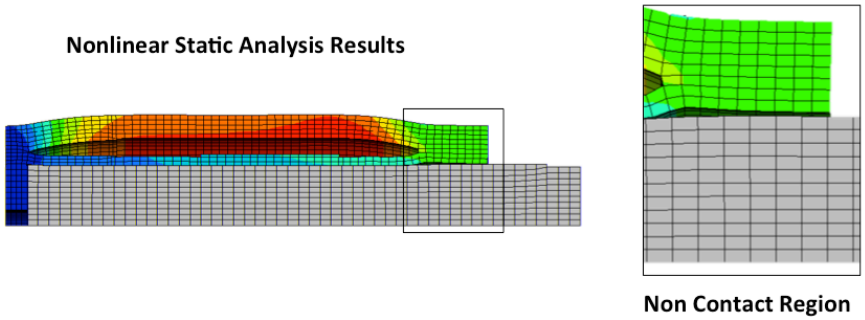

Figure 7.8 Static analysis contour plot. Model deformations increased by a factor 10.

Figure 7.8 shows analysis results. As highlighted, the front portion of tool-holder is not in contact with the tool shank, leading to an increased tool overhang. The model used for the static analysis is a reduced portion of the toolkit: its complete model, to be used for linear dynamic analyses, is created in the subsequent phase.

Nonlinear static analysis is post-processed evaluating actual tool projection length. This parameter is then used in toolkit modeling. In this phase components are meshed and then joined via glued contact. Tool and holder nodes lying in the non-contact region are not constrained, in order to model the overhang increase, while the remaining nodes are joined. In Figure 7.9 the proposed modeling technique is presented.

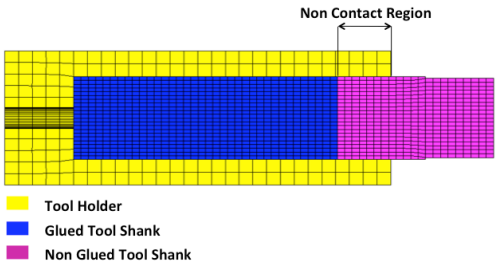

Figure 7.9 Example of the proposed method for hydraulic chuck toolkits modeling.

In conclusion the proposed hydraulic chuck modeling technique can be summarized in the following steps:

- Performing a static analysis on the pressure chamber portion of toolkit, imposing oil pressure as external load.
- Post processing static analysis to identify actual tool overhang.
- Assembling complete toolkit model without merging (or gluing) nodes lying inside the non-contact region, to accurately model contact conditions.

7.3. Experimental Validation

Proposed modeling strategies have been evaluated on the same test cases previously presented. Basically collet chuck and hydraulic toolkits (3, 4, 5 and 6) have been modeled according with the presented strategies and compared with experimental results and other modeling techniques. Particularly, collet is accurately modeled with longitudinal slots (Figure 7.10b) and compared with 3D solid axisymmetric (Figure 7.10a) as previously adopted.

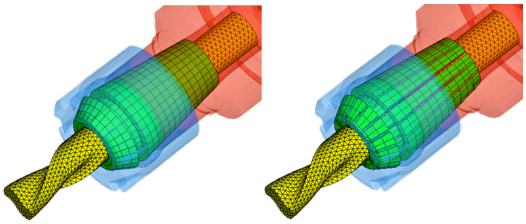

Figure 7.10 Axisymmetric collet modeling (a) and detailed collet modeling (b).

For what concern hydraulic chuck, actual overhang is calculated according with the proposed technique (Figure 7.11a) and compared with the nominal one (Figure 7.11b) used in the previous models. On the contrary shrink-fit connection does not required specific modeling technique: direct 3D modeling proposed in the previous Chapter is sufficient to return high-accurate results.

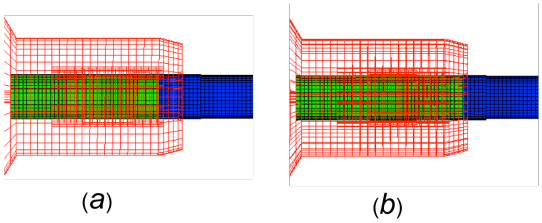

Figure 7.11 In green connection zones of proposed tool overhang (actual one) (a) and nominal overhang (b)

Results of the models comparisons are presented for toolkits 3, 4, 5 and 6 in the Table 7.2-Table 7.5. First two modes are compared.

Table 7.2 Correlation report on toolkit 3 with proposed modeling strategy

Figures			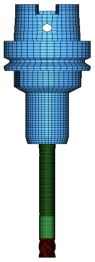		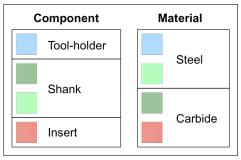		
3D modeling			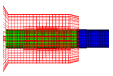 **Nominal Overhang**	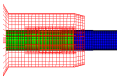 **Actual Overhang**			
Modes	**Experimental (Hz)**	**1D beam model (Hz)**	**3D solid model (Hz)**	**3D solid proposed modeling (Hz)**	**1D beam Error**	**3D solid Error**	**3D solid proposed modeling Error**
1	1304	1531	1452	1301	17.4%	11.4%	0.2%
2	4785	5696	5336	4767	19.0%	11.5%	1.5%

Table 7.3 Correlation report on toolkit 4 with proposed modeling strategy

Figures		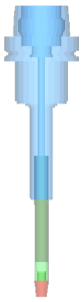	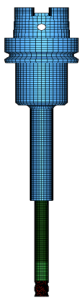	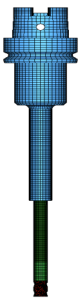	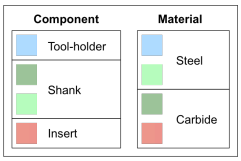		
3D modeling			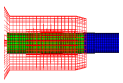 **Nominal Overhang**	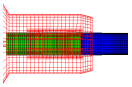 **Actual Overhang**			
Modes	**Experimental (Hz)**	**1D beam model (Hz)**	**3D solid model (Hz)**	**3D solid proposed modeling (Hz)**	**1D beam Error**	**3D solid Error**	**3D solid proposed modeling Error**
1	837	912	886	844	8.9%	5.7%	0.8%
2	2186	2355	2260	2206	7.8%	3.4%	0.9%

Table 7.4 Correlation report on toolkit 5 with proposed modeling strategy

Figures		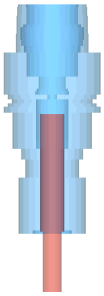	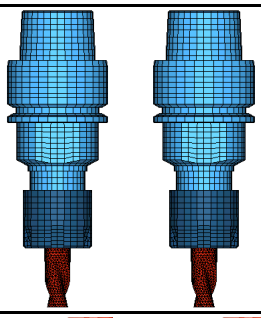		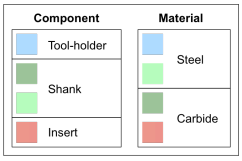		
3D modeling			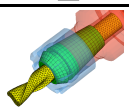 **Axisymmetric collet**	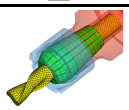 **Actual geometry**			
Modes	**Experimental (Hz)**	**1D beam model (Hz)**	**3D solid model (Hz)**	**3D solid proposed modeling (Hz)**	**1D beam Error**	**3D solid Error**	**3D solid proposed modeling Error**
1	10401	11670	10612	10379	12.2%	2.0%	-0.2%
2	16895	19193	17543	17363	13.6%	3.8%	2.8%

Table 7.5 Correlation report on toolkit 6 with proposed modeling strategy

Figures		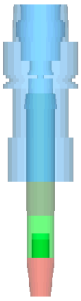	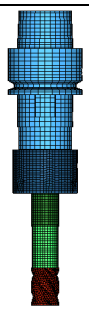		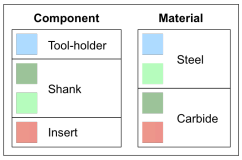		
3D modeling			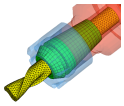 **Axisymmetric collet**	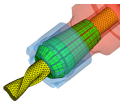 **Actual geometry**			
Modes	**Experimental (Hz)**	**1D beam model (Hz)**	**3D solid model (Hz)**	**3D solid proposed modeling (Hz)**	**1D beam Error**	**3D solid Error**	**3D solid proposed modeling Error**
1	4610	5284	4686	4634	14.6%	1.7%	0.5%
2	12744	14182	12869	12750	11.3%	1.0%	0.0%

As shown in the tables proposed modeling techniques return accurate results comparing with experimental natural frequencies in free-free boundary condition. For every toolkit an error less than 0.8% is identified on the first mode and less than 3% on the second one. Against an increase modeling complexity, higher accuracy is reached: this is crucial especially for hydraulic chuck that cannot be properly modeled with simplified modeling approaches, allowing a dramatic reduction of the provisional errors, which decrease for toolkit 3 from 17% of beam and 14% of solid to 0.2% (first mode). In Figure 7.12 histogram diagram of average errors on the first two modes is updated with the new results.

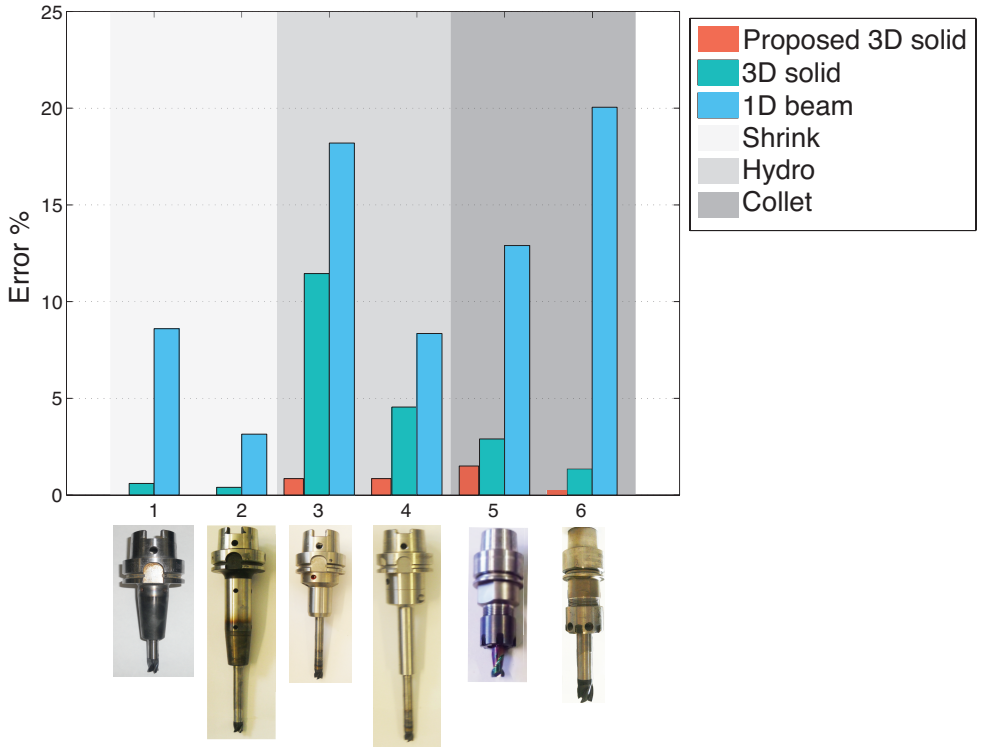

Figure 7.12 1D, axisymmetric 3D and proposed 3D modeling errors on selected toolkits

As summarized in the diagram in Figure 7.12 toolkits FE models can achieve accurate results (below 2%) if proper connection modeling is applied for all the connections analyzed.

7.4. Conclusion

In this Chapter fully predictive approaches for holder-tool connection modeling are presented. Proposed method allows achieving an accurate prediction of toolkit modal behavior without the need of experimental tests, generally used to identify connection stiffness. The most common connection types for milling application are analyzed. Specific modeling techniques are implemented for the considered connections. Experimental validation is provided. Correlation analysis between experimental and models points out that

the proposed techniques allow toolkit natural frequencies to be accurately identified. Results analyses allow the following conclusions to be drawn:

1. Collet chuck: collet geometry is important to achieve an accurate dynamics prediction. Detailed geometry connection ensures higher accuracy compared to axisymmetric approximation that leads to a slight connection stiffness increase.
2. Shrink-fit: this connection type is likely to be accurately modeled as a rigid connection. This makes shrink-fit the most suitable connection for 1D models implementation.
3. Hydraulic chuck: the increase of tool overhang during clamping operation significantly affects toolkit natural frequencies. Proposed modeling technique achieves high accurate results (less than 2% on the first two modes natural frequencies on the test cases). On the contrary toolkits models based on nominal overhang are proven to be stiffer than the real ones, leading to an unsatisfactory dynamics prediction. If an accurate prediction of toolkit dynamics is required, pre-process analysis to estimate actual tool projection length must be performed, as the one proposed in this work.

In conclusion, proposed modeling techniques provide a series of guidelines to accurately predict milling toolkit dynamics, focusing on holder-tool connection. For every analyzed connection type, critical factors affecting dynamic behavior are identified. This novel approach allows avoiding costly and time-consuming experimental tuning operations generally adopted for connection stiffness identification. Resulted accurate toolkit models are essential to efficiently evaluate tool-tip FRFs by means of receptance coupling technique, and simulate milling vibrations to select optimal cutting parameters. In next Chapter, the influence of modeling strategies on tool-tip FRFs is highlighted.

8. Hybrid experimental-numerical methods

In the last decades several authors investigated hybrid numerical-experimental approaches for tool-tip FRFs identification, in order to implement predictive models able to identify dynamics of different spindle-holder and tool configurations with the minimum set of measurements. As already mentioned, these methods are based on experimental tests on the machine without tool clamped (the fixed part), adding numerically toolkit dynamic contribution (changeable part). One of the most used coupling techniques is Receptance Coupling Substructure Analysis (RCSA), already briefly presented in Chapter 5.2.4, where it has been used to combine two FE models.

8.1. Receptance Coupling

This technique allows predicting frequency response of a specific system, combining its substructures frequency responses. The general method is presented in Ferreira and Ewins work [72] and it is going to be briefly synthesized. Let A and B be the two substructure to be coupled, let C be the assembled system. In both substructures joint and non-joint DOFs can be identified: joint DOFs describe connection points motion, while non-joint DOFs are related to the other structure points. To simplify the dissertation it is assumed that non-joint DOFs are present just in substructure A. Receptance coupling technique is based on imposing compatibility and equilibrium conditions. Compatibility conditions can be written as in equation (8.1):

$$\begin{cases} \vec{X}_{jA} = \vec{X}_{jB} = \vec{X}_{jC} \\ \vec{X}_{nA} = \vec{X}_{nC} \end{cases} \tag{8.1}$$

where X is a displacement vector, subscript j stands for joint DOFs and subscript n stands for DOFs. Basically with compatibility conditions, joint DOFs displacements in systems A, B and C are imposed to be equal, while non-joint DOFs have the same displacement in substructure A and in assembly C. Equilibrium conditions are presented in equation (8.2).

$$\begin{cases} \vec{F}_{jA} + \vec{F}_{jB} = \vec{F}_{jC} \\ \vec{F}_{nA} = \vec{F}_{nC} \end{cases} \tag{8.2}$$

where vector F represent a vector of forces acting on a specific DOFs set. These equations impose local equilibrium in each system point. Displacement and forces in systems A, B and C are linked by their receptance matrices as shown in equations (8.3), (8.4) and (8.5).

$$\begin{vmatrix} \vec{X}_{nA} \\ \vec{X}_{jA} \end{vmatrix} = \begin{vmatrix} G_{nnA}(\omega) & G_{njA}(\omega) \\ G_{jnA}(\omega) & G_{jjA}(\omega) \end{vmatrix} \begin{vmatrix} \vec{F}_{nA} \\ \vec{F}_{jA} \end{vmatrix} \tag{8.3}$$

$$\vec{X}_{jB} = G_{jjB}(\omega) \ \vec{F}_{jB} \tag{8.4}$$

$$\begin{vmatrix} \vec{X}_{nC} \\ \vec{X}_{jC} \end{vmatrix} = \begin{vmatrix} G_{nnC}(\omega) & G_{njC}(\omega) \\ G_{jnC}(\omega) & G_{jjC}(\omega) \end{vmatrix} \begin{vmatrix} \vec{F}_{nC} \\ \vec{F}_{jC} \end{vmatrix} \tag{8.5}$$

Therefore compatibility and equilibrium conditions can be rearranged introducing receptance matrices, and assembly response can be computed. It is easy to understand that this technique allows combining analytical (or numerical) and experimental models to predict assembled configuration FRFs, since it is not relevant if substructures are experimental or analytical models as long as compatibility and equilibrium conditions are respected.

As earlier mentioned, RCSA has been widely used in tool-tip frequency response prediction. T.L. Schmitz [39] is the first author to propose RCSA approach in machining field. In the paper evaluation of the tool-tip assembly response is presented, performing the following steps:

- Perform experimental characterization of the machine tool – tool holder assembly.
- Yield tool overhung portion FRFs from an analytical model (Euler-Bernoulli in his work [39]).
- Connect the two systems with an RCSA method.

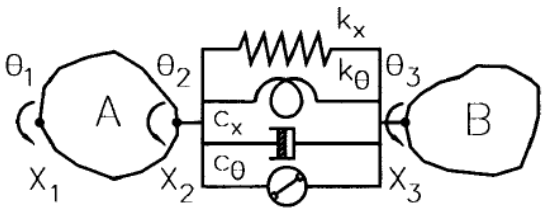

Figure 8.1 RCSA approach scheme [39]

In their paper connection stiffness between tool and tool-holder has been introduced, since a collet holder has been used (Figure 8.1). Authors affirm that this tool-clamping device cannot be considered rigid: compatibility conditions are not respected if collet compliance is not considered. RCSA allows the presence of compliant connection [72], but their stiffness and damping have to be identified. Schmitz's method [39] is suitable to include rotational degree of freedom responses: it means that in its RCSA formulation, compatibility and equilibrium conditions can be applied to points rotations too. Although this possibility, these conditions were not been considered, because experimental evaluation of rotational responses can present several complications. This modeling path has been proven to lead to inaccurate results [27], since holder-tool interface motion is characterized by both translations and rotations. Therefore rotational DOFs have to be considered in substructure analysis.

More recently, several papers on RCSA have been presented, proposing solutions to overcome connection and rotational response issues. An important step ahead has been done by Park et al. [27] , their method will be used in this work as reference to present proposed approaches. In their work, in which a reverse receptance coupling approach has been proposed, for rotational DOFs response identification.

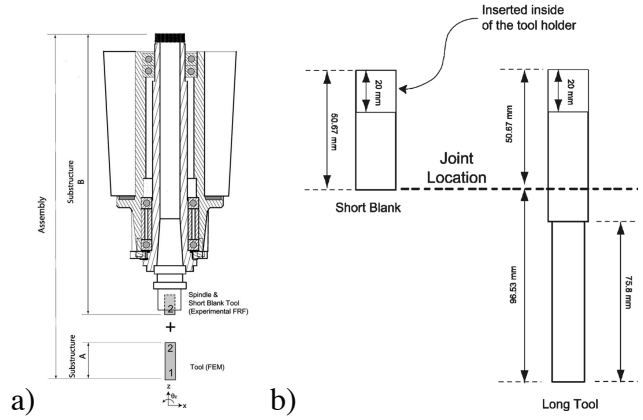

Figure 8.2 Park's work substructures and calibration tools [27]

Substructures for RCSA coupling were chosen as shown in Figure 8.2a, with connection point (point 2) outside the tool holder, in the overhung tool portion. Driving point translational response in point 2 for substructure B (Figure 8.2a), has been yielded via impact testing inserting short blank tool inside the tool holder (Short Blank in Figure 8.2b). Then a new test has been carried out with a calibration tool (Long Tool in Figure 8.2b), measuring FRFs in points 1 and 2. Tool H FRFs have been determined with a FE model and the second configuration tested has been used as reference to perform an inversion of receptance coupling approach to get system B rotational FRFs in point 2. This approach allows joint dynamics not to be modeled, since its contribution is included machine tool-tool holder assembly experimental response. Furthermore Park's work [27] provides an easy way for rotational response estimation, in order to overcome issues in their direct experimental acquisition. Thanks to the full FRF matrix, dynamic behavior of machine can be obtained accurately. This method is adopted in this work as reference for two main reasons: it is

assumed as reference and cited in other works [57], no other technique significantly improved accuracy and efficiency of this method.

Nevertheless the main limitations of this approach, as presented in the paper, are:

- Same holder tool connection geometry of the calibrator is required. This limits the application: new calibration tests must be performed for each tool-holder and connections before predicting dynamics of a new group of tools, therefore the number of tests required increases significantly compared to general RCSA.
- A calibration phase is required. Rotational FRFs are identified by an experimental phase with a calibration tool, increasing time required by the method.

8.2. Coupling machine-toolkit

As already mentioned, the first limitation can be overcome moving coupling point on holder standard section, an accurate model of the entire toolkit (holder and tool) as presented previously (Chapter 6 and 7), is hence required. In Figure 8.3 a scheme of proposed method application is presented and coupling point is identified.

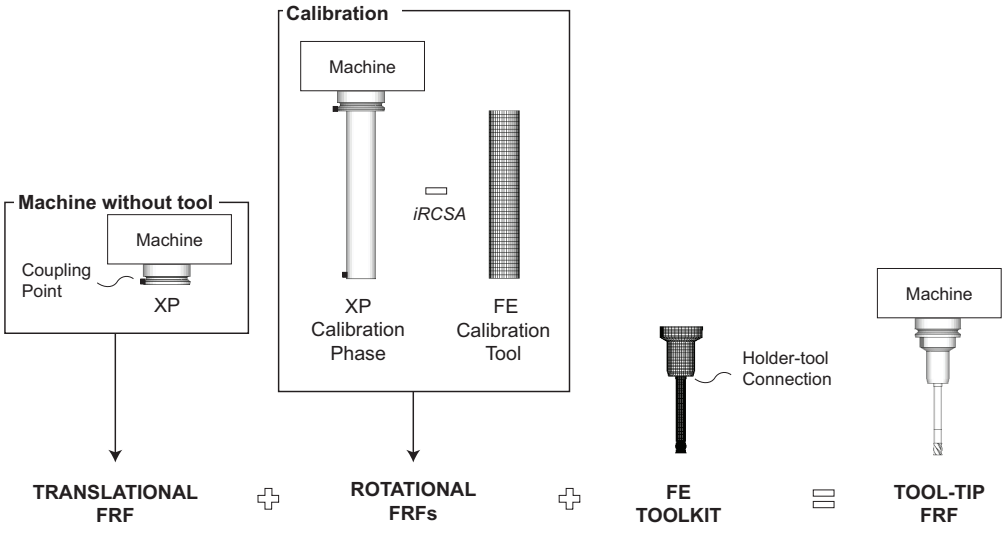

Figure 8.3 Park's method application to complete toolkit

Basically coupling point is set in the standard zone of holder: toolkit (holder and tool) becomes the changeable part and machine with standard zone of the holder the fixed one. For Park et al. [27] method this would lead to require, for any new toolkit mounted on the machine, only two measurements set-up: on the machine with only holder coupled, and a calibration phase with a proper calibration tool.

8.2.1. Case studies results

To show coupling machine-toolkit application and evaluate the influence of toolkit modeling accuracy on tool-tip FRF prediction, three test cases have been tested: toolkit 2, 3 and 5 as presented in the previous Chapters (6 and 7) and summarized in Table 6.8. Toolkit 2 is composed by a HSK64 shrink fit holder and a tool with about 100 mm overhang. In Toolkit 3 the same shank is housed in a HSK64 hydraulic chuck holder. Toolkit 5 is collet chuck HSK32 holder equipped with a short endmill (19 mm overhang).

Toolkits were connected to the milling machine tool (Mori Seiki NMV 1500 DCG for collect chuck test case, Fagima JAZZ for shrink-fit and hydraulic chuck test cases), acquiring tool-tip FRFs via impact testing. Proposed solid models and Timoshenko beam models, showed in the previous Chapters, were coupled with machine tool FRFs according with the method presented in section 8.2. Connection point between experimental and numerical model was set in correspondence of the ending section of the standardized holder portion, as previously shown (Figure 8.3). In Figure 8.4, Figure 8.5 and Figure 8.6 tool-tip FRFs of three different toolkits (one for each connection) are presented: experimental results is compared to the predicted ones. In Table 8.1, Table 8.2, Table 8.3 dominant mode parameters for the different configuration are reported.

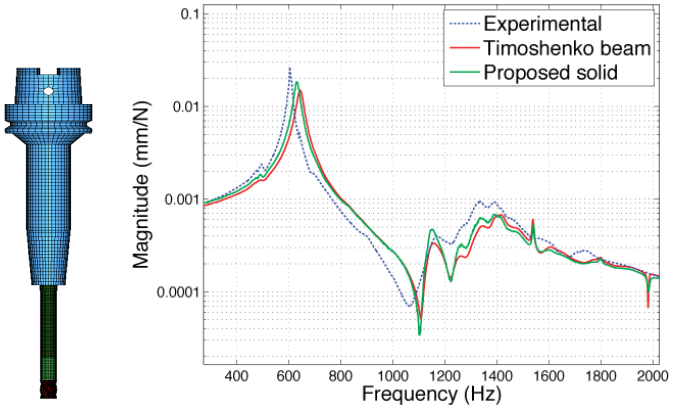

Figure 8.4 Tool-tip FRFs for toolkit 2

Table 8.1 Modal parameters of dominant mode for toolkit 2

	Natural Frequency (Hz)	Modal Damping	Stiffness (N/m)	Natural Frequency error
Experimental	605	0.008	1.45E6	-
Timoshenko beam	636	0.012	1.97E6	5.1%
Proposed solid	627	0.007	1.77E6	3.6%

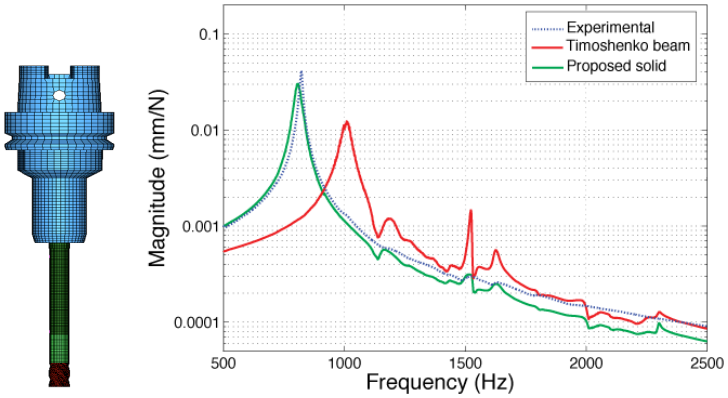

Figure 8.5 Tool-tip FRFs for toolkit 3

Table 8.2 Modal parameters of dominant mode for toolkit 3

	Natural Frequency (Hz)	Modal Damping	Stiffness (N/m)	Natural Frequency error
Experimental	821.5	0.008	1.58E6	-
Timoshenko beam	1004.3	0.020	2.74E6	22.3%
Proposed solid	798.3	0.010	1.73E6	-2.8%

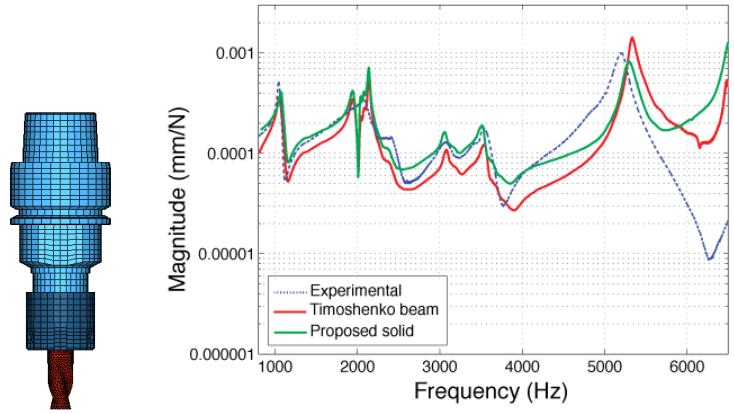

Figure 8.6 Tool-tip FRFs for toolkit 5

Table 8.3 Modal parameters of dominant mode for toolkit 5

	Natural Frequency (Hz)	Modal Damping	Stiffness (N/m)	Natural Frequency error
Experimental	5208	0.013	3.83E7	-
Timoshenko beam	5332	0.009	4.71E7	2.4%
Proposed solid	5226	0.012	4.41E7	0.3%

As expected, similar trend of free-free validation (Section 7.3) is obtained. Proposed solid models are in good agreement with experimental tool-tip FRFs in the three cases. As clear from Figure 8.5, Timoshenko beam model fails in computing tool-tip FRFs in hydraulic connection. On the contrary, Timoshenko beam and proposed solid model provide similar results for shrink-fit toolkit, in agreement with experimental FRF (Figure 8.4). For what concerns collet chuck, an intermediate condition is obtained (Figure 8.6): beam model accuracy is worse than proposed solid but closer compared to the high error obtained for hydraulic connection. These results show the high sensitivity of RCSA methods to toolkit FE models accuracy. Proposed modeling approaches improve tool-tip FRF prediction performance, however natural frequencies can not be predicted as accurately as in free-free condition: these errors (about 3%) are thought to be related to approximation introduced by RCSA method.

Once tool-tip FRF is identified chatter can be predicted. In order to show predicted FRFs application, SLDs of the three toolkits are computed. Zero-order analytical approach proposed by Altintas and Budak [25] (and presented in section 2.2) was applied to evaluate SLD. Chatter stability was predicted for a 1.5 mm radial depth of cut flank milling operation on steel (Ktc=2258 MPa, Krc=1554 MPa) for steel tools (Hydraulic and Shrink) using experimental and predicted FRFs. A slot operation on aluminum (Ktc= 796 MPa, Krc=196 MPa) for aluminum tool (Collet) is simulated. Results are shown in Figure 8.7, Figure 8.8 and Figure 8.9.

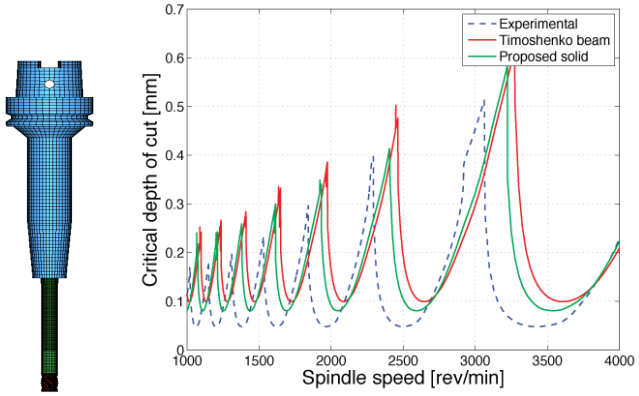

Figure 8.7 SLDs for toolkit 2

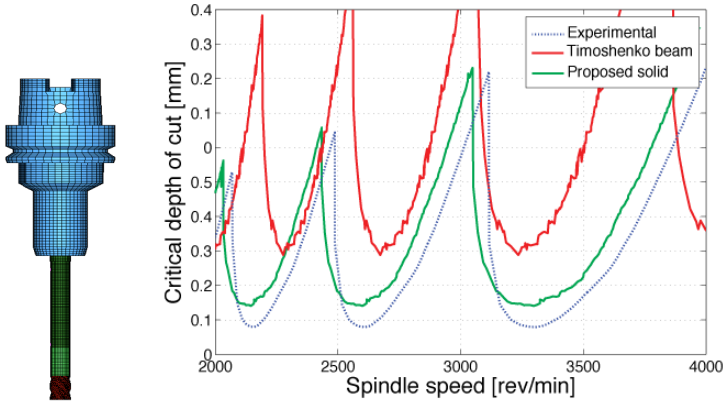

Figure 8.8 SLDs for toolkit 3

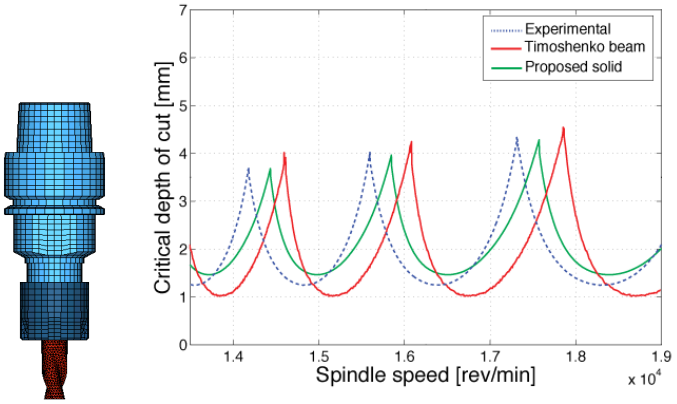

Figure 8.9 SLDs for toolkit 5

As expected, obtained SLDs are in agreement with tool-tip FRF prediction results. Stability prediction with 1D beam modeling is not reliable, especially for hydraulic toolkit. On the contrary proposed solid modeling strategies are in any case able to return good results. However some discrepancies, mainly in the predicted critical depth of cut, are obtained confirming the high sensitivity of SLD prediction to tool-tip FRF.

8.3. Proposed coupling analytical formulation

The second main limitation of Park's method is calibration phase required. This phase would be avoided if rotational FRFs could be identified with only one test set-up, some methodologies to achieve such results are presented in this section.

Some researchers [50, 57] tried to improve Park's work: however in all the cases rotational FRFs are identified by an experimental phase with a calibration tool, increasing time required by the method. Another way to improve RCSA applications is introducing a joint stiffness between tool and tool-holder: Movahhedy et al. [69] proposed a lumped model

equivalent to the joint, using two points of connection and two linear spring instead of the traditional single point with translational-rotational spring. Generally these approaches identify stiffness by means of iterative procedure based on experimental tests, therefore even in this case a calibration phase is required. Besides receptance coupling methods, other hybrid modeling approaches have been developed: Catania et al. [73] presented milling machine model obtained by coupling experimentally evaluated modal model of milling machine frame and spindle with an analytical discrete model of the tool, based on the continuous free-free beam shape analytical eigenfunctions. Also in their work an extensive experimental procedure is required to validate machine model.

In this work three coupling methods have been developed in order to overcome calibration phase issue. Two of them are based on RCSA approach, while the third one is based on a lumped machine holder-tool assembly model.

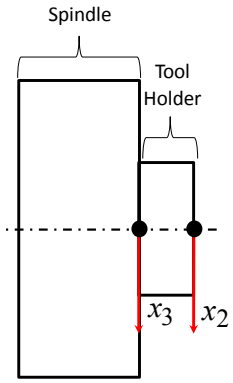

Figure 8.10 Machine-holder assembly experimental model used in the proposed coupling methods.

The common feature of these methods is that machine response is not evaluated just in one point, but in two points as shown in Figure 8.10. This allows reproducing joint rotations, as in Park's method, but without using calibration tools, hence experimental data needed to perform the coupling operation can be collected with just one machine set up configuration. This can be useful in practical industrial applications, in order to reduce machine tool downtime required for its experimental characterization. A FE model has been created in order to test coupling method in condition of complete fulfillment of basic hypotheses.

8.3.1. **Two points coupling method**

This first method is based on receptance coupling theory. The fundamental hypothesis is that tool holder overhung portion has a rigid behavior in frequency range of interest, hence considering the system in its bending can be neglected.

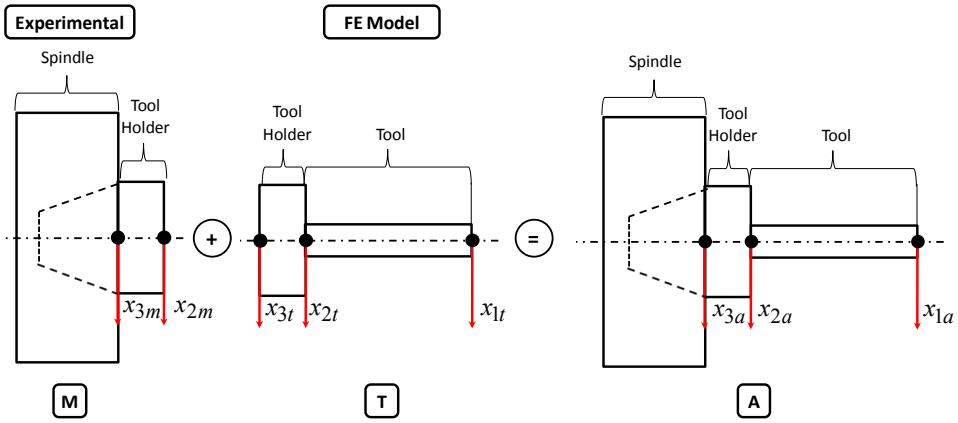

Figure 8.11 Substructures used for two points translation coupling method.

Joint rotation could be reproduced without rotational DOFs, introducing two connection points along tool axis and imposing equilibrium and compatibility conditions. Figure 8.11 summarizes substructures definitions for this coupling method:

- M system, machine tool – tool holder assembly, two DOFs, experimental model.
- T system, tool holder overhung portion – milling tool assembly, three DOFs, FE model.
- A system, assembled configuration.

As Figure 8.11 points out, tool holder part between point 2 and point 3 is present in both T and M system, therefore its contribution to assembly dynamics would be considered twice. This problem has been overcome, since the basic hypothesis is that the mentioned tool holder portion has a rigid behavior in the interest bandwidth, therefore its stiffness contribution can be considered twice without introducing any relevant error. Regarding mass contribution, it can be suppressed in FE model excluding mass matrices of the elements lying in the aforementioned zone from the assembly process. This strategy allows to consider tool holder overhung portion just in tool model.

Considering the mentioned hypothesis, mathematical formulation of coupling equations has been yielded. Receptance matrices for the three systems (T, M, A) are:

$$\begin{vmatrix} x_{1t} \\ x_{2t} \\ x_{3t} \end{vmatrix} = \begin{vmatrix} G_{11t}(\omega) & G_{12t}(\omega) & G_{13t}(\omega) \\ G_{21t}(\omega) & G_{22t}(\omega) & G_{23t}(\omega) \\ G_{31t}(\omega) & G_{32t}(\omega) & G_{33t}(\omega) \end{vmatrix} \begin{vmatrix} f_{1t} \\ f_{2t} \\ f_{3t} \end{vmatrix} \tag{8.6}$$

$$\begin{vmatrix} x_{2m} \\ x_{3m} \end{vmatrix} = \begin{vmatrix} G_{22m}(\omega) & G_{23m}(\omega) \\ G_{32m}(\omega) & G_{33m}(\omega) \end{vmatrix} \begin{vmatrix} f_{2m} \\ f_{3m} \end{vmatrix} \tag{8.7}$$

$$\begin{vmatrix} x_{1a} \\ x_{2a} \\ x_{3a} \end{vmatrix} = \begin{vmatrix} G_{11a}(\omega) & G_{12a}(\omega) & G_{13a}(\omega) \\ G_{21a}(\omega) & G_{22a}(\omega) & G_{23a}(\omega) \\ G_{31a}(\omega) & G_{32a}(\omega) & G_{33a}(\omega) \end{vmatrix} \begin{vmatrix} f_{1a} \\ f_{2a} \\ f_{3a} \end{vmatrix} \tag{8.8}$$

Compatibility and equilibrium conditions are expressed respectively in equations (**8**.**9**) and (**8**.**10**), whereas x_1 is the interest non-joint point (i.e., tool-tip) coordinate and x_2, x_3 are the joint coordinate:

$$\begin{cases} x_{1a} = x_{1t} \\ x_{2a} = x_{2t} = x_{2m} \\ x_{3a} = x_{3t} = x_{3m} \end{cases} \tag{8.9}$$

$$\begin{cases} f_{1a} = f_{1t} \\ f_{2a} = f_{2t} + f_{2m} \\ f_{3a} = f_{3t} + f_{3m} \end{cases} \tag{8.10}$$

Compatibility equations on joint coordinates for systems M and T can be written in terms of receptances functions:

$$\begin{vmatrix} G_{21t}(\omega) & G_{31t}(\omega) \\ G_{22t}(\omega) & G_{32t}(\omega) \\ G_{23t}(\omega) & G_{33t}(\omega) \end{vmatrix}^T \begin{vmatrix} f_{1t} \\ f_{2t} \\ f_{3t} \end{vmatrix} = \begin{vmatrix} G_{22m}(\omega) & G_{23m}(\omega) \\ G_{32m}(\omega) & G_{33m}(\omega) \end{vmatrix} \begin{vmatrix} f_{2m} \\ f_{3m} \end{vmatrix} \tag{8.11}$$

Equations (**8**.**11**) can be rearranged to eliminate M system forces using equilibrium conditions:

$$\begin{vmatrix} G_{21t}(\omega) & G_{31t}(\omega) \\ G_{22t}(\omega)+G_{22m}(\omega) & G_{32t}(\omega)+G_{32m}(\omega) \\ G_{23t}(\omega)+G_{23m}(\omega) & G_{33t}(\omega)+G_{33m}(\omega) \end{vmatrix}^T \begin{vmatrix} f_{1a} \\ f_{2t} \\ f_{3t} \end{vmatrix} = \begin{vmatrix} G_{22m}(\omega) & G_{23m}(\omega) \\ G_{32m}(\omega) & G_{33m}(\omega) \end{vmatrix} \begin{vmatrix} f_{2a} \\ f_{3a} \end{vmatrix} \tag{8.12}$$

$$\begin{vmatrix} G_{22t}(\omega)+G_{22m}(\omega) & G_{23t}(\omega)+G_{23m}(\omega) \\ G_{32t}(\omega)+G_{32m}(\omega) & G_{33t}(\omega)+G_{33m}(\omega) \end{vmatrix} \begin{vmatrix} f_{2t} \\ f_{3t} \end{vmatrix} = \ldots$$
$$\ldots \begin{vmatrix} G_{22m}(\omega) & G_{23m}(\omega) \\ G_{32m}(\omega) & G_{33m}(\omega) \end{vmatrix} \begin{vmatrix} f_{2a} \\ f_{3a} \end{vmatrix} - \begin{vmatrix} G_{21t}(\omega) \\ G_{31t}(\omega) \end{vmatrix} f_{1a} \tag{8.13}$$

Equation (**8**.**13**) allows f_{2t} and f_{3t} to be function of f_{1a}, f_{2a} and f_{3a}. This linear system has been solved using Matlab® symbolic math toolbox. These expressions can be simplified as:

$$\begin{cases} f_{2t} = A(\omega)f_{1a} + B(\omega)f_{2a} + C(\omega)f_{3a} \\ f_{3t} = L(\omega)f_{1a} + M(\omega)f_{2a} + N(\omega)f_{3a} \end{cases} \tag{8.14}$$

where capital letters coefficients are functions of machine system M and system T receptances functions. The first relation of equations (**8**.**9**) can be written down introducing receptance functions:

$$\begin{vmatrix} G_{11a}(\omega) \\ G_{12a}(\omega) \\ G_{13a}(\omega) \end{vmatrix}^T \begin{vmatrix} f_{1a} \\ f_{2a} \\ f_{3a} \end{vmatrix} = \begin{vmatrix} G_{11t}(\omega) \\ G_{12t}(\omega) \\ G_{13t}(\omega) \end{vmatrix}^T \begin{vmatrix} f_{1t} \\ f_{2t} \\ f_{3t} \end{vmatrix} \tag{**8.15**}$$

Using equations (**8**.**14**) and the equilibrium condition in point 1 (**8**.**10**):

$$\begin{vmatrix} G_{11a}(\omega) \\ G_{12a}(\omega) \\ G_{13a}(\omega) \end{vmatrix}^T \begin{vmatrix} f_{1a} \\ f_{2a} \\ f_{3a} \end{vmatrix} = \begin{vmatrix} G_{11t}(\omega) \\ G_{12t}(\omega) \\ G_{13t}(\omega) \end{vmatrix}^T \begin{vmatrix} f_{1a} \\ A(\omega)f_{1a} + B(\omega)f_{2a} + C(\omega)f_{3a} \\ L(\omega)f_{1a} + M(\omega)f_{2a} + N(\omega)f_{3a} \end{vmatrix} \tag{8.16}$$

Equation (**8**.**16**) has to be satisfied for every value of f_{1a}, f_{2a} and f_{3a}. Therefore an expression of $G_{11a}(\omega)$ can be yielded:

$$\begin{aligned} &G_{11a}(\omega)f_{1a} + G_{12a}(\omega)f_{2a} + G_{13a}(\omega)f_{3a} = \ldots \\ &(G_{11t}(\omega) + A(\omega)G_{12t}(\omega) + L(\omega)G_{13t}(\omega))f_{1a} + \ldots \\ &(B(\omega)G_{12t}(\omega) + M(\omega)G_{13t}(\omega))f_{2a} + \ldots \\ &(C(\omega)G_{12t}(\omega) + N(\omega)G_{13t}(\omega))f_{3a} \end{aligned} \tag{8.17}$$

$$G_{11a}(\omega) = G_{11t}(\omega) + A(\omega)G_{12t}(\omega) + L(\omega)G_{13t}(\omega) \tag{8.18}$$

Equation (**8**.**18**) allows to easily compute tool tip FRFs combining numerical (or analytical) tool response, and experimental machine response. Another great advantage of RCSA methods is that tool tip FRF is computed working by frequency step. It means that if experimental data are affected by measurement noise in a specific bandwidth, this will not contaminate assembled configuration FRF outside this bandwidth.

As earlier mentioned, before testing coupling method on a real machine-toolkit coupling, a numerical trial has been carried out. Figure 8.12 shows the structure used to test the method.

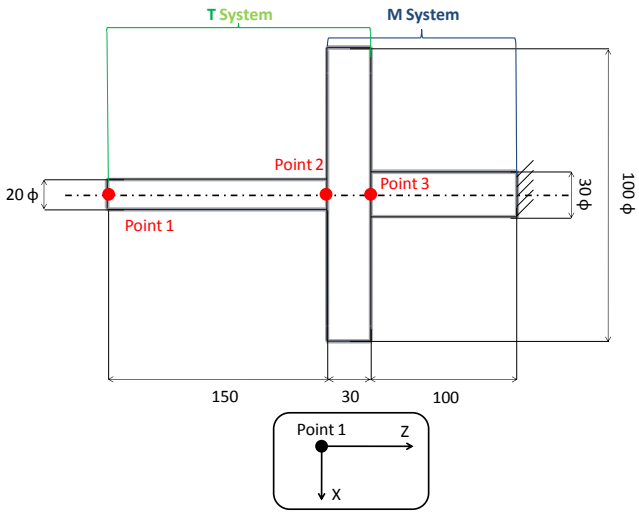

Figure 8.12: Structure used in method numerical trial.

This geometry has been created to meet the following guidelines:

- Contact zone should have a rigid behavior in the interest frequency range.
- In order to simulate an intense interaction between substructure dynamics, both T system and M system modes should be present in analysis frequency range.
- To approximate low frequency machine tool dynamics, M system should be constrained.

In Figure 8.12 structure has been modeled with Timoshenko beam elements, using the code implemented for milling tool modeling. Figure 8.13 shows FE models of the three systems, point 1, 2 and 3 are nodes marked by red spots. Material properties values used for these models are summarized in table 13 (same values for the three systems):

Table 8.4: Materials property values for FE models.

	E Young Modulus (MPa)	**ν** Poisson Ratio	**ρ** Density (tons/mm^3)	**η** Damping Ratio
Steel	2.1E+05	0.3	7.7E-09	0.01

As exposed in the beginning of the paragraph, mass matrices of the elements lying in the overlapping zone have been excluded from the assembly process. FRFs have been computed using algorithm written in Matlab® based on direct calculation, since analyzed models size does not involve excessive process time. Analysis results are shown in Figure 8.14.

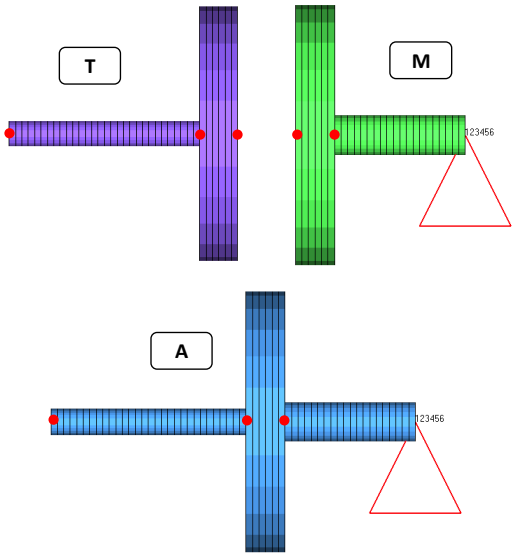

Figure 8.13: FE models used in numerical trials.

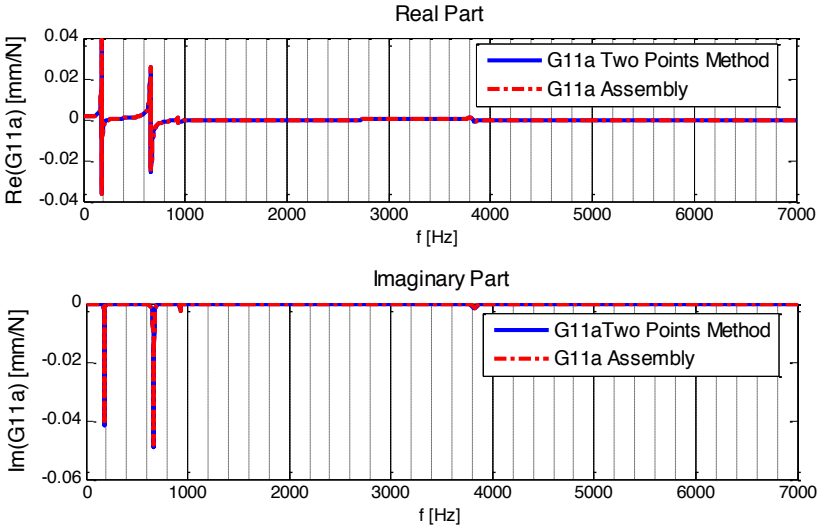

Figure 8.14: Results of two points method test on numerical model

The blue curve is the driving point FRF in point 1 computed with the proposed RCSA method and the red curve is the same FRF but computed on the assembled model (model A Figure 8.13). It is clear that if method hypotheses are completely fulfilled, assembled structure dynamics is correctly reproduced.

8.3.2. **One point coupling method**

The substructures used in this coupling method are summarized in Figure 8.15. The assembly is split in correspondence of holder-tool interface and, unlike in two points method, a rotational DOF is included for point 2.

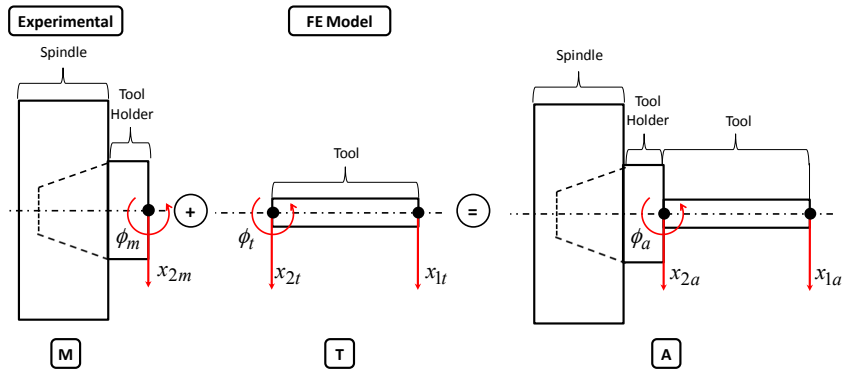

Figure 8.15: One point method substructures

During experimental characterization the same FRFs of two points method are acquired. Rotational FRFs for the machine tool – tool holder system are then yielded from measured data, using the hypothesis of rigid behavior of the tool holder overhung portion. Hence this method too requires just one machine set up configuration to collect the required FRFs. The following steps will show how rotational FRFs are obtained from translational ones, and how coupling process is carried out.

Equations (**8**.**19**), (**8**.**20**) and (**8**.**21**) summarize systems receptance matrices:

$$\begin{vmatrix} x_{1a} \\ x_{2a} \\ \phi_a \end{vmatrix} = \begin{vmatrix} G_{11a}(\omega) & G_{12a}(\omega) & G_{1\phi a}(\omega) \\ G_{21a}(\omega) & G_{22a}(\omega) & G_{2\phi a}(\omega) \\ G_{\phi 1a}(\omega) & G_{\phi 2a}(\omega) & G_{\phi\phi a}(\omega) \end{vmatrix} \begin{vmatrix} f_{1a} \\ f_{2a} \\ M_a \end{vmatrix} \tag{8.19}$$

$$\begin{vmatrix} x_{2m} \\ \phi_m \end{vmatrix} = \begin{vmatrix} G_{22m}(\omega) & G_{2\phi m}(\omega) \\ G_{\phi 2m}(\omega) & G_{\phi\phi m}(\omega) \end{vmatrix} \begin{vmatrix} f_{2m} \\ M_m \end{vmatrix} \tag{8.20}$$

$$\begin{vmatrix} x_{1t} \\ x_{2t} \\ \phi_t \end{vmatrix} = \begin{vmatrix} G_{11t}(\omega) & G_{12t}(\omega) & G_{1\phi t}(\omega) \\ G_{21t}(\omega) & G_{22t}(\omega) & G_{2\phi t}(\omega) \\ G_{\phi 1t}(\omega) & G_{\phi 2t}(\omega) & G_{\phi\phi t}(\omega) \end{vmatrix} \begin{vmatrix} f_{1a} \\ f_{2a} \\ M_a \end{vmatrix} \tag{8.21}$$

For every substructure present in this method the following notation is adopted:

- $G_{\phi i}(\omega)$ is the rotation in point 2 due to a unit force applied in DOF i.
- $G_{i\phi}(\omega)$ is the displacement of DOF i due to a unit moment applied in point 2.

- $G_{\phi\phi}(\omega)$ is the rotation of point 2 due to a unit moment applied in point 2.
- M is the moment applied in point 2.

Terms that must be yielded for the M system are $G_{2\phi m}(\omega)$, $G_{\phi 2m}(\omega)$ and $G_{\phi\phi m}(\omega)$.

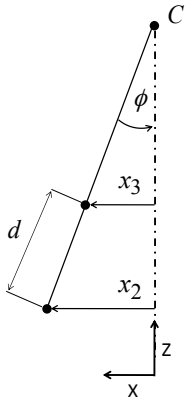

Figure 8.16: Tool holder overhung portion motion according to rigid behavior hypothesis.

If hypothesis of rigid behavior is satisfied, than the motion of the tool holder zone lying between point 2 and point 3 will be a pure rotation around its instantaneous center of motion (point C in Figure 8.16). Therefore the following relation can be considered:

$$\frac{x_3 - x_2}{d} = \phi \tag{8.22}$$

Instantaneous rotation center position is dependent by the considered frequency. (**8**.**22**) and FRFs reciprocity property allows to yield rotational FRFs:

$$G_{\phi 2}(\omega) = \frac{\phi}{f_2} = \frac{x_3 - x_2}{df_2} = \frac{1}{d}(G_{32}(\omega) - G_{22}(\omega)) \tag{8.23}$$

$$\begin{aligned} &G_{\varphi\varphi}(\omega) = \frac{\varphi}{M_2} = \frac{1}{d}\left(\frac{x_3}{M_2} - \frac{x_2}{M_2}\right) = \ldots \\ &\frac{1}{d}\left(\frac{\varphi}{f_3} - \frac{\varphi}{f_2}\right) = \frac{1}{d^2}\left(\frac{x_3 - x_2}{f_3} - \frac{x_3 - x_2}{f_2}\right) = \ldots \\ &\ldots\frac{1}{d^2}\left(G_{22}(\omega) + G_{33}(\omega) - G_{23}(\omega) - G_{32}(\omega)\right) \end{aligned} \tag{8.24}$$

$$\begin{cases} G_{\phi\phi}(\omega) = \dfrac{1}{d^2}\left(G_{22}(\omega) + G_{33}(\omega) - G_{23}(\omega) - G_{32}(\omega)\right) \\ G_{\phi 2}(\omega) = \dfrac{1}{d}\left(G_{32}(\omega) - G_{22}(\omega)\right) \\ G_{2\phi}(\omega) = G_{\phi 2}(\omega) \end{cases} \tag{8.25}$$

Equation (**8**.**25**) summarizes relations that allow obtaining rotational FRFs required for this coupling approach. For T system rotational FRFs can be directly computed by FE solver.

In equations (**8**.**26**) and (**8**.**27**) compatibility and equilibrium conditions for this substructures configuration are given:

$$\begin{cases} x_{1a} = x_{1t} \\ x_{2a} = x_{2t} = x_{2m} \\ \phi_a = \phi_t = \phi_m \end{cases} \tag{8.26}$$

$$\begin{cases} f_{1a} = f_{1t} \\ f_{2a} = f_{2t} + f_{2m} \\ M_a = M_t + M_m \end{cases} \tag{8.27}$$

Analytical expression of $G_{11a}(\omega)$ can be yielded using the same procedure presented for two points method.

As for two point method, a test on the numerical model has been carried out in order to verify method validity in conditions of completely fulfilled hypotheses. Model has not been changed since the two coupling techniques are based on the same hypotheses. Figure 8.17 shows results of comparison between real point 1 direct FRF and the predicted one. Results show that also this method is able to give a reliable prediction of assembly dynamics if the zone between point 2 and 3 can be approximated as rigid.

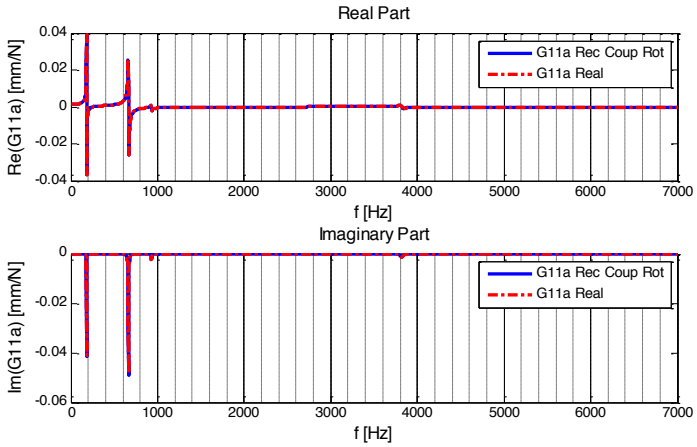

Figure 8.17: Comparison between estimated $G_{11a}(\omega)$ and the real one for numeric model

8.3.3. Frequency dependent stiffness method

This approach is not based on RCSA principles, but consists in using experimental data of machine holder-tool assembly to create a simple two DOF model with frequency dependent stiffness matrix. Considering the substructures layout already used in two points method, M system is represented by a 2 by 2 receptance matrix. Hence a two DOFs system describes dynamic behavior of all machine tool – tool holder assembly. The basic idea of this method is to yield stiffness and mass matrices of this system and assemble them with T system matrices, in order to perform an FRF analysis to obtain A system FRFs. The problem concerning this procedure is that a two DOFs system cannot fit the dynamic behavior of a complex system as machine tool – tool holder assembly, since it has just two normal modes, while the real system could show a more complex behavior, with an high number of modes in measurement bandwidth. This problem can be overcome considering a frequency dependent stiffness matrix. According to this assumption we can write down the following relation:

$$\begin{vmatrix} x_{2m} \\ x_{3m} \end{vmatrix} = \left(\begin{vmatrix} K_{22m}(\omega) & K_{23m}(\omega) \\ K_{32m}(\omega) & K_{33m}(\omega) \end{vmatrix} - \begin{vmatrix} M_{11} & 0 \\ 0 & M_{22} \end{vmatrix} \omega^2 \right) \begin{vmatrix} f_{2m} \\ f_{3m} \end{vmatrix} \tag{8.28}$$

where $K_{ijm}(\omega)$ are frequency dependent stiffness matrix terms and M_{ij} are mass matrix terms. The relation between M system matrices and measured FRFs is:

$$\begin{vmatrix} G_{22m}(\omega) & G_{23m}(\omega) \\ G_{32m}(\omega) & G_{33m}(\omega) \end{vmatrix} = \left(\begin{vmatrix} K_{22m}(\omega) & K_{23m}(\omega) \\ K_{32m}(\omega) & K_{33m}(\omega) \end{vmatrix} - \begin{vmatrix} M_{22m} & 0 \\ 0 & M_{33m} \end{vmatrix} \omega^2 \right)^{-1} \tag{8.29}$$

Performing an inversion on both sides of equation (**8.18**), and taking $U_{ijm}(\omega)$ as inverse receptance matrix terms:

$$\begin{vmatrix} K_{22m}(\omega) & K_{23m}(\omega) \\ K_{32m}(\omega) & K_{33m}(\omega) \end{vmatrix} = \left(\begin{vmatrix} U_{22m}(\omega) + M_{22m}\omega^2 & U_{23m}(\omega) \\ U_{32m}(\omega) & U_{33m}(\omega) + M_{33m}\omega^2 \end{vmatrix} \right) \tag{8.30}$$

$$\begin{cases} K_{22m}(\omega) = U_{22m}(\omega) + M_{22m}(\omega)\omega^2 \\ K_{23m}(\omega) = U_{23m}(\omega) \\ K_{32m}(\omega) = U_{32m}(\omega) \\ K_{33m}(\omega) = U_{33m}(\omega) + M_{33m}(\omega)\omega^2 \end{cases} \tag{8.31}$$

Equation (**8.31**) allows to compute stiffness matrix terms for every analysis frequency. Mass matrix terms can be chosen arbitrarily but they should be of the same order of tool mass, in order to avoid matrix bad conditioning issues during FRF analysis. It is important to underline that the stiffness matrix terms computed with this method are complex values functions, therefore machine tool – tool holder system damping is considered in this approach.

Once that M system stiffness matrix has been computed, FRF analysis can be performed. In this application direct method must be used, since M stiffness matrix frequency dependence does not allow to compute normal modes. In substructures matrices assembling process must be considered that, as in two points method, the tool holder overhung portion is present in both T and M models, therefore the hypothesis of rigid contact zone has to be assumed and mass matrices of the element between point 2 and point 3 have to be excluded from assembly process. That said assembly matrices M_a and $K_a(\omega)$ will be equal to M_t and K_t except for terms correspondent to point 2 and point 3 displacement in x direction (respectively specified by letters c and d):

$$M_a = \begin{vmatrix} M_{22m} + M_{cct} & \cdots & 0 & \cdots & M_{23m} & \cdots & 0 \\ \vdots & \ddots & & & \vdots & & \\ 0 & & 0 & & 0 & & \\ \vdots & & & \ddots & \vdots & & \\ M_{32m} & \cdots & 0 & \cdots & M_{33m} & \cdots & 0 \\ \vdots & & & & \vdots & \ddots & \\ 0 & & & & 0 & & 0 \end{vmatrix} \tag{8.32}$$

$$K_a = \begin{vmatrix} K_{22m}(\omega) + K_{cct} & \cdots & 0 & \cdots & K_{23m}(\omega) + K_{cdt} & \cdots & 0 \\ \vdots & \ddots & & & \vdots & & \\ 0 & & 0 & & 0 & & \\ \vdots & & & \ddots & \vdots & & \\ K_{32m}(\omega) + K_{dct} & \cdots & 0 & \cdots & K_{33m}(\omega) + K_{ddt} & \cdots & 0 \\ \vdots & & & & \vdots & \ddots & \\ 0 & & & & 0 & & 0 \end{vmatrix} \tag{8.33}$$

As pointed out in equation (**8.33**), assembly stiffness matrix is frequency dependent, therefore mass matrix assembling process can be done before running direct FRF analysis, while stiffness matrix assembly must be performed for every pulsation (frequency) step ω_i:

$$\vec{X}_a(\omega_i) = (K_a(\omega_i) - M_a)\vec{F}_a \tag{8.34}$$

As for the others coupling methods, a test on the already presented numerical model has been performed.

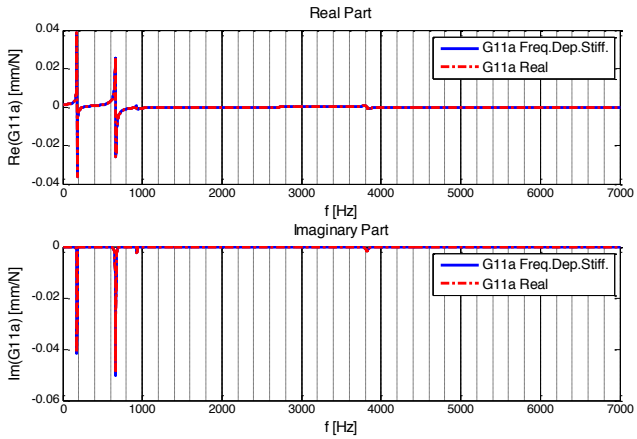

Figure 8.18 Comparison between estimated $G_{11a}(\omega)$ and the real one for numeric model

In Figure 8.18 a comparison between real and estimated Point 1 direct FRF is shown and as for the previous methods a good prediction of assembly dynamics can be provided. Figure 8.19 shows the computed frequency dependent stiffness function for the tested example.

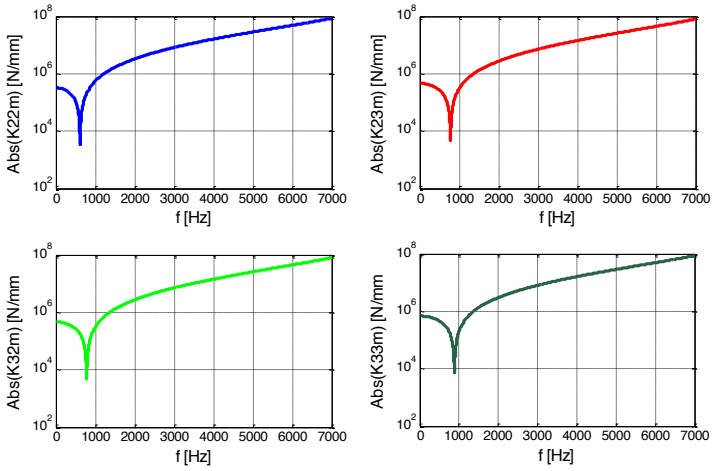

Figure 8.19 Frequency dependent stiffness plot

8.3.4. **Experimental validation**

Once that coupling methods have been validated numerically, a real machine tool case has been analyzed in order to verify if the proposed coupling methods could provide a reliable prediction of tooltip FRF. Tests have been carried out on a Mori Seiki NMV 1500 DCG five axis vertical milling center present in Manufacturing Technologies Research Lab. of the University of Firenze (Figure 8.20). Validation process has been carried out following these steps:

- Tool FE model implementation.
- Machine tool – tool holder assembly FRFs measurements.
- Tool tip FRF measurement for the completely assembled configuration.
- Tool tip FRF computing with proposed coupling methods.
- Comparison between computed and measured tool-tip FRF.

Coupling techniques have been validated on the dummy toolkit presented in toolkit modeling section (Chapter 6).

Figure 8.20 Mori Seiki NMV 1500 DCG five axis vertical milling center and machine axes representation

Figure 8.21 shows toolkit model, in which tool holder portion lying over point 3 has been removed according to substructures definition given in previous section. Connection points and tool-tip FRF measurement point have been located in the analysis coordinate system, as shown in Figure 8.21 and in Table 8.5.

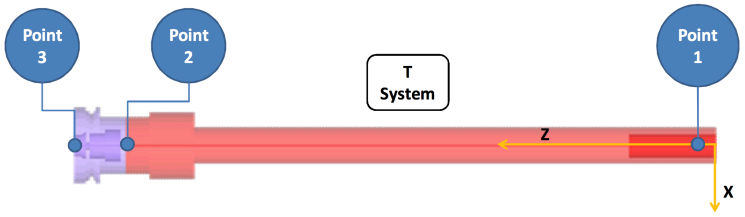

Figure 8.21 Tool model with connection points (2, 3) and tool-tip (1) positions and coordinate system.

Table 8.5 Connection points and tool tip point positions in the coordinate system

Point 1 Z coordinate (mm)	Point 2 Z coordinate (mm)	Point 3 Z coordinate (mm)
6.85	249	271

Experimental FRFs identifications on both assembled configuration and machine tool have been carried out with the impact testing technique. Accelerometers (PCB 352c22) have been placed in the positions identified in Table 8.5. Data acquisition and signal conditioning has been carried out using a LMS Scadas III frontend system and LMS Test.Lab software. Accelerometers have been calibrated before each test using a Bruel and Kjiaer handheld shaker type 4294 operating at fixed frequency (159.2 Hz) and known velocity (10 mm/s RMS).

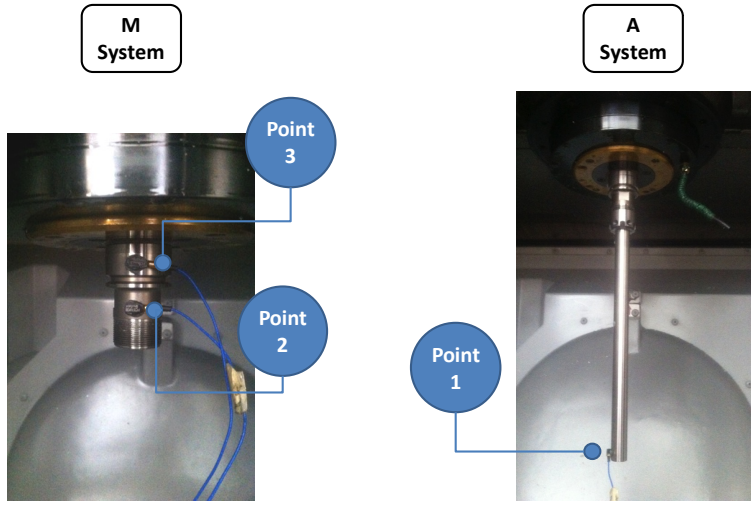

Figure 8.22 M system, and A system FRFs measurement layout.

Figure 8.22 shows accelerometers layout used in experimental tests. As earlier mentioned tool dynamic behavior can be approximated as axial symmetric without introduce any great error. However this approximation could not be valid for machine tool dynamics, therefore milling center has been excited along both its x and y axes (Figure 8.23) in order to verify if a dependency from excitation direction was present. These tests have shown that machine behavior in x and y directions can be considered equal, with good approximation. Measurement bandwidth has been 0-8192 Hz with a resolution of 1 Hz and all measured data show acceptable coherence function values (greater than 0.95) until approximately 7500 Hz. In order to reduce measurement noise influence on coupling results, M system measured FRFs have been processed to smooth the signals using a first degree polynomial model and performing local regression using weighted linear least squares. This signal smoothing has been performed since the operations executed on measured signals during the coupling process could lead to a noise amplification process.

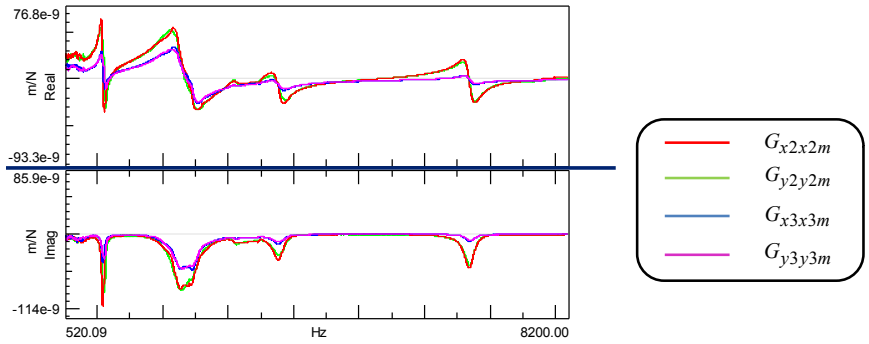

Figure 8.23 Machine tool – tool holder assembly driving point FRFs (points 2 and 3) in x and y directions

Once that experimental activity has been completed, coupling tests have been carried out using the implemented techniques. Estimated tool tip FRFs have been compared with the measured one, as shown in the following figures.

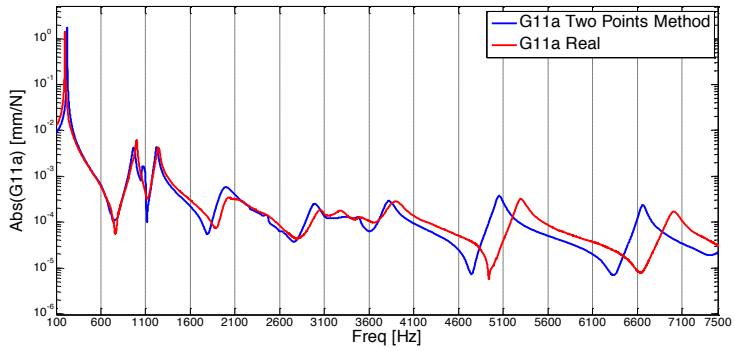

Figure 8.24 Two points coupling method results (Magnitude in log scale).

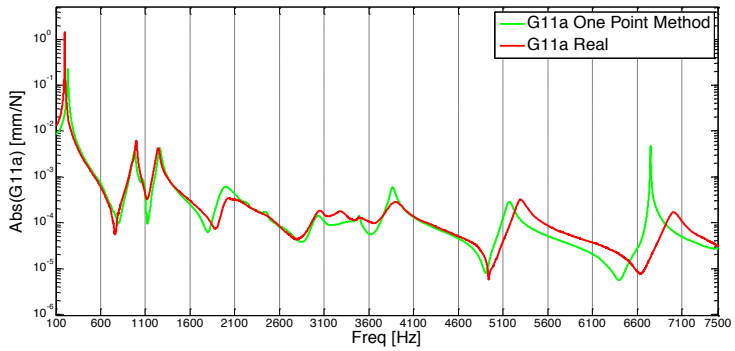

Figure 8.25 One point coupling method results (Magnitude in log scale).

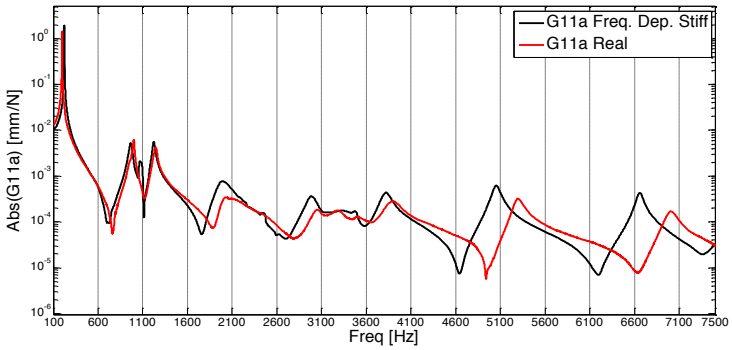

Figure 8.26 Frequency dependent stiffness coupling method results (Magnitude in log scale).

In Figure 8.24, Figure 8.25 and Figure 8.26, magnitude of tooltip FRF yielded by two points method, one point method and frequency dependent stiffness method are presented and compared with the experimental response.

Results of the three coupling techniques methods are slightly the same: one point method provides a worse fit than the other methods in low frequency range but better in high frequency range, two points method and frequency dependent stiffness method do not show relevant differences between each other in tool tip dynamics prediction, the only remarkable distinction has been observed in terms of computation time since frequency dependent stiffness method turned out to be the slowest of the three proposed procedures. Despite these differences is important to remark that all the implemented solutions were based in the same assumption: the rigid behavior of the tool holder overhang portion in interest frequency range. Tests on a numerical model have proven that if this hypothesis is verified, a single test configuration can provide all information required to predict FRFs of the assembled configuration. Tests carried out Mori Seiki milling center demonstrated that rigid behavior of the connection zone could be a realistic hypothesis in a real machine tool application.

8.4. Case studies results

In order to further assess new method accuracy, proposed coupling technique has been applied to cases studies previously presented and hence compared to Park et al. method. For the sake of brevity and clarity, only two points method (8.3.1) has been implemented. Same procedure and same toolkits (2, 3, 5) has been adopted to obtain both tool-tip FRFs and SLDs. Tool-tip FRFs are presented in Figure 8.27, Figure 8.28 and Figure 8.29. Dominant mode modal parameters are summarized in Table 8.6, Table 8.7 and Table 8.8.

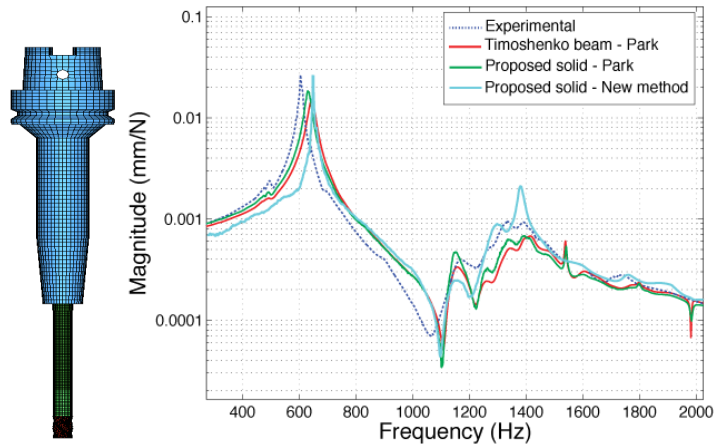

Figure 8.27 Tool-tip FRFs for toolkit 2 (two points method)

Table 8.6 Modal parameters of dominant mode for toolkit 2 (two points method)

	Natural Frequency (Hz)	Modal Damping	Stiffness (N/m)	Natural Frequency error
Experimental	605	0.008	1.45E6	-
Timoshenko beam	636	0.012	1.97E6	5.1%
Proposed solid	627	0.007	1.77E6	3.6%
Proposed solid – New method	642	0.007	1.572E6	6.1%

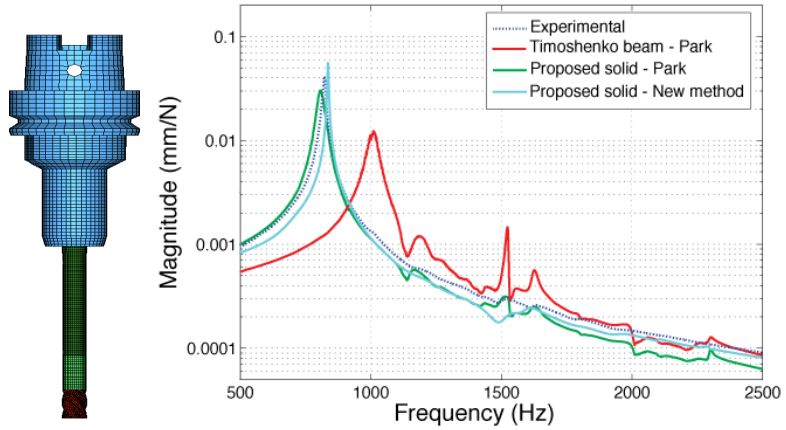

Figure 8.28 Tool-tip FRFs for toolkit 3 (two points method)

Table 8.7 Modal parameters of dominant mode for toolkit 3 (two points method)

	Natural Frequency (Hz)	Modal Damping	Stiffness (N/m)	Natural Frequency error
Experimental	822	0.008	1.58E6	-
Timoshenko beam	1004	0.020	2.74E6	22.3%
Proposed solid	798	0.010	1.73E6	-2.8%
Proposed solid – New method	839	0.004	2.02E6	2.1%

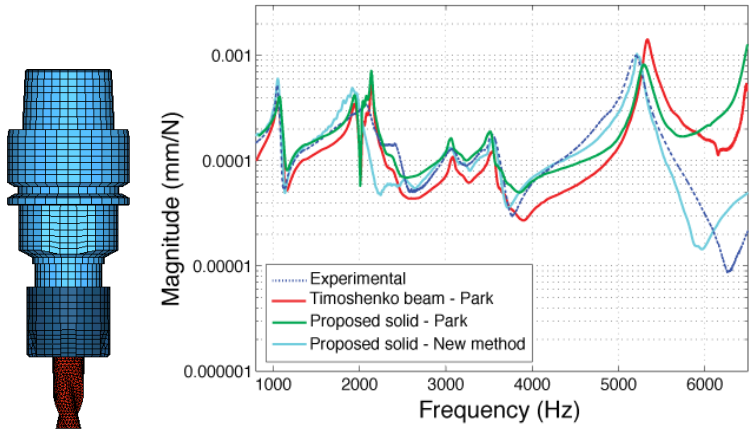

Figure 8.29 Tool-tip FRFs for toolkit 5 (two points method)

Table 8.8 Modal parameters of dominant mode for toolkit 5 (two points method)

	Natural Frequency (Hz)	Modal Damping	Stiffness (N/m)	Natural Frequency error
Experimental	5208	0.013	3.83E7	-
Timoshenko beam	5332	0.009	4.71E7	2.4%
Proposed solid	5226	0.012	4.41E7	0.3%
Proposed solid – New method	5213	0.012	3.98E7	0.1%

Results show how the two points method achieves similar accuracy compared to Park's one, but increasing efficiency thanks to a reduction of number of test required (no calibration phase). In particular comparing dominant natural frequency differences:

- For hydraulic holder, Park's method returns a lower dominant frequency (-2.8%) and new coupling method in a higher one with practically the same error compared to experimental results (+2.1%).
- In the shrink fit toolkit, Park's method results in higher accuracy (3.6%) compared to proposed method (6.1%).
- For collet toolkit on the other hand, two points method seems to provide very accurate results (0.1%).

High accuracy in collet toolkit is probably due to the different size of the holder, and positioning of measurement points (for collet HSK32 has been used). Proposed method, in fact, is influenced by experimental measurements noise that can be significant if accelerometers points are characterized by low mobility. Moreover proposed method extracts rotation information by the difference between two points displacements: if it is very low results will be affected by noise.

HSK63 is bigger and stiffer than HSK32: measurements points are characterized by lower mobility and then experimental results more affected by noise. Moreover in case of HSK63 toolkits (shrink fit and hydraulic ones) standard portion of holder was small and measurements points were located close together (Figure 8.30): this could have caused the higher discrepancies shown in the FRFs. On the contrary for HSK 32 measurements points were set more separated as presented for dummy tool (Figure 8.22).

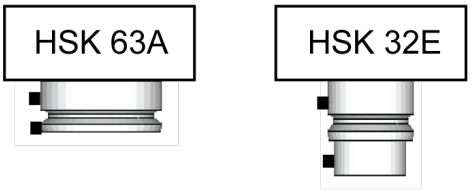

Figure 8.30 Coupling points positions for case studies

A deeper investigation on this aspect should be carried out studying the sensitivity of the different coupling methods to experimental measurements to analyze source of errors. However proposed method seems promising since allows to obtain tool-tip FRF with high accuracy (comparable to other methods) without the need of other experimental calibration phases. Tool-tip FRFs obtained are used to calculate SLDs in the same way presented previously, results are shown in Figure 8.31, Figure 8.32 and Figure 8.33. Same trend in the FRFs can be found in the SLD, as expected. Proposed method returns good prediction of SLD both in hydraulic and collet toolkits, on the other hand stable and unstable zone alternation is not effectively obtained for shrink fit toolkit: dominant frequency error (8.7%) is high to reach accurate results on lobes positioning.

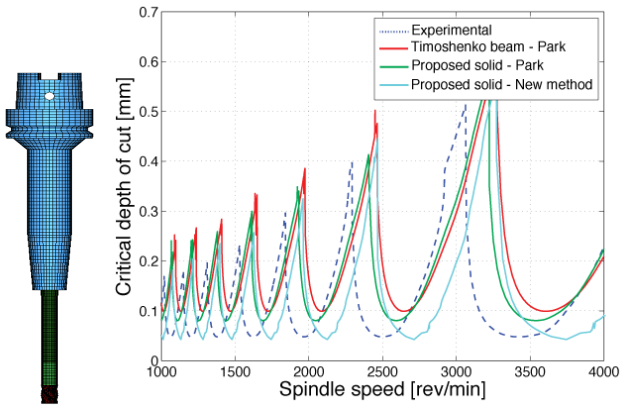

Figure 8.31 SLDs for toolkit 2 (two points method)

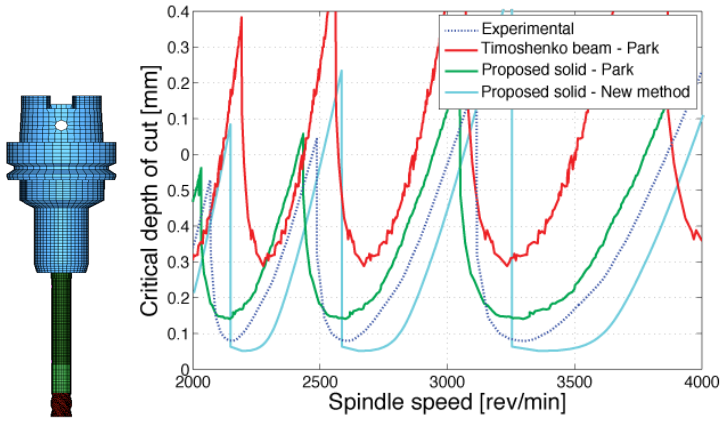

Figure 8.32 SLDs for toolkit 3 (two points method)

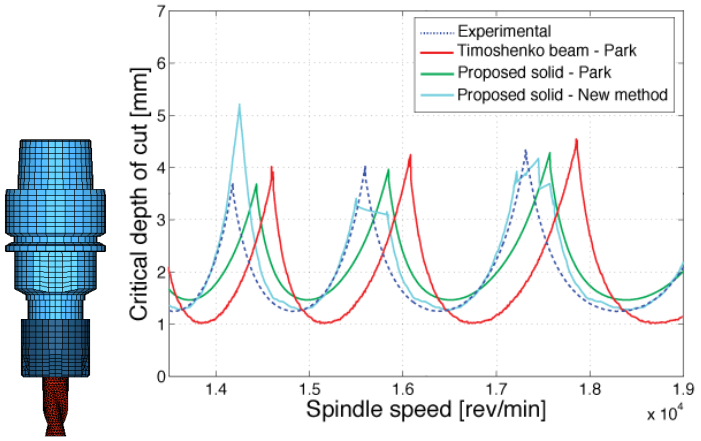

Figure 8.33: SLDs for toolkit 5 (two points method)

8.5. Simplified machine tool FE model

In this section a different approach to machine tool dynamics simulation is presented. Starting from the same assumption of analytical formulations, a procedure to create a simplified machine tool FE model is proposed. Compared to analytical formulations (i.e., Receptance Coupling) this method does not directly obtain FRFs but build a hybrid model in FE environment. Therefore the scope of this new simplified model prepares the ground to a simplified machine tool FE model that could be used for other applications, such as time-domain simulation or simplified flexible multi-body system.

Proposed method has been developed considering machine tool flexibility condensed in the spindle-holder-tool assembly in order to simplify the machine tool model and collate together easily the ever-changing toolkit. The idea is the same of analytical formulations based on frequency dependent stiffness but applied in FE environment: machine tool without tool is modeled by a lumped model, experimentally characterized by a set of FRFs

measurements on the tool-holder clamped to the spindle, without any tool. Frequency dependent springs are used in order to match, with a simple lumped model, the dynamic behavior of machine tool, generally composed by a large number of modes. The tool-tip FRF is then obtained coupling the lumped model with the FE model of the specific tool considered. Lumped model is connected with the tool by means of likely stiffness extracted by a numerical Craig-Bampton modal reduction [35] performed on the tool-holder in free-free configuration. To implement the proposed model are therefore required:

- A set of measurement on tool-holder clamped on the machine, no other calibration measurements are needed.
- FE model of tool-holder and tool

Starting from these inputs, proposed approach allows to identify tool-tip FRF to be used in chatter stability analysis. A flow chart of the proposed method is presented in Figure 8.34.

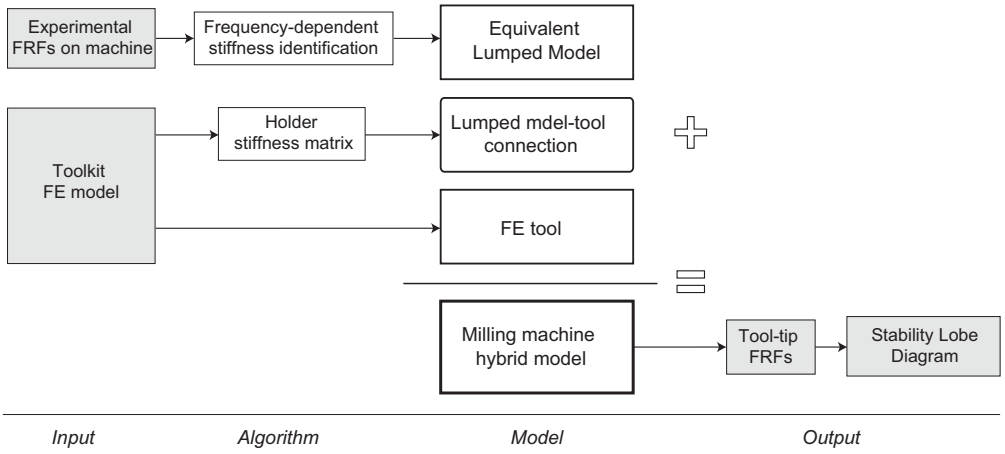

Figure 8.34 Flow chart of the proposed method

8.5.1. **Machine tool lumped model**

The lumped model is chosen as simple as possible: a two-degree of freedom (DOF) model is selected as the simplest one able to take into account the rotational DOF that cannot be neglected for accurate FRF identification at the tool-tip [27].

The proposed model is composed by two masses rigidly connected and three grounded frequency dependent stiffness springs: two translational (K_1 e K_2) and one rotational (K_θ) that constrain the model, lumped model is presented in Figure 8.35 where θ is the relative rotation between point 1 and 2.

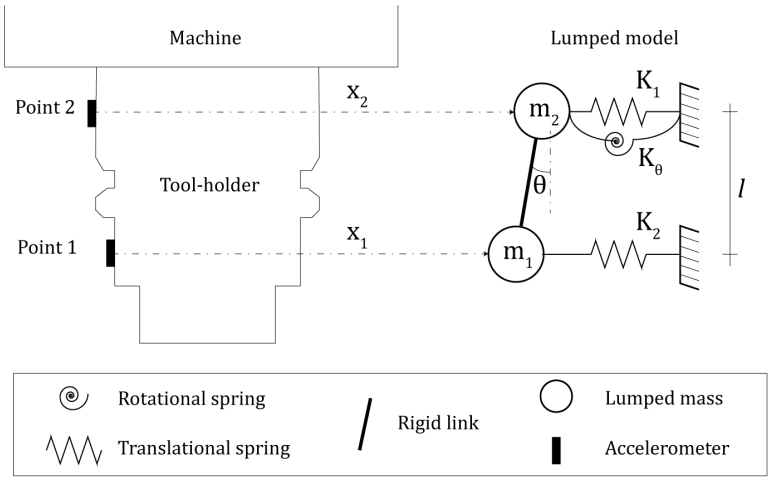

Figure 8.35 Lumped model scheme

Model is thus described by three complex springs, characterized by structural damping as in equation (8.35):

$$K_j(f) = k_j(f)(1 + ih_j) \tag{8.35}$$

where capitol K is the complex stiffness composed by stiffness *k* and structural damping *h*.

For every frequency (*f*) the stiffness are calculated by means of experimental measurements performed on the machine tool with only the tool-holder clamped on the spindle. Two points on tool-holder are chosen to measure dynamic response (FRFs) and distance between points is measured. To obtain an equivalent lumped model the experimental receptance matrix (G) is required. Defined model enables to avoid rational FRF measurements: θ angle is identified through nodes translations according with equation (8.36):

$$\theta = (x_2 - x_1)/l \tag{8.36}$$

where x_1 and x_2 are the translational displacements and l is distance between the two masses chosen equal to the one between the two measurements points. Equation (8.36) is valid as long as segment between point 1 and point 2 is considered rigid, same assumption proposed in the analytical formulations presented in section 8.3. This is an acceptable approximation: proximity of the points and stiffness of tool-holders suggest this behavior in the frequency range of interest (within 20kHz).

The result of this approximation is a 2x2 matrix composed only by translational FRFs. Three FRFs should be then measured: Point 1 driving point (G_{11}), Point 2 driving point (G_{22}) and cross Points 1 and 2(G_{12}). FRF matrix is presented in equation (8.37).

$$[G(f)] = \begin{bmatrix} G_{11}(f) & G_{12}(f) \\ G_{12}(f) & G_{22}(f) \end{bmatrix} \tag{8.37}$$

These FRFs are used to extract lumped model parameters (mass, stiffness and damping) according to the (8.38) and (8.39) formulas:

$$[H(f)] = [G(f)]^{-1} \tag{8.38}$$

$$[K(f)] = [H(f)] + [M](2\pi f)^2 \tag{8.39}$$

where:

$$[M] = \begin{bmatrix} m_1 & 0 \\ 0 & m_2 \end{bmatrix} \tag{8.40}$$

$$[K(f)] = \begin{bmatrix} K_1(f) + \dfrac{K_\theta(f)}{l^2} & -\dfrac{K_\theta(f)}{l^2} \\ -\dfrac{K_\theta(f)}{l^2} & K_2(f) + \dfrac{K_\theta(f)}{l^2} \end{bmatrix} \tag{8.41}$$

No univocal solution for the system can be obtained: more than one equivalent lumped model can be found. In this work mass values are fixed and frequency dependent stiffness hence calculated according to the equations (8.42), (8.43) and (8.44):

$$K_\theta(f) = k_\theta(f)(1 + ih_\theta) = -l^2 H_{12}(f) \tag{8.42}$$

$$K_1(f) = k_1(f)(1 + ih_1) = H_{11} - K_\theta / l^2 + m_1(2\pi f)^2 \tag{8.43}$$

$$K_2(f) = k_2(f)(1 + ih_2) = H_{22} - K_\theta / l^2 + m_2(2\pi f)^2 \tag{8.44}$$

In this way thanks to real and imaginary part of *H,* for each frequency, stiffness (*k*) and structural damping (*h*) can be calculated to be included in the lumped model. Stiffness and mass matrices values are not physically related to the machine structure but allow the lumped model to be dynamically equivalent to the milling machine without tool. Thanks to frequency dependent stiffness a simple 2 DOFs model can accurately represent machine dynamic behavior generally characterized by a large number of modes.

8.5.2. **Tool**

The proposed method requires tool-holder and tool FE model. The method has been implemented in FE environment; therefore any kind of FE elements can be used (e.g., beam, solid). In order to apply proposed approach to any tool clamped to the machine with only one measurement set-up, also tool-holder is included in the modeling approach. Tool-holder FE model is essential for the method: this component is the link between machine and tool, i.e., experimental measurements and numerical model.

8.5.3. **Machine – Tool connection**

Connection between the two points of measurements and tool is ensured by tool-holder flexibility, in order to model properly this connection, lumped model and FE tool will be coupled with holder stiffness between the points of interest. This stiffness is obtained using the Craig-Bampton modal reduction [35] of the tool-holder FE model, same technique adopted in Chapter 4. This reduction method allows reducing the size of a finite element model, resulting in an equivalent model constituted only by a small subset of reference nodes. This equivalent reduced model (called "superelement" in MSC Nastran) is composed by new reduced mass and stiffness matrices. In this case this technique is used to obtain connection stiffness matrix, reducing tool-holder in free-free configuration to:

- Connection nodes with lumped model, positioned in the measurements points.
- Interface nodes between tool-holder and tool.

Only stiffness matrix is extracted from modal reduction, mass is not needed because already included in the experimental tests and thus in the lumped model.

A scheme of the connection nodes is reported in Figure 8.36.

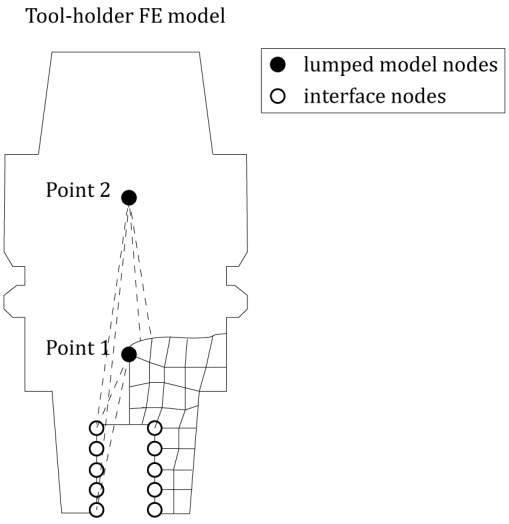

Figure 8.36 Connection scheme

8.6. Experimental validation

Proposed approach has been experimentally validated on a Mori Seiki NMV 1500 DCG milling machine using a DIEBOLD HSK 32E R16x60 tool-holder with collet chunk connection, an ISCAR Multi-Master shank has been used as tool.

8.6.1. Experimental characterization of lumped model

Tool-holder chosen has been mounted on the machine without tool (no collet, nut and shank are attached). Experimental modal analysis (EMA) has been performed on two points in the positions presented in Figure 8.37.

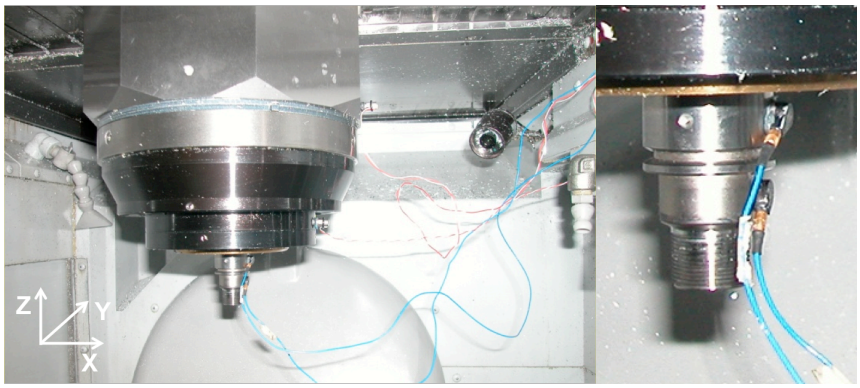

Figure 8.37 Experimental set-up for lumped model definition

Two accelerometers (PCB 352C22) have been attached to the tool-holder and FRFs measurements have been performed by means of impact hammer (Brüel & Kjær 8202). Both driving and cross FRFs have been acquired with only one measurements set up. Starting from these measurements lumped model is created: nodes distance l has been chosen equal to distance between the two measurements points (19.6 mm), fictitious masses (m_1 and m_2) have been set equal to half total tool-holder mass (0.086 kg). Frequency variable stiffness and damping values have been calculated according to proposed method. Direct FRFs simulations performed on lumped model using MSC Nastran have confirmed dynamic equivalence between experimental and model response as imposed; results are presented in Figure 8.38 for one of the driving point FRF.

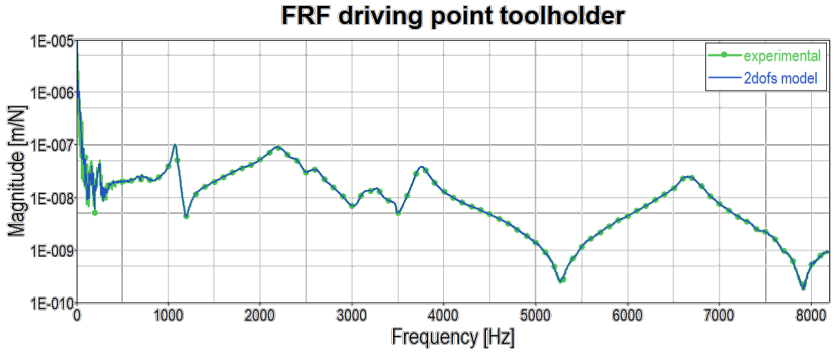

Figure 8.38 FRFs comparison between lumped model and experimental machine tool

8.6.1. **FE model**

3D solid FE elements have been used to model tool-holder and tool assembly composed by: tool-holder, collet, nut and shank. Solid elements have been adopted because beam elements fail to model properly elastic collect connection: a detailed solid model is thus required (Chapter 6). Preliminary sensitivity studies have been conducted in order to get a suitable balance between computational time and accuracy of the numerical simulations. The mesh size has been chosen smaller than required by convergence analysis, to achieve a better components geometry description. Interchangeable cutting head that can be added to the shank has been modeled as a lumped mass. Tool-holder and tool assembly, its FE model and components are shown in Figure 8.39.

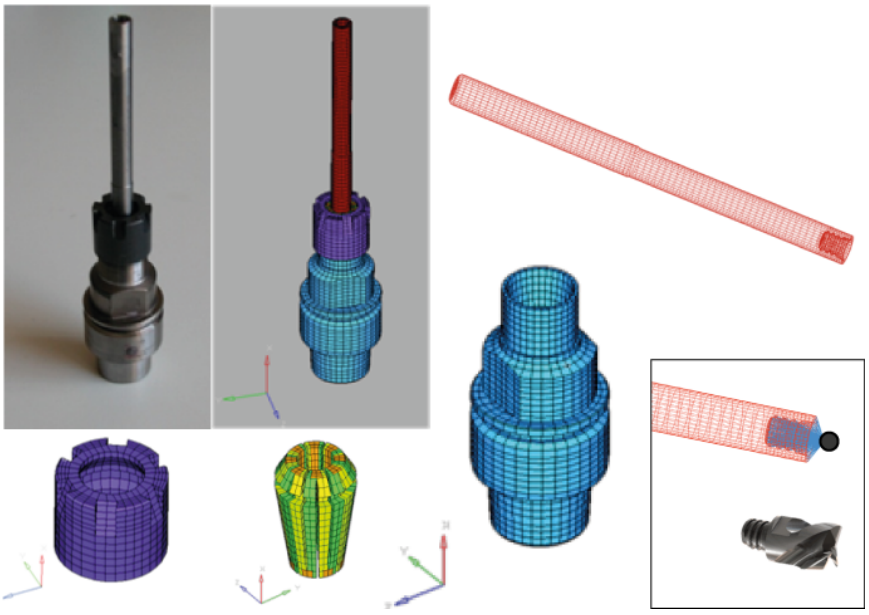

Figure 8.39 Finite element models of the tool-holder tool assembly

Every single part has been validated by experimental modal analysis in free-free configuration. In order to exclude modeling errors from method validation, materials proprieties have been then optimized to match experimental results, as presented in section 6.4.4. In this procedure accelerometer masses have been taken into account, including them in the model as concentrated mass (CONM2 in Nastran). So that identified material proprieties are not affected by accelerometers masses.

In Figure 8.40 is reported, as example, the test setup and the FRFs comparison for the shank and the collet. Same procedure has been repeated for all the components and the assembly. MSC Nastran© has been used to obtain the numerical results.

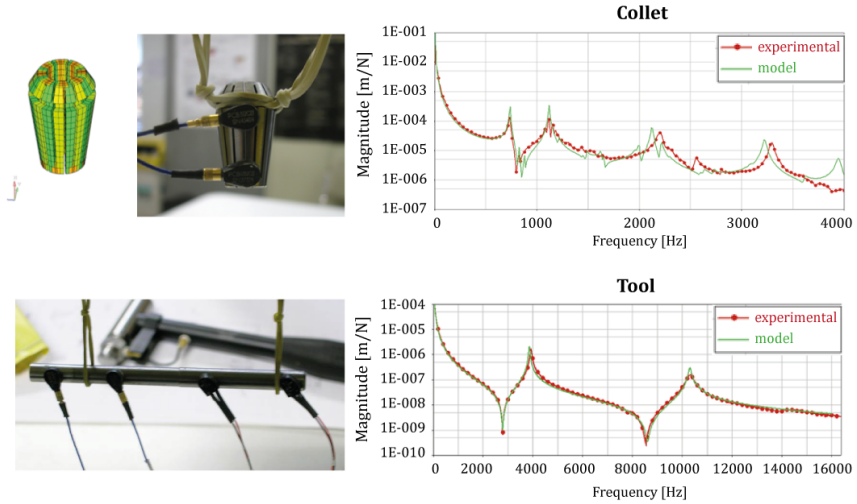

Figure 8.40 Test setup and FRFs comparison between experimental and numerical results

In Table 8.9 the optimized values for steel and carbide used in the numerical simulation (a damping ratio value of 0.005 has been chosen for each component) are summarized.

Table 8.9 Mechanical characteristics of the materials used in the simulation

	Type	Material	Young Modulus (N/mm^2)	Densitiy (kg/m^3)	Poisson coefficient
Tool-holder	HSK32E	Steel	2.0 E+11	7881	0.25
Nut	.	Steel	2.1 E+11	7800	0.31
Tapered Collet	R16 Φ8	Steel	2.0 E+11	7860	0.31
Tool	Shank 110mm Φ8	Carbide	6.6 E+11	13466	0.24

This validation and optimization procedure has been carried out in order to present method results without the effect of inaccuracy of FE model of the tool. Adjustment of material proprieties is therefore not required in general. Nevertheless in the same way of every method based on FE model, an accurate model is required to return accurate results.

8.6.2. **Coupling and validation**

Lumped model and tool model are connected via stiffness matrix extracted from reduced tool-holder model to interface nodes with collet and connection nodes positioned in measurements points. Tool-holder reduction nodes are presented in Figure 8.41.

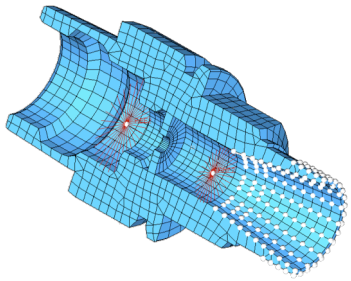

Figure 8.41 Tool-holder reduction nodes

A simplified hybrid experimental-FE model of the machine is created, shown in Figure 8.42

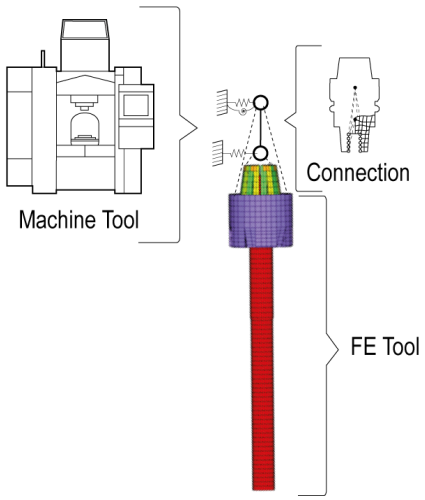

Figure 8.42 Simplified machine tool model

Machine tool model allows predicting dynamics at the tool-tip for chatter stability analysis. Simulated results have been experimentally verified. Impact tests have been performed on machine tool at the tool-tip, with different overhang (86.1 and 70.7 mm), with and without the interchangeable cutting head (Figure 8.43). A Brüel & Kjaer Type 8202 impulse hammer, LMS Scadas III frontend, LMS Test.Lab 11A software, and PCB 352C22 accelerometers (0.4 g) have been used.

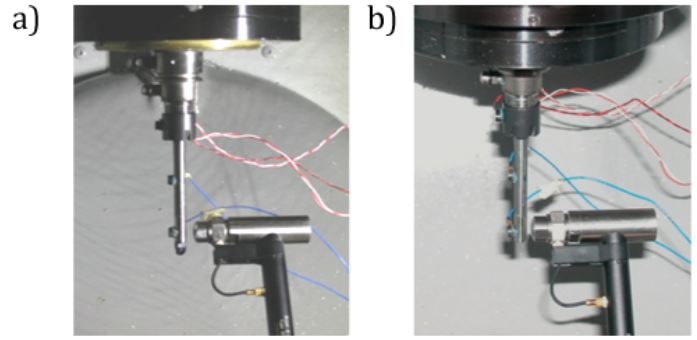

Figure 8.43 Experimental validation set-up. Test with (a) and without (b) cutting head

The comparison shows an excellent agreement between numerical and experimental FRFs, as reported in Figure 8.44.

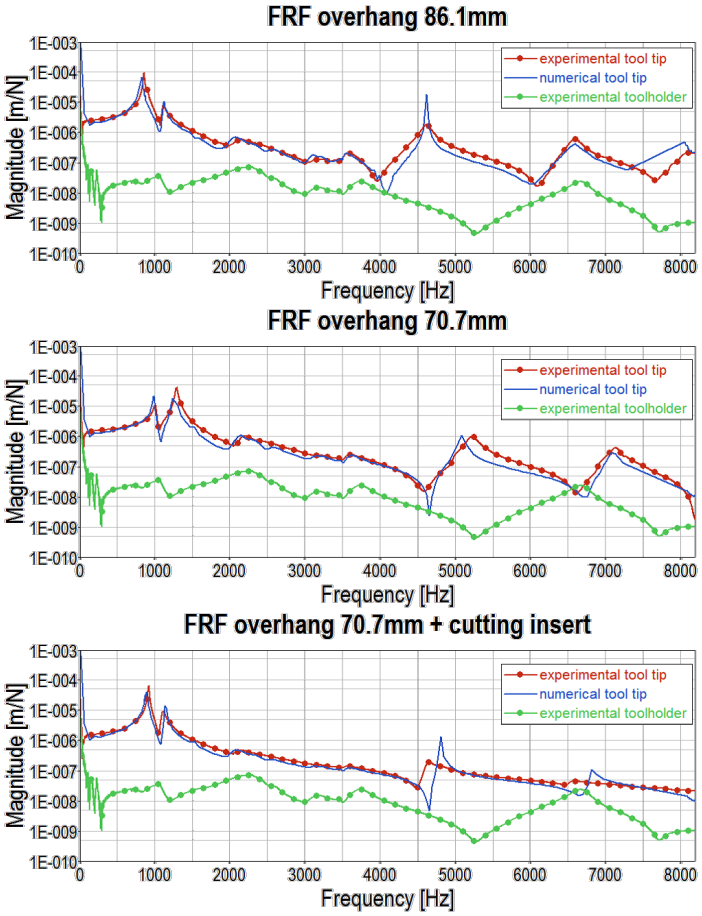

Figure 8.44 Experimental and simulated tool-tip FRFs.

FRFs prediction is accurate in a very large frequency range (till 8192Hz), although some discrepancies are detected at high frequency and for what concerns damping. This could be caused by FE model inaccuracies (more significant at high frequency) and FE model damping modeling not analyzed deeply in this paper.

8.6.3. **Stability prediction**

Tool-tip FRFs simulated can be used for stability prediction. In this section Stability Lobe Diagram (SLD) according to Altintas and Budak theory [25], are calculated with both experimental and numerical FRFs in order to present method chatter prediction capability. Tool-holder and tool presented for validation is used: 70.7mm overhang and cutting insert is considered (2 flutes 8 mm diameter). A side milling operation on Aluminum 7075-T6 (cutting coefficients Ktc= 796 MPa, Krc=196 MPa) at 1 mm radial depth of cut is simulated. Results are shown in Figure 8.45 in which stability lobe diagrams for experimental and proposed method FRFs are plotted.

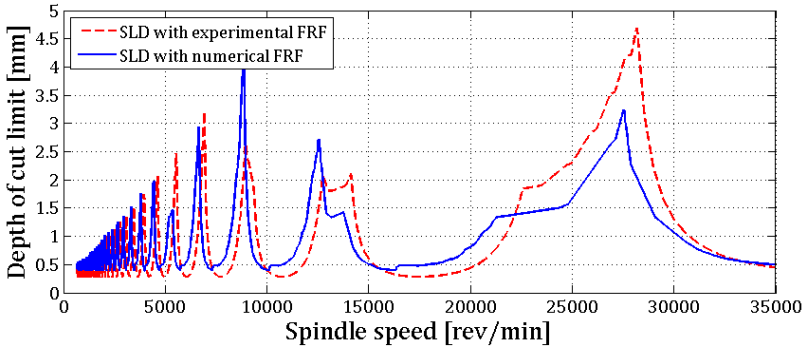

Figure 8.45 Comparison between stability lobes obtained by experimentally measured FRF and predicted FRF

8.7. Conclusions

In this Chapter hybrid experimental-numerical methods have been investigated. Firstly state of the art method by Park et al. has been implemented with the FE model of entire toolkit. In this way the number of experimental tests required for each machine tool is reduced, although a calibration phase is always needed. Then a series of new methods has been proposed that do not require calibration test but only a single test set-up with two measurement points. This allows further reducing number of tests required, increasing efficiency of RCSA methods that could become more attractive for industrial application. Presented methods have been applied to real test cases and compared: a good agreement with experimental tests is obtained with similar results for both methods. Moreover test cases results show the high sensitivity of RCSA methods to toolkit FE models and how SLD prediction is strictly dependent on tool-tip FRF accuracy

A hybrid FE-experimental model that uses an experimental characterization of machine tool dynamics at the tool-holder, coupled together to a FE representation of the tool has been developed. The tests carried out using this approach in different conditions (e.g.,

overhang) have proven a good capability to predict FRF of the machine at the tool-tip. As the analytical methods, only one measurement set-up on the machine without tool is required, no other calibration tests are needed. This method differs from analytical formulations building a simplified FE model of the milling machine. Obtained model can be effectively used to evaluated tool-tip FRF and Stability Lobe Diagram but could be adapted to be used for other applications, e.g., time-domain simulation.

9. Speed-varying cutting force coefficients

9.1. Overview

Besides machine tool dynamics, accurate cutting force simulation is essential to obtain a reliable chatter stability prediction (see Chapter 1). Various cutting force models have been developed on this purpose and presented in literature [6, 74, 75]. Despite the differences between the existing force models, it is practically universally assumed that cutting forces are related to uncut chip area, through cutting force coefficients that could be obtained by means of experimental tests. The accuracy in cutting force prediction, and consequently in process simulation, is mainly related to the accuracy achieved in identifying such coefficients. There are mainly two ways to identify cutting force coefficients: using the mechanics of cutting and tool geometry or specific coefficients from direct experimental results. Regarding the first approach, the most used method is the one developed by Budak et al. [8] and known as "orthogonal to oblique transformation": a general approach that allows to identify cutting force coefficients for different cutting tools and operations from data extracted from orthogonal cutting tests. Coefficients obtained using the mechanics of cutting are more versatile, since they can be applied to any different tool geometry thanks to the orthogonal to oblique transformation; nevertheless some approximations are included in this approach. On the other hand specific coefficients are consistent only for the same tool-material combination used in the experimental tests but accuracy achieved with this approach could be higher. There are different ways to obtain specific cutting coefficients from experimental results; among them, the most common are based on average forces measurements per revolution in slot milling tests [6, 76] but other methods based on simulation and instantaneous forces [77-79] have been proposed. In instantaneous approaches force coefficients are identified using an inverse method by fitting simulated and measured forces in time domain.

General approach to specific cutting force coefficients identification is based on low speed experimental tests to limit dynamic issue of cutting force measurement devices [6]. The main drawback of this approach is that the so-identified coefficients are employed in simulation of general machining operation at different spindle speeds. This could be an issue considering that cutting process and chip formation mechanics change varying cutting speed, suggesting a change in coefficients as well. Speed dependence of cutting force coefficients has not been widely investigated in literature showing partial and conflicting results. In [80, 81] a variation of cutting coefficients with speed is presented and this trend appears relevant

especially for tangential forces: according to these studies coefficients are higher at low speed, showing a decrease and then increasing again in high speed area. On the contrary according to Wang et al. [82] cutting coefficients are constant varying cutting velocity, but only a limited range of speed has been tested (500-1500 rpm). Anyhow all these analysis are affected by uncertainties and errors derived from measuring cutting forces at high rotational speeds. Evaluating coefficients with high speed milling tests, in fact, is challenging due to the frequency bandwidth of commercial force sensors that is inadequate for high spindle speeds (dynamometer's frequency response limits measurements to low speed).

In this work speed-varying cutting force coefficients are investigated, overcoming dynamometer dynamics issues by means of an improved compensation technique, based on Kalman filter estimator [83]. With this technique a more reliable estimation of specific cutting forces coefficients has been carried out by means of milling tests over a wide range of speed (1,000-30,000 rpm). An improved instantaneous coefficients identification approach is proposed and implemented: a trochoidal cutting edges path for chip thickness identification has been chosen as already presented in [77] but a more accurate analytical formulation [84] has been used including run-out in order to better fit measured forces with simulated ones. Fitting procedure has been performed by means of Genetic Algorithm (GA): this way all the coefficients and run-out values can be obtained from one set of force measurements, properly compensated, with reasonable computational effort. Differences between the two identification methods have been presented both in coefficients values and fitting curves, analyzing compensation effects on cutting force prediction reliability.

Experimental tests have finally been conducted on Aluminum 6082-T4 alloy, employing nine different spindle speeds: cutting speed influence on cutting force coefficients for linear force model has been consequently evaluated. Thanks to this investigation cutting speed dependency of specific coefficients is highlighted and the effectiveness of the improved identification technique validated. Based on cutting speed dependent force coefficients, a method to create analytical Stability Lobe Diagram [25] has been developed, taking into account different cutting coefficients changing continuously with spindle speed. The reliability of obtained stability lobe diagram for HSM has been proved by experimental tests.

9.2. Cutting force coefficients identification methods

9.2.1. Cutting force model

Coefficients estimation is based on the linear cutting force model presented by Altintas in [6] where cutting force is expressed by three components (tangential, radial and axial) and six different specific coefficients as shown in equation (9.1).

$$\begin{aligned} dF_t &= K_{tc} H db + K_{te} dl \\ dF_r &= K_{rc} H db + K_{re} dl \\ dF_a &= K_{ac} H db + K_{ae} dl \end{aligned} \tag{9.1}$$

where dl is the edge length of each discrete element in which cutting edge is discretized, H is the underformed chip thickness, db is the chip width. The equation (9.1) describes each component by two contributions: one related to material shearing and proportional to chip thickness, given by K_{ic}, and one related to friction and ploughing, given by K_{ie} coefficients (where i refers to tangential, radial, or axial).

The tangential, radial and axial components are then transformed to the X (feed), Y (normal) and Z (axial) directions by the transformations [6] in Eq. (9.2):

$$\begin{Bmatrix} dF_X \\ dF_Y \\ dF_Z \end{Bmatrix} = \begin{bmatrix} -\cos(\varphi) & -\sin(\varphi)\sin(\kappa) & -\sin(\varphi)\cos(\kappa) \\ \sin(\varphi) & -\cos(\varphi)\sin(\kappa) & -\cos(\varphi)\cos(\kappa) \\ 0 & \cos(\kappa) & -\sin(\kappa) \end{bmatrix} \begin{Bmatrix} dF_t \\ dF_r \\ dF_a \end{Bmatrix} \tag{9.2}$$

where φ is the spindle rotation angle and κ is the approach angle of the cutting edge.

Forces are calculated for each plane in which tool is discretized (Figure 9.1a) and integrated to obtain total force acting on the tool.

9.2.2. **Average method**

The fastest and most used technique for calibrating specific cutting force coefficients from milling tests is called average force method [6] which requires a set of milling tests at different feed rates, but at constant axial and radial immersion. The average cutting forces can be expressed as linear functions of the feed rate, therefore average forces at different feed rates are measured and coefficients are estimated by data linear regression.

Slot-milling tests are generally performed to simplify identification, in this case cutting force coefficients are calculated as shown in Eq. (9.3).

$$\begin{aligned} K_{tc} &= \frac{4\underline{F}_{yc}}{Na} & K_{te} &= \frac{\pi \underline{F}_{ye}}{Na} \\ K_{rc} &= \frac{-4\underline{F}_{xc}}{Na} & K_{re} &= \frac{-\pi \underline{F}_{xe}}{Na} \\ K_{ac} &= \frac{\pi \underline{F}_{zc}}{Na} & K_{ae} &= \frac{2\underline{F}_{ze}}{Na} \end{aligned} \tag{9.3}$$

where $\underline{F}_{ic}$ is the proportional contribution and $\underline{F}_{ie}$ is the offset of the linear regression of data related to feed rate. In this work slotting operations have been performed at five different feed rates and repeated at different spindle speeds in order to collect cutting coefficients for each cutting velocity.

9.2.3. **Instantaneous method**

Another approach to obtaining specific cutting force coefficients is based on fitting measured and simulated forces in time domain. In this paper this approach is called "instantaneous method" [77]: it is more complex than average method because it implies to

hypothesize a formulation to simulate cutting forces in time domain and a fitting method, on the other hand it requires only one set of measurements for coefficients estimation.

Chip thickness formulation

Chip thickness is required to calculate cutting forces as presented in equation 1. In order to accurately simulate them for "instantaneous" method, an accurate prediction of underformed chip thickness is needed. Different approaches are presented in literature, the most used method entails a circular tool-path approximation, neglecting the actual trochoidal tool motion. To reach a more accurate simulation, trochoidal motion is considered in this paper (as in [77]), in addition specific run-out formulation has been implemented. This feature, not yet implemented in usual cutting coefficient identification techniques, could represent a sensible advantage in accurately identifying both the cutting force coefficients and run-out parameters by means of a single experimental test.

A particular analytical formulation for chip thickness simulation presented by Kumanchik and Schmitz in [84] has been applied to the proposed approach. In their work trochoidal path of the i-th tooth in a milling cut is described as:

$$x_i = \rho\theta + r_i \sin(\theta + \varphi_i) \qquad y_i = r_i \cos(\theta + \varphi_i) \tag{9.4}$$

where $\rho=V_f/n$ is the radius of the circle that defines the cycloidal motion of the tooth, V_f the linear feed rate, n is the rotational speed of the tool, r_i is the radius of the i-th tooth including run-out, θ the instantaneous cutter angle, and φ_i is the angle between θ and the i-th tooth (Figure 9.1a).

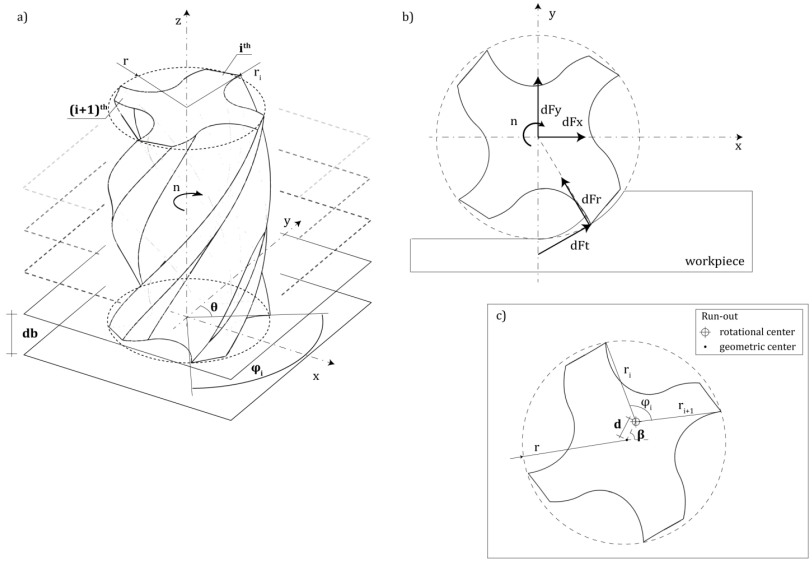

Figure 9.1 Tool scheme: a) Variables, b) Force components, c) Run-out formulation

Starting from this, chip thickness formulation is calculated as:

$$H_i = r_i - \sqrt{\rho^2(\theta_0 - \theta)^2 + 2\rho \cdot r_{i+1}(\theta_0 - \theta)\sin(\theta_0 + \varphi_i) + r_{i+1}{}^2} \tag{9.5}$$

where:

$$\theta_0 = \theta - \frac{\varphi_{i+1} - \varphi_i}{(\rho / r_{i+1})\cos(\theta + \varphi_i) + 1} \tag{9.6}$$

Thanks to this formulation the real geometric trochoidal path is analytically computed, improving reliability of simulated forces. Circular approximation, in fact, entails errors in the chip thickness calculation as shown in Figure 9.2, where trochoidal (Figure 9.2a) and circular (Figure 9.2b) tool-paths are compared (two flutes tool is considered as example).

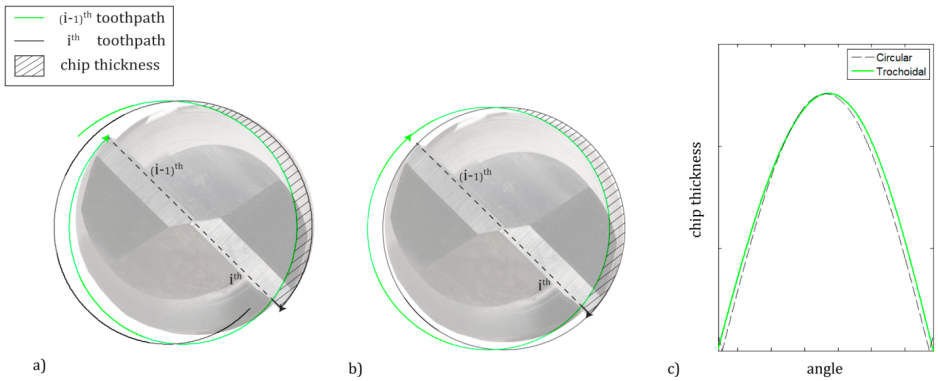

Figure 9.2 Trochoidal tool-path (a) compared to circular (b) for chip thickness identification (c)

Run-out

As already mentioned, thanks to the improved chip thickness formulation also run-out can be taken into account: any cutting edge, in fact, can be characterized by radius (r_i) and angle (φ_i). To consider valid values for run-out, a correlation between cutting edges radii and angles has been implemented. The effect of run-out has been included considering the position of rotational center shifted with respect to tool geometric center. Therefore cutting edges parameters have been calculated by the distance (d) from geometric center and the angular position (β) of rotational center as shown in Figure 9.2c. This formulation allows to introduce run-out by two variables, excluding non-physical values, very useful feature in fitting application.

Fitting method

Once forces are simulated starting from chip thickness formulation, a fitting method is required to identify optimal cutting force coefficients. In this paper Genetic Algorithm has been used to optimize fitting of simulated and measured forces. Genetic algorithms are efficient search algorithms based on the mechanics of natural genetics. They imitate nature with their "survival-of-the-fittest" approach, performing fitting procedure in a very efficient way compared to more-conventional search technique. GA is nowadays widely used to solve

optimization problems in different research field, including machining [85, 86]. In this paper, the simple genetic algorithm to least mean square (LMS) curve fitting [87] is implemented.

Nine variables are considered:

- Six cutting force coefficients (K_{tc}, K_{te}, K_{rc}, K_{re}, K_{ac}, K_{ae});
- Two parameters for run-out presented above (d and β)

Thanks to cutting and tool parameters and these nine variables, chip thickness and forces are simulated and compared with measured ones. Fitting has been performed by minimizing the fitness function in equation (9.7):

$$fo = \left|F_{sim} - F_{xp}\right|^2 / \left|F_{xp}\right|^2 \quad \textbf{(9.7)}$$

Fitting procedure has been performed for the three components (X, Y, Z) at the same time: resulting fitness function is the sum of the three specific function.

9.2.4. **Dynamics compensation**

Measuring cutting forces at higher spindle speeds entails acquiring signals characterized by frequencies contribution that could approach the transducer resonant frequency or even exceed it. This could result in appreciable distortion of the measured force signals in general applications. Although this is a known issue, just a few references in literature can be highlighted regarding specific compensation of force transducers, outlining three major approaches. The most intuitive technique is based on identifying the transfer functions (TFs) between measured and applied forces, hence reconstructing the original signal by multiplying the measured force signal for the identified transfer function matrix inverse. Such technique has been presented by Ricardo Castro et al. [88] and latter by Girardin et al. [89], including crosstalk contributions. This technique shows two major drawbacks since existence of the TF matrix inverse is not always ensured and small errors in TF identification could result in measurement noise amplification. An alternative technique, generally referred to as “accelerometrical compensation”, is based on measuring dynamometer cover plate accelerations and removing inertial force contributions by estimating an equivalent mass, as presented by Lapoujoulade et al. [90]. This technique revealed some accuracy problems and limited compensated bandwidth, moreover it requires a number of additional sensors (accelerometers). The most promising technique seems to be the one based on Kalman filter estimation, as presented by Albrecht et al. [91] and later by Chae and Park [92], where an hybrid formulation contemplating the implementation of additional accelerometrical signals is described. This technique seems to be more robust and accurate since it requires no direct matrix inversion and it should be less influenced by measurement noise, as a consequence of Kalman filter formulation.

In this work an improved technique has been developed following the technique described in [91] but including some adjustments that have been needed to overcome numerical limitations and extend compensation bandwidth over a wide frequency range, as presented in [83].

Improved compensation technique

A crucial process in determining global and local accuracy of these techniques is fitting the measured FRFs into mathematical TFs formulations to numerically compute the compensation filters. Instead of using a modal identification approach, a technique mainly based on the rational fraction polynomial method (RFP) [93] has been implemented. This technique allowed better global accuracy, even if still not adequate over some specific frequency ranges as shown in Figure 9.3. Some evident accuracy improvements have hence been achieved by using the results obtained with this technique as initial estimates for a fitting algorithm based on the damped Gauss-Newton method for iterative search [94]. This approach ensured adequate accuracy is maintained over the entire frequency range and revealed to be computationally efficient.

This second technique has demonstrated to be sensibly more accurate and has been preferred to the modal curve fitting techniques given that no interest is put in modal parameter identification and accuracy was found to be definitely not adequate, at least in this specific application. Figure 9.3 shows a comparison between the fitting results obtained using the two described fitting techniques over one of the experimentally identified FRFs.

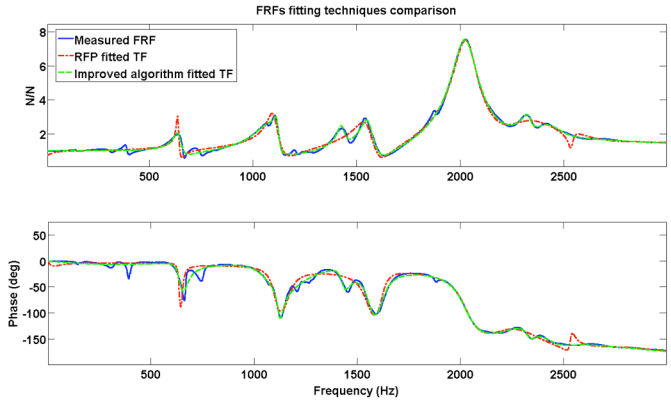

Figure 9.3 FRFs fitting techniques comparison over the 0-3000hz frequency range, using 21st order polynomials.

Figure 9.3 exemplifies that sufficient fitting accuracy could be achieved only using high order TF polynomials, even if the superior algorithm is used. The curve fitted TF generally leads to ill-conditioned system matrices and this issue gets more relevant as the polynomial order increases, actually preventing numerical filter computation in this specific application. Approaches such as system rescaling or similarity transformations could only partially solve the problem when the interest is put in compensating dynamic behavior over a wide frequency range with FRFs presenting many modes, as the one measured in this work. Hence to effectively extend the compensation bandwidth maintaining adequate accuracy over the entire frequency range a specific approach has been developed and allowed to extend the implementation of the described compensation technique to most practical applications, even in HSM if needed. Since the polynomials used could not exceed a given order without determining numerical limitations, the maximum allowable polynomial order has been imposed for the fitting algorithm and the fitting frequency range has been reduced as much as needed to ensure adequate accuracy over the desired fitting range. By doing so accuracy is maximized over a specific frequency range overcoming numerical limitations, on

the other hand the compensable bandwidth would result way too narrow for general applications.

To extend the compensable bandwidth as much as needed, while maintaining sufficient accuracy over the entire frequency range of interest, a sort of "parallel elaboration" approach has been developed. This approach is based on computing different compensation filters for specific discrete frequency ranges over the entire range of interest, maximizing accuracy without exceeding polynomial order limitations. The measured force signals could hence be frequency-partitioned over those specific frequency ranges using zero-phase band-pass filters; the single frequency contributions could then be processed with the specifically developed compensation filters, finally the compensated force signal could be reassembled by summing the single compensated contributions together. The "parallel elaboration" approach is exemplified in Figure 9.4.

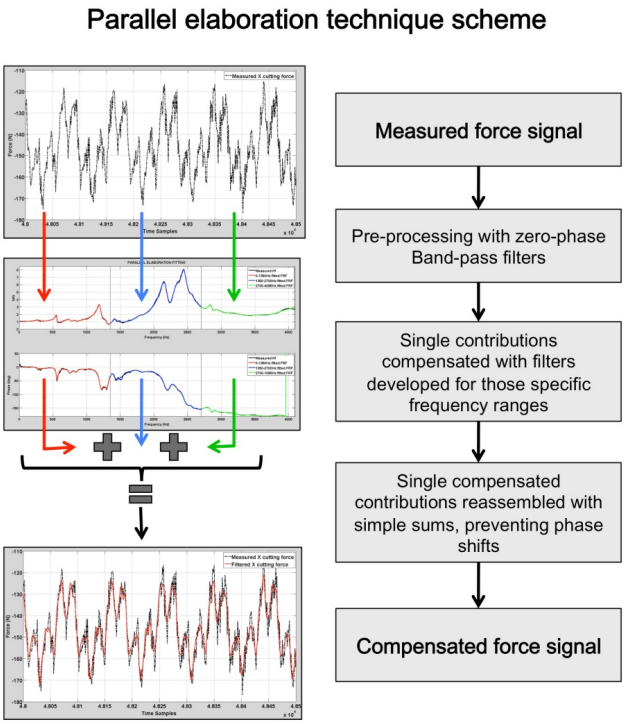

Figure 9.4 Parallel elaboration technique scheme.

This method allows to overcome most of the limitations experienced, but its effectiveness and accuracy mostly depend on the pre-process filtering phase that could become computationally demanding if complex filters are used. Nevertheless in this specific application good results in term of accuracy have been achieved even using computationally efficient 8^{th} order Butterworth filters. The successive steps necessary for filter computation have been accomplished in accordance with the method reported in [91]. Results obtained by the compensation techniques in cutting coefficients estimation will be fully discussed in a following paragraph. The improved compensation technique has been validated by means of

experimental tests and supporting results have been obtained in terms of accuracy and effectiveness.

9.3. Experimental validation

To investigate identified cutting coefficients speed-dependence, using both the average and instantaneous force methods, some experimental cutting tests have been conducted; slot milling operations were chosen, as requested for simplifying the average force method implementation.

9.3.1. Instantaneous method

Experimental cutting force coefficients identification has been carried out using a CNC vertical machine, a Mori Seiki NMV1500DCG. The material used for the machining tests was an Aluminum 6082-T4 alloy. Workpiece used was a bar 60x60x150mm clamped to dynamometer with two screws (Figure 9.5b). A three-component Kistler dynamometer type 9254 A, has been mounted on machine table and coordinates system has been set to level force sensor surfaces (Figure 9.5a). LMS Scadas III frontend and LMS Test.lab 11A software have been used to acquire signals. Tool has been chosen in order to ensure stable depth of cut in slotting operations. Different tools and overhangs have been tested, identifying tool-tip FRF and calculating Stability Lobe Diagram (SLD) with coefficients measured by the authors in [80] at low speed: a two flutes Garant 201770 with 8 mm diameter have been selected and mounted with a 20mm overhang on HSK32ER20 tool-holder (Figure 9.5c). In Figure 9.6, stability diagram is presented, 2.5mm minimum critical depth of cut is identified, slot milling of 1.5mm are performed considering an adequate uncertainty margin. In order to determine the average cutting force coefficients, cutting forces have been measured during slotting at different spindle speeds (Figure 9.5d). For each speed five different feed rates have been tested for better computing linear regression in average method, cutting and tool parameters are summarized in Table 1. Feed rates have been chosen in accordance to the one suggested by cutting tool manufacturer (0.03 mm).

Table 9.1 Cutting and tool parameters for speed-varying cutting force coefficients investigation

Tool parameters					
Diameter (mm)	8		**Helix angle**	45°	
Flutes number	2		**Material**	Carbide	
Cutting parameters for milling tests					
Spindle speed (rpm)	995	3979	7958	11937	15916
	19894	23873	27852	31831	
Feed per tooth (mm)	0.02	0.025	0.03	0.035	0.04
Axial depth of cut (mm)	1.5		**Radial depth of cut (mm)**	Slotting	

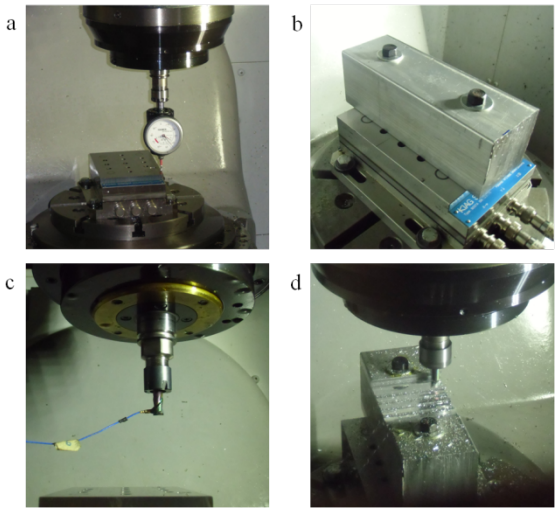

Figure 9.5 Tests set-up (a) dynamometer (b) workpiece (c) tool (d) slotting tests

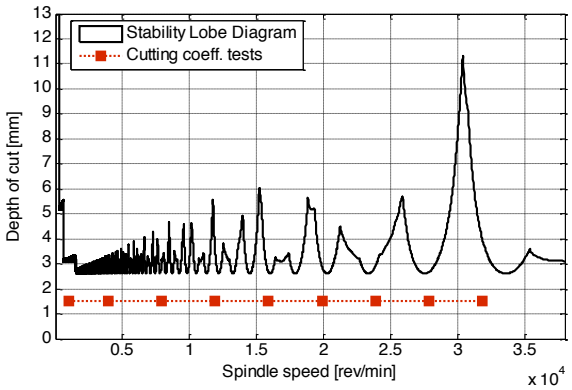

Figure 9.6 Stability Lobe Diagram for tests of coefficients identification

9.3.2. **Compensation**

To investigate coefficients estimation using the instantaneous force method at various spindle speed ensuring accuracy of cutting force measurements is maintained, the compensation technique described in previous section (and presented in [83]) has been used. Kistler reports a resonant frequency around 2.5kHz for the dynamometer used [95]. Referring to Kistler documentation about 5% amplitude rise can be expected at approximately 1/5 of the resonant frequency (f_n). So the expected usable frequency range of this dynamometer should be around 0 – 500 Hz, actually limiting the employable spindle speeds for cutting tests. In Figure 9.7 this aspect is exemplified.

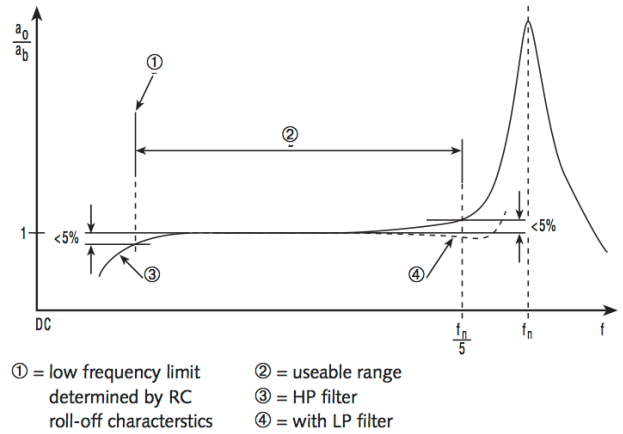

Figure 9.7 Typical dynamometer frequency response curve [95].

To estimate the actual measurable bandwidth of the Kistler 9257A table dynamometer used some impact modal tests have been conducted using a Brüel & Kjaer Type 8202 impulse hammer, LMS Scadas III frontend and LMS Test.lab 11A software. In Figure 9.8 the measured FRFs for each of the three dynamometer axis are reported.

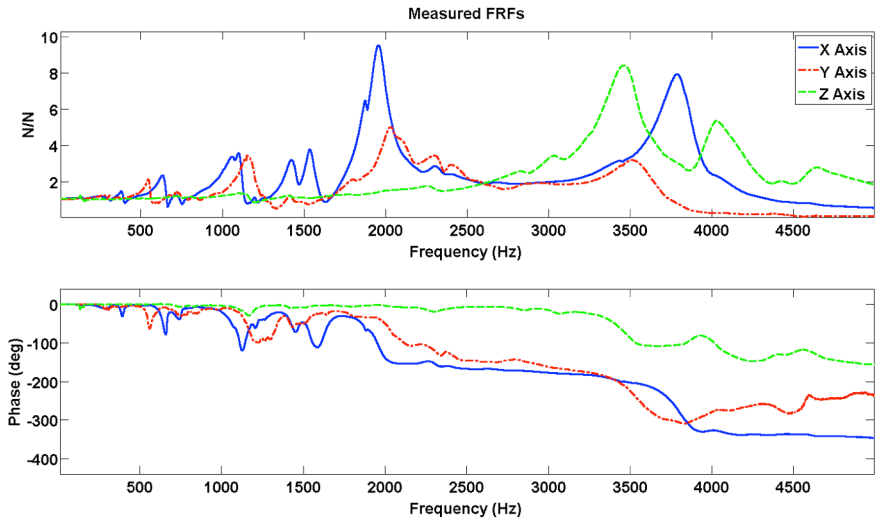

Figure 9.8 Measured Transmissibility FRFs for each of the Kistler 9257A dynamometer axis.

As shown even in the 0 – 500 Hz range some appreciable modes are presents, reducing the actual measurable bandwidth and confirming again the need of an effective and accurate compensation technique to extend the range of investigable cutting velocities. As a matter of fact, if no compensation is used, the highest spindle speed employable for the experimental tests could not exceed 3000rpm, resulting in around 100Hz tooth passing frequency with a two-teeth mill such as the one used in the experimental tests. The investigable range of cutting velocities would hence results not sufficient to define a general

trend of cutting coefficients speed-dependency. As anticipated the compensation technique effectiveness mostly depends on the FRFs measurements accuracy, but these FRFs could change over time due to workpiece material removal. Should be clear that this aspect is only relevant for table dynamometers. To ensure accuracy of the compensation technique is maintained over the entire cutting test session, the FRFs have been measured at three different times during the milling tests. In Figure 9.9 the results obtained for the X-axis of the dynamometer in the three different impact tests are shown.

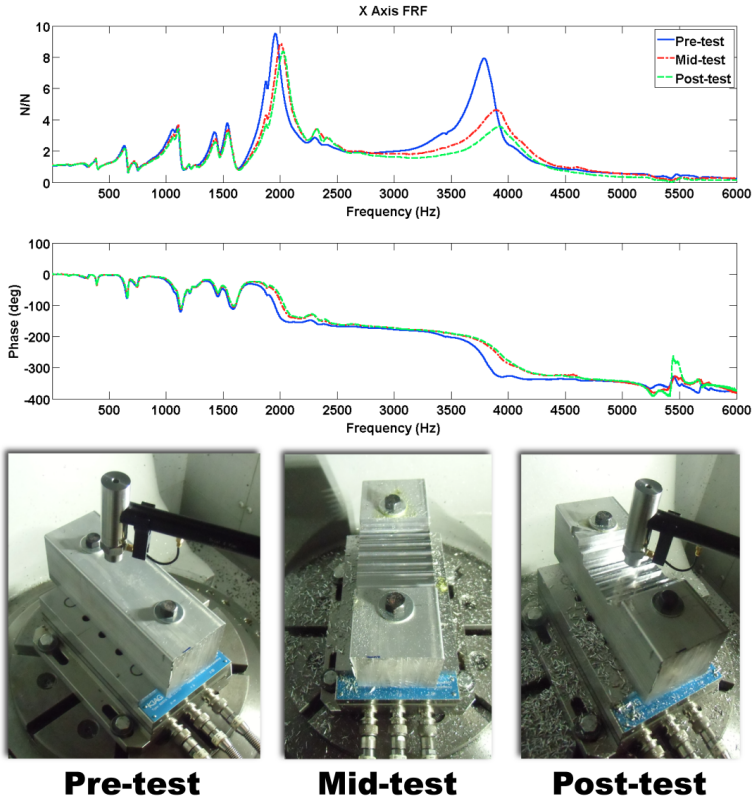

Figure 9.9 Measured transmissibility FRF-X in different times.

By doing so the compensation filters could be developed on experimentally measured FRFs that more closely represents the actual system dynamics during the specific cutting tests, ensuring that accuracy and effectiveness of the compensation technique is maintained all over the entire experimental test session. As shown in Figure 9.9 the changes in the measured FRFs are appreciable, especially below the transducer resonant frequency, confirming that neglecting the FRFs evolution would result in misleading compensated forces and not reliable coefficients estimation.

As should be expected by analyzing the FRFs the errors induced in force measurements by the system dynamic are appreciable and for some milling tests the difference in cutting force magnitude resulted as high as 60% comparing the measured and compensated force signals. This confirms again that an accurate and effective compensation

technique is an absolute requirement if interest is focused on cutting force measurements, even at relatively low spindle speeds.

In Figure 9.10 a comparison of measured and compensated forces for some of the milling tests is shown both in time domain (Figure 9.10) and frequency domain (Figure 9.10b).

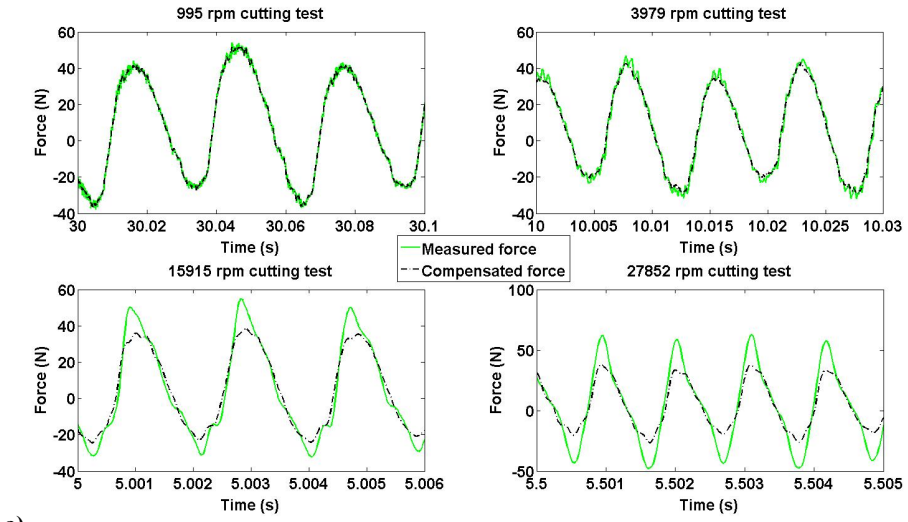

a)

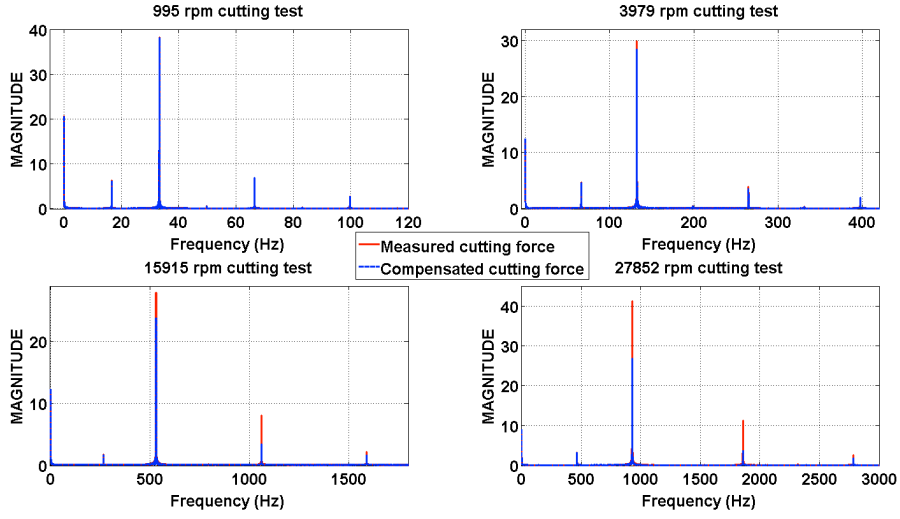

b)

Figure 9.10 Compensated and measured force signals for four different spindle speeds along X-axis of the dynamometer, Time domain (a) Frequency domain (b).

Effects of the compensation technique are highlighted in Figure 9.11 where a comparison between measured and compensated forces is shown over the measured FRF.

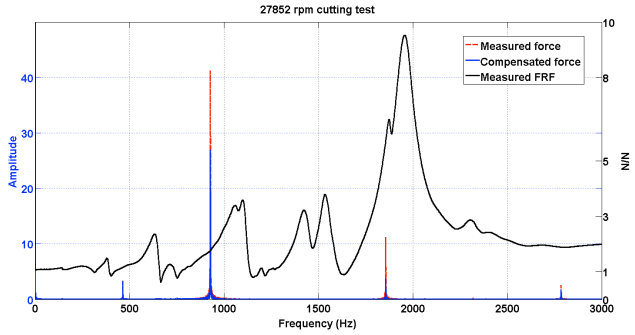

Figure 9.11 Detailed Frequency domain force signals related to measured transmissibility FRF

As reported in the figure the errors on the measured force signal are in accordance with the distortion imposed by system dynamics. Even if the differences between measured and compensated forces are appreciable, should be pointed out that no real need exists in compensating force signals if the average force method for cutting coefficient estimation is used since the mean force results not to be affected by system dynamics. This effect could be explained by pointing out that cutting force signals are actually composed of a mean constant (i.e., 0 Hz) contribution and some frequency contributions related to the tooth passing frequency and its harmonics [6]. While the frequency contributions could be affected by errors induced by system dynamic, as already shown in Figure 9.9 and Figure 9.10, the constant contribution should not be distorted by any dynamic effect, since the FRFs should have magnitude one and zero phase at 0 Hz, for physical reasons (i.e., rigid motion frequency). This aspect is exemplified by Figure 9.12, where a comparison between measured and compensated mean forces for one of the experimental tests is shown.

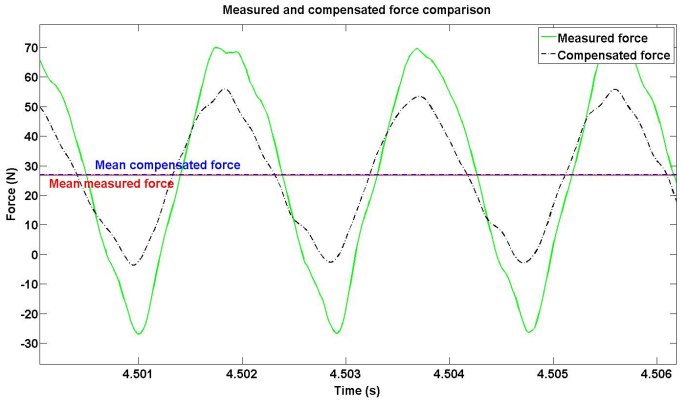

Figure 9.12 Mean compensated and mean measured forces comparison

On the other hand if interest is put in implementing the instantaneous force method, the effects of the compensation technique are definitely appreciable, as will be discussed more in detail in the results section.

9.3.3. **Methods implementation**

On the basis of force signals acquired in the cutting tests, average force method has been applied to obtain cutting force coefficients. For each spindle speed, average forces at the five feed rates have been calculated; linear regression of the data has been performed to identify cutting coefficients. Having chosen slotting operations, y direction force has been used to identify tangential coefficients, x for radial and z for axial (e.g., in Figure 9.13).

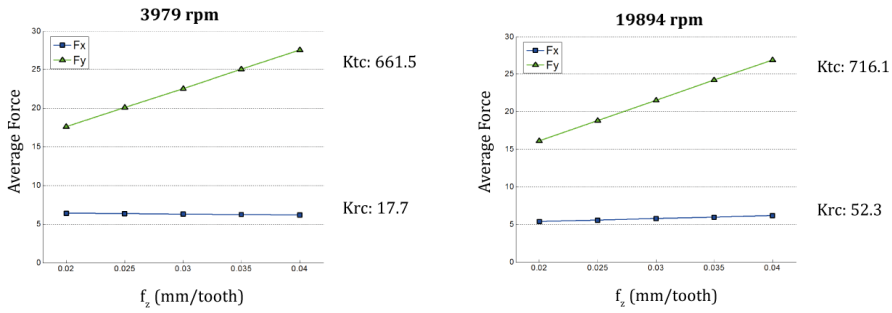

Figure 9.13 Linear fitting for average method

This procedure has been repeated for each spindle speed: by doing so speed-varying coefficients have been estimated.

For what concerns instantaneous method, coefficients have been calculated for a single feed rate, the one suggested by tool manufacture (0.03 mm/tooth). For each spindle speed, genetic algorithm has been implemented to match simulated and measured forces. This fitting has been applied to a small part of the force signal, only one tool revolution. In order to reduce influence of possible local measurements errors in the acquired force signals that could result in misleading coefficient estimation, different samples of each single measured force signal have been selected at different acquisition times. The identified samples have then been averaged to smooth the potential effects of local measurement errors.

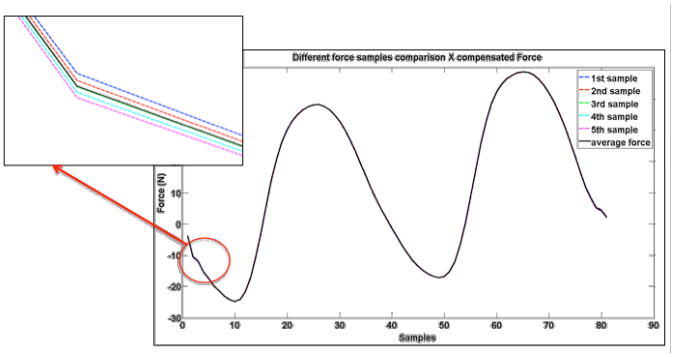

Figure 9.14 Comparison of five different cutting force samples and average cutting force.

Analogous results have been obtained for all the measured cutting force signals. As a matter of fact in this specific application the effects of measurement errors could have been neglected, as shown in Figure 9.14.

9.3.4. Coefficients identification methods and compensation results

In this section resulting cutting force coefficients are presented highlighting the influence of compensation on identification procedure and their dependence on cutting speed. Coefficients have been calculated for each spindle speed both with average and instantaneous method using compensated and uncompensated measurements. As already pointed out, compensation does not influence average method, thus only instantaneous method has been applied to both compensated and non-compensated measurements. In addition thanks to the improved instantaneous approach run-out value has been estimated around 1 μm for all the experimental tests.

In Figure 9.15 force measurements at two different spindle speeds (low speed: 3979 rpm and high speed: 27852 rpm) are shown as an example compared to simulated forces using cutting force coefficients obtained by the different methods. Significant variables are presented in the figure (coefficients K_{tc} and K_{rc} and Least Mean Square fitting error between curves).

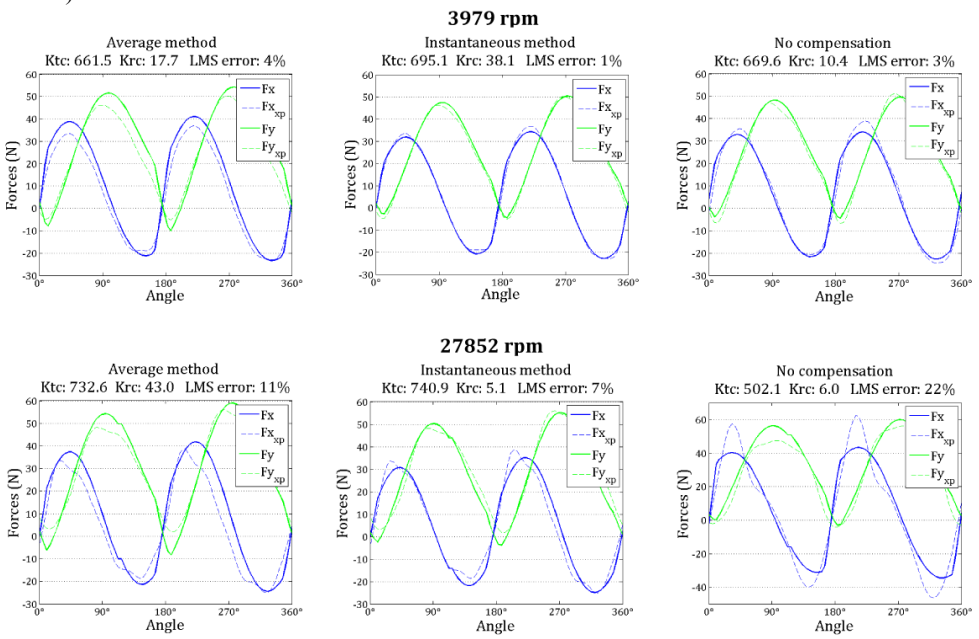

Figure 9.15 Comparison between cutting forces simulated with coefficients obtained by different methods and experimental forces

As shown in Figure 9.15, cutting coefficients applied to simulated chip thickness by means of improved formulation including run-out effect lead to accurate results. Comparing the two estimation approaches, instantaneous method is more accurate compared to average method that nevertheless results in an adequate accuracy without the need of compensation. Particularly at high speed, compensation is essential to return proper results following the instantaneous approach: at 27852 rpm force signals are sensibly distorted and identification of coefficients from these signals would lead to significant errors. This is even clearer examining spindle-speed-varying coefficients presented in Figure 9.16 limiting analysis to the two more significant coefficients, K_{tc} and K_{rc} (required for analytical stability prediction).

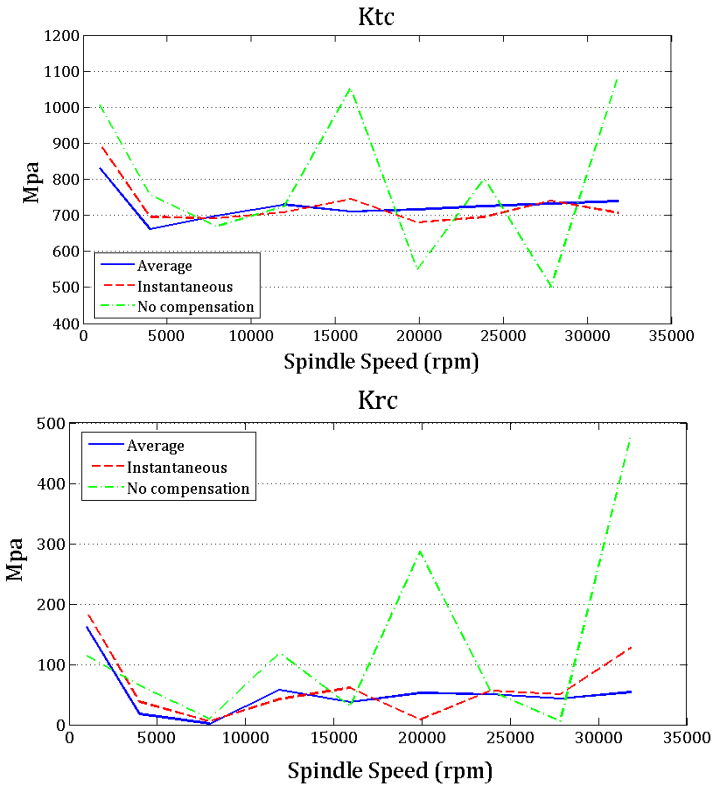

Figure 9.16: Cutting force coefficients Ktc and Krc varying with spindle speed

Instantaneous method applied to non-compensated force signals gets unreliable increasing spindle speed. Average force method and instantaneous method applied to compensated signals result in similar coefficients and similar trend. Coefficients variations in the spindle speed range tested are appreciable: estimated coefficients are, in fact, higher at low speed decreasing quickly then increasing again at higher speed. It is important to point out this trend: generally cutting force coefficients are evaluated only at low speed to avoid transducers dynamics influence and they are used even in higher speed applications. This approach could lead to significant errors, reducing reliability of higher speed simulation. Moreover should be pointed out that speed-dependent coefficients identification can be investigated by means of average force method since results obtained by this approach are not affected by transducers dynamic effects. Therefore for this technique no real need exists in limiting experimental test at low speed such as generally suggested if interest is put in cutting force simulation at higher speed, given that otherwise misleading results could be obtained. On the contrary for more complex and accurate method, as the instantaneous one presented in this paper, distorted force signals influence coefficients identification: a compensation technique as the one proposed is definitely needed.

9.3.5. **Speed varying cutting force coefficients**

In this section the trend of force coefficients, changing with cutting velocity is highlighted for the average method. In order to improve robustness and investigate

repetitiveness of the resulted coefficients, the cutting tests have been repeated 13 times in the same configuration and parameters. Based on these tests, error bars for each spindle speed and coefficient have been considered in accordance with [31]. Particularly 95% confidential intervals have been computed and presented in Figure 9.17 as error bars for shearing and edge coefficients.

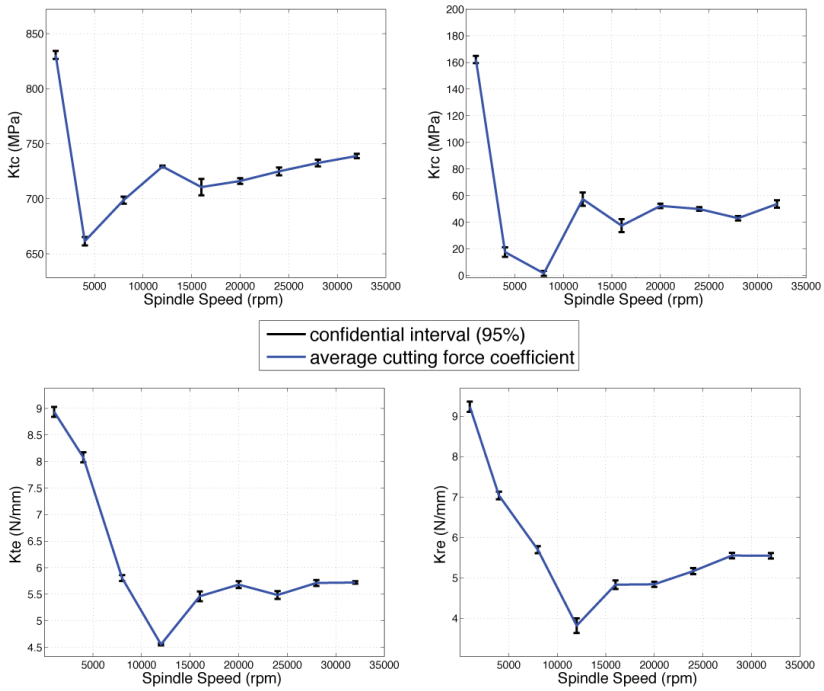

Figure 9.17 Error bars of average cutting force coefficients varying with spindle speed

As shown in the Figure 9.17 both shearing and edge coefficients change significantly over spindle speed. Thanks to error bars, robustness of the presented results is highlighted: calculated coefficients at different velocity are quite repeatable, low statistic spread is identified confirming coefficients dependency on cutting speed.

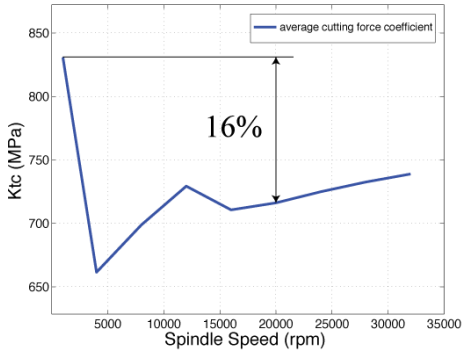

Figure 9.18 Estimation of coefficient K_{tc} error for 19894 rpm

Cutting force coefficients are traditionally evaluated at low speed to avoid influence of dynamometer dynamics: these coefficients are considerably different respect to the ones at high speed, reducing reliability of simulated forces. For example 16% error on K_{tc} is committed considering coefficient at 995 rpm to simulate forces at 19894 rpm, 8% considering coefficient identified at 3979 rpm, as exemplified in Figure 9.18.

9.4. Coefficients results and discussion

Cutting force simulation is essential to predict chatter stability. Cutting force models are generally based on experimentally estimated coefficients, the accuracy of which is crucial to accurately simulate cutting forces. These coefficients are generally evaluated at low speed to avoid influence of dynamometer dynamics on measurements, to overcome this limitation an improved compensation technique is presented and experimentally implemented. Specific cutting force coefficients have been evaluated by means of both average and instantaneous methods resulting in similar values. An advanced instantaneous method has been developed by authors to reduce computational effort by means of genetic algorithm and including tool run-out thanks to an improved chip thickness formulation.

The main conclusions of this investigation are:

1. Cutting force coefficients could change appreciably with spindle speed as mechanics of cutting change, this is an issue especially for HSM: using cutting force coefficients evaluated at low speed for higher speed simulations could lead to significant errors. In some applications speed-varying coefficients should be useful to sensibly improve reliability of simulated forces.
2. Speed-varying specific cutting coefficients can be computed without compensating dynamometer dynamics in case of average cutting force method but this technique requires four-five measurements at different feed rates to ensure reliable results.
3. Only one series of measurements is needed for instantaneous force based methods, but an effective compensation technique, as the one presented here, must be applied. Instantaneous force method is more accurate than average method; moreover in case of using an improved formulation for chip thickness in the fitting approach, also run-out values can be estimated with the same procedure. On the other hand a specific compensation filter is needed for each application, if the workpiece or fixture is changed, nevertheless this approach is more time-efficient once compensation algorithm is developed than the average approach since few experimental tests are needed.

9.5. Speed-varying stability prediction

Once speed-varying cutting force coefficients have been identified, they can be used to improve reliability of chatter prediction. In this section a method to include these coefficients in the stability theory is presented and obtained Stability Lobe Diagram is experimentally validated. Stability theory adopted is based on analytical zero-order approximation [25] as explained in Chapter 2.2.1 and already used in this work.

According with analytical stability theory, K_{tc} and K_{rc}, respectively the tangential and the radial cutting force coefficients, are needed to create SLD. Chatter stability changes as these parameters vary.

Different approaches could be applied to build an accurate SLD, which take into account the dependence of the cutting coefficients on the spindle speed. Cao [96] proposed a method based on the same analytical stability approach (zero-order) but for FRFs varying with spindle speed: the basic idea was to check stability according to equation (2.6) for discrete spindle speeds, considering different depth of cut. This approach implies depth of cut discretization and consequently an approximation compared to the original theory. In this paper a different approach is proposed, and the speed-dependent stability lobe diagram is calculated by the procedure summarized below and displayed in Figure 9.19:

1. According to the number of calculated coefficients, global spindle speed range is divided in different zones.
2. Analytical stability diagram is then calculated, changing coefficients for every single zone, creating a step diagram.
3. Starting from the diagram at point 2, a new continuous line diagram is calculated interpolating depth of cut limit between zones (e.g., linear).

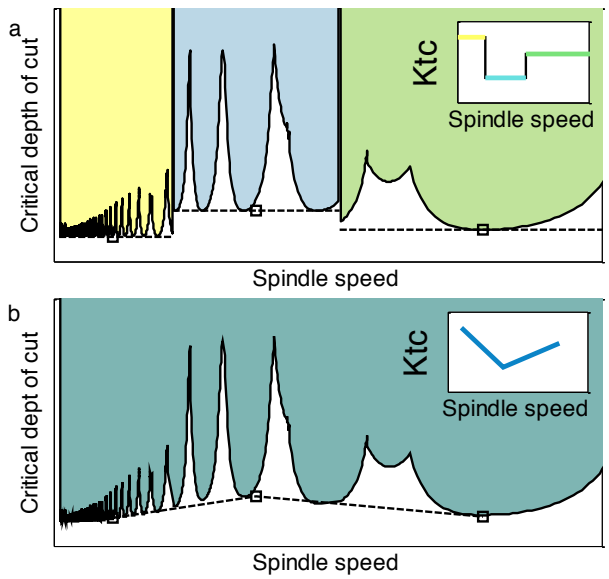

Figure 9.19. Speed-varying coefficients stability lobe diagram(a) Step diagram (phase 2); (b) Continuous diagram (phase 3).

9.5.1. Speed-varying SLD experimental validation

Calculated cutting force coefficients have been applied to the Stability Lobe Diagrams theory presented. Speed-varying K_{tc} and K_{rc} have been allocated in different zone portioning the spindle speed range, as presented in Figure 9.20.

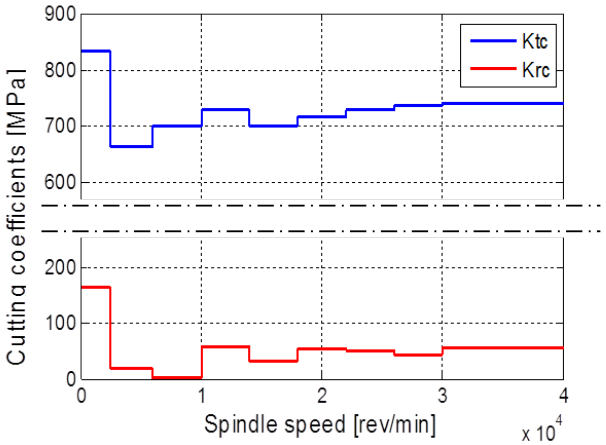

Figure 9.20 Cutting force coefficients for stability analysis

Stability Lobe Diagram is then calculated. Same tool used for coefficients estimation (Table 9.1) has been used with different overhang (36.5 mm), so different FRFs have been obtained by impact testing and used in SLD calculation for the same operation (i.e., slotting) and material. Resulting SLD (blue line) is compared with the traditional theory (black line) built considering as coefficients the ones obtained by low speed test (i.e., 995 rpm), as shown in Figure 9.21. Analyzing stability diagrams different cutting tests have been performed in order to experimentally validate proposed approach.

To check chatter onset, table dynamometer and microphone signals have been acquired by LMS Scadas III and elaborated in LMS Test.Lab software. Frequency spectra of the data have been calculated to check chatter frequency evolution. In Figure 9.21 results are shown. Chatter mark (red square) is indicated when chatter frequency is dominant on the spectrum, in the limit points (violet triangle) chatter frequency is growing but it's not dominant, no significant chatter frequency is identified in the stable points (green square). As evident from the figure, speed-varying coefficients stability is more accurate than traditional approach, anyway some discrepancies are shown, experimental-suggested diagram is presented (dot line).

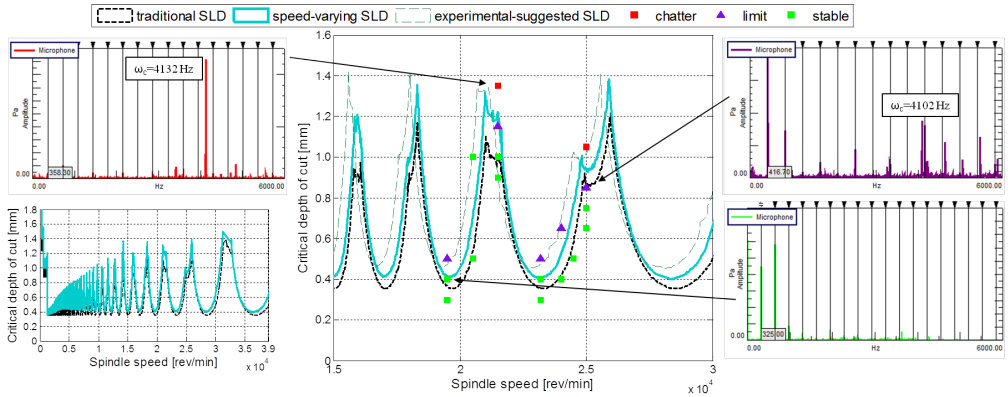

Figure 9.21 Stability Lobe Diagrams for experimental validation

The differences could be imputed to the variation of FRFs with spindle speed, dependency that has not been considered in this work. As presented in literature [97] [96] [60], at high spindle speed an increase of damping is expected, causing an increase of depth of cut. Moreover the difference between the chatter frequency experimentally determined, and the ones coming from SLD theory suggest the presence of a frequency shift of the resonant modes of the tool, due to the high spindle speed. Consequently a lobes shift can be hypothesized as shown in Figure 9.21.

In conclusion chatter stability is determined by machine tool dynamics and by the cutting force coefficients: both could change at different cutting velocity. For HSM applications, cutting force coefficient have to be experimentally evaluated with different spindle speed, in order to predict more reliable stability limits. In this Chapter a method to include speed-dependent cutting force coefficients to traditional chatter stability theory is presented. The presented research has demonstrate that cutting force coefficients could be effectively calculated without compensate the dynamometer dynamics, only if the average cutting force method is used; otherwise, as in case of instantaneous force based methods, a compensation algorithm, as the one presented, is needed.

Experimental validation shows the increased accuracy of the proposed approach, nevertheless more accurate results could be obtained introducing speed-varying FRFs, not considered in this application.

10. Experimental stability lobes identification

Predictive methods, as investigated in the previous sections, are effective because they can estimate chatter without performing cutting tests, avoiding time-consuming trial and error approach. However Stability Lobe Diagram accuracy is strongly affected by reliability of data entries, as reported in this work. Both machine tool dynamics and cutting force coefficients are influenced by different factors. As presented in Chapter 2, machine tool dynamics varies changing tool and position. In addition tool-tip Frequency Response Functions (FRFs) are evaluated in stationary condition, but could change significantly increasing spindle speed due to thermal effect and ball bearing stiffness under load condition [60, 97]. Moreover in some conditions (e.g., thin-wall machining) workpiece dynamics should be also taken into account [98], and the main drawback is that it changes during the machining process [15]. Besides cutting forces are influenced by tool geometry, type of operation, cutting parameters, e.g., cutting speed as presented in the previous Chapter.

Taking these sources of variability into account, in general is not easy to accurately identify tool-tip FRFs and cutting forces and this could reflect in a wrong prediction of chatter conditions. This method can consequently return a rough prediction of Stability Lobe Diagram that generally could be improved by experimental approaches in which cutting tests are performed to identify chatter onset.

These methods generally analyze signals of sensors mounted on the machine in order to detect chatter. Different chatter indicators have been developed in order to reliably identify chatter occurrence. Despite the differences almost every indicator is based on the signal frequency spectrum: when chatter frequency amplitude exceeds a certain threshold value, chatter is detected. Different kinds of sensors have been tested: Liao et al. [99] presented an on-line method based on force transducer, Kuljanic et al. [100] a multi-sensors approach using two accelerometer and a dynamometer, but the most interesting sensor has revealed to be microphone because of its simplicity and low-cost: this sensor has shown good chatter identification capabilities [101]. Schmitz et al. [102, 103] proposed a chatter detection approach by statistically evaluating milling sound variance. Bediaga et al. [104] developed an algorithm that uses sound signals to detect chatter and suggests alternative machining parameters. The aim of experimental methods is creating a stability experimental map to be exploited for selecting stable machining parameters. This approach is reliable but more time-consuming. The most used technique consists in performing cutting tests for each single condition in order to detect the presence of chatter. Identification of chatter is carried out both on the surface finish (checking distinctive marks) and on sensors signals. A large

number of tests are thus required to reconstruct SLD, limiting its application to validation of predictive approaches. In order to extend this approach to industrial context more efficient tests have been proposed: Quintana et al. [105] proposed a new test in which axial depth of cut is increased gradually until chatter is identified: a single test can investigate chatter behavior at one spindle speed. Anyway if a wide range of spindle speed has to be analyzed, many tests should be performed. Ismail and Soliman [106] introduced a different method: in their test spindle speed is increased and chatter is detected thanks to a statistical indicator [107]. They performed a slow ramp of the spindle speed in which feed per tooth is varying working out of the optimal cutting parameters: this leads to some drawbacks in chatter identification. Moreover the use of a statistical indicator instead of a frequency analysis is less reliable: it is not possible to validate chatter occurrence on frequency content of signals and isolate it from other effect (e.g., force vibrations). Method is not able to return chatter frequency values, useful to analyze and understand process behavior.

In this work a novel experimental method to detect chatter and create an experimental stability map is presented. The proposed test has been called Spindle Speed Ramp-up (SSR). Spindle speed is increased continuously in the test, increasing simultaneously feed in order to keep feed per tooth constant, with fixed depth of cut for each test. Different sensors (accelerometer, dynamometer, and microphone) have been tested and analyzed using the Order Analysis (OA) technique to detect chatter frequencies. As a result a frequency map changing spindle speed has been obtained, and chatter detected checking chatter frequency onset. This very quick test, based on the OA technique, has revealed to be a very efficient way to identify process damping, and stable and unstable zones for a single depth of cut. Moreover repeating the test with different depths of cut an accurate experimental stability map in the range of spindle speed can be efficiently obtained.

10.1. Proposed test

SSR test aims at reducing number of tests required to experimentally identify stability limits of a machining operation. The idea is to compress large number of tests at different spindle speed in a single test in which spindle speed is increased in the entire range of interest. Therefore compared to Quintana's test [105] depth of cut is not increased but is kept constant increasing spindle speed instead (Figure 10.1). The main advantage of the proposed method is to obtain exploitable results with just one test: a single SSR test can extract stable cutting parameters for a working condition. This is relevant for industrial context in which could be enough to obtain the optimal spindle speed for a given depth of cut, because this allows to enhance the process without changing the toolpath, which could be a time consuming issue that reduces the possibility to enable an on-line optimization.

Moreover as shown in Figure 10.1, with few tests it is possible to investigate the entirely SLD, drastically reducing the experimental effort usually required.

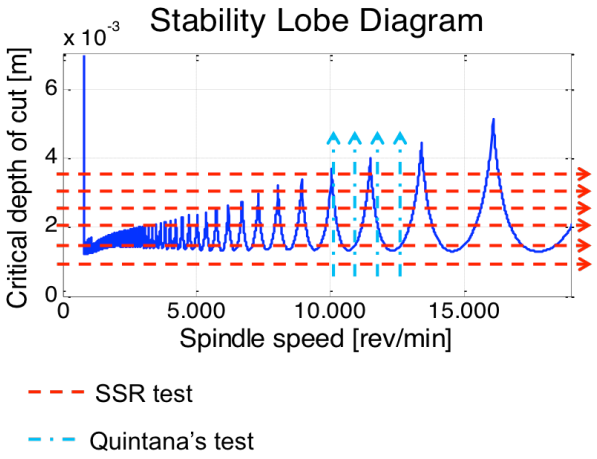

Figure 10.1 SSR test compared to Quintana's approach [105] for SLD identification

In order to obtain such result some shrewdness should be taken into account. First feed should be simultaneously increased with spindle speed in order to keep feed per tooth constant. In this way suggested cutting parameter for the tool are respected and cutting forces do not vary significantly. Then spindle speed should be increased linearly for mainly two reasons:

- Avoiding chatter growing uncontrollably: a continuous increase of spindle speed does not give time for chatter vibration to become dangerous for tool and machine because a new condition is reached immediately after;
- Easily and properly applying frequency analysis of the signals, as presented in the next section.

These features could be attained thanks to a proper definition of the NC code of the test, where the spindle speed and feed are changed linearly and accordingly.

10.2. Analysis method

During SSR cutting test sensors signals are acquired and used to identify stable and unstable cutting parameters of the operation. As proposed in other works [99-101, 105], chatter vibration characteristic frequency (i.e., chatter frequency) is used to detect instability. Therefore frequency analysis of the acquired signals is required. Due to the continuously changing spindle speed, OA technique [108], usually adopted for rotor-dynamics analysis and health monitoring [109] of rotors, such as turbines [110] or petrol engines, is performed on data.

During a run-up or run-down the structural resonances are excited by the fundamental or the harmonics of the rotational speed: OA allows the separation of rotational and structural noise and vibration phenomena and it is used to investigate critical speeds, resonances and instabilities in rotating machinery. Orders are the normalization of the rotational speed: the first order is the rotational speed, and order n is n times the rotational speed. The goal of this technique is to track sound and vibrations over operating rotational range: signals are collected and post-processed calculating spectrum data based on rpm. Two

main methods are generally used: frequency analysis and order-tracking analysis. They differ in sampling frequency: fixed in frequency analysis, in order-tracking it changes with revolution speed. Frequency analysis is thus more focused on frequency but it suffers smearing of frequency content issue especially at high frequency. Order-tracking analysis is suitable for high frequency and focused on orders evolution. In this paper frequency analysis is adopted because the goal is chatter frequency identification. Results of this analysis are spectra of signals calculated at different rotation speeds, generally presented as a 3D waterfall plot (also called Campbell diagram) where amplitudes of signals vibrations as function of frequency are plotted against rotation speed (Figure 10.2a). Harmonic components (i.e., Orders) appear on lines diverging from the origin (0 Hz, 0 RPM) while vibrations phenomena (e.g., resonances) appear on lines parallel to spindle speed axis (constant frequency), as shown in the scheme in Figure 10.2b.

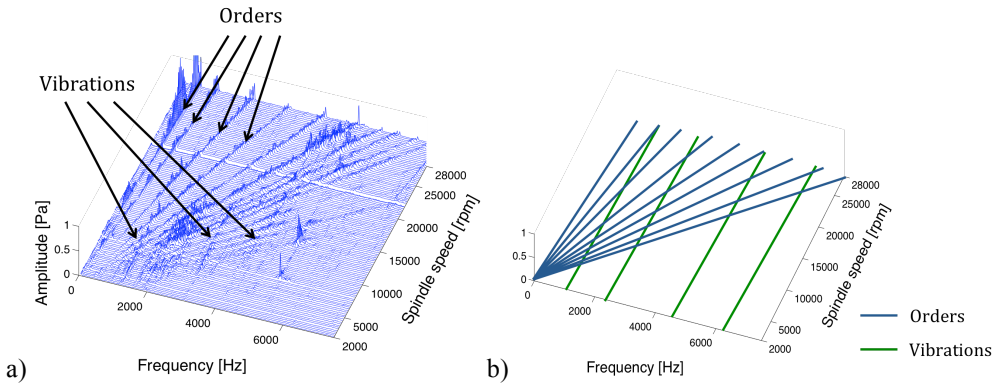

Figure 10.2 3D Waterfall diagram example (a) Diagram reading scheme (b)

In machining, order components are related to tooth passing frequency and its harmonics. Frequency contributions of acquired signals should be excited by orders. This is verified until chatter occurs: chatter frequency will appear in the data irrespective of frequency content of forces. Therefore, thanks to this technique, it will be easy to identify stable and unstable parameters at a defined depth of cut by analyzing evolution of the spectrum over spindle speed. Essential element of OA is rotational speed measurement. If possible, this could be provided by a synchronized tachometer mounted on the spindle or directly by machine tool encoders. Otherwise post processing acquired signals such as sound, vibration or force could return tooth pass frequency and hence identify the instantaneous speed. OA of the signals can be performed both on-line and off-line on time histories previously collected. During acquisition and further analysis three main parameters have to be set: sampling frequency of the signals, frequency resolution of the spectra, rpm resolution.

Once signals are acquired during SSR test, can be processed in frequency domain. Auto Power Spectrum of the signals is calculated, FFT analysis is performed every spindle speed interval with the frequency resolution set. Results are presented as waterfall 3D diagram or color map (e.g., in Figure 10.6). In the waterfall spectra on X-axis represents frequency, Y spindle speed and Z amplitude of the spectra. Thereby each calculated spectrum is presented in X-Z plane. In the color map the same information is provided: colors represent amplitude of the spectra.

10.3. Experimental set-up

Experimental tests have been performed in order to show method implementation.

Tests have been carried out on a Mori Seiki 5 axis milling machine, a NMV 1500 DCG, equipped with an high speed spindle (40.000 rpm max). A series of SSR tests at different depth of cut in slotting (i.e., full radial immersion) operation has been performed.

The material used for the machining test is a bar of Aluminum 6082-T4 alloy and a two flutes end mill (8 mm diameter Garant 201770) has been used. An optical tachometer able to detect the spindle speed till its maximum has been installed on the machine. The workpiece has been rigidly clamped to a three-component Kistler dynamometer type 9254 A. The machine has been equipped also with a microphone (Bruel & Kjaer type 4165) installed inside the cutting chamber close to the cutting zone and a 3-axis accelerometer (PCB U356A15) on Z-axis. The signals have been acquired by LMS Scadas III and elaborated in LMS Test.Lab software. Test set-up is presented in Figure 10.3.

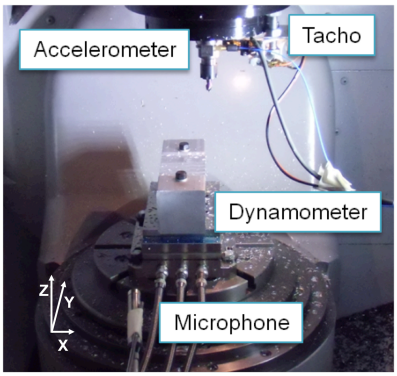

Figure 10.3 Test set-up

Six different axial depths of cut have been tested, ranging from 1 to 3.5 mm. Cutting parameters are summarized in Table 10.1.

Table 10.1 Cutting and tool parameters for SSR tests

Tool parameters						
Diameter (mm)	8			**Helix angle**	45°	
Flutes number	2			**Material**	Carbide	
Cutting parameters for milling tests						
Spindle speed (rpm)	2000	-	280000			
Feed per tooth (mm)	0.03			**Radial depth of cut (mm)**	Slotting	
Axial depth of cut (mm)	1	1.5	2	2.5	3	3.5

A spindle acceleration of 9000 rpm/s has been set for the tests, two SSR tests for each depth of cut have been performed: from 2000 to 8000 rpm and from 8100 rpm to 28000 in order to avoid the transient due to the power commutation of spindle unit during test. The time history of the spindle speed acquired by the tachometer is presented in Figure 10.4a. SSR test

has been implemented thanks to a simple NC code based on spindle acceleration and feed per tooth: a sample of the code used for this test is presented in Figure 10.4b.

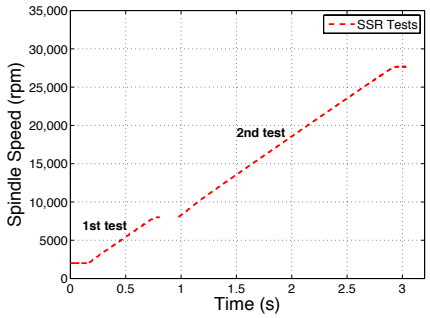

a)

```
G01
...
X6.240 S6500 F390
X6.444 S6800 F408
X6.657 S7100 F426
X6.879 S7400 F444
X7.110 S7700 F462
X7.350 S8000 F480
...
```

b)

Figure 10.4 Spindle speed evolution during test (a), sample of the NC code (b)

As shown, the proposed test is very fast: each depth of cut can be investigated in about 3 seconds. OA technique has been applied: parameters are listed in Table 10.2 and results are presented in the next section.

Table 10.2 Order Analysis parameters

Order Analysis parameters			
Sampling frequency (Hz)	25600	**Spindle acceleration (rpm/s)**	9000
Frequency resolution (Hz)	10	**Rpm resolution (rpm)**	25

Before performing SSR test impact tests on the tool-tip has been carried out with a Brüel & Kjaer Type 8202 impulse hammer and PCB 352C22 accelerometers (0.4 g) in order to validate and compare OA results. Frequency Response Functions (FRFs) on both directions (X and Y) are presented in Figure 10.5. Tool-tip FRFs has been presented to check machine tool dynamics behavior, focusing on dominant modes that, according to chatter theory, are accountable of instability occurrence. In the reported test case X and Y direction present similar behavior with a dominant mode at around 5100 Hz.

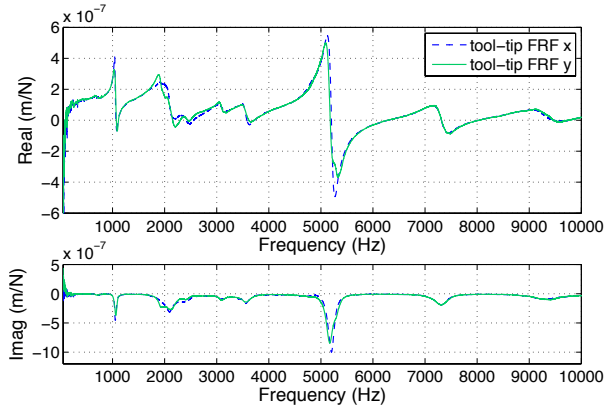

Figure 10.5 Tool-tip FRFs – Real and Imaginary part

10.4. Results and Exploitation

10.4.1. Chatter detection

Results of OA for low depth of cut (1 mm) and high depth of cut (3mm) are presented in Figure 10.6 and Figure 10.7, using as example the Z-axis force signal. Both waterfall and color map are shown.

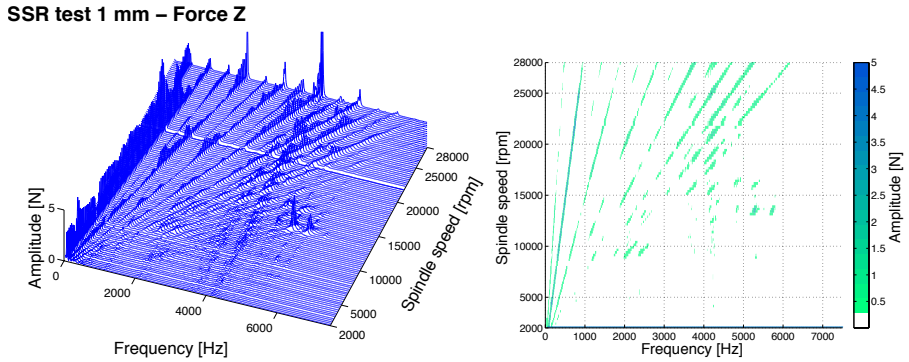

Figure 10.6 Waterfall diagram and color map for chatter detection (1 mm test Force Z)

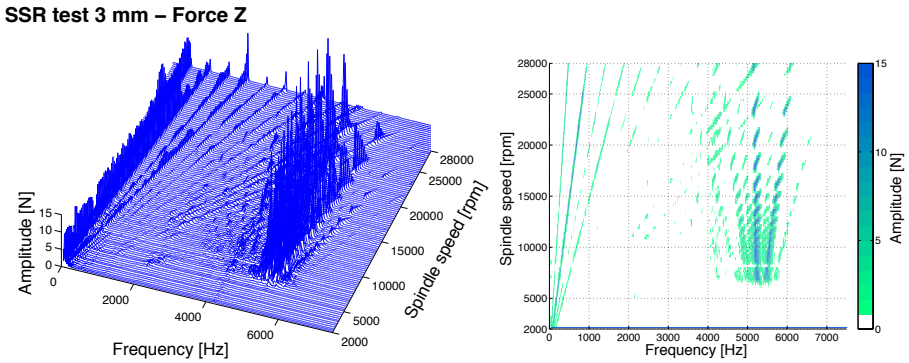

Figure 10.7 Waterfall diagram and color map for chatter detection (3 mm test Force Z)

As already mentioned, in a stable condition, the main contributions of the frequency spectrum of the sensors signals must be found on frequencies related to the tooth passing frequency and its harmonics. In case of instability, a chatter frequency will appear (becoming dominant) in the spectrum, this frequency is not consistent with the tooth pass frequency or one of its harmonics and remains almost constant varying spindle speed. Detecting chatter stable zones (including process damping) over spindle speed range is hence an easy task: in stable zones no dominant frequency (i.e., chatter frequency) out of tooth pass frequency and its harmonics is present. In Figure 10.6, at 1 mm depth of cut only tooth pass frequency and harmonics (orders) are dominant in the spectra: process is hence stable in the entire range of spindle speed. In Figure 10.7, at 3 mm depth of cut a dominant frequency out of the orders is present at some spindle speeds: at those spindle speeds, chatter will affect cutting operation.

Stable and unstable zones are evident using color map: in case of chatter, amplitude of the spectrum at the chatter frequency is very high (blue) becoming low (white) in the stable zones.

Therefore analyzing chatter frequency evolution stable and unstable zones can be obtained, as shown in Figure 8 for 3mm depth of cut test. Chatter starts when, for a specific spindle speed, chatter frequency becomes relevant. To evaluate when a chatter frequency becomes relevant it is necessary to use a threshold on its amplitude as proposed in other work [4,21]; for the proposed method the threshold value has been experimentally defined, using some preliminary tests, for which the surface has been studied, as a reference; the defined value for the amplitude of Z force is equal to 2 N. Using this rule it is possible to define chatter free spindle speeds and unstable speeds for each tested depth of cut.

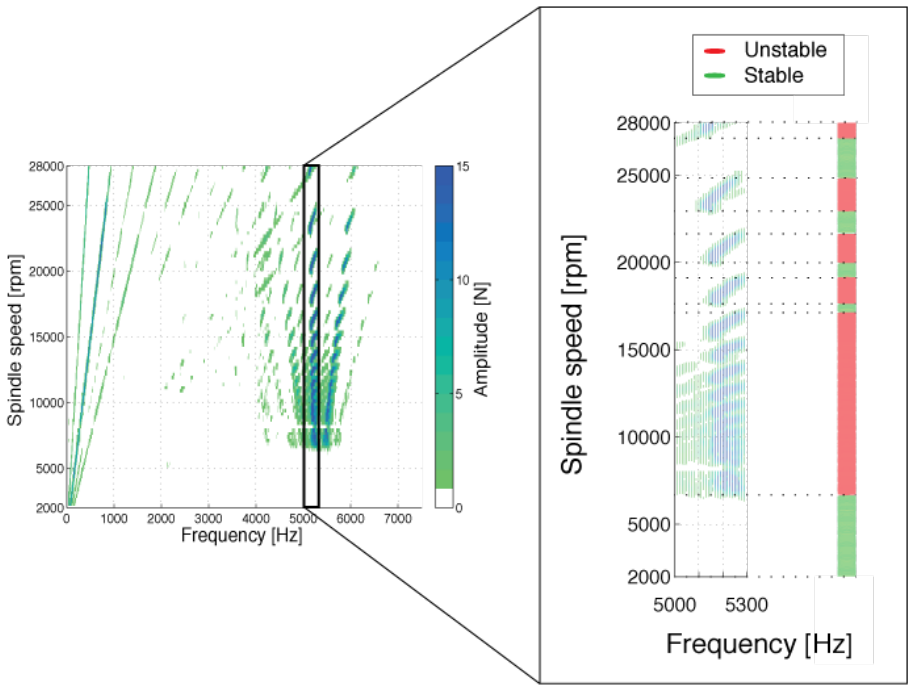

Figure 10.8 Stable and unstable zones identification example (3mm SSR test)

For example, by analyzing Figure 10.8 one could identify that no relevant chatter frequency contribution is present in the range of around 25000-27000 rpm, this range is thus identified as stable (green in the figure). On the contrary the 23000-25000 rpm range is characterized by evident chatter frequency contribution and is thus identified as unstable (red in the figure).

Presented experimental results are in accordance with chatter stability theory: chatter frequency evolution, and stable and unstable zones alternation are in agreement with SLD prediction models. Moreover, as expected, chatter frequency value around 5200 Hz is close to machine tool dominant mode natural frequency (5100 Hz, Figure 10.5) as chatter prediction theories present (Chapter 2.2).

10.4.2. **Sensors comparison**

In this section a comparison between signals is presented in order to show the application of the proposed method using different sensors. This investigation has been carried out to highlight the capability of each sensor used for the proposed approach and identify the most suitable one.

Proposed method has been applied to every source acquired. In Figure 10.9, Figure 10.10 and Figure 10.11 results for accelerometer, dynamometer and microphone in the 3 mm depth of cut test are presented.

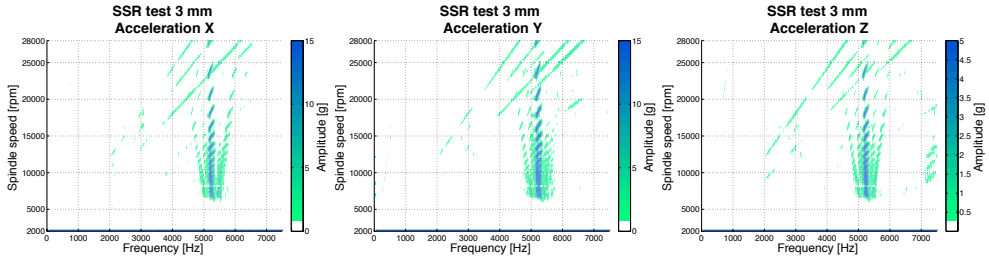

Figure 10.9 Accelerometer signals color maps for 3 mm SSR test

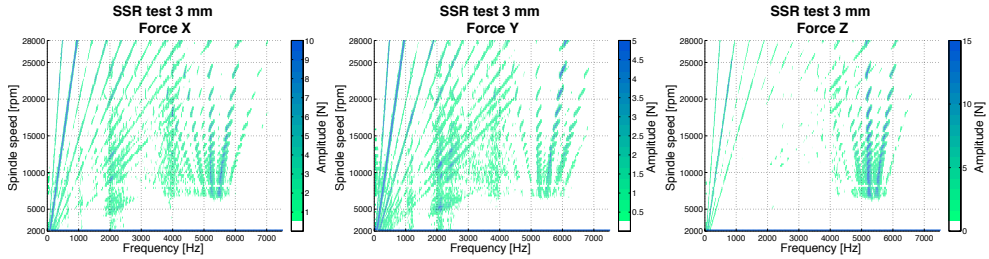

Figure 10.10 Dynamometer signals color maps for 3 mm SSR test

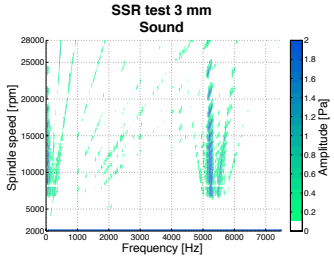

Figure 10.11 Microphone signals color maps for 3 mm SSR test

As shown in the Figure 10.9, Figure 10.10 and Figure 10.11 every signal gives similar information: chatter frequency occurrence is detected in the same way from each source. The main differences are:

- X-Y force signals are affected by some noise: this is probably due to influence of dynamometer and surrounding system dynamics on the acquired signal. Amplitude

values are not reliable especially increasing frequency: an effective compensation as the one proposed in the previous section and developed in [83] is required.

- Z force is more reliable than X-Y forces as already pointed out in [100]: on Z direction, influence of dynamometer and surrounding system is less significant, at least in the tested frequency range because of the higher resonant frequency. Signal is suitable both for order identification and chatter frequency detection.
- Accelerometer signals are accurate to detect chatter frequency, but not in identifying orders, that could be used to extract spindle speed values information if tachometer cannot be used.
- Microphone signal returns good results in terms of orders and chatter frequency. However signal is affected by environmental noise.

According to these considerations, Z-axis force signal seems to be the more reliable for both order and chatter frequency detection. Nevertheless accelerometer and microphone are more convenient and easy-to use and could give good results if some precautions are applied (filter for microphone and external tachometer for accelerometer). A sensor fusion strategy for these two sensors could be a promising future development.

10.4.3. Spindle acceleration influence

One of the main parameter to be set in the SSR test is spindle acceleration. Spindle acceleration determines operation time of the test and removed material. This aspect becomes significant when very high spindle speeds are reached: keeping feed per tooth constant, feed rate increase and more material is needed. Increasing spindle acceleration, identified stable and unstable states could be different because of inertia between phenomenon occurrence and its detection. In this section the influence of this parameter on the analysis results is presented. Different spindle accelerations (3000, 5000, 7000, 9000 rpm/s) have been tested to discuss the effect on stable and unstable zones detection. Moreover a ramp-down test with spindle speed starting at high speed and decrease to low speed is proposed. In order to compare results, tests with the same parameters (tool, operation and depth of cut of 1.5 mm) have been carried out and results in terms of stable regions are presented in Figure 10.12.

Stable and unstable points have been obtained analyzing chatter frequency evolution, as presented in the previous section.

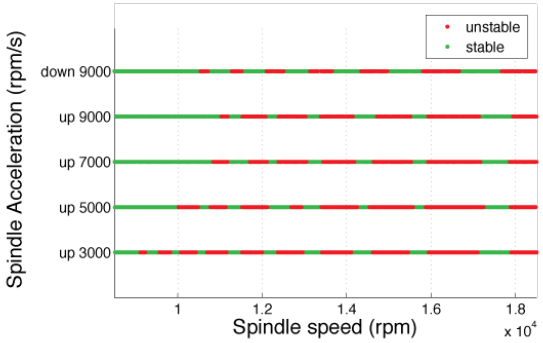

Figure 10.12 Spindle acceleration influence on 1.5 mm SSR test

Results presented in Figure 10.12 show discrepancies between different spindle acceleration. Particularly increasing spindle acceleration, accuracy on detection at low speed is reduced, this is probably due to the inertia of the system entering and exiting unstable conditions. On the contrary at high speed stable and unstable zones are quite the same between the different tests. For what concern test with decreasing spindle speed, also in this case there are differences between ramp up and down at 9000 rpm/s. These differences are significant at lower speed: stable and unstable zones appear shifted between the two tests.

In conclusion spindle acceleration influences results basically at lower speed, in order to improve method accuracy low acceleration is needed if low spindle speed has to be investigated. On the other hand high spindle acceleration can be adopted for high spindle speed, condition in which high spindle acceleration is beneficial because of high feed rate.

10.4.4. **Stability Experimental Map**

In order to present method capability of creating an experimental map of stable and unstable zones more depth of cut have been tested. OA has been applied to signals acquired for each depth of cut. This analysis will be limited to 9000 rpm/s acceleration and Z-force according with previous section considerations, same procedure can be carried out for different signals. In accordance with the main stability theories, increasing the depth of cut the process become more unstable: analyzing the signals of the tests chatter frequency becomes dominant in a wider range of spindle speed, as shown in Figure 10.13.

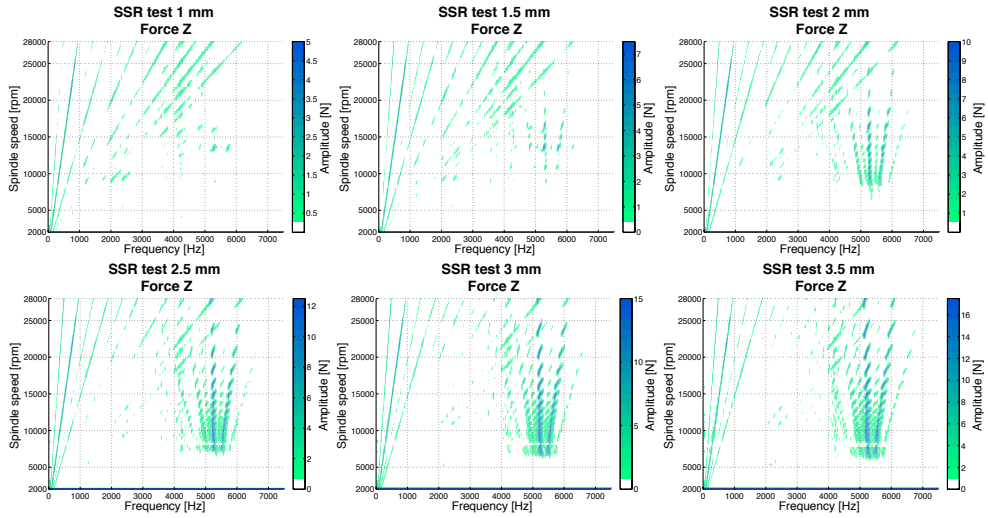

Figure 10.13 Color maps at different depth of cut

Merging together the results of the different tests is possible to create an experimental stability map, as shown in Figure 10.14. Based on chatter frequency threshold for each depth of cut, stable (green points) and unstable (red points) zones are identified. These zones are then connected together to create chatter limits and reconstruct Stability Lobe Diagram (Figure 10.14).

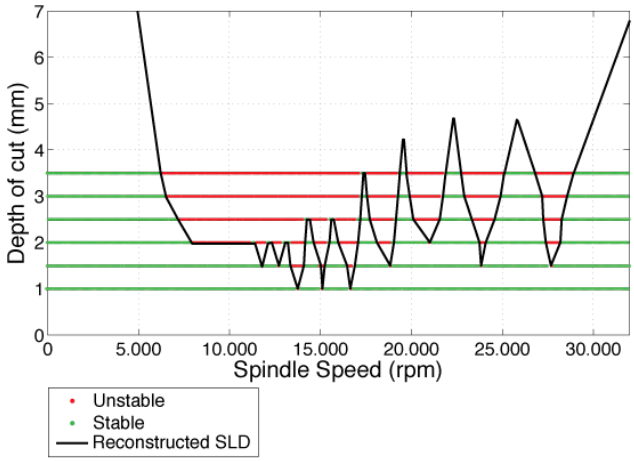

Figure 10.14 Stable and unstable zones for different depth of cut and reconstructed SLD

In this work this procedure is based on linear interpolation and extrapolation of the data: limit points between stable and unstable zones are connected by linear interpolation, then linear extrapolation has been used to predict zones at higher depth of cut (Figure 10.15).

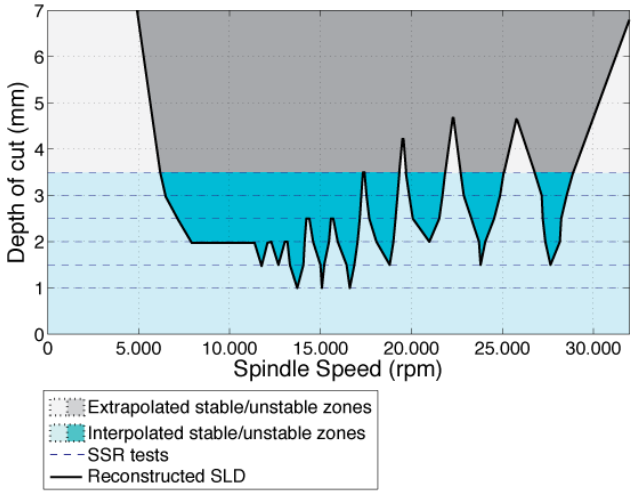

Figure 10.15 Reconstruction methods for SLD detection

Thanks to few tests an experimental stability diagram can hence be created. In order to validate reconstructed SLD some experimental tests have been carried out with constant parameters (single points in the diagram). Some spindle speeds have been tested changing depth of cut in order to detect chatter: chatter occurrence has been evaluated based on frequency signals of sensors and checking distinctive marks on the surface. Validation of the diagram has been limited to a high spindle speeds range in which according to previous

section 9000 rpm/s is suitable for chatter identification. Figure 10.16 shows single tests results compared to reconstructed SLD.

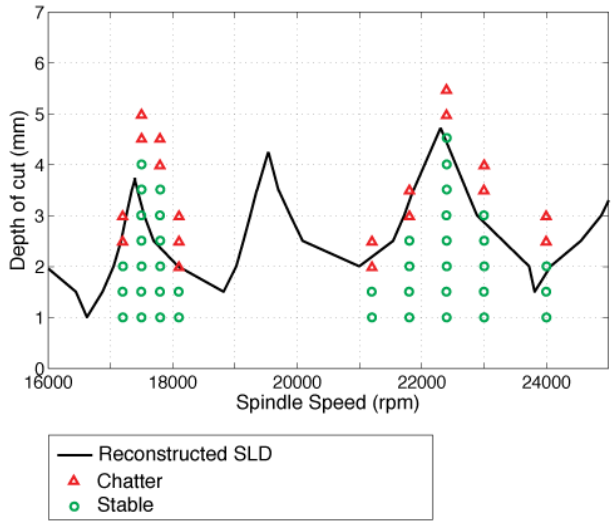

Figure 10.16 Experimental validation of the reconstructed SLD

As shown in Figure 10.16 reconstructed SLD seems to provide accurate results both in terms of depth of cut limit and positioning of the lobes: only few discrepancies are detected (e.g., 17800 rpm) probably due to inertia of the test but without resulting in significant inaccuracy. This experimental stability map is suitable to be directly applied at shop floor level and to experimentally validate chatter prediction approaches efficiently. This method is able to detect SLD experimentally avoiding all the issues related to predictive approaches such as process damping and input data accuracy. Moreover the proposed method takes into account every possible modification to the process and system including tool-tip FRF and forces changing with spindle speed. On the other hand this approach is valid only for the specific operation, tool and workpiece, like every SLD experimental identification technique: a new test is needed for each different set-up.

10.5. Speed-varying tool-tip FRF

In order to further investigate SSR test potentials, a comparison between reconstructed and predicted SLDs has been performed. Based on Altintas and Budak theory [25], (already extensively adopted in this work and briefly presented in Chapter 2), SLD has been computed and compared with the one reconstructed by SSR technique (Figure 10.17). In order to achieve this goal, both cutting force coefficients for workpiece material and tool-tip FRFs are experimentally obtained. For the case study, acquired tool-tip FRFs show symmetric dynamic behavior: no significant differences in X and Y direction are found as shown in Figure 10.5 (only FRF on Y direction is thus presented in Figure 10.19 as dotted blue line).

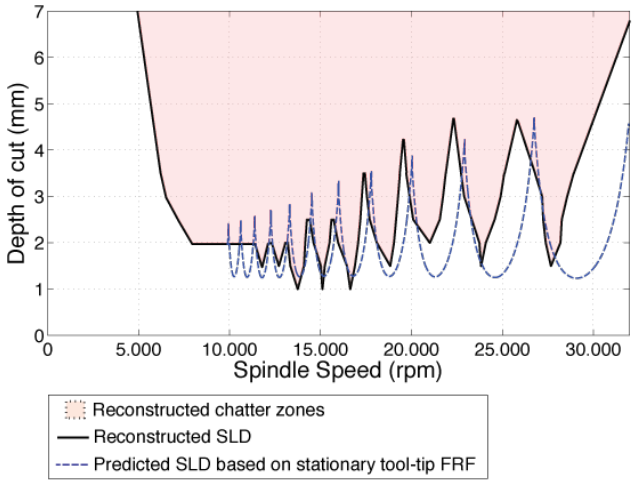

Figure 10.17 Reconstructed and predicted SLD

As shown in the figure, predicted SLD is in agreement with experimental one at low speed, but there are discrepancies in lobe positioning at very high speed. This could be caused by tool-tip FRF: predicted SLD is calculated based on FRF extracted via EMA in stationary condition, however tool-tip FRF could vary with spindle speed (as already reported in section 9.5). This aspect is confirmed and quantified analyzing chatter frequency evolution: a comparison between predicted and experimental chatter frequencies is reported in Figure 10.18. Experimental chatter frequencies are extracted from 3 mm depth of cut SSR test.

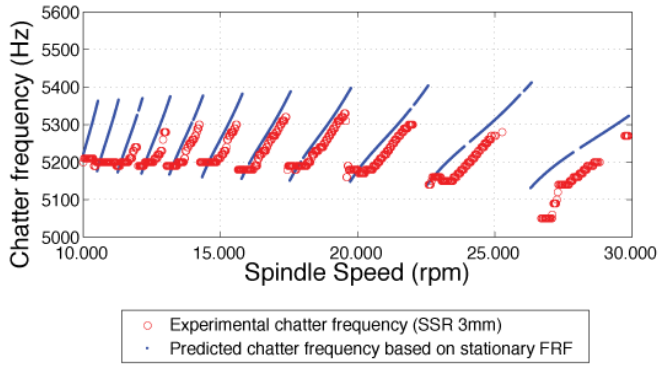

Figure 10.18 Experimental and predicted chatter frequency evolution

Experimental chatter frequency evolution is in agreement with the prediction theory, but a slight chatter frequency values decrease is observed (about 100 Hz in the spindle speed range 10.000-30.000). This behavior causes discrepancies between predicted and experimental chatter frequency values at high speed. Chatter frequency decrease is not modeled in the predictive theory and it could be imputed to speed-dependent tool-tip FRF.

To preliminarily investigate this behavior, SLD has been calculated based on a different tool-tip FRF. Starting from stationary tool-tip FRF, a new FRF is obtained shifting natural frequencies of 100 Hz (Figure 10.19).

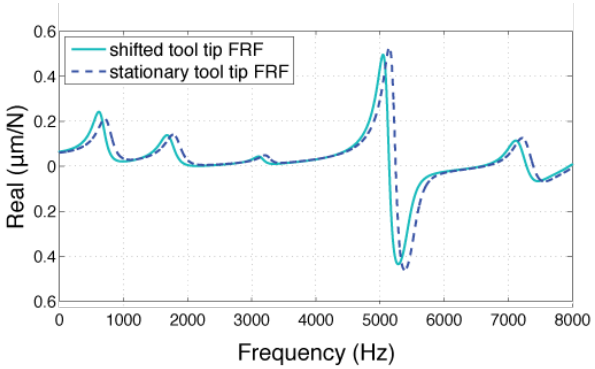

Figure 10.19 Stationary and shifted tool-tip FRF

Thanks to this shifted FRF a new comparison between predicted and experimental SLD is performed and shown in Figure 10.20.

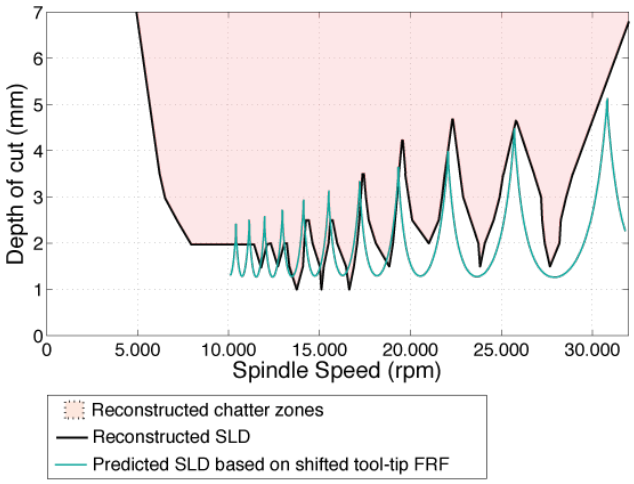

Figure 10.20 Reconstructed and predicted with shifted FRF SLD

Adjusting FRFs to 30.000 rpm chatter frequency value, predicted SLD and experimental results are now in good agreement at that speed, suggesting the speed-dependency of tool-tip FRF. This is clear even analyzing chatter frequency evolution, reported in Figure 10.21. Predicted chatter frequency trend now matches the experimental one at high speed.

According with this scheme, starting from comparison between predicted and experimental chatter frequency values tool-tip FRF for each spindle speed could be extracted. The actual speed-dependent tool-tip FRF in the range of 10.000-30.000 rpm would be a gradual shift from the stationary to the shifted one.

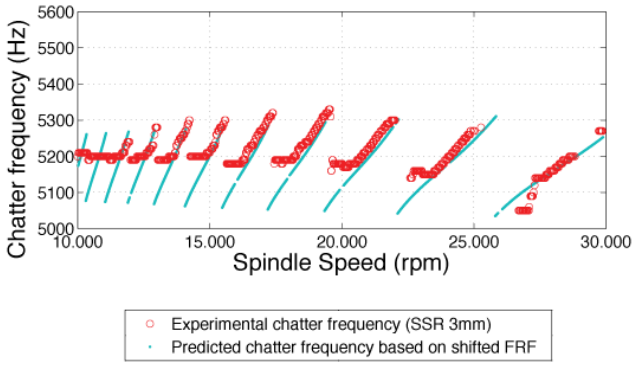

Figure 10.21 Experimental and predicted with shifted FRF chatter frequency evolution

This preliminary analysis shows how SSR test could be useful even to investigate speed dependency of tool-tip FRF, identifying the correct FRF at different speed. Thanks to frequency analysis of the signals and chatter frequency values speed-varying tool-tip FRF could be calculated (e.g., adapting the procedure proposed in [111]). This indirect measure could be very efficient and effective technique to identify speed-varying tool-tip FRF, without requiring complex and expensive equipment [60] or time-consuming and hard-to-validate spindle FE models [96, 97]. A more structured and comprehensive technique is needed to achieve this goal and form part of future works.

10.6. Conclusion

In this work a novel experimental method for chatter detection has been proposed. A simple and fast test, called Spindle Speed Ramp-up (SSR), has been presented to detect stable and unstable spindle speed at a specific depth of cut. The test is carried out increasing linearly the spindle speed maintaining constant the feed per tooth and the depth of cut. Chatter detection has been performed by frequency analysis of sensors signals thanks to Order Analysis technique. Method performances have been proven by experimental application to a slotting operation on aluminum. Different measurement devices can be used in the method: accelerometer, dynamometer and microphone have been compared in the paper providing similar results on chatter frequency evaluation.

The proposed test could be effectively used to:

- Obtain stable cutting parameters for a specific working condition (i.e., maintaining the design depth of cut) with just one test: this is an important advantage for the application in an industrial plant that usually requires a chatter-free spindle speed identification technique that could allow to maintain the programmed tool-path;
- Evaluate experimentally the SLD performing few tests changing depth of cut;
- Validate SLD predictive approaches and investigate process behavior such as machine tool dynamics changing with spindle speed thanks to the analysis of chatter frequency evolution.

The developed test has proven to be an efficient and effective way to experimentally identify stable and unstable cutting parameters, reducing drastically number of tests

generally required. Moreover proposed technique could be adopted to investigate tool-tip FRF changing with spindle speed thanks to the analysis of chatter frequency evolution.

11. Conclusions and final remarks

This thesis deals with prediction and experimental detection of chatter vibration, one of the most important limiting factors to milling performances.

The final output of chatter investigation is generally Stability Lobe Diagram: a chart that provides stable cutting parameters (spindle speed and engagement conditions). Unfortunately SLD identification is not easily applicable to the shop floor. This thesis deals with the main criticalities related to the implementation of SLD identification in the industrial context, inheriting its motivation from the benefits that an accurate SLD can provide to milling process performances and consequently to the competiveness of precision manufacturing enterprises. The final goal of this thesis is thus the investigation and development of SLD identification techniques suitable for industrial application. This goal is achieved by studying both predictive and experimental approaches. For what concern chatter prediction the effort in this thesis is mainly focused on input data, considering the high sensitivity of SLD accuracy on these parameters. A significant part of the thesis is focused on machine tool dynamics identification methods since it is the most influent input for chatter prediction: different machine tool dynamics identification techniques have been proposed focusing on their industrial relevance (simplification, and reduction of experimental tests have been the main goals). Both numerical (FEM) techniques and hybrid experimental-numerical approaches have been investigated. Two fully numerical approaches are developed in order to reduce pre-processing and analysis time. Novel hybrid experimental-numerical techniques are proposed, reducing the number of tests required. Toolkit FE modeling is investigated using both 1D and 3D modeling and developing holder-tool connection modeling techniques. The other inputs required by predictive models are cutting force coefficients. In this thesis guidelines to study and investigate their dependency on cutting speed are proposed both for average force methods and instantaneous ones. Dynamometer dynamics influence issue has been overcome thanks to a compensation technique proper developed for milling application. Once speed-varying cutting force coefficients have been identified, a method to include them on chatter prediction has been developed and experimentally validated.

Together with predictive approaches, experimental methods are also investigated. A new experimental technique called Spindle Speed Ramp-up has been developed. This technique has proven to be an interesting and efficient way to quickly obtain experimentally SLD. Thanks to few cutting tests SLD can be identified accurately without approximations or simplifications that characterized predictive approaches.

The research presented in this thesis yields nine important general conclusions in view of its final goal:

- Starting from a validated machine tool FE model, dynamics changing with position or tool orientation can be identified and consequently used for chatter prediction with very high efficiency and without lack of accuracy.
- Hybrid experimental-numerical approaches for tool-tip FRF identification can reduce drastically the number of tests required if applied to entire toolkit (holder and tool).
- Tool-tip FRF resulted by hybrid approaches is highly influenced by tool FE model accuracy.
- 1D beam modeling is not always suitable for toolkit modeling in hybrid approaches because of mainly two parameters: slenderness and holder-tool connection.
- Accurate holder-tool connection is a key factor in toolkit modeling and can be achieved by means of fully predictive numerical approach without the need of experimental iterative procedures.
- An effective receptance coupling approach without calibration phase can be achieved.
- Starting from the same hypothesis of receptance coupling method a simplified machine tool FE model can be obtained, preparing the ground to its application to time-domain simulation.
- Cutting force coefficients could change with cutting speed, and this dependency can be investigated thanks to dynamometer dynamics compensation.
- Chatter experimental detection can be achieved efficiently and accurately by means of a test in which spindle speed change continuously and the application of Order Analysis technique.

11.1. Summary of the principal achievements

In summary main contributions are:

- Efficient and effective position-dependent dynamics identification technique based on full FE model of the machine tool and commercial FE solver.
- Orientation-dependent stability technique based on receptance coupling and machine tool FE model, suitable for gimbal head machine structures.
- Fully predictive numerical approaches for the main holder-tool connections (shrink-fit, collet and hydraulic chuck).
- Accurate receptance coupling method without the need of calibration test.
- Simplified machine tool model definition method.
- Chatter stability prediction approach using speed-varying cutting force coefficients.
- Spindle Speed Ramp-up test: an efficient and accurate chatter experimental detection technique.

11.2. Industrial application of the developed techniques

As already pointed out, this thesis is focused on improving existing techniques for industrial applications. Many of the techniques developed are already promising to be used on the shop floor level. Both predictive approaches and experimental methods developed can be effectively applied in order to introduce SLD in the industrial context and improve process productivity thanks to chatter-free cutting parameters selection.

Hybrid experimental-numerical approaches here presented could be applied to obtain a preliminary chatter prediction without the need of the large number of experimental tests generally required. Proposed techniques, in fact, are able to return accurate results with only one test for each machine tool: only toolkit FE model is then required. As presented in this thesis, FE toolkit models is significantly influencing tool-tip FRF results, it is thus essential to provide a procedure to achieve this scope effectively but at the same time efficiently and automatic, applicable to the industrial context. 1D beam modeling algorithm proposed in this thesis is efficient and automatic but this type of element are not always suitable for toolkit modeling (slenderness and holder-tool connection are key factors). Although 3D modeling technique, as proposed in this work, return accurate results but is more difficult to automate. An intermediate solution should be developed.

Alternatively a rough model could be updated based on experimental test in free-free boundary condition, as presented in section 6.4.4. These experimental tests are not carried out inside the machine tool and they are not consequently affecting machine downtime. Moreover it could be possible to introduce this tuning experimental test in a new smart pre-setting machine, including it in a consolidated procedure. Anyhow it is clear how this technique can return preliminary stability estimation due to the high number of uncertainties and approximation; in order to improve predictive approach chatter estimation, experimental tests could be used.

Proposed SSR technique is ready to be used with this purpose since it requires only simple and very quick tests and cheap sensors. In this thesis the technique was applied and validated for force sensors but it is also shown how other sensors can be used, such as cheap and non-contact microphone. It will be possible to create an easy-to-use software and device to operate this test before real cutting, identifying easily and without any time-consuming test the optimal cutting parameters.

11.3. General ideas for future works

Ideas for future research related to the developed technique can be summarized in:

- Further investigations on full FE model techniques thanks to their experimental validation could be carried out.
- Toolkit 1D beam models thanks to connection modeling guidelines identified in this work could be improved. Shrink fit seems properly modeled by rigid connection, no action are needed. Hydraulic chuck actual overhang could be introduced in the beam model according with 3D modeling approach proposed in this work, or developing simplified analytical formulations. Collet chuck requires accurate axisymmetric 3D modeling to return high accurate results, a simplified method to include this behavior in beam model could be investigated, e.g., equivalent lamped stiffness based on 3D model response.
- Simplified machine tool model proposed could be applied to time-domain simulation in order to investigate machine tool behavior in time domain.
- Additional tests for cutting force coefficients estimation could be performed with different materials in order to investigate speed-varying trend. Chatter technique based on speed varying cutting force coefficients could be improved with a more robust and structured approach.

- An extended validation of SSR test should be carried out and a simple hardware-software system should be developed in order to perform this test in a industrial context
- According with proposed results, SSR test could be used to study machine tool dynamics evolution over spindle speed thanks to chatter frequency values, comparing them with predicted ones. This could lead to accurate tool-tip FRF identification varying with spindle speed.
- Thanks to accurate speed-varying tool-tip FRF, a technique to update experimental FRFs on the machine by inverting hybrid experimental-numerical technique could be an interesting development. Starting from this updated machine FRFs, a more reliable speed-varying tool-tip FRF could be obtained by hybrid experimental-numerical approach as the one proposed in this work.

Acknowledgements

The present thesis work was carried out in the Department of Industrial Engineering of the University of Florence. Foremost, I would like to express my sincere gratitude to all the people working in this Department, starting from my supervisors, Dr. Antonio Scippa and Dr. Gianni Campatelli. I would like to thank Massimiliano who guided me from the very beginning, and all my laboratory colleagues (Filippo, Lorenzo, Riccardo, Francesco, Andrea e Alessandro) and graduates.

I am also deeply grateful to Prof. Yusuf Altintas that gave me the opportunity to be part of Manufacturing Automation Laboratory, supporting me in my research activities and letting me enjoy Vancouver. A special thanks goes to Dr. Mohit Law and to all the people from MAL (Svenja, Keivan, Alex, Sneha, Jin, Hasan, Oguzhan, Murat).

I would like to acknowledge Prof. Yamazaki, Prof. Soshi and Dr. Mori as MTTRF (Machine Tool Technology Research Foundation) for the loaned machine tool, essential for my research, and for conferences that helped me to grew in my research and gives the opportunity to meet people from all around the world, as Prof. Ryuta Sato from Kobe University: I am grateful to him for his help to my work.

Finally I would like to thank my friends (firstly Claudio, Lorenzo, Gabriele, Lorenzo and Marco), my family and Stefania for their constant and generous support.

References

[1] M. Law, N. Grossi, A. Scippa, A.S. Phani, Y. Altintas, Modeling the Orientation-Dependent Dynamics of Machine Tools with Gimbal Heads, in: 3rd International Chemnitz Manufacturing Colloquium ICMC 2014, Chemnitz, Germany 2014.

[2] G. Campatelli, A. Scippa, N. Grossi, A. Velenosi, Hybrid FE-experimental modeling of machine tool dynamics, in: MTTRF Annual Meeting 2012, Iga, Japan, 2012.

[3] N. Grossi, A. Scippa, G. Campatelli, Tool point dynamics prediction using a hybrid FE-experimental modeling of milling machine, in: XI Convegno dell'Associazione Italiana Tecnologia Meccanica (AITeM), San Benedetto del Tronto, 2013.

[4] N. Grossi, L. Sallese, A. Scippa, G. Campatelli, Chatter Stability Prediction in Milling Using Speed-varying Cutting Force Coefficients, Procedia CIRP, 14 (2014) 170-175.

[5] N. Grossi, A. Scippa, L. Sallese, R. Sato, G. Campatelli, Spindle speed ramp-up test: A novel experimental approach for chatter stability detection, International Journal of Machine Tools and Manufacture.

[6] Y. Altintas, Manufacturing Automation: Metal Cutting Mechanics, Machine Tool Vibrations, and CNC Design, in, Cambridge University Press, USA, 2012.

[7] S. Smith, J. Tlusty, Current Trends in High-Speed Machining, Journal of Manufacturing Science and Engineering, 119 (1997) 664-666.

[8] G. Tlusty, Manufacturing Process and Equipment, Prentice Hall, New York, 2000.

[9] C. Brecher, M. Esser, S. Witt, Interaction of manufacturing process and machine tool, CIRP Annals - Manufacturing Technology, 58 (2009) 588-607.

[10] R. Furness, Engineering for High Performance Machining Systems, in: CIRP - High Performance Cutting, Berkeley, 2014.

[11] J.-V. Le Lan, A. Marty, J.-F. Debongnie, A stability diagram computation method for milling adapted to automotive industry, in: CIRP - High performance cutting, Vancouver, 2006.

[12] G. Quintana, J. Ciurana, Chatter in machining processes: A review, International Journal of Machine Tools and Manufacture, 51 (2011) 363-376.

[13] Y. Altintas, M. Weck, Chatter Stability of Metal Cutting and Grinding, CIRP Annals - Manufacturing Technology, 53 (2004) 619-642.

[14] F. Haase, The investigation and design of a piezoelectric active vibration control system for vertical machining centres, University of Huddersfield, 2005.

[15] A. Scippa, N. Grossi, G. Campatelli, FEM based Cutting Velocity Selection for Thin Walled Part Machining, Procedia CIRP, 14 (2014) 287-292.

[16] A. Scippa, N. Grossi, G. Campatelli, Milled Surface Generation Model for Chip Thickness Detection in Peripheral Milling, Procedia CIRP, 8 (2013) 450-455.

[17] A. Scippa, N. Grossi, A. Velenosi, G. Campatelli, Milled surface generation model for time domain simulation, in: MTTRF Annual Meeting 2013, San Francisco, U.S., 2013.

[18] T.L. Schmitz, B.P. Mann, Closed-form solutions for surface location error in milling, International Journal of Machine Tools and Manufacture, 46 (2006) 1369-1377.

[19] S.A. Tobias, Machine Tools Vibrations, in, URMO, Spain, 1961.

[20] F.W. Taylor, On the art of cutting metals, American Society of mechanical engineers, New York, 1907.

[21] U. Naterwalla, Chatter Theory Fundamentals, in: Modern Machine Shop magazine, 2000.

[22] J. Tlusty, M. Polacek, Besipiele der behandlung der selbsterregten Schwingung der Werkzeugmaschinen, FoKoMa, Hanser Verlag, Munchen, (1957).

[23] S.A. Tobias, W. Fiswick, Theory of Regenerative Machine Tool Chatter, Engineering, 258 (1958).

[24] Y. Altintas, G. Stepan, D. Merdol, Z. Dombovari, Chatter stability of milling in frequency and discrete time domain, CIRP Journal of Manufacturing Science and Technology, 1 (2008) 35-44.

[25] Y. Altintas, E. Budak, Analytical Prediction of Stability Lobes in Milling, CIRP Annals - Manufacturing Technology, 44 (1995) 357-362.
[26] W.X. Tang, Q.H. Song, S.Q. Yu, S.S. Sun, B.B. Li, B. Du, X. Ai, Prediction of chatter stability in high-speed finishing end milling considering multi-mode dynamics, Journal of Materials Processing Technology, 209 (2009) 2585-2591.
[27] S.S. Park, Y. Altintas, M. Movahhedy, Receptance coupling for end mills, International Journal of Machine Tools and Manufacture, 43 (2003) 889-896.
[28] M. Law, Y. Altintas, A. Srikantha Phani, Rapid evaluation and optimization of machine tools with position-dependent stability, International Journal of Machine Tools and Manufacture, 68 (2013) 81-90.
[29] G. Bianchi, F. Paolucci, P. Van den Braembussche, H. Van Brussel, F. Jovane, Towards Virtual Engineering in Machine Tool Design, CIRP Annals - Manufacturing Technology, 45 (1996) 381-384.
[30] A. Velenosi, G. Campatelli, A. Scippa, Axis geometrical errors analysis through a performance test to evaluate kinematic error in a five axis tilting-rotary table machine tool, Precision Engineering.
[31] G. Reinhart, M. Weissenberger, Multibody simulation of machine tools as mechatronic systems for optimization of motion dynamics in the design process, in: Advanced Intelligent Mechatronics, 1999. Proceedings. 1999 IEEE/ASME International Conference on, 1999, pp. 605-610.
[32] M. Zaeh, D. Siedl, A New Method for Simulation of Machining Performance by Integrating Finite Element and Multi-body Simulation for Machine Tools, CIRP Annals - Manufacturing Technology, 56 (2007) 383-386.
[33] M. Law, Position-dependent dynamics and stability of machine tools, in, University of British Columbia, 2013.
[34] P.D. Fonseca, Simulation and Optimization of the Dynamic Behavior of Mechatronics Systems, in, Katholieke Universiteit Leuven, 2000.
[35] M.C.C. Bampton, J.R.R. Craig, Coupling of substructures for dynamic analyses, AIAA Journal, 6 (1968) 1313-1319.
[36] M. Law, S. Ihlenfeldt, M. Wabner, Y. Altintas, R. Neugebauer, Position-dependent dynamics and stability of serial-parallel kinematic machines, CIRP Annals - Manufacturing Technology, 62 (2013) 375-378.
[37] M.S.C. Software Corporation, MD/MSC Nastran 2010 Quick Reference Guide, in, 2010.
[38] J.-P. Hung, Y.-R. CHen, T.-L. Luo, Effect of Tool Orientation on the Machining Stability of a Milling Machine with Swinging Head, World Accademy of Science, Engineering and Technology, 77 (2013) 957-964.
[39] T.L. Schmitz, R.R. Donalson, Predicting High-Speed Machining Dynamics by Substructure Analysis, CIRP Annals - Manufacturing Technology, 49 (2000) 303-308.
[40] Y. Cao, Y. Altintas, Modeling of spindle-bearing and machine tool systems for virtual simulation of milling operations, International Journal of Machine Tools and Manufacture, 47 (2007) 1342-1350.
[41] L. Uriarte, M. Zatarain, D. Axinte, J. Yagüe-Fabra, S. Ihlenfeldt, J. Eguia, A. Olarra, Machine tools for large parts, CIRP Annals - Manufacturing Technology, 62 (2013) 731-750.
[42] K. Niehues, S. Schwarz, M.F. Zaeh, Reliable material damping ratio determination in machine tool structures, Prod. Eng. Res. Devel., 6 (2012) 475-484.
[43] O.C. Zienkiewicz, R.L. Taylor, D. Fox, The Finite Element Method for Solid and Structural Mechanics, in, Butterworth-Heinemann, Oxford, 2014.
[44] A. Ertürk, H.N. Özgüven, E. Budak, Analytical modeling of spindle–tool dynamics on machine tools using Timoshenko beam model and receptance coupling for the prediction of tool point FRF, International Journal of Machine Tools and Manufacture, 46 (2006) 1901-1912.
[45] M. Namazi, Y. Altintas, T. Abe, N. Rajapakse, Modeling and identification of tool holder–spindle interface dynamics, International Journal of Machine Tools and Manufacture, 47 (2007) 1333-1341.
[46] A. Ertürk, H.N. Özgüven, E. Budak, Effect analysis of bearing and interface dynamics on tool point FRF for chatter stability in machine tools by using a new analytical model for spindle–tool assemblies, International Journal of Machine Tools and Manufacture, 47 (2007) 23-32.
[47] S.P. Timoshenko, Strength Of Materials Part I Elementary Theory and Problems, 1st ed., D. Van Nostrand Company, 1930.
[48] E.B. Kivanc, E. Budak, Structural modeling of end mills for form error and stability analysis, International Journal of Machine Tools and Manufacture, 44 (2004) 1151-1161.
[49] B. Bediz, U. Kumar, T.L. Schmitz, O. Burak Ozdoganlar, Modeling and experimentation for three-dimensional dynamics of endmills, International Journal of Machine Tools and Manufacture, 53 (2012) 39-50.
[50] P. Albertelli, M. Goletti, M. Monno, A new receptance coupling substructure analysis methodology to improve chatter free cutting conditions prediction, International Journal of Machine Tools and Manufacture, 72 (2013) 16-24.

[51] B.A. Mascardelli, S.S. Park, T. Freiheit, Substructure Coupling of Microend Mills to Aid in the Suppression of Chatter, Journal of Manufacturing Science and Engineering, 130 (2008) 011010-011010.
[52] T.L. Schmitz, M.A. Davies, M.D. Kennedy, Tool Point Frequency Response Prediction for High-Speed Machining by RCSA, Journal of Manufacturing Science and Engineering, 123 (2001) 700-707.
[53] T.L. Schmitz, G.S. Duncan, Three-Component Receptance Coupling Substructure Analysis for Tool Point Dynamics Prediction, Journal of Manufacturing Science and Engineering, 127 (2005) 781-790.
[54] K. Ahmadi, H. Ahmadian, Modelling machine tool dynamics using a distributed parameter tool–holder joint interface, International Journal of Machine Tools and Manufacture, 47 (2007) 1916-1928.
[55] R. Madoliat, S. Hayati, A. Ghasemi Ghalebahman, Investigation of chatter suppression in slender endmill via a frictional damper, Scientia Iranica, 18 (2011) 1069-1077.
[56] V. Ostasevicius, M. Ubartas, R. Gaidys, V. Jurenas, S. Samper, R. Dauksevicius, Numerical–experimental identification of the most effective dynamic operation mode of a vibration drilling tool for improved cutting performance, Journal of Sound and Vibration, 331 (2012) 5175-5190.
[57] I. Mancisidor, A. Urkiola, R. Barcena, J. Munoa, Z. Dombovari, M. Zatarain, Receptance coupling for tool point dynamic prediction by fixed boundaries approach, International Journal of Machine Tools and Manufacture, 78 (2014) 18-29.
[58] J.R. Hutchinson, Shear Coefficients for Timoshenko Beam Theory, Journal of Applied Mechanics, 68 (2000) 87-92.
[59] I.H. Shames, C.L. Dym, Energy and Finite Element Methods in Structural Mechanics, 1995.
[60] M. Rantatalo, J.-O. Aidanpää, B. Göransson, P. Norman, Milling machine spindle analysis using FEM and non-contact spindle excitation and response measurement, International Journal of Machine Tools and Manufacture, 47 (2007) 1034-1045.
[61] Y. Cao, Modeling of high-speed machine-tool spindle systems, in: Mechanical Enginnering, University of British Columbia, Vancouver, Canada, 2006.
[62] C. Okwudire, Modeling and control of high speed machine tool feed drives, in, University of British Columbia, 2009.
[63] D.J. Ewins, Modal Testing: Theory, Practice, and Application, Wiley, 2000.
[64] R.J. Allemang, The Modal Assurance Criterion (MAC): Twenty Years of Use and Abuse, in: IMAC 20, the International Modal Analysis Conference, Los Angeles, 2002, pp. 397-405.
[65] B. Peeters, H. Van der Auweraer, P. Guillaume, J. Leuridan, The PolyMAX Frequency-Domain Method: A New Standard for Modal Parameter Estimation?, Shock and Vibration, 11 (2004).
[66] I.M. Hanna, J.S. Agapiou, D.A. Stephenson, Modeling the HSK Toolholder-Spindle Interface, Journal of Manufacturing Science and Engineering, 124 (2002) 734-744.
[67] W. Xiao, K. Mao, M. Zhu, B. Li, S. Lei, X. Pan, Modelling the spindle–holder taper joint in machine tools: A tapered zero-thickness finite element method, Journal of Sound and Vibration, 333 (2014) 5836-5850.
[68] T.L. Schmitz, K. Powell, D. Won, G. Scott Duncan, W. Gregory Sawyer, J.C. Ziegert, Shrink fit tool holder connection stiffness/damping modeling for frequency response prediction in milling, International Journal of Machine Tools and Manufacture, 47 (2007) 1368-1380.
[69] M.R. Movahhedy, J.M. Gerami, Prediction of spindle dynamics in milling by sub-structure coupling, International Journal of Machine Tools and Manufacture, 46 (2006) 243-251.
[70] V. Ostasevicius, R. Gaidys, J. Rimkeviciene, R. Dauksevicius, An approach based on tool mode control for surface roughness reduction in high-frequency vibration cutting, Journal of Sound and Vibration, 329 (2010) 4866-4879.
[71] E.I. Rivin, J. Agapiou, C. Brecher, M. Clewett, R. Erickson, F. Huston, Y. Kadowaki, E. Lenz, T. Moriwaki, A. Pitsker, S. Shimizu, T. Schulte, M.H. Schulz, K.S. Smith, M. Tsutsumi, A.G. Ulsoy, M. Weck, K. Yokoyama, Tooling Structure: Interface between Cutting Edge and Machine Tool, CIRP Annals - Manufacturing Technology, 49 (2000) 591-634.
[72] J.V. Ferreira, D.J. Ewins, Nonlinear Receptance Coupling Approach Based on Describing Functions, Proceedings of the 14th International Modal Analysis Conference, Dearborn. MI (1995) 1034-1040.
[73] G. Catania, N. Mancinelli, Theoretical–experimental modeling of milling machines for the prediction of chatter vibration, International Journal of Machine Tools and Manufacture, 51 (2011) 339-348.
[74] O. Kienzle, H. Victor, Spezifische schnittkrafte bei der metallbearbeitung, Werkstoffteechnik und Machinenbau, 47 (1957) 224-225.
[75] E.J.A. Armarego, R.H. Brown, The machining of metals, in, Prentice-Hall, Englewood Cliffs, N.J., 1969.
[76] J.J.J. Wang, C.M. Zheng, Identification of shearing and ploughing cutting constants from average forces in ball-end milling, International Journal of Machine Tools and Manufacture, 42 (2002) 695-705.
[77] O. Gonzalo, J. Beristain, H. Jauregi, C. Sanz, A method for the identification of the specific force coefficients for mechanistic milling simulation, International Journal of Machine Tools and Manufacture, 50 (2010) 765-774.

[78] Z.-Q. Yao, X.-G. Liang, L. Luo, J. Hu, A chatter free calibration method for determining cutter runout and cutting force coefficients in ball-end milling, Journal of Materials Processing Technology, 213 (2013) 1575-1587.
[79] Q. Cao, J. Zhao, S. Han, X. Chen, Force coefficients identification considering inclination angle for ball-end finish milling, Precision Engineering, 36 (2012) 252-260.
[80] G. Campatelli, A. Scippa, Prediction of Milling Cutting Force Coefficients for Aluminum 6082-T4, Procedia CIRP, 1 (2012) 563-568.
[81] J. Salguero, M. Batista, M. Calamaz, F. Girot, M. Marcos, Cutting Forces Parametric Model for the Dry High Speed Contour Milling of Aerospace Aluminium Alloys, Procedia Engineering, 63 (2013) 735-742.
[82] M. Wang, L. Gao, Y. Zheng, An examination of the fundamental mechanics of cutting force coefficients, International Journal of Machine Tools and Manufacture, 78 (2014) 1-7.
[83] A. Scippa, L. Sallese, N. Grossi, G. Campatelli, Improved dynamic compensation for accurate cutting force measurements in milling applications, Mechanical Systems and Signal Processing.
[84] L.M. Kumanchik, T.L. Schmitz, Improved analytical chip thickness model for milling, Precision Engineering, 31 (2007) 317-324.
[85] M. Subramanian, M. Sakthivel, K. Sooryaprakash, R. Sudhakaran, Optimization of Cutting Parameters for Cutting Force in Shoulder Milling of Al7075-T6 Using Response Surface Methodology and Genetic Algorithm, Procedia Engineering, 64 (2013) 690-700.
[86] P.E. Amiolemhen, A.O.A. Ibhadode, Application of genetic algorithms—determination of the optimal machining parameters in the conversion of a cylindrical bar stock into a continuous finished profile, International Journal of Machine Tools and Manufacture, 44 (2004) 1403-1412.
[87] C.L. Karr, B. Weck, D.L. Massart, P. Vankeerberghen, Least median squares curve fitting using a genetic algorithm, Engineering Applications of Artificial Intelligence, 8 (1995) 177-189.
[88] L. Ricardo Castro, P. Viéville, P. Lipinski, Correction of dynamic effects on force measurements made with piezoelectric dynamometers, International Journal of Machine Tools and Manufacture, 46 (2006) 1707-1715.
[89] F. Girardin, D. Remond, J.-F. Rigal, High Frequency Correction of Dynamometer for Cutting Force Observation in Milling, Journal of Manufacturing Science and Engineering, 132 (2010) 031002-031002.
[90] F. Lapoujoulade, G. Coffignal, J. Pimont, Cutting forces evaluation during high speed milling, in: 2ième Conf. Int. IDMME'98, Compiègne, France, 1998.
[91] A. Albrecht, S.S. Park, Y. Altintas, G. Pritschow, High frequency bandwidth cutting force measurement in milling using capacitance displacement sensors, International Journal of Machine Tools and Manufacture, 45 (2005) 993-1008.
[92] J. Chae, S.S. Park, High frequency bandwidth measurements of micro cutting forces, International Journal of Machine Tools and Manufacture, 47 (2007) 1433-1441.
[93] M.H. Richardson, D.L. Formenti, Global Curve Fitting of Frequency Response Measurements using Rational Fraction Polynomial Method, in: 3RD IMAC Conference, Orlando, FL, 1985.
[94] J.E. Dennis, R.B. Schnabel, Numerical Methods for Unconstrained Optimization and Nonlinear Equations, Society for Industrial and Applied Mathematics, 1996.
[95] Kistler, Document 20.290e-05.04, in.
[96] H. Cao, B. Li, Z. He, Chatter stability of milling with speed-varying dynamics of spindles, International Journal of Machine Tools and Manufacture, 52 (2012) 50-58.
[97] V. Gagnol, B.C. Bouzgarrou, P. Ray, C. Barra, Model-based chatter stability prediction for high-speed spindles, International Journal of Machine Tools and Manufacture, 47 (2007) 1176-1186.
[98] S. Ratchev, S. Liu, W. Huang, A.A. Becker, An advanced FEA based force induced error compensation strategy in milling, International Journal of Machine Tools and Manufacture, 46 (2006) 542-551.
[99] Y .S. Liao, Y.C. Young, A new on-line spindle speed regulation strategy for chatter control, International Journal of Machine Tools and Manufacture, 36 (1996) 651-660.
[100] E. Kuljanic, G. Totis, M. Sortino, Development of an intelligent multisensor chatter detection system in milling, Mechanical Systems and Signal Processing, 23 (2009) 1704-1718.
[101] T. Delio, J. Tlusty, S. Smith, Use of Audio Signals for Chatter Detection and Control, Journal of Manufacturing Science and Engineering, 114 (1992) 146-157.
[102] T.L. Schmitz, K. Medicus, B. Dutterer, Exploring once-per-revolution audio signal variance as chatter indicator, Machining Science and Technology, 6 (2002) 215-233.
[103] T.L. Schmitz, Chatter recognition by a statistical evaluation of the synchronously sampled audio signal, Journal of Sound and Vibration, 262 (2003) 721-730.
[104] I. Bediaga, J. Muñoa, J. Hernández, L.N. López de Lacalle, An automatic spindle speed selection strategy to obtain stability in high-speed milling, International Journal of Machine Tools and Manufacture, 49 (2009) 384-394.

[105] G. Quintana, J. Ciurana, D. Teixidor, A new experimental methodology for identification of stability lobes diagram in milling operations, International Journal of Machine Tools and Manufacture, 48 (2008) 1637-1645.
[106] F. Ismail, E. Soliman, A new method for the identification of stability lobes in machining, International Journal of Machine Tools and Manufacture, 37 (1997) 763-774.
[107] F. Ismail, E.G. Kubica, Active suppression of chatter in peripheral milling Part 1. A statistical indicator to evaluate the spindle speed modulation method, Int J Adv Manuf Technol, 10 (1995) 299-310.
[108] I. Bucher, D.J. Ewins, Modal analysis and testing of rotating structures, Philosophical Transactions of the Royal Society of London. Series A: Mathematical, Physical and Engineering Sciences, 359 (2001) 61-96.
[109] H.A.H. Al-Khazali, M.R. Askari, Analyzing Rotating Data for Machines Rotor with High Speeds Using the Spectral Map Wizard, International Journal of Scientific & Engineering Research, 3 (2012).
[110] M. Luczak, M. Firla, D. Sporna, S. Manzato, B. Peeters, Structural monitoring of the small wind turbine test stand, in: 8th International Conference on Structural Dynamics, EURODYN 2011, Leuven, Belgium, 2011.
[111] O. Özşahin, E. Budak, H.N. Özgüven, In-process tool point FRF identification under operational Conditions using inverse stability solution, International Journal of Machine Tools and Manufacture.